Selim Gürgen *Editor*

Shear Thickening Fluid

Theory and Applications

Springer

Shear Thickening Fluid

Selim Gürgen
Editor

Shear Thickening Fluid

Theory and Applications

Springer

Editor
Selim Gürgen
Department of Aeronautical Engineering
Eskişehir Osmangazi University
Eskişehir, Turkey

ISBN 978-3-031-25716-2 ISBN 978-3-031-25717-9 (eBook)
https://doi.org/10.1007/978-3-031-25717-9

This Springer imprint is published by the registered company Springer Nature Switzerland AG
The registered company address is: Gewerbestrasse 11, 6330 Cham, Switzerland

Contents

1 Introduction 1
Selim Gürgen

2 Rheology of Shear Thickening Fluid 3
Miguel Montenegro, Laura Campo-Deaño, and Francisco J. Galindo-Rosales

3 Multi-Phase Shear Thickening Fluid 33
Mohammad Rauf Sheikhi and Mahdi Hasanzadeh

4 Multi-Functional Systems Based on Shear Thickening Fluid 53
Xinglong Gong, Junshuo Zhang, and Shouhu Xuan

5 Vibration Damping Systems with Shear Thickening Fluid 77
Mohammad Rauf Sheikhi, Selim Gürgen, and Melih Cemal Kuşhan

6 Shear Thickening Fluid in Surface Finishing Operations 99
Ziyan Man and Li Chang

7 Shear Thickening Fluid–Based Protective Structures Against Low Velocity Impacts 115
Unsanhame Mawkhlieng, Mukesh Bajya, and Abhijit Majumdar

8 Shear Thickening Fluid-Based Protective Structures Against High Velocity Impacts 139
Neelanchali Asija Bhalla

Index 153

Chapter 1
Introduction

Selim Gürgen

The term "smart" describes an intellectual concept that is associated with human behavior. However, the smart concept has been adapted to engineering materials by the technological developments in recent years [1]. A great interest from every sector has been devoted to gain smart properties for various materials that are used to produce smart components, structures, and systems. Smart materials are known as the engineered materials that have controlled behavior by the external stimulations. The controlled behavior can be related to one or more properties such as electrical, magnetic, chemical, physical, thermal, and mechanical [2]. Shear thickening is one of non-Newtonian behaviors widely seen in colloidal suspensions. Despite the smart properties of shear thickening behavior, it has been considered as a problem in the industrial applications for a long time. In the chemical and textile industries, mixers generally suffer from overloading-based failures, while spray nozzles encounter with blockage downtimes due to the shear thickening of suspensions [3]. Over the last two decades, researchers have made significant achievements about shear thickening and consequently benefitting from this non-Newtonian behavior in various engineering fields [4]. Shear thickening rheology has been investigated by many researchers to find out the main factors in a controllable fashion so that the smart concept has been obtained for shear thickening fluid (STF). A set of factors has been listed in recent publications regarding the controllable properties of STF. Upon understanding the shear thickening principles, STF has been adapted to several applications such as multi-functional systems, damping devices, protective structures, manufacturing operations, etc.

This book provides a comprehensive source on shear thickening rheology and STF applications for engineers, researchers, and scientists. The basics of STF rheology are given while discussing the determining factors on shear thickening

S. Gürgen (✉)
Department of Aeronautical Engineering, Eskişehir Osmangazi University, Eskişehir, Turkey
e-mail: sgurgen@ogu.edu.tr

S. Gürgen (ed.), *Shear Thickening Fluid*,
https://doi.org/10.1007/978-3-031-25717-9_1

behavior. In addition, a novel concept, namely multi-phase STF, is described. Multi-phase STF, which includes various filler materials in an STF, dates back to less than a decade ago; however, there have been an increasing number of attempts on this novel concept. For example, shear thickening properties are enhanced by using rigid fillers while conductivity is developed with conductive fillers in STF. In addition to rheological side, various applications are given in this book. Multi-functional systems have been widely investigated in recent years. Based on the desired multi-functional properties, multi-phase STF systems are designed by using proper filler materials. Furthermore, STF-based vibration damping devices are discussed with the help of a literature survey. Shear thickening rheology provides adaptive properties for damping systems, thereby ensuring the design of smart damping devices. Surface finishing processes also take advantage of shear thickening rheology to design effective polishing slurries and, therefore, STF-based surface processing is given in this book. Protective structures are the main application field for STF. There are several studies on STF-included protective systems to benefit from shear thickening rheology for designing flexible and lightweight structures. STF-based protective structures are discussed with two chapters in this book so that focusing on low and high velocity threats respectively.

References

1. A. Hajalilou, S. Amri Mazlan, H. Lavvafi, K. Shameli, Introduction, in *Field Responsive Fluids as Smart Materials [Internet]*, (Springer Singapore, Singapore, 2016), pp. 1–3. [cited 2022 Sep 8]. (Engineering Materials). https://doi.org/10.1007/978-981-10-2495-5_1
2. S.L. Vieira, C. Ciocanel, P. Kulkarni, A. Agrawal, N. Naganathan, Behaviour of MR fluids in squeeze mode. Int. J. Veh. Des. **33**(1/2/3), 36 (2003)
3. H.A. Barnes, Shear-thickening ("Dilatancy") in suspensions of nonaggregating solid particles dispersed in Newtonian liquids. J. Rheol. **33**(2), 329–366 (1989)
4. S. Gürgen, M.C. Kuşhan, W. Li, Shear thickening fluids in protective applications: A review. Prog. Polym. Sci. **75**, 48–72 (2017)

Chapter 2
Rheology of Shear Thickening Fluid

Miguel Montenegro, Laura Campo-Deaño, and Francisco J. Galindo-Rosales

Nomenclature

BET	Back extrusion technique
CST	Continuous shear thickening
CSR	Controlled shear rate
CSS	Controlled shear stress
DST	Discontinuous shear thickening
d_0	Initial diameter (m)
d_f	Final diameter (m)
$d_{\min}$	Minimum diameter (m)
F	Force (N)
g	Gravitational acceleration (m^2/s)
G'	Storage modulus (Pa)
G''	Loss modulus (Pa)
h_0	Initial height
L	Length (m)

M. Montenegro · L. Campo-Deaño
CEFT—Centro de Estudos de Fenómenos de Transporte, Departmento de Engenharia Mecânica, Faculdade de Engenharia da Universidade do Porto, Porto, Portugal

ALiCE—Laboratório Associado em Engenharia Química, Faculdade de Engenharia da Universidade do Porto, Porto, Portugal

F. J. Galindo-Rosales (✉)
ALiCE—Laboratório Associado em Engenharia Química, Faculdade de Engenharia da Universidade do Porto, Porto, Portugal

CEFT—Centro de Estudos de Fenómenos de Transporte, Departmento de Engenharia Química, Faculdade de Engenharia da Universidade do Porto, Porto, Portugal
e-mail: galindo@fe.up.pt

S. Gürgen (ed.), *Shear Thickening Fluid*,
https://doi.org/10.1007/978-3-031-25717-9_2

LAOS	Large amplitude oscillatory shear
LVR	Linear viscoelastic region
MRSTF	Magnetorheological shear thickening fluid
N_1	First normal stress difference
N_2	Second normal stress difference
PCC	Precipitated calcium carbonate
Q	Flow rate (m^3/s)
r	Radius (m)
SAOS	Small amplitude oscillatory shear
SBE	Short back extrusion
SHPB	Split-Hopkinson pressure bar
STF	Shear thickening fluid
t	Time (s)
wt	Mass fraction (%)
δ	Phase angle (rad)
Δp	Pressure drop (Pa)
γ	Strain
$\dot{\gamma}$	Shear rate (s^{-1})
$\dot{\gamma}_w$	Shear rate at wall (s^{-1})
$\dot{\epsilon}$	Extension rate (s^{-1})
η	Shear viscosity (Pa•s)
η^+	Transient viscosity (Pa•s)
Λ_0	Initial aspect ratio
ρ	Density (kg/m^3)
σ	Surface tension (N/m)
τ	Shear stress (Pa)
τ_w	Shear stress at wall (Pa)
Ψ_1^+	First normal stress coefficient
Ψ_2^+	Second normal stress coefficient
ω	Angular frequency (rad/s)

2.1 Introduction

Rheology is the field of science that studies the deformation and flow of complex materials [1]. A complex fluid is a sort of complex material that does not obey Newton's law of viscosity: it exhibits a nonlinear relationship between the imposed stress and the measured strain rate or vice versa [2]. In order to understand and model that relationship between stress and strain, we need to poke the material and observe how the material functions depend on the loading time scale, loading amplitude, external electromagnetic fields, temperature, etc. [3]. Rheometry is a branch of rheology dedicated to measuring the different material functions [4], which are determined under standard flows, such as shear and extensional flows that can provide complementary information to get a complete rheological characterization [5].

Shear thickening fluids (STFs) are complex fluids, typically consisting of dense suspensions of solid particles dispersed in an inert carrier fluid, that exhibit an increase in viscosity under the application of a shear rate/stress over a critical value [6]. In other words, the stress required to shear an STF increases faster than linearly with the shear rate [7], as shown in Fig. 2.1. In his seminal work of 1989 [10], Barnes stated that shear thickening behavior is normally conditioned by different parameters (Table 2.1). Subtle changes in the local particle arrangements are responsible for the transitions between shear thinning, Newtonian, and shear thickening regimes [9]. In recent years, it is common to distinguish between continuous shear thickening (CST) and discontinuous shear thickening (DST); the former is exhibited at intermediate packing fractions and the viscosity increase is relatively mild due to the formation of hydroclusters [11]; increasing the packing fraction, the viscosity increase becomes steeper up to a point where the viscosity exhibits a discontinuous increase beyond a critical shear rate, as result of the contact between particles [7].

Although shear thickening behavior may cause technical problems in flow processes, such as blockage of spraying nozzles or insufficient mold filling [12], thanks to their viscous dissipative nature and the possibility of tuning their viscosity curves, these fluids have allowed the development of important engineering solutions to different applications, namely in energy dissipation systems, such as vibration or impact absorption, which have accelerated in the last years [6, 13]. Even though STF has undergone dynamic loads in most of the applications, it is traditionally characterized by means of viscosity curves, which represent the equilibrium shear viscosity values reached at different steady shear rates. It is hard to believe that the STF will undergo steady simple shear flow in its final application, most probably the flow will be transient and complex, a combination of shear and extensional flows; this mismatch, both in terms of timescale and flow type, between the rheological

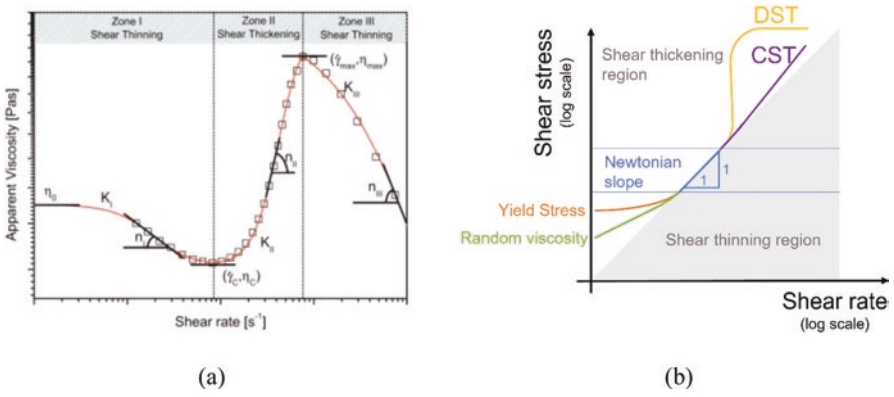

Fig. 2.1 (**a**) Sketch of a viscosity curve exhibited by STF transiting from Newtonian to shear thinning and shear thickening (CST) regimes [8]. (**b**) Sketch of different flow curves exhibiting CST and DST [9]. Reprinted by permission from Elsevier

Table 2.1 Parameters for conditioning the shear thickening behavior [10]

Particle	• Particle size • Particle size distribution • Particle shape • Particle-particle interaction • Volume fraction
Continuous phase	• Liquid phase viscosity
Flow field	• Type of deformation (shear or extension, steady or unsteady) • Rate of deformation • Time of deformation

information provided and the final deformation under real conditions, may result in a wrong performance of the fluid [14].

This chapter aims at providing a guide about how to perform a full rheological characterization of STF useful for both fitting and developing constitutive models and tweaking the formulations toward obtaining an optimal rheological performance of the fluid.

2.2 Shear Rheometry of STF

2.2.1 Steady Shear Flow

In shear rheometry, the fluid sample undergoes simple shear flow, which can be imposed either by rotational rheometers or by capillary (both at macro and microscales) ones [2]. Steady shear measurements allow obtaining either the viscosity curve, which provides information about the dependence of the steady shear viscosity on the shear rate, or the flow curve, which relates the steady shear stress with the shear viscosity.

There are two kinds of rotational rheometers: strain-controlled and stress-controlled rheometers, the latter commonly equipped with control systems allowing for operating in pseudo-strain-controlled mode. As highlighted by Mewis and Wagner [15], it is very important to bear in mind that "controlling stress allows one to move systematically through the transition, whereas in a strain-controlled device the discontinuous shear thickening region is generally not accessible". Rotational rheometers enable the imposition of steady simple shear flow covering a wide range of shear rates/stresses by working with the right geometry, i.e., concentric cylinders, cone-plate or plate-plate, and the right dimensions. Whereas cone plate geometry ensures a homogeneous shear rate throughout the whole volume sample, for STF, plate-plate geometries are very convenient, particularly if wall slip would be an issue, as they can operate with grooved surfaces and different gaps to avoid it. Concentric cylinders can also be used with STF, as long as a small gap is being used to minimize the change of shear rate inside the gap and to avoid particle migration; however, loading a very viscous STF in a concentric cylinder geometry is more

difficult than in other rotational geometries [16, 17]. Some other precautions must be considered when working with STF, not because of its rheological behavior, but because STF mostly consists of a dense suspension of particles [15]: regarding the gap size, either operating with cone-plate or plate-plate geometry, it is of paramount importance ensuring that the ratio of gap size to particle/aggregate size is large enough, between 10 and 50; when the formulation consists of particles not neutrally buoyant with the carrier fluid and large enough to avoid the Brownian motion so that sedimentation dominates, a vertical concentration gradient will be developed and the top moving plate will "feel" an apparent reduction in the viscosity of the sample; as in many suspensions, some shear thickening samples may require a pre-shear protocol to ensure reproducibility in the measurements [18]; partial evaporation of the carrier fluid may be also an issue when working with volatile solvents, which can be avoided either by fractioning the range of shear rates to be covered in a single experiment or by reducing the shearing time at each shear rate.

The experimentalist is responsible for being aware of the instrument's resolution, instrument inertia, sample inertia, boundary effects, and volumetric effects to avoid bad data [3] when operating the rotational rheometer. Working with STF, the maximum torque of the rheometer may be reached with ease if working with a cone-plate or plate-plate geometry. To avoid misinterpretations of the steady shear flow measurements, the experimental window must be properly identified, because the data set obtained below the minimum torque line can be misinterpreted as shear thinning behavior and data beyond the onset of secondary flows can be misunderstood as shear thickening behavior.

When performing steady shear flow measurements with STF in a rotational rheometer equipped with crosshatched, serrated, or grooved plates, it is important to perform several preliminary tests: the experimentalist should test different gap sizes in order to ensure that the measurements are gap independent [19], as the roughness of the plates may introduce gap dependency; surplus of material around the plates should be carefully trimmed, otherwise the presence of a few milliliters of suspension left on the bottom plate in contact with the paste between the two plates may strongly affect the critical shear rate and induce gap dependency [20].

Any complex fluid would be fully characterized under steady shear flow with three material functions [21], i.e., the variation with shear rate of the shear viscosity and the first and second normal stress differences, $N_1 = \sigma_{11} - \sigma_{22}$ and $N_2 = \sigma_{22} - \sigma_{33}$ respectively [22], where by convention 1, 2, and 3 are the velocity, velocity gradient, and vorticity directions, respectively, in a viscometric shear flow. For isotropic materials, N_1 has always been found to be positive (unless it is zero) and N_2 negative and smaller than N_1 in terms of magnitude [23]. If the material is an ideal solid (purely elastic), then the value of N_2 would be zero. Typically, a negative value of N_1 means that one is dealing with a shear thinning behavior. When dealing with STF, however, it has been found that the value of N_1 can also be negative and with an absolute value equal to the applied stress [24]. Andrade et al. [25] reported in their work that the transition from $N_1 \approx 0$ to a negative value of the first normal stress difference in their colloidal suspensions with DST behavior appeared at rates lower than the onset of the shear thickening regime and was also related to a lower volume

fraction, indicating contributions from lubrication forces, instead of the transition $N_1 \approx 0$ to positive (beyond critical shear rate) that suggested frictional interactions from contacts between particles. Pan et al. [26] also observed that increasing particle diameters in shear thickening granular suspensions led to the growing importance of hydrodynamic interactions, resulting in negative normal stresses. N_2, however, generally remained very much neglected [27]; Laun [24] back in 1990s reported that $N_2 \approx -N_1/2$ in opposition to most of the reported measurements and numerical simulations [28]. Thus, as the measurement of both normal stress differences may be limited by capillary stresses as discussed by Brown and Jaeger [7, 29] and shown by Garland et al. [30], the information regarding the normal stresses can alternatively obtained by means of extensional experiments.

Capillary rheometry has been typically used for determining the viscosity curves of polymer melts, providing reliable information at high shear rates, beyond the limits of rotational rheometers, and in similar conditions to the industrial process. The latter reasoning could be also applied to STF, as in many industrial processes, such as injection of pastes or ceramics inside molds, dense suspensions are extruded through a capillary and the shear thickening or jamming transition may happen in the process. The functioning principle of a capillary rheometer is very simple: the fluid sample flows at a controlled flow rate (Q) through a tube having a well-defined radius (r), and the pressure drop (Δp) between two points, within the fully developed region and separated by a certain distance (L), is measured. A non-slip condition is assumed to be held at the wall. As the shear rate at the wall ($\dot{\gamma}_w$) is directly proportional to the flow rate and the shear stress at the wall (τ_w) is also proportional to the pressure drop, the shear viscosity is just given by dividing one by the other $\left(\eta = \tau_w / \dot{\gamma}_w\right)$. The basic principle of a capillary rheometer is illustrated in Fig. 2.2.

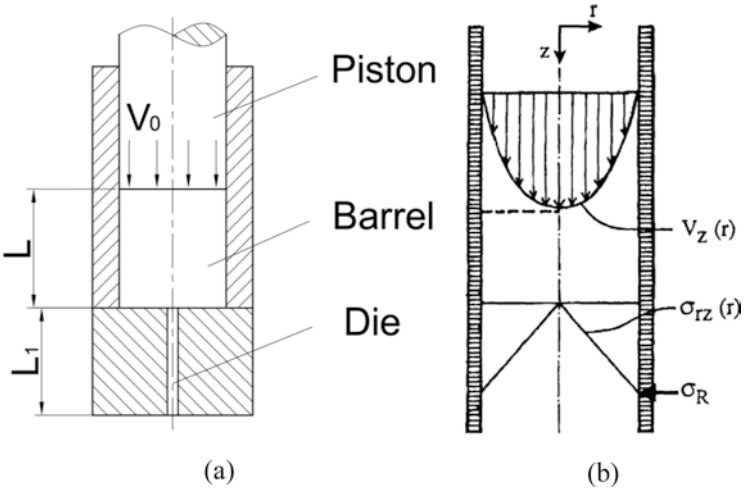

Fig. 2.2 (**a**) Schematic diagram of a high-pressure capillary rheometer [31]. (**b**) Velocity and shear stress profiles [32]. Reprinted by permission from Elsevier

This works well for Newtonian fluids; however, when dealing with shear thinning fluids, the Weissenberg-Rabinowitsch-Mooney (WRM) correction is required [23] because the shear rate at the wall is not linearly related to the flow rate. In principle, this correction also remains valid when working at the microscale with planar slit microfluidic devices [33]. However, the recent experimental results reported by Bossis and co-workers [34] discourage the use of capillary rheometry with STF, at least for those exhibiting DST. They realized that upon jamming, there is no longer a suspension flowing through a capillary, but instead a less concentrated suspension flows through a porous medium developed by the jammed particles; moreover, they also reported that the jamming does not occur inside the capillary but rather before its entrance, and finally, the fluctuations of pressure observed at constant shear rate are probably produced by the intermittent collapse of the jammed structure at the entrance of the die. However, they managed to get useful results [16] and, based on them, successfully modified the model proposed by Wyart and Cates [35]. Another interesting result from Bossis et al. [36] is that the jamming transition, which in the rotational rheometer occurs in a fraction of the inverse shear rate, exhibited in the extrusion a much slower dynamics than in the case of stress imposed on a rotational geometry. This latter observation supports the idea that characterizing STF under simple steady shear experiments in a rotational rheometer is by far insufficient to provide the required information to understand and predict the behavior of these fluids in practical applications.

Besides the information provided above, it is also important to note that capillary rheometry requires a larger amount of fluid sample than rotational rheometry, slip can often be a problem difficult to determine, and capillary rheometers are much less versatile than rotational ones since neither transient, oscillatory, nor normal stress measurements are possible [15]. Because of all the argued reasons, capillary rheometry does not seem to be the most convenient approach for steady shear flow measurements with STF.

2.2.2 Transient Shear Flows

As mentioned before, STF will find practical applications in which its time-dependent behavior is of paramount importance, irrespective of whether it will be used in anti-impact protective equipment or in anti-vibration systems. Moreover, it is known that STF exhibits a much different rheological response when undergoing transient impact experiments than under the steady shear state, as described in the previous section; for instance, DST suspensions support stress orders of magnitude larger under impact conditions than inferred from steady state rheometer measurements [37–39]. Again, these transient results support the idea that any generalized Newtonian fluid model [8, 40–49] will provide information with limited utility from the practical point of view [50]. Thus, a more complete rheological characterization including both the steady state and transient behaviors would be required to provide

theoreticians with useful data sets to develop a constitutive model able to predict time-dependent behaviors such as kinetic models [51].

Transient shear experiments cannot be executed with a capillary rheometer, but by means of rotational rheometers, and, ideally, they should always be performed with a cone-plate geometry, since the shear rate is constant throughout the volume sample. The use of parallel plates is discouraged because the shear strain and stress vary in the radial direction, which is even more inconvenient in transient experiments than in steady shear measurements because it causes a variable shear history throughout the volume sample that complicates the interpretation of the results [15].

In this section, transient experiments are referred to as unsteady shear flows under continuous rotation of the geometry in the rotational rheometer. Oscillatory experiments will be considered as a different group of unsteady shear flow. The variety of transient experiments available in the literature is quite wide [1]; hereafter, the different experiments, the information that they can provide, the precautions that should be considered, and the usefulness for characterizing STF will be considered.

Startup experiments, when applied to STF, should be preferably performed in control-stress mode, for the same reason argued in the previous section. Before the beginning of the experiment ($t < 0$), the fluid sample is at rest; at $t = 0$ constant shear stress is imposed on the fluid: $\tau(t \geq 0) = \tau_0$. This experiment aims at looking at the time evolution of the transient viscosity ($\eta^+(t, \tau_0)$), first normal stress coefficient $\left(\Psi_1^+\left(t,\tau_0\right)\right)$, and second normal stress coefficient $\left(\Psi_2^+\left(t,\tau_0\right)\right)$, which will also depend on the magnitude of the applied shear stress. This sort of experiment allowed Rathee et al. [52] to study localized stress fluctuations in dense suspension, for instance.

Tassieri and his co-workers [53] have developed a Fourier transform-based method (i-Rheo) to determine the viscoelastic moduli from raw startup experimental data in control-stress mode. The efficacy of i-Rheo was validated with colloidal suspensions, both in the fluid and in the glass states [54]; nevertheless, they did not validate it for STF. In this sense, i-Rheo might be an excellent tool for determining the viscoelastic moduli of STF at high frequencies, beyond the limits of rotational rheometers, which are related either to the instrument or to the fluid inertia [3].

From the practical point of view, it may be important to understand how the STF relaxes upon releasing the load [50], how long it will take to be ready for the next load, or even whether it comes to the same initial structure prior to the released load (anti-thixotropy or rheopexy) [55–58]. *Stress relaxation* experiments consist of observing how the shear stress relaxes with time when the flow is abruptly stopped, which allows to determine a relaxation time in shear; this kind of experiment was used by Cho et al. [59] to discover that STF exhibiting DST retains its memory of the level of frictional contacts prior to the flow cessation even after the relaxation ends, despite the presence of the inter-particle repulsions that enable DST.

Concatenated stepwise experiments have been typically used for characterizing thixotropy, but they have been also proven to be useful for characterizing anti-thixotropy or rheopexy (Fig. 2.3). Rubio-Hernández et al. [51] used this experimental protocol to verify that fumed silica suspensions with CST behavior exhibited

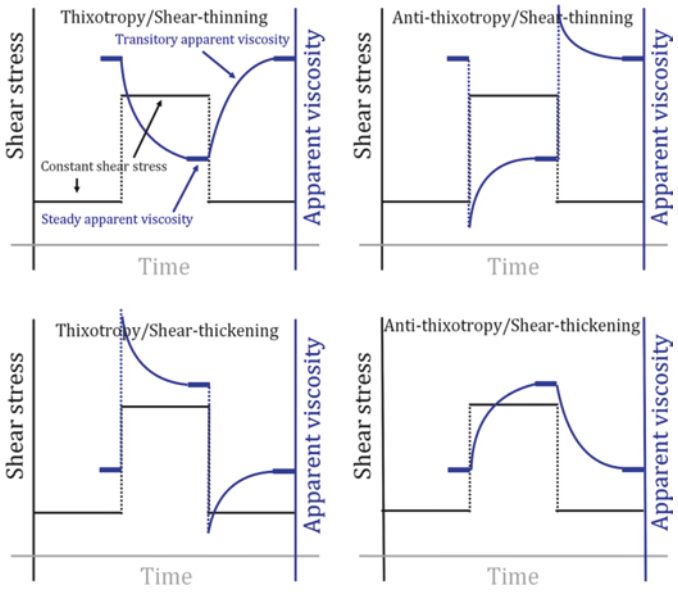

Fig. 2.3 Possible evolution in the apparent viscosity with time in a three-step test applied to shear thinning and shear thickening materials [51]. Reprinted by permission from AIP Publishing

thixotropy within the shear thinning region and anti-thixotropy in the shear thickening region [51].

Hysteresis loops have also been traditionally used to determine thixotropic behavior, although the existence of hysteresis loops is not a synonym of thixotropy; as aforementioned, the existence of thixotropy can only be determined with concatenated stepwise experiments. The hysteresis loop experiment consists of imposing an increasing ramp in shear rate with time followed by a decreasing ramp with the same slope, and register the time evolution of the transient viscosity for each ramp, i.e., $\eta_1^+\left(t,\dot{\gamma}_1\right)$ for the increasing ramp with slope $\dot{\gamma}_1$ and $\eta_2^+\left(t,\dot{\gamma}_2\right)$ for the decreasing ramp with slope $\dot{\gamma}_2=-\dot{\gamma}_1$. Results are typically represented as η^+ vs $\dot{\gamma}$, and if the curves given by η_1^+ and η_2^+ do not overlap, it is said that there is a hysteresis loop; nevertheless, they can also be found in terms of stress versus shear rate (Fig. 2.4).

In STF, if the first and second ramps lie within the limit of the shear thinning region $(\dot{\gamma}<\dot{\gamma}_c)$, then the presence of a hysteresis loop would mean that there is a difference between the kinematics of the destruction of the microstructure during the increasing ramp and the kinematics of construction of the microstructure during the decreasing ramp; if the first and second ramps go within the limits of the shear thickening region $(\dot{\gamma}_c<\dot{\gamma}<\dot{\gamma}_{\max})$, then the kinematics of construction of the shear-induced microstructure during the increasing ramp is different from the kinematics of destruction of the microstructure dominated by repulsive forces during the decreasing ramp. If the experiment provides overlapping curves, then it would mean

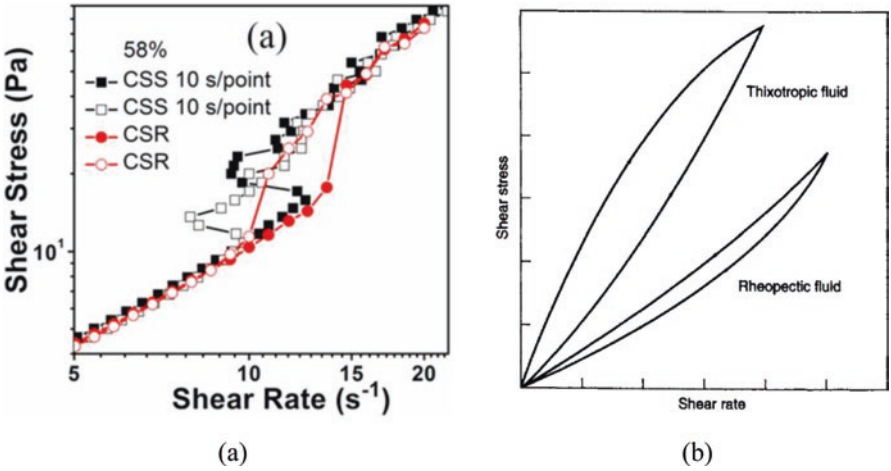

Fig. 2.4 (**a**) Up and down flow curves displaying hysteresis of shear thickening suspensions. Filled symbols for increasing stress and open symbols for decreasing stress sweeps [60]. Reprinted by permission from American Physical Society. (**b**) Schematic shear-stress rate behavior for time-dependent fluid behavior [61]. Reprinted by permission from Elsevier

that both kinematics responsible for building and destroying microstructure are essentially equal. It is recommendable to test different slopes as in [62].

Flow reversal tests consist of imposing a shearing flow in one direction and instantaneously changing the direction of the flow while the magnitude of the shear rate remains the same [63]. This kind of test has been traditionally used to validate constitutive models for thixotropic fluids, which typically exhibit a two-step relaxation of shear stress caused by the presence of a viscoelastic relaxation and a kinematic hardening relaxation [58]. Nevertheless, there is no fundamental reason for not using the flow reversal tests in validating kinematic models for time-dependent behavior of STF; however, to the best of the author's knowledge, the state of the art lacks this experimental data sets.

It can be found in the literature that unsteady shear flow tests are typically complemented with simultaneous confocal microscopy [64], boundary stress microscopy [65] X-ray [66] pressure measurements [67], or ultrasound imaging [68] in order to provide extra information regarding the presence or the evolution of microstructures, heterogeneities, vortices bands, etc., developed in the fluid sample along the experiment.

2.2.3 Oscillatory Shear Flows

Oscillatory shear flow experiments allow to decouple the viscoelastic response of a complex fluid into the elastic contribution and the viscous contribution; these viscous and elastic forces lead to an additional time scale and help to provide more

insight into a controllable alternative shear history in comparison to steady shear experiments [69].

Typically, a sinusoidal shear stress or strain is imposed, and the resulting strain or stress is recorded; therefore, the material functions (G' and G'') are defined with the output signal. This way, when a sinusoidal strain signal is applied, the stress wave that is in phase with the applied strain wave divided by the amplitude of the strain wave is called the *storage modulus* (G'). On the other way, the amplitude of the stress wave that is out of phase with the strain wave divided by the strain amplitude is called *loss modulus* (G''). If the sample is a Hookean solid, both signals are in phase ($G'' = 0$); in the case of a Newtonian liquid, the signals are shifted by $\frac{\pi}{2}$ ($G' = 0$), and in the case of a viscoelastic liquid, the signals are shifted by a phase angle $0 < \delta < \frac{\pi}{2}\left(G' \text{and} G'' \neq 0\right)$ as illustrated in Fig. 2.5.

The first step to analyze a sample by means of an oscillatory test is to perform an amplitude sweep. This test consists in applying a strain or stress amplitude sweep at a constant frequency and the typical results are represented in Fig. 2.6. These results allow one to determine the limit of the linear viscoelastic region (LVR), in which the viscoelastic moduli do not vary with the strain amplitude indicating that the structure is still preserved.

The frequency sweep test must then be developed by choosing a strain within the LVR. The frequency sweep test gives information on the time-dependent behavior of the sample in a non-destructive interval of strain/stress and consists in applying a

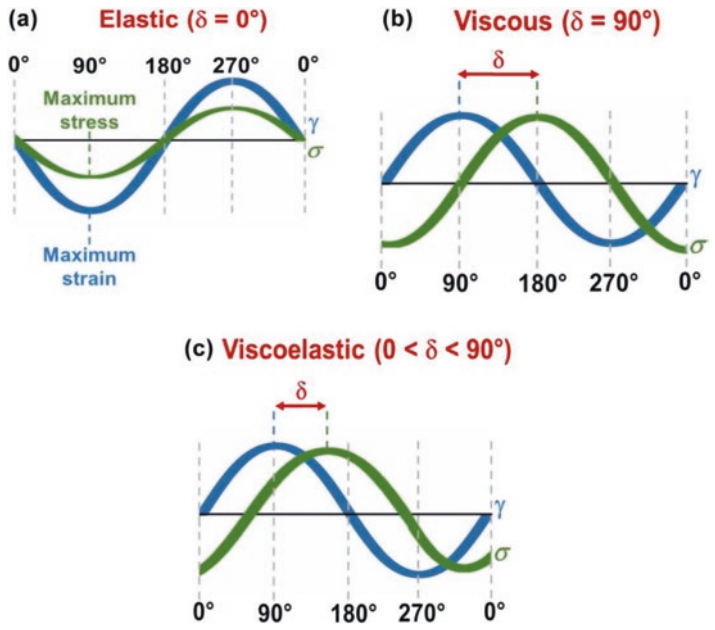

Fig. 2.5 Stress and strain wave relationships for (**a**) a purely elastic (ideal solid), (**b**) a purely viscous (ideal liquid), and (**c**) a viscoelastic material [70]. Under the Creative Commons license

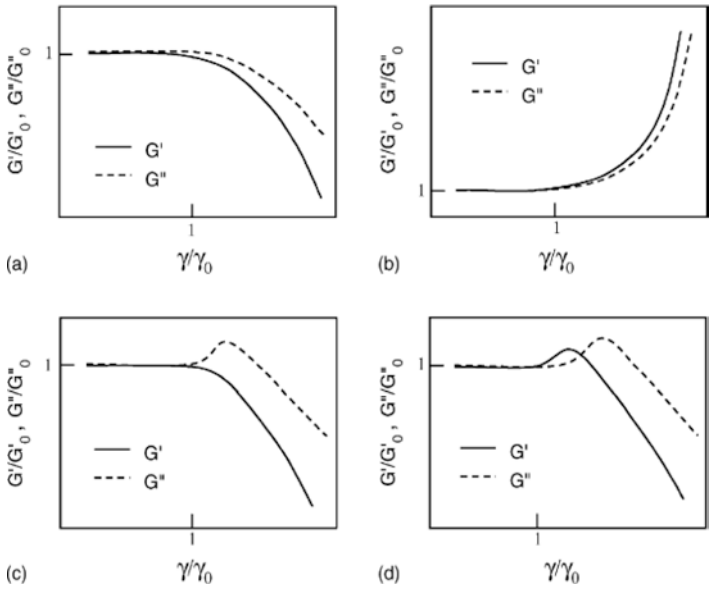

Fig. 2.6 Types of LAOS behavior: (**a**) strain thinning, (**b**) strain hardening, (**c**) weak strain overshoot, (**d**) strong strain overshoot [71]. Reprinted by permission from Elsevier

frequency sweep at a constant strain from the LVR. However, the complex behavior of STF is not observed in this kind of experiment because of the small magnitude of the applied strain. Under certain conditions (high deformation, high volume fraction, high frequency, etc.), the signal response is no longer sinusoidal indicating the limit of the LVR and more harmonics appear that can give valuable information about the microstructure of the sample. Experimental tests performed in this region are called large oscillatory shear tests (LAOS) as opposed to their counterparts developed at low deformations, small amplitude oscillatory tests (SAOS). Several studies have been carried out during decades to understand the dynamic behavior of STF using oscillatory tests: e.g., Laun et al. [72], Boersma et al. [73], Raghavan and Khan [74], Yziquel et al. [75], Mewis and Biebaut [69], Lee and Wagner [76], Fischer et al. [77], Chang et al. [78], Khandavalli and Rothstein [79], Lee et al. [80], Rathee et al. [65].

Hyun et al. [71] wrote about the importance of LAOS experiments to characterize complex fluids such as STF. They basically classified the complex fluids into four types: type I, with G' and G'' decreasing (strain thinning); type II, with G' and G'' increasing (strain hardening); type III, with G' decreasing and G'' increasing followed by a decrease (weak strain overshoot); and type IV, with both G' and G'' increasing followed by a decrease (strong strain overshoot). Figure 2.6 is a schematic representation of these types of LAOS behaviors. Typically type IV is very representative of STF as is shown in Raghavan and Khan [74] and Galindo-Rosales et al. [18], for example.

Boersma et al. [73] studied the nonlinear viscoelastic behavior of dispersions of silica (SiO_2) particles in a glycerol/water mixture and dispersions of glass particles in a glycerol/water mixture. They found that G'' dominates over G', indicating a liquid-like behavior because of the absence of flocculation. A nonlinear response was observed after a critical combination of frequency and deformation. When larger strain amplitudes and frequencies are applied to STF, the viscoelastic modulus increases abruptly (strain hardening). Raghavan and Khan [74] analyzed the rheological behavior under oscillatory tests of suspensions of fumed silica in polypropylene glycol. They reported strain hardening behavior and demonstrated that this behavior at high strain amplitudes is quite similar to shear thickening in steady flow experiments. This correlation can be represented using a modified Cox-Merz rule (proposed by Doraiswamy et al. [81]) in which the results of the complex viscosity as a function of dynamic shear rate ($\gamma_0 \bullet \omega$) can be superposed with the results of the viscosity in steady shear experiments. Also, three different fumed silica particles suspended in polypropylene glycol and in paraffin oil were used by Yziquel et al. [75] to analyze the linear and nonlinear rheological behavior. They observed solid-like behavior ($G' > G''$) for the three different silica particles at 8.2 wt% in paraffin oil. It was not possible to observe the linear regime as the loss modulus increased with the strain amplitude at low values of strain, possibly due to the breakdown of the structure. On the contrary, for the suspension in polypropylene glycol, the loss modulus was higher than the elastic modulus, indicating a liquid-like behavior. In the nonlinear regime, they observed excess dissipation energy (calculated from amplitudes sweeps) because of the breakdown of the 3D structure of the fumed silica suspensions. Mewis and Biebaut [69] observed also a strain hardening in oscillatory flow for monodispersed silica core particles with a grafter layer of poly(butyl methacrylate) (PBMA) in octanol. They found that the critical stress at which the strain hardening occurs is independent of the frequency and is also the same as the critical shear stress in steady flow measurement when the shear thickening appears. They also concluded that for their systems, the onset for the strain hardening is independent of the flow history, since in the oscillatory flow, the critical conditions are obtained periodically and lead to the same effect as reaching the critical conditions in continuous regime. Lee and Wagner [76] investigated the critical strain amplitude able to provoke shear thickening in oscillatory flow and the frequency dependence. They showed that neither the extent nor the modified Cox-Merz rules were able to correlate the dynamic and the steady state viscosities in the shear thickening regime or in the onset of the shear thickening. They proposed a superposition of the two viscosities at the point when the shear thickening regime can be observed by plotting the data versus the average stress magnitude. For low frequencies, the critical strain varies inversely with the frequency, but for high frequencies, an apparent plateau appears because of a large amount of slip. Fischer et al. [77] used in their studies concentrated suspensions of hydrophilic fumed silica in polypropylene glycol. They performed frequency sweep experiments for a wide range of strain amplitudes and found a power law correlation showing a decrease in the viscosity with frequency before and after the transition, being the effect more marked at frequencies after the transitions, leading to think that the shear thickening

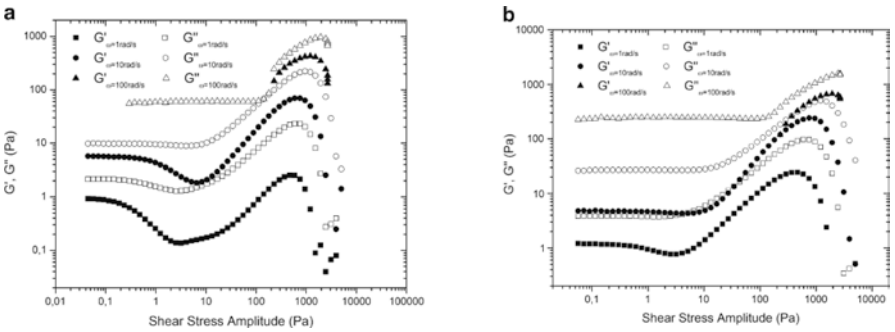

Fig. 2.7 Amplitude sweeps of Aerosil R816 suspensions in (**a**) PPG400, (**b**)PPG2000 [18]. Reprinted by permission from Springer

could disappear at sufficiently high frequencies. Galindo-Rosales et al. [18] used hydrophobic fumed silica in polypropylene glycol. Fig. 2.7 shows the results of the amplitude sweep tests: the loss modulus (G'') is higher than the elastic modulus (G'), typical of a liquid-like behavior, but both moduli present relatively low values according to the non-flocculated nature of the suspensions. As it was reported previously, at a certain value of the stress amplitude, both moduli increase abruptly revealing the strain hardening behavior.

A deep-inside analysis of the LAOS experiments was developed by Khandavalli and Rothstein [79]; they evaluated the rheological properties of three different suspensions—fumed silica in polyethylene oxide, fumed silica in polypropylene glycol, and cornstarch in water—and found a type III and type II LAOS behaviors for G' and G'' for the fumed silica in polyethylene oxide and in polypropylene glycol respectively (according to the classification of Hyun et al. [71]). For the cornstarch in water suspension, the results were $G' \geq G''$, and as the strain amplitude increased, the moduli declined, but at large strain amplitudes, G' and G'' increased showing a strain-rate thickening behavior. The Lissajous-Bowditch curves were useful to analyze the viscoelastic nonlinearities which revealed strong differences between the samples. Rathee et al. [65] also analyzed the LAOS response of colloidal suspensions formulated with silica particles in a glycerol/water mixture in a regime of discontinuous shear thickening, obtaining results consistent with the ones of Khandavalli and Rothstein [79].

The analysis of the viscoelastic properties in the nonlinear regime by means of LAOS experiments is of great importance for the development of damping materials and their applications to energy absorption and vibration control. The analysis of the energy dissipation capacity of a damper is normally done through a hysteresis curve in which the enclosed area is the consumed energy of the structure in one cycle, similarly to the Lissajous-Bowditch curves obtained in LAOS experiments. Some work related to the development of optimized dampers aimed to develop dynamic models for dampers with STF (Zhao et al. [82], Zhang et al. [83], Lin et al.

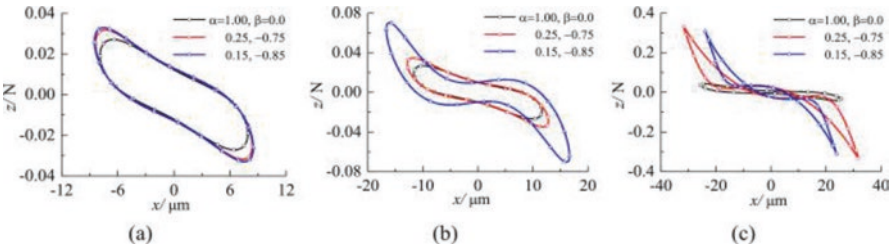

Fig. 2.8 Hysteric curves with different excitation frequency and amplitude: (**a**) $f = 35$ Hz, F = 2 N, (**b**) $f = 50$ Hz, F = 2 N, (**c**) $f = 50$ Hz, F = 5 N [85]. Reprinted by permission from Elsevier

[84], Zhao et al. [85]). The hysteretic curves with different excitation frequency and amplitude developed by Zhao et al. [85] are shown in Fig. 2.8 and can be easily compared with the data from LAOS.

2.2.4 Superposition Rheology

Superposition in rheology means that during the experiment, both steady shear deformation and oscillatory motion are simultaneously applied to the sample. The directions of the velocity vectors of each motion can be either parallel, thus designating a parallel superposition, or at right angles, known as transverse or orthogonal superposition. The parallel shear stress superposition is represented in Fig. 2.9 and given by $\tau_{yx}\left(\dot{\gamma},\gamma_0,t\right)=\eta\left(\dot{\gamma}\right)\bullet\dot{\gamma}+G_{\|}^{*}\left(\omega,\dot{\gamma},\gamma_0\right)\bullet\gamma_0\bullet\sin\left(\omega\bullet t\right)$, where $G_{\|}^{*}$ is the parallel complex modulus, $\dot{\gamma}$ is the steady shear rate, $\eta\left(\dot{\gamma}\right)$ is the steady shear viscosity, and γ_0 and ω are the amplitude and frequency of the superimposed oscillation, respectively [87, 88].

Although data interpretation regarding superposition rheology is still under investigation since the viscoelastic superposition response on a microscopic level is rather complex, the technique is very powerful as it provides valuable information regarding the material's viscoelasticity under nonlinear perturbation [89]. The effects of parallel superposition have been gradually investigated in shear thickening suspensions, such as in the work of Mewis and Biebaut [69] where suspensions of silica particles in poly(butyl methacrylate) (PBMA) were subjected to parallel superposition eliminating or reducing the contributions from the longest relaxation times during the experiments and evidencing shear thickening behavior before the steady state viscosities start to increase. Recently, Rubio-Hernández [86] tested a concentrated fumed silica suspension in polypropylene glycol (PPG) with parallel superposition rheology. They concluded that, for simple oscillatory measurements, the loss modulus dominated $G'' > G'$, contrary to what happened with superimposed testing, where $G' > G''$, suggesting that the microstructure of the STF evolved from few and big hydroclusters on the onset of the shear thickening region to many and small ones when shearing increases.

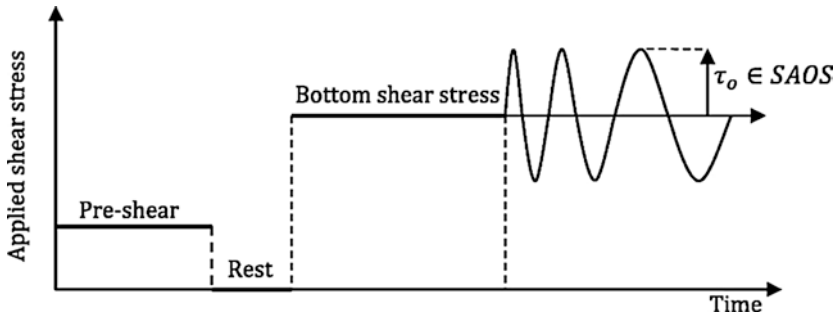

Fig. 2.9 Parallel superposition (steady shear rate and SAOS) protocol [86]. Reprinted by permission from Elsevier

2.3 Extensional Rheometry of STF

Even though most of the real flow conditions are complex—i.e., they consist of a combination of shear, rotation, and extensional flows, and it has become evident that just by shear rheometry, it is not possible to properly model the behavior of complex fluids—the truth is that extensional rheometry is underdeveloped when compared to shear rheometry. The reason is that imposing a surface-free uniaxial extensional flow is challenging, particularly for mobile liquids, such as suspensions or polymeric solutions. Only the Filament Stretching Extensional Rheometer (FiSER™) and the Capillary Breakup Extensional Rheometer (CaBER®) have given proof of merits for rheometric purposes. Both devices are based on the filament stretching approach, but whereas the FiSER™ imposes a constant extension rate, the CaBER® device imposes a step-strain deformation out of the equilibrium and the filament thinning process is performed under capillary forces and at an uncontrolled extension rate. In any case, they are both considered accurate methods for characterizing viscoelastic polymeric solutions, particularly when operated with simultaneous high-speed imaging [5]; nevertheless, in recent years, their use has been extended to other complex fluids such as emulsions [90, 91] or suspensions [25, 92–97]. The extensional properties of STF have also been characterized with success by means of the FiSER™ [25, 49, 98–100] and the CaBER® [25, 101, 102] devices in the recent years.

In both devices, the initial aspect ratio $\left(\Lambda_0 = \frac{h_0}{d_0}\right)$ introduces an important shearcomponent in the flow at the early stages of the experiment. In order to minimize the shear effects, the FiSER™ device can impose two steps in the stretching protocol: in the first step, the liquid bridge is stretched at a small extension rate, well below the onset of extensional thickening and when the aspect ratio is large enough, ide-ally $\frac{1}{\Lambda_0^4} \sim 0$; and in the second step, the desired extension rate ($\dot{\epsilon}$) is imposed [25]. Further investigations about the influence of systematically introducing a controlled pre-deformation history can be found in [103]. The force sensors provide information about the time evolution of the pulling force exerted by the liquid on the

plates, $F(t)$, and then the tensile stress difference generated within the filament canbe calculated: $\tau_{zz}-\tau_{rr}=\frac{4F(t)}{\pi d_{\min}^2(t)}+\frac{1}{2}\frac{\rho g\pi h_0 d_0^{\,2}}{4\pi d_{\min}^2(t)}-\frac{2\sigma}{d_{\min}(t)}$. Thus, the transient extensional viscosity is given by $\eta_E^+(t)=\frac{\tau_{zz}-\tau_{rr}}{\dot{\epsilon}}$. Although CaBER® can provide interesting information about the extensional rheometry of STFs, it possesses three significant drawbacks: (i) it cannot perform the two-step stretching protocol and, therefore, the experimentalist must take that into account for the analysis of the results; (ii) it can only control the initial extension rate until reaching the final separation, upon when then the filament thinning process undergoes an uncontrolled extension rate, which has to be calculated from the time evolution of the minimum diameter as $\dot{\epsilon}=\frac{-2}{d_{\min}(t)}\frac{d\left(d_{\min}(t)\right)}{dt}$; (iii) CaBER® is not originally equipped with a force transducer, thus the extensional viscosity can only be estimated by means of surface tension and the time evolution of the filament radius $\left(\eta_E^+\approx\frac{-\sigma}{d(d_{\min}(t))/dt}\right)$.

Temperature control in the FiSER™ and CaBER® is not as good as in the rotational rheometers, where the bottom plate geometry is typically equipped with a Peltier temperature controller. Thus, if it is intended to work at a different temperature, it is recommended to have the sample in an external bath at the required temperature and quickly load the sample and run the experiments, which are very fast and temperature evolution could be neglected.

2.4 Field-Responsive STF

In magnetorheology [104] and electrorheology [105], an external magnetic and electric field is imposed, respectively, to the fluid sample while the rheological experiment is undergone. For this purpose, commercial rotational rheometers can be equipped with a magnetorheological cell or an electrorheological cell and, in both cases, the external field imposed is steady and perpendicular to the direction of the flow field. The presence of either the electric field or the magnetic field induces a microstructure of particles aligned in the direction of the field, which typically results in an increase of the yield stress. Very recently, M. Terkel and J. de Vicente have developed a new magnetorheological cell able to impose unsteady and triaxial magnetic fields [106, 107]. Consequently, exotic magnetic mesostructures can be generated, resulting in an enrichment of the magnetorheological response. Nevertheless, this degree of freedom in terms of control of the direction and unsteadiness of the electric field has not been reached yet for the electrorheological cells of the rotational rheometers.

Regarding the extensional rheometry, researchers from the Transport Phenomena Research Center [108] have recently developed a series of magnetorheological [92,

Table 2.2 Possible field flow configurations currently available in - and electrorheometry

Field	Configuration	Shear flow	Extensional flow
Magnetic	Parallel	Possible	Possible
	Perpendicular	Possible	Possible
Electric	Parallel	Not possible	Possible
	Perpendicular	Possible	Not possible

94] and electrorheological [94] cells able to impose steady and uniaxial external magnetic fields and electric fields, respectively, to the fluid sample when characterized under extensional flow in the CaBER® device. In the case of extensional magnetorheometry, two add-ons were designed allowing to choose the direction of the magnetic field either parallel or perpendicular to the extensional flow, whereas in the case of extensional electrorheometry, only one add-on was created and the electric field can only be imposed aligned with the direction of the flow. Table 2.2 summarizes the current state of the art in terms of possible configurations to perform magneto- and electrorheological measurements.

Despite the magnetorheological effect being traditionally linked to an increase in viscosity and yield stress under shear flow operating in the perpendicular configuration, it is possible to formulate magnetorheological STF (MRSTF) by dispersing carbonyl iron particles in a carrier fluid exhibiting shear thickening behavior [109–113], allowing to control the shear thickening behavior with the presence of the external magnetic field. Very recently, Bossis et al. [114] reported an outstanding magnetorheological effect based on discontinuous shear thickening. Their MRSTF was formulated by dispersing carbonyl iron particles in water using a superplasticizer molecule, which allowed to reach a volume fraction as high as 62% with a small yield stress and a still low plastic viscosity. The DST behavior is the consequence of particle-particle friction [115]. In their rheological characterization, they used parallel plates with serrated surfaces to avoid slip, and the results showed that by increasing the intensity of the magnetic field, the jamming transition occurred at smaller shear rates. Because the torque range in the rotational rheometer is too low for this kind of samples and because the radial stress developed during the jamming expels the particles from the suspension, they designed a viscometer able to hold ten times larger torques and based on a double helix geometry, which behaves approximately as a cylinder and avoids sedimentation, thanks to the induced small flow along the axis; the outer cylinder had vertical stripes to prevent wall slip.

In the electrorheological effect, the presence of an external electric field also results in an increase in the viscosity and yield stress under shear flow operating in the perpendicular configuration. Nevertheless, the application of an external electric field is also able to affect the shear thickening behavior of certain suspensions. That is the case of the E-FiRST (Electric Field Responsive Shear Thickening), which was first reported by Shenoy et al. [116]; instead of enlarging the shear thickening response of the fluid, in the E-FiRST effect, the presence of an external field allows to suppress the onset of shear thickening and, subsequently, the resistance to flow at high shear rates. In that study, non-serrated plates were used in a strain-controlled

rheometer. Tian and co-workers [117, 118] reported a reversible shear thickening of electrorheological fluids above a low critical shear rate and a high critical electric field strength; their fluid sample consisted of a dispersion of NaY zeolite particles coated with glycerin in silicone oil, which was tested in a two concentric cylinder geometry by means of shear rate ramp tests.

2.5 Non-conventional Rheometry of STF

Apart from the latest works on the application of STF for polishing optical components and vibration control [119, 120], most of the vast research related to STF is dedicated to protective applications [6], such as the development of anti-impacts [121–125], anti-blast [126–128], bullet proof [129, 130], or stab/spike-resistant [131–135] materials.

In these impact protection applications, STF undergoes either low or high velocity impacts, which impose a flow to the liquid that is intrinsically transitory and, therefore, obviously far from the experimental conditions imposed in the rotational rheometer leading to the steady state viscosity/flow curves. Moreover, even if the rheologist wanted to measure the "instantaneous" flow curve in the rheometer, that curve would only be reliable if the time between points would be over 15 ms, because of the instrument and fluid's inertias [14]. In low-velocity impact tests, the characteristic timescale for the composite providing the maximum force in its response is smaller than 5 ms, which will be much shorter in the case of bullet proof, stab/spike-resistant, or anti-blast applications. So, there is no doubt that new experimental approaches are required to provide the determination of the time-resolved viscosity curve of a liquid sample with a time resolution of the order of milliseconds at most.

Sliding plate rheometers [136–138] have proven to be an alternative to rotational rheometers for the characterization of shear thinning fluids under "large, rapid, transient shear deformations", allowing the measurement of normal stresses [139] and reaching high frequencies when reducing the gap size down to the microscale [140–142]. This latter feature, characterizing STF at frequencies in the order of 10 kHz, is of paramount importance because, on the one hand, it enables a fine analysis of the interplay between local scale hydrodynamics and inter-particle forces [143], and that information can help in the development of new formulations of STF; on the other hand, it allows developing fluid models that can be used in practical dampers' design for motion stages [144]. Sliding cylinder rheometers are similar to sliding plate rheometers, but they prevent edge effects and bearing friction issues. The principle of the sliding cylinder rheometer is also similar to the principle of the falling rod viscometer, which is considered a precise method for measuring the absolute viscosity of Newtonian fluids ranging from 10 to 10^7 Pa·s [145, 146]. In these three kinds of rheometers, when the relative gap between the plates or cylinders is very small, there is no need to know the constitutive equation of the fluid to calculate the shear strain and shear rate, as in the rotational rheometer. Although they have proven

to be useful for highly viscous systems, such as polymer melts [147] and others [144, 145], to the best of the authors' knowledge, it has not been reported in the literature their performance when dealing with STF.

Bikerman's penetroviscometer [146] for determining the viscosity of Newtonian fluids under steady state conditions is able to provide viscosity measurements between 10^2 and 10^5 Pa·s with an error below 3.5%. As in the falling rod viscometer, the fluid sample is contained between two coaxial cylinders in which the inner one moves downward and the outer is fixed; however, unlike the falling rod rheometer, the area of contact does not remain constant in the penetroviscometer and the fluid is forced to flow upward through the annular gap between the two cylinders. This kind of flow is currently known as back extrusion flow or annular pumping flow, which is the basis of the back extrusion technique (BET) [148], which is mainly used in food engineering [149–152] to evaluate the rheological properties of the power-law or Herschel-Bulkley fluids in general, but it can also be used for determining the viscoelastic moduli of concentrated polymer solutions by imposing an axially oscillatory movement with a very small amplitude to the inner cylinder [153]. Based on the BET, Hoshino [154–156] has recently developed the Short Back Extrusion (SBE) method, which is able to provide good agreement with the steady viscosity curves measured with a rotational rheometer; however, SBE is not suited for high speed measurements. Fakhari and Galindo-Rosales [14] analyzed the possibility of measuring transient shear viscosity at large, rapid, and transient shear deformation by imposing a back extrusion flow; an analytical expression for the instantaneous viscosity relating the friction force at the inner cylinder wall to its velocity by means of a geometric factor was validated providing an accuracy of ~93% for Newtonian fluids and for the right set of parameters in the experiment within a timescale of the order of ~2 ms; however, it has not been validated yet for STF, neither analytically, numerically, nor experimentally.

The split-Hopkinson pressure bar (SHPB) is typically used for the characterization of dynamic mechanical properties of materials and it has also been used for characterizing STF in transient squeeze flows at high compression rates, which are characteristics of an impact event [157–160]. It consists of a gas gun and three cylindrical bars, i.e., a striker bar, an incident bar, and a transmission bar; during the experiment, the incident wave, the reflection wave, and the transmission wave are recorded by means of strain gauges (Fig. 2.10). Lim et al. [162] discussed in detail the conditions under which classic SHPB data analysis is applicable for Newtonian fluid samples and they found a good agreement between the theory and the experiment obtained for thin specimens (~1 mm) across a wide range of shear strain rates (over 105 s^{-1}). Despite this technique providing useful information for the development of STF to be used under high-velocity impact applications, further work is still required for determining the material properties from the SHPB measurements, as it was done previously for Newtonian fluids [162]. For STF, this would require a robust constitutive model and/or independent measurements of the kinematics in the sample during deformation [157].

Very recently, Madsen et al. [163] developed a non-intrusive technique able to provide instantaneous viscosity up to a timescale on the order of 20 μs. They

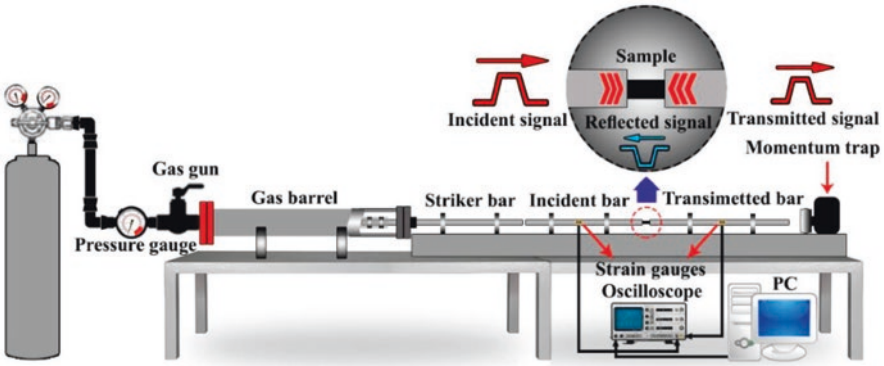

Fig. 2.10 Schematics of the split-Hopkinson pressure bar (SHPB) [161]. Under the Creative Commons license

developed a structured-light detection system that allows particle tracking over femtometer length scales and 16 ns timescales, which allows the determination of the instantaneous velocity of a trapped particle in an optical tweezer. In the ballistic regime, where the measurement is fast compared to the particle's momentum relaxation time, the viscosity can be obtained more directly through its connection to kinetic energy dissipation. Neglecting hydrodynamic memory effects, collisions with molecules in the fluid exponentially damp the velocity of the particle over the momentum relaxation time. This momentum relaxation typically occurs at a much faster rate than the position relaxation, which allows for reducing the integration time required for precise viscosity measurements and, therefore, increases the speed of the measurement. The method was only validated for Newtonian fluids with viscosities ranging from 0.3 to 1.9 mPa•s with temporal resolution between 20 μs and 1 ms; therefore, further research would be required to validate it for STF.

2.6 Future Perspectives

In the last decade, STF has proven to be very popular in protective applications [6]. Most of the published work aims the application of STF in fabric development for body protection technology. The range of STF application is quite extensive. There are several works in the literature regarding sports products (athletic rackets), medical products (surgical gloves or gowns), space technology, electronics and sensing, or even the petrochemical industry [164].

Rheology is a powerful tool that has been only exploited to its most in the characterization of STF when scientists tried to unveil the physics behind this fluid. The use of rheology has been typically limited to providing just their viscosity curves. It is essential to understand that STF will undergo transient and complex flows in real applications, and viscosity curves will fall short in predicting their response. Therefore, a complete rheological characterization can better predict how STF will perform in real flow conditions.

It becomes evident that to better predict the fluid-flow features of STF under real conditions allowing the development of new composites, it is of paramount importance to develop new and more realistic constitutive models for STF that goes beyond the current generalized Newtonian fluid models. These new constitutive models should be able to predict the viscoelastic nature based on the experimental information that a complete rheological characterization is able to provide. This is a challenge for the rheology community in the years to come.

Acknowledgments Authors would like to acknowledge the financial support from FEDER funds through COMPETE2020-Programa Operacional Competitividade e Internacionalização (POCI) and FCT/MCTES LA/P/0045/2020 (ALiCE), UIDB/00532/2020, UIDP/00532/2020 (CEFT), and UI/BD/150887/2021, funded by national funds through FCT/MCTES (PIDDAC) and NORTE-01-0145-FEDER-000054.

References

1. F.A. Morrison, A.P.C.E.F.A. Morrison, *Understanding Rheology* (Oxford University Press, 2001) https://books.google.pt/books?id=bwTn8ZbR0C4C
2. F.J. Galindo-Rosales, Complex fluids and Rheometry in microfluidics, in *Complex Fluid-Flows in Microfluidics*, ed. by F.J. Galindo-Rosales, (Springer International Publishing, Cham, 2018), pp. 1–23
3. R. Ewoldt, M. Johnston, *Caretta L* (How to Avoid Bad Data, Experimental Challenges of Shear Rheology, 2015), pp. 207–241
4. Official symbols and nomenclature of the Society of Rheology. J. Rheol. **57**(4), 1047–1055 (2013). https://doi.org/10.1122/1.4811184
5. F.J. Galindo-Rosales, M.A. Alves, M.S.N. Oliveira, Microdevices for extensional rheometry of low viscosity elastic liquids: A review. Microfluid. Nanofluid. **14**(1), 1–19 (2013). https://doi.org/10.1007/s10404-012-1028-1
6. S. Gürgen, M.C. Kuşhan, W. Li, Shear thickening fluids in protective applications: A review. Prog. Polym. Sci. **75**, 48–72 (2017) https://www.sciencedirect.com/science/article/pii/S0079670017300035
7. E. Brown, H.M. Jaeger, Shear thickening in concentrated suspensions: Phenomenology, mechanisms and relations to jamming. Rep. Prog. Phys. **77**(4), 046602 (2014). https://doi.org/10.1088/0034-4885/77/4/046602
8. F.J. Galindo-Rosales, F.J. Rubio-Hernández, A. Sevilla, An apparent viscosity function for shear thickening fluids. J. Non-Newtonian Fluid Mech. **166**(5), 321–325 (2011) https://www.sciencedirect.com/science/article/pii/S0377025711000024
9. E. Brown, H.M. Jaeger, Through thick and thin. Science **333**(6047), 1230–1231 (2011). https://doi.org/10.1126/science.1211155
10. H.A. Barnes, Shear-thickening ("Dilatancy") in suspensions of nonaggregating solid particles dispersed in Newtonian liquids. J. Rheol. **33**(2), 329–366 (1989). https://doi.org/10.1122/1.550017
11. N.J. Wagner, J.F. Brady, Shear thickening in colloidal dispersions. Phys. Today **62**(10), 27–32 (2009) https://www.scopus.com/inward/record.uri?eid=2-s2.0-70349779635&doi=10.1063%2f1.3248476&partnerID=40&md5=96a696a15746a2d14f974ec019d87f7c
12. T.G. Mezger, C. Sprinz, A. Green, *Applied Rheology: With Joe Flow on Rheology Road* (Anton Paar, 2018) https://books.google.pt/books?id=xmgBjwEACAAJ
13. F.J. Galindo-Rosales, Complex fluids in energy dissipating systems. Appl. Sci. **6**(8), 206 (2016)

14. A. Fakhari, F.J. Galindo-Rosales, Parametric analysis of the transient back extrusion flow to determine instantaneous viscosity. Phys. Fluids **33**(3), 033602 (2021). https://doi.org/10.1063/5.0033560
15. J. Mewis, N.J. Wagner, *Colloidal Suspension Rheology* (Cambridge University Press, Cambridge, 2011) https://www.cambridge.org/core/books/colloidal-suspension-rheology/E4C1D16944B043534881158BC62D3E59
16. G. Bossis, Y. Grasselli, O. Volkova, Capillary flow of a suspension in the presence of discontinuous shear thickening. Rheol. Acta **61**(1), 1–12 (2022). https://doi.org/10.1007/s00397-021-01305-0
17. A. Fall, A. Lemaître, F. Bertrand, D. Bonn, G. Ovarlez, Shear thickening and migration in granular suspensions. Phys. Rev. Lett. **105**(26), 268303 (2010). https://doi.org/10.1103/PhysRevLett.105.268303
18. F. Galindo-Rosales, F. Rubio-Hernández, J. Velázquez-Navarro, Shear-thickening behavior of Aerosil® R816 nanoparticles suspensions in polar organic liquids. Rheol. Acta **48**, 699–708 (2009). https://doi.org/10.1007/s00397-009-0367-7
19. Y. Madraki, S. Hormozi, G. Ovarlez, É. Guazzelli, O. Pouliquen, Enhancing shear thickening. Phys. Rev. Fluids **2**(3), 033301 (2017). https://doi.org/10.1103/PhysRevFluids.2.033301
20. A. Fall, N. Huang, F. Bertrand, G. Ovarlez, D. Bonn, Shear thickening of Cornstarch suspensions as a Reentrant jamming transition. Phys. Rev. Lett. **100**(1), 018301 (2008). https://doi.org/10.1103/PhysRevLett.100.018301
21. J.M. Dealy, J. Wang, Viscosity and normal stress differences, in *Melt Rheology and its Applications in the Plastics Industry*, ed. by J.M. Dealy, J. Wang, (Springer Netherlands, Dordrecht, 2013), pp. 19–47
22. C.D. Cwalina, N.J. Wagner, Material properties of the shear-thickened state in concentrated near hard-sphere colloidal dispersions. J. Rheol. **58**(4), 949–967 (2014). https://doi.org/10.1122/1.4876935
23. C.W. Macosko, *Rheology: Principles, Measurements, and Applications* (VCH, New York, NY, 1994)
24. H.M. Laun, Normal stresses in extremely shear thickening polymer dispersions. J. Non-Newtonian Fluid Mech. **54**, 87–108 (1994) https://www.sciencedirect.com/science/article/pii/0377025794800162
25. R.J.E. Andrade, A.R. Jacob, F.J. Galindo-Rosales, L. Campo-Deaño, Q. Huang, O. Hassager, et al., Dilatancy in dense suspensions of model hard-sphere-like colloids under shear and extensional flow. J. Rheol. **64**(5), 1179–1196 (2020). https://doi.org/10.1122/1.5143653
26. Z. Pan, H. de Cagny, M. Habibi, D. Bonn, Normal stresses in shear thickening granular suspensions. Soft Matter **13**(20), 3734–3740 (2017). https://doi.org/10.1039/C7SM00167C
27. O. Maklad, R.J. Poole, A review of the second normal-stress difference; its importance in various flows, measurement techniques, results for various complex fluids and theoretical predictions. J. Non-Newtonian Fluid Mech. **292**, 104522 (2021) https://www.sciencedirect.com/science/article/pii/S0377025721000458
28. J.F. Morris, Shear thickening of concentrated suspensions: Recent developments and relation to other phenomena. Annu. Rev. Fluid Mech. **52**(1), 121–144 (2020). https://doi.org/10.1146/annurev-fluid-010816-060128
29. E. Brown, H.M. Jaeger, The role of dilation and confining stresses in shear thickening of dense suspensions. J. Rheol. **56**(4), 875–923 (2012). https://doi.org/10.1122/1.4709423
30. S. Garland, G. Gauthier, J. Martin, J.F. Morris, Normal stress measurements in sheared non-Brownian suspensions. J. Rheol. **57**(1), 71–88 (2012). https://doi.org/10.1122/1.4758001
31. W. Wu, K. Zeng, B. Zhao, F. Duan, F. Jiang, New considerations on the determination of the apparent shear viscosity of polymer melt with micro capillary dies. Polymers **13**(24), 4451 (2021). https://doi.org/10.3390/polym13244451
32. P.J. Carreau, D.C.R. De Kee, R.P. Chhabra, 3- Rheometry, in *Rheology of Polymeric Systems*, ed. by P.J. Carreau, D.C.R. De Kee, R.P. Chhabra, 2nd edn., (Hanser, 2021), pp. 69–130

33. C.J. Pipe, T.S. Majmudar, G.H. McKinley, High shear rate viscometry. Rheol. Acta **47**(5), 621–642 (2008). https://doi.org/10.1007/s00397-008-0268-1
34. G. Bossis, O. Volkova, Y. Grasselli, O. Gueye, Discontinuous shear thickening in concentrated suspensions. Philos. Trans. R. Soc. A Math. Phys. Eng. Sci. **377**(2143), 20180211 (2019). https://doi.org/10.1098/rsta.2018.0211
35. M. Wyart, M.E. Cates, Discontinuous shear thickening without inertia in dense non-Brownian suspensions. Phys. Rev. Lett. **112**(9), 098302 (2014). https://doi.org/10.1103/PhysRevLett.112.098302
36. G. Bossis, Y. Grasselli, A. Ciffreo, O. Volkova, Tunable discontinuous shear thickening in capillary flow of MR suspensions. J. Intell. Mater. Syst. Struct. **32**(12), 1349–1357 (2020). https://doi.org/10.1177/1045389X20959458
37. S.R. Waitukaitis, H.M. Jaeger, Impact-activated solidification of dense suspensions via dynamic jamming fronts. Nature **487**(7406), 205–209 (2012). https://doi.org/10.1038/nature11187
38. I.R. Peters, H.M. Jaeger, Quasi-2D dynamic jamming in cornstarch suspensions: Visualization and force measurements. Soft Matter **10**(34), 6564–6570 (2014). https://doi.org/10.1039/C4SM00864B
39. R. Maharjan, S. Mukhopadhyay, B. Allen, T. Storz, E. Brown, Constitutive relation for the system-spanning dynamically jammed region in response to impact of cornstarch and water suspensions. Phys. Rev. E **97**(5), 052602 (2018). https://doi.org/10.1103/PhysRevE.97.052602
40. S. Gürgen, M.A. Sofuoğlu, M.C. Kuşhan, Rheological compatibility of multi-phase shear thickening fluid with a phenomenological model. Smart Mater. Struct. **28**(3), 035027 (2019). https://doi.org/10.1088/1361-665X/ab018c
41. M. Wei, L. Sun, P. Qi, C. Chang, C. Zhu, Continuous phenomenological modeling for the viscosity of shear thickening fluids. Nanomater. Nanotechnol. **8**, 1847980418786551 (2018). https://doi.org/10.1177/1847980418786551
42. A. Ghosh, I. Chauhan, A. Majumdar, B.S. Butola, Influence of cellulose nanofibers on the rheological behavior of silica-based shear-thickening fluid. Cellulose **24**(10), 4163–4171 (2017). https://doi.org/10.1007/s10570-017-1440-5
43. M. Wei, K. Lin, L. Sun, Shear thickening fluids and their applications. Mater. Des. **216**, 110570 (2022) https://www.sciencedirect.com/science/article/pii/S0264127522001915
44. K. Lin, J. Qi, H. Liu, M. Wei, H. Peng, A phenomenological theory-based viscosity model for shear thickening fluids. Mater. Res. Express. **9**, 015701 (2022)
45. J. David, P. Filip, A.A. Kharlamov, Empirical modelling of nonmonotonous behaviour of shear viscosity. Adv. Mater. Sci. Eng. **2013**, 658187 (2013). https://doi.org/10.1155/2013/658187
46. M. Wei, K. Lin, Q. Guo, H. Sun, Characterization and performance analysis of a shear thickening fluid damper. Meas. Control **52**, 002029401881954 (2019)
47. F.J. Galindo-Rosales, F.J. Rubio-Hernández, A. Sevilla, R.H. Ewoldt, How Dr. Malcom M. cross may have tackled the development of "an apparent viscosity function for shear thickening fluids". J. Non-Newtonian Fluid Mech. **166**(23), 1421–1424 (2011) https://www.sciencedirect.com/science/article/pii/S0377025711002011
48. T. Shende, V.J. Niasar, M. Babaei, An empirical equation for shear viscosity of shear thickening fluids. J. Mol. Liq. **325**, 115220 (2021) https://www.sciencedirect.com/science/article/pii/S0167732220374626
49. S. Khandavalli, J.A. Lee, M. Pasquali, J.P. Rothstein, The effect of shear-thickening on liquid transfer from an idealized gravure cell. J. Non-Newtonian Fluid Mech. **221**, 55–65 (2015) https://www.sciencedirect.com/science/article/pii/S0377025715000592
50. R. Maharjan, E. Brown, Giant deviation of a relaxation time from generalized Newtonian theory in discontinuous shear thickening suspensions. Phys. Rev. Fluids. **2**(12), 123301 (2017). https://doi.org/10.1103/PhysRevFluids.2.123301
51. F.J. Rubio-Hernández, J.H. Sánchez-Toro, N.M. Páez-Flor, Testing shear thinning/thixotropy and shear thickening/antithixotropy relationships in a fumed silica suspension. J. Rheol. **64**(4), 785–797 (2020). https://doi.org/10.1122/1.5131852

52. V. Rathee, D.L. Blair, J.S. Urbach, Localized stress fluctuations drive shear thickening in dense suspensions. Proc. Natl. Acad. Sci. **114**(33), 8740–8745 (2017). https://doi.org/10.1073/pnas.1703871114
53. M. Tassieri, J. Ramírez, N.C. Karayiannis, S.K. Sukumaran, Y. Masubuchi, I-Rheo GT: Transforming from time to frequency domain without artifacts. Macromolecules **51**(14), 5055–5068 (2018). https://doi.org/10.1021/acs.macromol.8b00447
54. R. Rivas-Barbosa, M.A. Escobedo-Sánchez, M. Tassieri, M. Laurati, I-Rheo: Determining the linear viscoelastic moduli of colloidal dispersions from step-stress measurements. Phys. Chem. Chem. Phys. **22**(7), 3839–3848 (2020). https://doi.org/10.1039/C9CP06191F
55. F. Juliusburger, A. Pirquet, Thixotropy and rheopexy of V2O5-sols. Trans. Faraday Soc. **32**, 445–452 (1936). https://doi.org/10.1039/TF9363200445
56. J. Mewis, Thixotropy - a general review. J. Non-Newtonian Fluid Mech. **6**(1), 1–20 (1979) https://www.sciencedirect.com/science/article/pii/0377025779870019
57. J. Lyklema, H. Van Olphen, Terminology and symbols in colloid and surface chemistry part 1.13. Definitions, terminology and symbols for rheological properties. Pure Appl. Chem. **51**(5), 1213–1218 (1979). https://doi.org/10.1351/pac197951051213
58. R.G. Larson, Y. Wei, A review of thixotropy and its rheological modeling. J. Rheol. **63**(3), 477–501 (2019). https://doi.org/10.1122/1.5055031
59. J.H. Cho, A.H. Griese, I.R. Peters, I. Bischofberger, Lasting effects of discontinuous shear thickening in cornstarch suspensions upon flow cessation. Phys. Rev. Fluids. **7**(6), 063302 (2022). https://doi.org/10.1103/PhysRevFluids.7.063302
60. Z. Pan, H. de Cagny, B. Weber, D. Bonn, S-shaped flow curves of shear thickening suspensions: Direct observation of frictional rheology. Phys. Rev. E **92**(3), 032202 (2015). https://doi.org/10.1103/PhysRevE.92.032202
61. R.P. Chhabra, J.F. Richardson, Chapter 1 - Non-Newtonian fluid behaviour, in *Non-Newtonian Flow in the Process Industries*, ed. by R.P. Chhabra, J.F. Richardson, (Butterworth-Heinemann, Oxford, 1999), pp. 1–36
62. F.J. Galindo-Rosales, F.J. Rubio-Hernández, Transient study on the shear thickening behaviour of surface modified Fumed silica suspensions in polypropylene glycol. AIP Conf. Proc. **1027**(1), 686–688 (2008). https://doi.org/10.1063/1.2964809
63. Y. Wei, M.J. Solomon, R.G. Larson, A multimode structural kinetics constitutive equation for the transient rheology of thixotropic elasto-viscoplastic fluids. J. Rheol. **62**(1), 321–342 (2017). https://doi.org/10.1122/1.4996752
64. X. Cheng, H. McCoy Jonathan, N. Israelachvili Jacob, I. Cohen, Imaging the microscopic structure of shear thinning and thickening colloidal suspensions. Science **333**(6047), 1276–1279 (2011). https://doi.org/10.1126/science.1207032
65. V. Rathee, D.L. Blair, J.S. Urbach, Dynamics and memory of boundary stresses in discontinuous shear thickening suspensions during oscillatory shear. Soft Matter **17**(5), 1337–1345 (2021). https://doi.org/10.1039/D0SM01917H
66. G. Ovarlez, A. Vu Nguyen Le, W.J. Smit, A. Fall, R. Mari, G. Chatté, et al., Density waves in shear-thickening suspensions. Sci. Adv. **6**(16), eaay 5589 (2020). https://doi.org/10.1126/sciadv.aay5589
67. A. Gauthier, M. Pruvost, O. Gamache, A. Colin, A new pressure sensor array for normal stress measurement in complex fluids. J. Rheol. **65**(4), 583–594 (2021). https://doi.org/10.1122/8.0000249
68. B. Saint-Michel, T. Gibaud, S. Manneville, Uncovering instabilities in the spatiotemporal dynamics of a shear-thickening Cornstarch suspension. Phys. Rev. X **8**(3), 031006 (2018). https://doi.org/10.1103/PhysRevX.8.031006
69. J. Mewis, G. Biebaut, Shear thickening in steady and superposition flows effect of particle interaction forces. J. Rheol. **45**(3), 799–813 (2001). https://doi.org/10.1122/1.1359761
70. H. Ramli, N.F.A. Zainal, M. Hess, C.H. Chan, Basic principle and good practices of rheology for polymers for teachers and beginners. Chemistry Teacher International **4**(4), 307–326 (2022). https://doi.org/10.1515/cti-2022-0010

71. K. Hyun, S.H. Kim, K.H. Ahn, S.J. Lee, Large amplitude oscillatory shear as a way to classify the complex fluids. J. Nonnewton Fluid Mech **107**, 51–65 (2002). https://doi.org/10.1016/S0377-0257(02)00141-6
72. H.M. Laun, R. Bung, F. Schmidt, Rheology of extremely shear thickening polymer dispersions (passively viscosity switching fluids). J. Rheol. **35**(6), 999–1034 (1991) https://www.scopus.com/inward/record.uri?eid=2-s2.0-76149128078&doi=10.1122%2f1.550257&partnerID=40&md5=0debbc1882216f1a2b2f19ea4ffbc7bc
73. W.H. Boersma, J. Laven, H.N. Stein, Viscoelastic properties of concentrated shear-thickening dispersions. J. Colloid Interface Sci. **149**(1), 10–22 (1992) https://www.sciencedirect.com/science/article/pii/002197979290385Y
74. S.R. Raghavan, S.A. Khan, Shear-thickening response of Fumed silica suspensions under steady and oscillatory shear. J. Colloid Interface Sci. **185**(1), 57–67 (1997) https://www.sciencedirect.com/science/article/pii/S0021979796945816
75. F. Yziquel, P.J. Carreau, P.A. Tanguy, Non-linear viscoelastic behavior of fumed silica suspensions. Rheol. Acta **38**(1), 14–25 (1999). https://doi.org/10.1007/s003970050152
76. Y.S. Lee, N.J. Wagner, Dynamic properties of shear thickening colloidal suspensions. Rheol. Acta **42**(3), 199–208 (2003). https://doi.org/10.1007/s00397-002-0290-7
77. C. Fischer, C.J.G. Plummer, V. Michaud, P.-E. Bourban, J.-A.E. Månson, Pre- and post-transition behavior of shear-thickening fluids in oscillating shear. Rheol. Acta **46**(8), 1099–1108 (2007). https://doi.org/10.1007/s00397-007-0202-y
78. L. Chang, K. Friedrich, A.K. Schlarb, R. Tanner, L. Ye, Shear-thickening behaviour of concentrated polymer dispersions under steady and oscillatory shear. J. Mater. Sci. **46**(2), 339–346 (2011). https://doi.org/10.1007/s10853-010-4817-5
79. S. Khandavalli, J.P. Rothstein, Large amplitude oscillatory shear rheology of three different shear-thickening particle dispersions. Rheol. Acta **54**(7), 601–618 (2015). https://doi.org/10.1007/s00397-015-0855-x
80. J. Lee, Z. Jiang, J. Wang, A.R. Sandy, S. Narayanan, X.-M. Lin, Unraveling the role of order-to-disorder transition in shear thickening suspensions. Phys. Rev. Lett. **120**(2), 028002 (2018). https://doi.org/10.1103/PhysRevLett.120.028002
81. D. Doraiswamy, A.N. Mujumdar, I. Tsao, A.N. Beris, S.C. Danforth, A.B. Metzner, The Cox–Merz rule extended: A rheological model for concentrated suspensions and other materials with a yield stress. J. Rheol. **35**(4), 647–685 (1991). https://doi.org/10.1122/1.550184
82. Q. Zhao, Y. He, H. Yao, B. Wen, Dynamic performance and mechanical model analysis of a shear thickening fluid damper. Smart Mater. Struct. **27**(7), 075021 (2018). https://doi.org/10.1088/1361-665X/aac23f
83. X.Z. Zhang, W.H. Li, X.L. Gong, The rheology of shear thickening fluid (STF) and the dynamic performance of an STF-filled damper. Smart Mater. Struct. **17**(3), 035027 (2008). https://doi.org/10.1088/0964-1726/17/3/035027
84. K. Lin, A. Zhou, H. Liu, Y. Liu, C. Huang, Shear thickening fluid damper and its application to vibration mitigation of stay cable. Structure **26**, 214–223 (2020) https://www.sciencedirect.com/science/article/pii/S2352012420301727
85. Q. Zhao, J. Yuan, H. Jiang, H. Yao, B. Wen, Vibration control of a rotor system by shear thickening fluid dampers. J. Sound Vib. **494**, 115883 (2021) https://www.sciencedirect.com/science/article/pii/S0022460X20307203
86. F.J. Rubio-Hernández, Testing a shear-thickening fumed silica suspension with parallel superposition rheology. J. Mol. Liq. **365**, 120179 (2022) https://www.sciencedirect.com/science/article/pii/S0167732222017184
87. P. Moldenaers, J. Mewis, On the nature of viscoelasticity in polymeric liquid crystals. J. Rheol. **37**(2), 367–380 (1993). https://doi.org/10.1122/1.550448
88. BA de L Costello. Parallel superposition rheology of an associatively thickened latex. TA Instruments applications note RH-060
89. Tianhong Chen. Parallel Superposition Studies on Paint Using An ARES-G2 Rheometer. TA Instruments applications note RH093

90. K. Niedzwiedz, H. Buggisch, N. Willenbacher, Extensional rheology of concentrated emulsions as probed by capillary breakup elongational rheometry (CaBER). Rheol. Acta **49**(11), 1103–1116 (2010). https://doi.org/10.1007/s00397-010-0477-2
91. L. Martinie, H. Buggisch, N. Willenbacher, Apparent elongational yield stress of soft matter. J. Rheol. **57**(2), 627–646 (2013). https://doi.org/10.1122/1.4789785
92. F.J. Galindo-Rosales, J.P. Segovia-Gutiérrez, F.T. Pinho, M.A. Alves, J. de Vicente, Extensional rheometry of magnetic dispersions. J. Rheol. **59**(1), 193–209 (2014). https://doi.org/10.1122/1.4902356
93. S.H. Sadek, H.H. Najafabadi, F.J. Galindo-Rosales, Capillary breakup extensional magnetorheometry. J. Rheol. **64**(1), 55–65 (2019). https://doi.org/10.1122/1.5115460
94. S.H. Sadek, H.H. Najafabadi, F.J. Galindo-Rosales, Capillary breakup extensional electrorheometry (CaBEER). J. Rheol. **64**(1), 43–54 (2019). https://doi.org/10.1122/1.5116718
95. J.H. García-Ortiz, F.J. Galindo-Rosales, Extensional Magnetorheology as a tool for optimizing the formulation of ferrofluids in oil-spill clean-up processes. PRO **8**(5) (2020)
96. J.M. Nunes, F.J. Galindo-Rosales, L. Campo-Deaño, Extensional Magnetorheology of viscoelastic human blood analogues loaded with magnetic particles. Materials **14**(22), 6930 (2021)
97. H.C.H. Ng, A. Corker, E. García-Tuñón, R.J. Poole, GO CaBER: Capillary breakup and steady-shear experiments on aqueous graphene oxide (GO) suspensions. J. Rheol. **64**(1), 81–93 (2019). https://doi.org/10.1122/1.5109016
98. E. White, M. Chellamuthu, J. Rothstein, Extensional rheology of a shear-thickening cornstarch and water suspension. Rheol. Acta **49**, 119–129 (2009)
99. M. Chellamuthu, E. Arndt, J. Rothstein, Extensional rheology of shear-thickening nanoparticle suspensions. Soft Matter **5**, 2117–2124 (2009)
100. M.I. Smith, R. Besseling, M.E. Cates, V. Bertola, Dilatancy in the flow and fracture of stretched colloidal suspensions. Nat. Commun. **1**(1), 114 (2010). https://doi.org/10.1038/ncomms1119
101. S. Khandavalli, J.P. Rothstein, Extensional rheology of shear-thickening fumed silica nanoparticles dispersed in an aqueous polyethylene oxide solution. J. Rheol. **58**(2), 411–431 (2014). https://doi.org/10.1122/1.4864620
102. M. Roché, H. Kellay, H.A. Stone, Heterogeneity and the role of normal stresses during the extensional thinning of non-Brownian shear-thickening fluids. Phys. Rev. Lett. **107**(13), 134503 (2011). https://doi.org/10.1103/PhysRevLett.107.134503
103. S.L. Anna, G.H. McKinley, Effect of a controlled pre-deformation history on extensional viscosity of dilute polymer solutions. Rheol. Acta **47**(8), 841–859 (2008). https://doi.org/10.1007/s00397-007-0253-0
104. J.R. Morillas, J. de Vicente, Magnetorheology: A review. Soft Matter **16**(42), 9614–9642 (2020). https://doi.org/10.1039/D0SM01082K
105. P. Sheng, W. Wen, Electrorheological fluids: Mechanisms, dynamics, and microfluidics applications. Annu. Rev. Fluid Mech. **44**(1), 143–174 (2011). https://doi.org/10.1146/annurev-fluid-120710-101024
106. M. Terkel, J. de Vicente, Magnetorheology of exotic magnetic mesostructures generated under triaxial unsteady magnetic fields. Smart Mater. Struct. **30**(1), 014005 (2020). https://doi.org/10.1088/1361-665X/abcca3
107. M. Terkel, J. Tajuelo, J. de Vicente, Enhancing magnetorheology with precession magnetic fields. J. Rheol. **66**(1), 67–78 (2021). https://doi.org/10.1122/8.0000356
108. Transport Phenomena Research Center. Smart Fluids: CEFT; Available from https://ceft.fe.up.pt/fluids/smart-fluids/
109. X. Zhang, W. Li, X.L. Gong, Study on magnetorheological shear thickening fluid. Smart Mater. Struct. **17**(1), 015051 (2008). https://doi.org/10.1088/0964-1726/17/1/015051
110. C. Qian, Y. Tian, Z. Fan, Z. Sun, Z. Ma, Investigation on rheological characteristics of magnetorheological shear thickening fluids mixed with micro CBN abrasive particles. Smart Mater. Struct. **31**(9), 095004 (2022). https://doi.org/10.1088/1361-665X/ac7bbd

111. Y. Ming, X.M. Huang, D.D. Zhou, Q. Zeng, H.Y. Li, Rheological properties of magnetic field-assisted thickening fluid and high-efficiency spherical polishing of ZrO2 ceramics. Int. J. Adv. Manuf. Technol. **121**(1), 1049–1061 (2022). https://doi.org/10.1007/s00170-022-09344-4
112. J. Yang, S. Sun, W. Li, H. Du, G. Alici, M. Nakano, Development of a linear damper working with magnetorheological shear thickening fluids. J. Intell. Mater. Syst. Struct. **26**(14), 1811–1817 (2015). https://doi.org/10.1177/1045389X15577653
113. A. Rendos, S. Woodman, K. McDonald, T. Ranzani, K.A. Brown, Shear thickening prevents slip in magnetorheological fluids. Smart Mater. Struct. **29**(7), 07LT2 (2020). https://doi.org/10.1088/1361-665X/ab8b2e
114. G. Bossis, Y. Grasselli, A. Meunier, O. Volkova, Outstanding magnetorheological effect based on discontinuous shear thickening in the presence of a superplastifier molecule. Appl. Phys. Lett. **109**(11), 111902 (2016). https://doi.org/10.1063/1.4962467
115. F. Vereda, J.P. Segovia-Gutiérrez, J. de Vicente, R. Hidalgo-Alvarez, Faceted particles: An approach for the enhancement of the elasticity and the yield-stress of magnetorheological fluids. Appl. Phys. Lett. **108**(21), 211904 (2016). https://doi.org/10.1063/1.4952394
116. S.S. Shenoy, N.J. Wagner, J.W. Bender, E-FiRST: Electric field responsive shear thickening fluids. Rheol. Acta **42**(4), 287–294 (2003). https://doi.org/10.1007/s00397-002-0289-0
117. Y. Tian, M. Zhang, J. Jiang, N. Pesika, H. Zeng, J. Israelachvili, et al., Reversible shear thickening at low shear rates of electrorheological fluids under electric fields. Phys. Rev. E **83**(1), 011401 (2011). https://doi.org/10.1103/PhysRevE.83.011401
118. J. Jiang, Y. Liu, L. Shan, X. Zhang, Y. Meng, H.J. Choi, et al., Shear thinning and shear thickening characteristics in electrorheological fluids. Smart Mater. Struct. **23**(1), 015003 (2013). https://doi.org/10.1088/0964-1726/23/1/015003
119. S. Gürgen, M.A. Sofuoğlu, Vibration attenuation of sandwich structures filled with shear thickening fluids. Compos. Part B **186**, 107831 (2020) https://www.sciencedirect.com/science/article/pii/S1359836819355131
120. S. Gürgen, M.A. Sofuoğlu, Experimental investigation on vibration characteristics of shear thickening fluid filled CFRP tubes. Compos. Struct. **226**, 111236 (2019) https://www.sciencedirect.com/science/article/pii/S0263822319316988
121. L. Sun, M. Wei, J. Zhu, Low velocity impact performance of fiber-reinforced polymer impregnated with shear thickening fluid. Polym. Test. **96**, 107095 (2021) https://www.sciencedirect.com/science/article/pii/S0142941821000453
122. H. Taş, I.F. Soykok, Investigation of the low velocity impact behaviour of shear thickening fluid impregnated Kevlar, hybrid (Kevlar/carbon) and carbon fabrics. Fibers Polym. **22**(9), 2626–2634 (2021). https://doi.org/10.1007/s12221-021-1358-2
123. F. Pinto, M. Meo, Design and manufacturing of a novel shear thickening fluid composite (STFC) with enhanced out-of-plane properties and damage suppression. Appl. Compos. Mater. **24**(3), 643–660 (2017). https://doi.org/10.1007/s10443-016-9532-1
124. E. Selver, Impact and damage tolerance of shear thickening fluids-impregnated carbon and glass fabric composites. J. Reinf. Plast. Compos. **38**(14), 669–688 (2019). https://doi.org/10.1177/0731684419842648
125. F. Galindo-Rosales, S. Martínez-Aranda, L. Campo-Deaño, Cork STFμfluidics – A novel concept for the development of eco-friendly light-weight energy absorbing composites. Mater. Des. **82** (2015)
126. A. Haris, H.P. Lee, V.B.C. Tan, An experimental study on shock wave mitigation capability of polyurea and shear thickening fluid based suspension pads. Def. Technol. **14**(1), 12–18 (2018) https://www.sciencedirect.com/science/article/pii/S2214914717301150
127. M.A. Dawson, Composite plates with a layer of fluid-filled, reticulated foam for blast protection of infrastructure. Int. J. Impact Eng. **36**(10), 1288–1295 (2009) https://www.sciencedirect.com/science/article/pii/S0734743X09000621
128. M.A. Dawson, G.H. McKinley, L.J. Gibson, The dynamic compressive response of open-cell foam impregnated with a Newtonian fluid. J. Appl. Mech. **75**(4), 041015 (2008). https://doi.org/10.1115/1.2912940

129. S. Gürgen, M.C. Kuşhan, The ballistic performance of aramid based fabrics impregnated with multi-phase shear thickening fluids. Polym. Test. **64**, 296–306 (2017) https://www.sciencedirect.com/science/article/pii/S0142941817313478
130. A.F. Ávila, A.M. de Oliveira, S.G. Leão, M.G. Martins, Aramid fabric/nano-size dual phase shear thickening fluid composites response to ballistic impact. Compos. A: Appl. Sci. Manuf. **112**, 468–474 (2018) https://www.sciencedirect.com/science/article/pii/S1359835X18302689
131. M. Hasanzadeh, V. Mottaghitalab, The role of shear-thickening fluids (STFs) in ballistic and stab-resistance improvement of flexible Armor. J. Mater. Eng. Perform. **23**(4), 1182–1196 (2014). https://doi.org/10.1007/s11665-014-0870-6
132. K. Yu, H. Cao, K. Qian, L. Jiang, *Li HJF* (Europe TiE, Synthesis and Stab Resistance of Shear Thickening Fluid (STF) Impregnated Glass Fabric Composites, 2012)
133. M.J. Decker, C.J. Halbach, C.H. Nam, N.J. Wagner, E.D. Wetzel, Stab resistance of shear thickening fluid (STF)-treated fabrics. Compos. Sci. Technol. **67**(3), 565–578 (2007) https://www.sciencedirect.com/science/article/pii/S0266353806002983
134. S. Gürgen, T. Yıldız, Stab resistance of smart polymer coated textiles reinforced with particle additives. Compos. Struct. **235**, 111812 (2020) https://www.sciencedirect.com/science/article/pii/S0263822319337614
135. S. Gürgen, M.C. Kuşhan, The stab resistance of fabrics impregnated with shear thickening fluids including various particle size of additives. Compos. A: Appl. Sci. Manuf. **94**, 50–60 (2017) https://www.sciencedirect.com/science/article/pii/S1359835X1630447X
136. J.M. Dealy, A.J. Giacomin, Sliding plate and sliding cylinder rheometers, in *Rheological Measurement*, ed. by A.A. Collyer, D.W. Clegg, (Springer Netherlands, Dordrecht, 1998), pp. 237–259
137. A.J. Giacomin, T. Samurkas, J.M. Dealy, A novel sliding plate rheometer for molten plastics. Polym. Eng. Sci. **29**(8), 499–504 (1989). https://doi.org/10.1002/pen.760290803
138. K.C. Ortman, N. Agarwal, A.P.R. Eberle, D.G. Baird, P. Wapperom, G.A. Jeffrey, Transient shear flow behavior of concentrated long glass fiber suspensions in a sliding plate rheometer. J. Non-Newtonian Fluid Mech. **166**(16), 884–895 (2011) https://www.sciencedirect.com/science/article/pii/S0377025711000930
139. J. Xu, S. Costeux, J.M. Dealy, M.N. De Decker, Use of a sliding plate rheometer to measure the first normal stress difference at high shear rates. Rheol. Acta **46**(6), 815–824 (2007). https://doi.org/10.1007/s00397-006-0156-5
140. C. Clasen, G.H. McKinley, Gap-dependent microrheometry of complex liquids. J. Non-Newtonian Fluid Mech. **124**(1), 1–10 (2004) https://www.sciencedirect.com/science/article/pii/S0377025704002381
141. D. Moon, A.J. Bur, K.B. Migler, Multi-sample micro-slit rheometry. J. Rheol. **52**(5), 1131–1142 (2008). https://doi.org/10.1122/1.2955511
142. T. Athanasiou, G.K. Auernhammer, D. Vlassopoulos, G. Petekidis, A high-frequency piezoelectric rheometer with validation of the loss angle measuring loop: Application to polymer melts and colloidal glasses. Rheol. Acta **58**(9), 619–637 (2019). https://doi.org/10.1007/s00397-019-01163-x
143. B. Schroyen, D. Vlassopoulos, P. Van Puyvelde, J. Vermant, Bulk rheometry at high frequencies: A review of experimental approaches. Rheol. Acta **59**(1), 1–22 (2020). https://doi.org/10.1007/s00397-019-01172-w
144. C.A.M. Verbaan, G.W.M. Peters, M. Steinbuch, Linear viscoelastic fluid characterization of ultra-high-viscosity fluids for high-frequency damper design. Rheol. Acta **54**(8), 667–677 (2015). https://doi.org/10.1007/s00397-015-0862-y
145. R.A. Secco, M. Kostic, J.R. de Bruyn, Fluid viscosity measurement, in *Measurement IaSH*, ed. by J.G. Webster, H. Eren, (Imprint CRC Press, 2014) p. 46-1: 31
146. J.J. Bikerman, A penetroviscometer for very viscous liquids. J. Colloid Sci. **3**(2), 75–85 (1948) https://www.sciencedirect.com/science/article/pii/0095852248900592

147. F. Koran, J.M. Dealy, A high pressure sliding plate rheometer for polymer melts. J. Rheol. **43**(5), 1279–1290 (1999). https://doi.org/10.1122/1.551046
148. A. Perrot, D. Rangeard, Y. Mélinge, Prediction of the Ram extrusion force of cement-based materials. Appl. Rheol. **24**(5), 34–40 (2014). https://doi.org/10.3933/applrheol-24-53320
149. K.D. Dolan, J.F. Steffe, R.G. Morgan, Back extrusion and simulation of viscosity development during starch gelatinization. J. Food Process Eng. **11**(2), 79–101 (1989). https://doi.org/10.1111/j.1745-4530.1989.tb00023.x
150. G.H. Brusewitz, H. Yu, Back extrusion method for determining properties of mustard slurry. J. Food Eng. **27**(3), 259–265 (1996) https://www.sciencedirect.com/science/article/pii/0260877495000089
151. K. Autio, T. Kuuva, K. Roininen, L. Lähteenmäki, Rheological properties, microstructure and sensory perception of high-amylose starch-pectin mixed gels. J. Texture Stud. **33**(6), 473–486 (2002). https://doi.org/10.1111/j.1745-4603.2002.tb01362.x
152. F. Nasaruddin, N.L. Chin, Y.A. Yusof, Effect of processing on instrumental textural properties of traditional Dodol using back extrusion. Int. J. Food Prop. **15**(3), 495–506 (2012). https://doi.org/10.1080/10942912.2010.491932
153. T.L. Smith, J.D. Ferry, F.W. Schremp, Measurements of the mechanical properties of polymer solutions by electromagnetic transducers. J. Appl. Phys. **20**(2), 144–153 (1949). https://doi.org/10.1063/1.1698326
154. T. Hoshino, Analysis of viscosity measurements obtained using the short back extrusion method. Part 1: Theory of short back extrusion in viscometry. J. Texture Stud. **51**(2), 201–213 (2020). https://doi.org/10.1111/jtxs.12501
155. T. Hoshino, Analysis of viscosity measurements obtained using the short back extrusion method. Part 2: Verification of short back extrusion in viscometry. J. Texture Stud. **51**(2), 214–224 (2020). https://doi.org/10.1111/jtxs.12510
156. T. Hoshino, Analysis of the flow properties of a Herschel–Bulkley fluid using short back extrusion viscometry and considering time-dependent and stress growth behaviors. Rheol. Acta **59**(11), 809–819 (2020). https://doi.org/10.1007/s00397-020-01243-3
157. A.S. Lim, S.L. Lopatnikov, N.J. Wagner, J.W. Gillespie, Investigating the transient response of a shear thickening fluid using the split Hopkinson pressure bar technique. Rheol. Acta **49**(8), 879–890 (2010). https://doi.org/10.1007/s00397-010-0463-8
158. N. Asija, H. Chouhan, S.A. Gebremeskel, N. Bhatnagar, High strain rate characterization of shear thickening fluids using Split Hopkinson pressure bar technique. Int. J. Impact Eng. **110**, 365–370 (2017) https://www.sciencedirect.com/science/article/pii/S0734743X16306534
159. Z. Tan, J. Ge, H. Zhang, P. Zhai, W. Li, Dynamic response of shear thickening fluid reinforced with SiC nanowires under high strain rates. Appl. Phys. Lett. **111**(3), 031902 (2017). https://doi.org/10.1063/1.4994066
160. Y. Guo, Y. Wei, J. Zou, C. Huang, X. Wu, Z. Liu, et al., Impact and usage of the shear thickening fluid (STF) material in damping vibration of bolted flange joints. Smart Mater. Struct. **28**(9), 095005 (2019). https://doi.org/10.1088/1361-665X/aaef6c
161. A. Azimi, G.M. Owolabi, H. Fallahdoost, N. Kumar, G. Warner, High strain rate behavior of ultrafine grained AA2519 processed via multi axial cryogenic forging. Metals **9**(2), 115 (2019)
162. A.S. Lim, S.L. Lopatnikov, J.W. Gillespie, Development of the split-Hopkinson pressure bar technique for viscous fluid characterization. Polym. Test. **28**(8), 891–900 (2009) https://www.sciencedirect.com/science/article/pii/S0142941809001342
163. L.S. Madsen, M. Waleed, C.A. Casacio, A. Terrasson, A.B. Stilgoe, M.A. Taylor, et al., Ultrafast viscosity measurement with ballistic optical tweezers. Nat. Photonics **15**(5), 386–392 (2021). https://doi.org/10.1038/s41566-021-00798-8
164. M. Zarei, J. Aalaie, Application of shear thickening fluids in material development. J. Mater. Res. Technol. **9**(5), 10411–10433 (2020) https://www.sciencedirect.com/science/article/pii/S2238785420315489

Chapter 3
Multi-Phase Shear Thickening Fluid

Mohammad Rauf Sheikhi and Mahdi Hasanzadeh

Nomenclature

STF	Shear thickening fluid
EG	Ethylene glycol
PMMA	Poly(methyl methacrylate)
PEO	Poly(ethylene oxide)
PEG	Polyethylene glycol
AF	Aramid fiber
CNTs	Carbon nanotubes
GO	Graphene oxide
GNs	Graphene nanoplatelets
UHMWPE	Ultra-high molecular weight polyethylene
MWCNTs	Multi-walled carbon nanotubes
FTIR	Fourier transform infrared spectroscopy
CNFs	Cellulose nanofibers
ODT	Order-disorder transition
SiC	Silicon carbide
PDA	Polydopamine

M. R. Sheikhi (✉)
State Key Laboratory for Strength and Vibration of Mechanical Structures, Shaanxi ERC of NDT and Structural Integrity Evaluation, School of Aerospace Engineering, Xi'an Jiaotong University, Xi'an, China

Key Laboratory of Traffic Safety on Track of Ministry of Education, School of Traffic & Transportation Engineering, Central South University, Changsha, Hunan, China
e-mail: 4121999205@stu.xjtu.edu.cn

M. Hasanzadeh
Department of Textile Engineering, Yazd University, Yazd, Iran

S. Gürgen (ed.), *Shear Thickening Fluid*,
https://doi.org/10.1007/978-3-031-25717-9_3

PS–AA	Poly(styrene–acrylic acid)
ZIF-8	Zeolitic imidazolate framework-8
Al_2O_3	Aluminum oxide
ZrO_2	Zirconium dioxide
Nd_2O_3	Neodymium oxide

3.1 Introduction

Shear thickening fluid (STF) is a type of non-Newtonian fluid whose viscosity increases as shear rate increases. In other words, at high shear rates, the viscosity of STF rises dramatically, and it behaves like a solid. However, once the impact stress is removed, STF reverts to a liquid-like state as soon as shear is removed. The reversible process is considered as the main favorable feature of STF. This phenomenon is of special interest for both scientific and technological issues in developing engineering applications [1, 2]. Notably, this phenomenon was initially defined as a problem in many industrial processes such as coating and mixing. For instance, shear thickening leads to the failure of mixer motors due to overloading. However, the unique characteristics of the STF have been used in developing smart materials and structures more recently. For instance, STF has been combined with high performance fabrics to provide a uniquely thin, flexible, cost-effective material that is comparable to or even better than the present protective materials in terms of ballistic, stab, and puncture protection. The idea of impregnating fabric with STF to increase the impact resistance of textile structures has recently attracted a lot of attention [3–8]. The absorption of the shock waves from the earthquake or severe wind conditions and the integration of STF within the damper systems are other applications of STF that have been recently investigated [9]. STF is recommended for structural components to increase the vibratory and damage resistance of systems and to avoid unexpected accelerations; it should also limit the range of motion in the shoulders, knees, elbows, ankles, and hips [10]. Figure 3.1 depicts the rise of STF-related publications over the past ten years based on the Scopus database.

STF is a suspension of nano- or micro-particles like silica or silicon dioxide in a Newtonian fluid-like water or polyethylene glycol (PEG). This combination produces a material with extraordinary properties. Common types of STF are silica suspended in ethylene glycol (EG) [6], polyvinylchloride in dioctyl phthalate [11], kaolin clay in glycerol [12], poly(methyl methacrylate) (PMMA) in PEG [13], fumed silica in propylene glycol [14, 15], and silica suspended in PEG [16]. Among these, the suspension of silica particles in PEG has been extensively investigated and frequently reported in STF literature (Table 3.1).

Multi-phase STF suspensions with particle additives have recently been fabricated to benefit from additives. In this chapter, the literature on the rheological characteristics of multi-phase STF is thoroughly reviewed. We discuss the shear thickening mechanism in concentrated colloidal suspension and the crucial factors affecting the rheological characteristics of multi-phase STF. We also explain

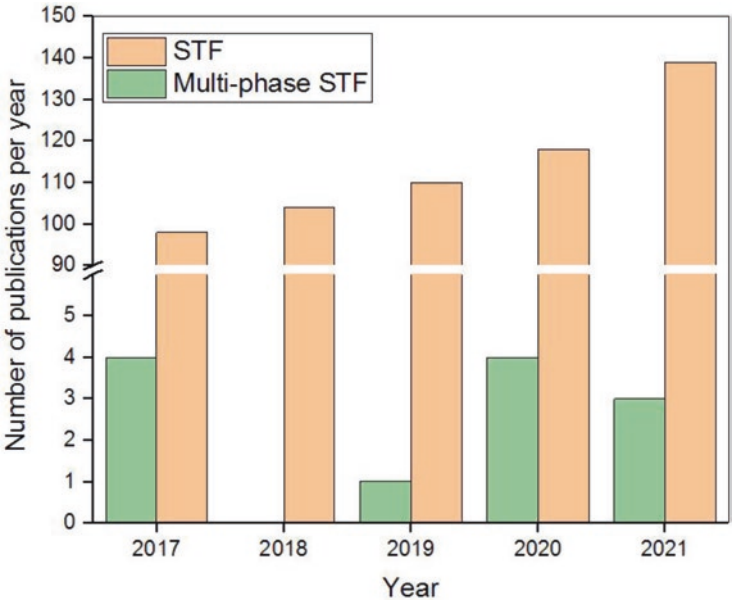

Fig. 3.1 The number of publications related to STF and multi-phase STF

how additional particles like carbon nanotubes, graphene, and nanoparticles affect the rheology of multi-phase STF systems. It is persuaded that a thorough analysis of the rheological characteristics of multi-phase STF is a crucial first step in comprehending the function of multi-phase STFs in the creation of engineering structures.

3.2 Shear Thickening Mechanism

STF, as a non-Newtonian fluid, is usually identified by a drastic increase in viscosity as the applied shear rate reaches a critical value. Figure 3.2 shows a schematic representation of shear thickening behavior. In the equilibrium state, the particles are well dispersed in the medium. STF exhibits reduced viscosities at lower shear rates before the critical point. The chaotic nature of the particles under the applied stress leads to the formation of particle layers as shear rate increases. When shear rate increases to further levels, hydroclusters are formed, thereby causing the particles to agglomerate. After the stress is removed from the medium, the suspension reverts into an easy-flowing state and resumes flowing like any other liquid. The shear thickening phenomenon is fully reversible.

Based on the literature, researchers have brought forth some theories to account for the fundamental reasons behind the shear thickening behavior. The "order-disorder transition" (ODT) [30–34] and the "hydrocluster" mechanism [35, 36]

Table 3.1 Single-phase STFs prepared by different particles and liquid mediums

Particles	Particle size (nm)	Weight fraction (%)	Liquid medium	Molecular weight (g/mol)	Application	Ref.
Colloidal silica	N/A	40	EG	N/A	Ballistic protection with STF-impregnated textiles	[6]
Spherical silica	15	40	PEG	200	Stab protection with STF-impregnated textiles	[7]
Nanosilica	500	34–38	EG	N/A	Stab protection with STF-impregnated textiles	[8]
Silica and PMMA	N/A	N/A	PEG	200	Puncture protection with STF-impregnated textiles	[13]
Spherical silica	650	75–88	PEG	N/A	Rheological properties of STF	[17]
Fumed silica	12	4–9	PEG	200 and 400	Rheological properties of STF	[18]
Fumed silica	14	20, 30, and 40	EG	N/A	Vibration damping with STF	[19]
Spherical silica and fumed silica	120 300–400	5–65	EG and PEG	200	Stab and ballistic protection with STF-impregnated textiles	[20]
Silica and PMMA	500	0.64 and 0.51	PEG	200	Impact protection with STF-impregnated textiles	[21]
Spherical silica	100, 300, 500	65	PEG	200	Ballistic protection with STF-impregnated textiles	[22]
Silica in aqueous dispersion	100	50, 60, and 70	PEG	200	Ballistic protection with STF-impregnated textiles	[23]
Colloidal silica	450	67	PEG	200	Puncture protection with STF-impregnated textiles	[24]
Silica	450	35–40	EG	N/A	Rheological properties of STF	[25]
Clay	30	N/A	PEO	400,000	Microstructural properties of STF	[26]
ZIF-8	240–400	51–56	EG	N/A	Rheological properties of STF	[27]
Core-shell structured silica@PDA	360	58–64	PEG	200	Rheological properties of STF	[28]
PS-AA nanospheres	330	50–56	EG	N/A	Rheological properties of STF	[29]

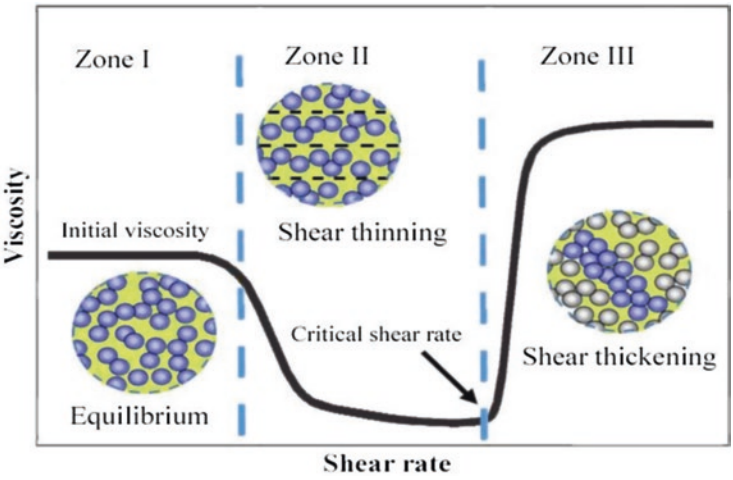

Fig. 3.2 Standard STF viscosity graph illustrating colloidal suspensions' shear thinning and thickening behavior

provide a more comprehensive explanation of this behavior than the other ideas. The ODT explains how the application of shear rate causes the particle arrangements to break down in the suspension, increasing the drag forces between the particles. Hoffman [37], one of the pioneers to research shear thickening in depth, created a micromechanical model of shear thickening as a flow-induced ODT based on this information. He suggested that the shear thickening tendency was the result of a change from a layer-ordered easy-flowing state to a disordered state. He claimed that the van der Walls-London, electric double layer, and shear stress forces acting on a collection of particles are responsible for this transformation. Additionally, it was proposed that the particles within the moving layers undergo hydrodynamically induced forces, which will cause the particles to be pushed out of their layer and disturb the orderly flow. When shear rate reaches a critical point, this transition shows a sharp increase in viscosity. Particle interactions in a liquid medium are the generation of the hydrocluster mechanism. Based on this, it can be stated that hydrodynamic lubricating forces between particles are the source of shear thickening behavior in concentrated colloidal suspensions. Hydrodynamic pressure increases when particles suspended in a fluid collide upon applying shear stress. Due to the formation of clusters under shear force, the drag forces between the particles grow stronger. Rheological, rheo-optic, and flow-SANS studies, as well as computer simulations, are used to experimentally support the hydrocluster mechanism [38]. Although the microscopic mechanisms have been proposed to explain the shear thinning phenomenon, the "hydrocluster" mechanism is more accurate and generalized.

Even though shear thinning is thought to be more common than shear thickening, it has been proposed that shear thickening can occur in all dense mixtures under certain conditions [15]. However, one of the major challenges is determining why

not all dense mixtures show shear thickening properties. One of the more perplexing questions is why mixtures with soft particles, which can easily deform, do not exhibit shear thickening behavior, whereas densely packed mixtures with hard particles do. A recent research has shown that nanoparticle behavior varies significantly for hard spheres due to strong electrostatic, charge-dipole, dipole-dipole, and van der Waals interactions. In particular, the interactions between the nanoparticles as well as those between the nanoparticle and liquid medium in such systems influence the state of the nanoparticles. The literature indicates that lubricating forces and frictional forces play a substantial role in the shear thickening process. To determine the hydrodynamic and contact force contributions to the shear thickening process, Lin et al. [39] investigated the shear thickening behavior in the interaction of micron-sized silica and latex particles. They found that as the suspension gets thickened, increasing the shear rate causes the contact contribution to growing while the hydrodynamic contribution stays the same. This phenomenon shows how contact forces have a significant impact on the shear thickening of dense colloidal suspensions. Based on the contact rheology models [39, 40], hydrodynamic lubrication forces produce a Newtonian behavior or shear thinning at low shear rates (Zone I) as a result of the insignificant interactions between particles. Lubrication breaks down when the shear rate (Zone II) is increased. As a result, frictional forces result in force chains, which cause discontinuous shear thickening [41]. The force network becomes tighter as shear rate increases (Zone III), eventually reaching a fully shear jammed state. Large clusters are produced when shear rearranges the particles into anisotropic formations. While frictionless contact results in a smooth and reversible viscosity increase associated with continuous shear thickening, frictional hydrodynamic interactions between suspended particles produce large jumps while rapid increase in viscosity associated with strong and discontinuous shear thickening [37].

3.3 STF Rheology

Up till now, several investigations on the rheological characteristics of STF under steady-state and dynamic conditions have been conducted [18, 20]. It has been observed that some influencing elements including particles, flow field, suspending medium, additives, and the interaction between particles and additives affect the STF rheology [15, 21, 42]. Table 3.2 summarizes the key factors influencing the rheological properties. Particle properties (shape, solid volume fraction, size distribution, and interaction with other particles), suspending phase properties (viscosity and molecular weight of carrier liquid), and STF properties are the main factors influencing the rheological properties.

Barnes [15] suggested that above the particle volume fraction of 0.5, the fluid's behavior changes dramatically with shear rate. The critical shear rate (the shear rate at which shear thickening begins) decreases as the volume fraction of the particle increases. Similarly, Kang et al. [20] investigated the effect of silica loading on the

Table 3.2 Key factors on STF rheology

Parameter	Description	Effects on the rheology of STF
Particles	Shape	Decreasing the critical shear rate by increasing the aspect ratio of particles
	Size	Decreasing the critical shear rate with increasing the particle size
	Size distribution	Decreasing the critical shear rate with narrow particle size distribution
	Solid volume fraction	Decreasing the critical shear rate by increasing the solid volume fraction
	Particle-particle interaction	Deflocculated suspensions exhibit shear thickening at a high shear rate
	Hardness	Better shear thickening behavior for silica particles with higher hardness
Suspending phase	Molecular weight and viscosity	Decreasing the critical shear rate by increasing the molecular weight of suspending phase
STF properties	Temperature	Decreasing the critical shear rate with decreasing STF temperature
	pH	Increasing the critical shear rate with increasing the pH of STF

shear thickening properties. They stated that critical shear rate develops at lower shear rates as silica particle concentration increases. Moreover, with increasing the silica particle concentration, the shear thickening phenomenon realizes sharply. Wetzel et al. [43] found that when the aspect ratio of the particles grows, lower volume percentages of particles are sufficient to trigger the shear thickening behavior. According to Maranzano et al. [42] particle size significantly affects the transition from reversible shear thickening to dense colloidal suspensions. They also noted that the flow curves systematically change to decrease shear stresses as particle size increases. Lee et al. [22] also observed a similar pattern of behavior. Kang et al. [20] reported the temperature effect on the critical shear rate and STF viscosity. From this work, as temperature increases, hydrodynamic interactions grow stronger due to the increased Brownian motion with the colloidal particles and, thus, critical shear rate slightly moves toward higher shear rates.

Is there a regulating factor, such as a range above or below which the critical shear rates appear to be lower? As was already mentioned, the solid volume percentage affects how colloidal suspensions thicken under shear. However, due to variations in form, size, size distribution, and interaction with other particles, distinct nanoparticles display different shear thickening rheology. The solid particle amount cannot, therefore, be the only determining factor. Another difficulty is knowing how to change STF characteristics. Creating a straightforward and organized way of showing the interrelated effects of elements is another challenge. There has not been any publication on comprehensive quantitative analysis of effective parameters yet in the literature.

3.4 Rheology of Multi-phase STF

Several studies on the rheological behavior of STF have been conducted up to now. Integrating particle additives into STF and studying the rheological behavior of multi-phase STF have recently received much attention. As mixtures of single-phase STF and different additives, multi-phase STF offers the opportunity to tune the rheological behavior of suspension concerning the application field. For example, Hasanzadeh and Mottaghitalab [44] investigated the use of multi-walled carbon nanotubes (MWCNTs) as an additive to tune the rheological properties of a fumed silica/PEG-based STF. Rheological measurements revealed that MWCNTs have a significant impact on the rheology of STF. Even at low concentrations of MWCNTs (0.4 wt.%), the critical viscosity of the STF decreases with the addition. Furthermore, shear thickening appears at higher shear rates in the multi-phase STF system. In other words, the MWCNTs interfere with the shear thickening behavior. The proposed mechanism of MWCNT incorporation and shear thickening behavior of a multi-phase STF system is depicted in Fig. 3.3. According to this mechanism, the increased interactions between the fumed silica nanoparticles, PEG as a carrier fluid, and MWCNTs are responsible for affecting the shear thickening properties. The silanol groups on the surface of fumed silica nanoparticles form hydrogen bonds with the PEG hydroxyl groups and the internal oxygen atoms. When MWCNTs are added to the STF, the hydroxyl/carboxyl groups on the MWCNT surfaces can form hydrogen bonding with silica particles and PEG. However, hydrogen bonds are more likely to be formed with PEG than with silica particles. Fourier transform infrared spectroscopy (FTIR) confirms that the hydrogen bonding in the MWCNT-silica-PEG suspension enhances. As a result of the strong interactions between MWCNTs and PEG, higher shear force is needed to withstand the strong interactions, and the thickening in the mixture is postponed to higher critical shear rates. Finally, the presence of MWCNTs in the STF reduces the thickening ratio so that the shear thickening properties.

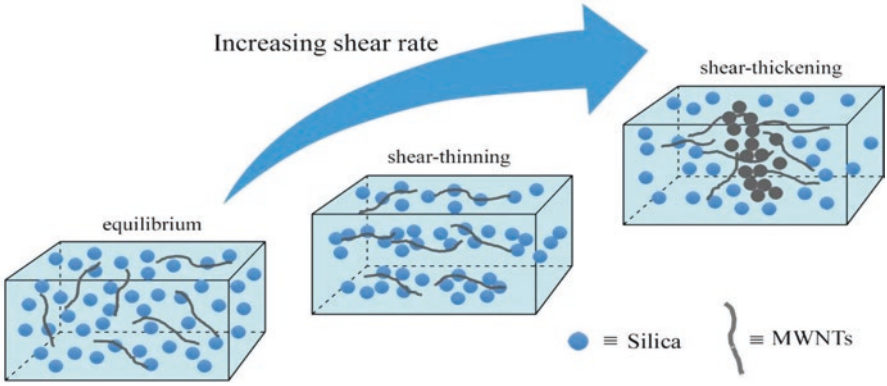

Fig. 3.3 The mechanism of incorporation of MWCNTs additive on the rheological behavior of multi-phase STFs

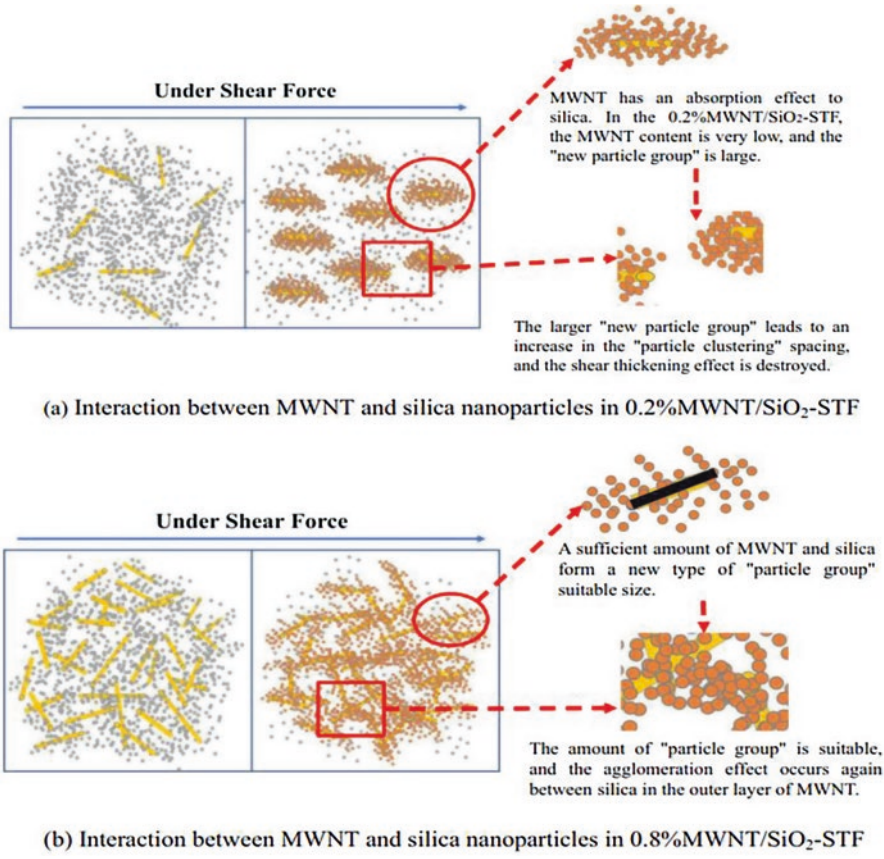

Fig. 3.4 The schematic of the mechanism of interaction between silica and MWCNTs in multi-phase STF [45]. Reprinted by permission from Springer

A similar study on the rheological behavior of multi-phase STF with MWCNTs additive was carried out by Wei et al. [45]. They found that the peak viscosity of the multi-phase STF with 1 wt.% MWCNTs increases about 360% and the critical shear rate decreases about 70%. Investigation of the variation of the mass fraction of MWCNT additives shows the irregular change in the viscosity of multi-phase STF. For instance, the multi-phase STF with 0.2 wt.% MWCNTs does not show shear thickening behavior, which is likely due to the hindering of the flow by flocculent structure and the large aspect ratio of MWCNT. Figure 3.4 shows the schematic of the interaction mechanism between silica and MWCNTs. In multi-phase STF with a low mass fraction of MWCNT, a large amount of silica nanoparticles adsorbs on a small amount of MWCNT and forms a larger new particle group containing MWCNT. Due to the no "particle clustering" mechanism, the multi-phase STF (2 wt.% MWCNT) has no obvious shear thickening effect. However, when the mass fraction of MWCNTs increases, the "particle clustering" mechanism

develops. The reason is that increasing the mass fraction of MWCNT leads to an increase in the interaction forces between the particles as well as the number of new particles, which decreases the inter-particle distances and thereby hinders their flow. Hence, a significant shear thickening phenomenon occurs. Wei et al. [45] also studied the thermal effect on the rheology of multi-phase STF and found a significant effect of temperature on the shear thickening behavior. The temperature sensitivity of multi-phase STF is similar to that of single-phase STF and dominates by silica nanoparticles. The MWCNT can significantly enhance the shear thickening effect without influencing the temperature sensitivity. At higher temperatures, the shear thickening properties of multi-phase STF weaken due to the poor hydrogen bonds. This phenomenon may be due to the good thermodynamic properties and high thermal conductivity of MWCNTs. Hence, the temperature of each component in the STF is similar and the particle distribution is uniform due to the effective heat transfer at an elevated temperature environment.

Li et al. [46] studied the shear thickening rheology of a silica and PEG-based STF using oxygen-plasma-modified MWCNTs for improving the quasi-static stab resistance of textiles. They modified the MWCNTs with plasma treatment, due to the van der Waals interactions and the hydrophobicity of MWCNTs, which led to the agglomeration in STF. The rheology of multi-phase STF was investigated in different mass friction of modified-MWCNTs (0.02–0.06 wt.%). The results showed that the multi-phase STF with 0.06 wt.% of modified MWCNTs exhibits an enhanced peak viscosity of about 120%. Similarly, the critical shear rate reduces by 80%. The multi-phase STF displays higher yield stress in comparison with the single-phase STF. The stronger network formed by the modified-MWCNTs enhances the interaction between the M-MWCNTs and silica particles. This is likely due to the presence of oxygen-containing functional groups, such as hydroxyl and carboxyl groups, on the surface of the modified-MWCNTs, which facilitate the formation of hydrogen bonds with silanol groups on the surface of silica. Hence, more interaction between silica particles and modified-MWCNTs leads to the easy formation of "hydrocluster" and consequently shear thickening at a lower shear rate.

In another study by Gürgen et al. [47, 48], various ceramic particles have been used in a silica-based STF. They found that the incorporation of ceramic particles into STF disrupts the thickening behavior. Moreover, the thickening behavior is dependent on the parameters, including the amount and particle size of additives. For example, at higher loadings of ceramic particles, the volume fraction of silica falls below the effective limit and the shear thickening behavior of suspension fades away. They suggested that the incorporation of additive particles to STF may disrupt the thickening behavior in two ways: (i) lowering the silica percentage of particles by adding additives and (ii) shortening the hydrocluster networks along suspensions due to interstitial additive particles. According to the hydrocluster thickening mechanism, the more the extended hydroclusters, the more the powerful shear thickening behavior. The ceramic micro-particles in suspension occupy the large volume in silica nanoparticles medium and thereby hinders the extension of hydroclusters. Hence, in the multi-phase STFs, the contact networks of silica particles are less likely to form than in the single-phase STF. Moreover, the coarser particles have

significant effects on the weakening of shear thickening behavior in comparison to finer particles. This is likely attributed to the larger distance between silica particles in the flow induced by the coarser particles. The ceramic particles with smaller sizes have less effect on the hydroclusters and thickening behavior. The results show that the coarser ceramic particles lead to a decrease in the critical shear rate and the thickening properties of the suspension.

The rheological properties of multi-phase STF were also investigated by using graphene oxide (GO) as an additive. Huang et al. [49] prepared a multi-phase STF using fumed silica (15 wt.%) and PEG-based suspension. The multi-phase STFs with various amounts (from 0 to 0.3 wt.%) of GO additives were rheologically measured and compared with the single-phase STF. They found that the addition of GO particles leads to a remarkable increase in the viscosity and a decrease in the critical shear rate. Moreover, the thickening ratio gradually decreases with increasing GO content. These results are similar to the output of ceramic particles and MWCNTs investigated by Gürgen et al. [47, 48] and Hasanzadeh and Mottaghitalab [44] respectively. Due to the sheet-like structure of GO, they have a stronger hydrodynamic field effect than that of the silica particles. Hence, GO additives can cause a stronger congestion effect and, therefore, hydro-clusters can be formed at lower shear rates. Moreover, the strong interaction between the GO additives and silica particles leads to more aggregation of silica nanoparticles on the GO surfaces. However, the incorporation of GO into the STF prevents the hydrocluster elongations and consequently lowers the viscosity increase in the multi-phase STF.

Halloysite nanotubes as an additive (1 to 5 wt.%) in multi-phase STFs have been investigated by Passey [50]. Fumed silica (7 nm) as a solid phase and PEG200 as a liquid medium were utilized for the preparation of the STF. The rheological studies revealed that the halloysite nanotubes disrupt the thickening mechanism of STF and reduce the viscosity of the suspension. They suggested the formation of strong hydrogen bonding between the fumed silica and halloysite nanotubes. The hydrodynamic forces progressively take control of the suspension as shear rate increases, and the nanotubes align themselves in a layered and parallel orientation. The extension of the clusters in the suspension is suppressed by the formation of hydroclusters around the halloysite nanotubes as shear rate is further increased. The inclusion of more halloysite nanotube additives leads to an increase in the critical shear rates. The addition of halloysite nanotubes enhances the surface area of the particles due to the cylindrical morphology and, consequently, more hydrodynamic forces are required for cluster formation. Similarly, Laha et al. [51] studied the multi-phase STF system using halloysite nanotubes in a spherical silica and PEG200-based STF. However, they discovered that adding more halloysite nanotubes to suspensions causes the critical shear rate to drop. The results demonstrated that the halloysite nanotubes enhance the shear thickening behavior. Although Passey [50] and Laha et al. [51] used the same type of additives, the rheology of the suspensions is completely different. Laha et al. [51] discovered that halloysite nanotubes act as bases for the hydroclusters in which the spherical silica particles are collected around the halloysite nanotubes. In the study by Passey [50], the halloysite nanotubes do not attract fumed silica while the additives prevent the hydrocluster

formation by intercepting the growing of the silica chains. The interaction between the halloysite nanotubes and silica may differ depending on the shape of the silica particles as the spherical silica may be attractive while the fumed silica may be repulsive to the halloysite nanotubes. However, the particle morphology of silica may not be the only factor influencing the interactions between the silica and additives. Fumed silica, for example, can exist in both hydrophobic and hydrophilic forms, which have a direct impact on the suspension rheology. Hydrophilic silica contains silanol groups, which exhibit enhanced thickening in low polarity media due to strong hydrogen bonds, whereas hydrophobic silica exhibits thickening in high polarity media due to weak hydrogen bonding [52].

Sha et al. [53] studied the rheology of a multi-phase STF using graphene nanoplatelets (GNs) and carbon nanotubes (CNTs). The rheology of the STF with spherical silica in a PEG was investigated as well as the effects of GNs and CNTs as additives. They discovered that the suspension viscosity increases as the additive concentration in the STF rises. Additionally, the viscosity of the multi-phase STF can be increased more effectively by CNTs in comparison to GNs. Because CNTs are shaped like long tubes and PEG has long chemical chains, their relative lubricating forces are stronger than those between GNs and PEG. The GNs play as bridges between the silica particles in a liquid, forming hydrogen bonds and thus connecting the aggregated silica groups. Consequently, shear thinning occurs at lower shear rates. PEG-CNTs have a much weaker internal force than PEG-GNs because GNs are sheet-like additives. As a result, phase separation occurs more easily in the CNT suspensions than in the GN suspensions. Furthermore, CNTs having rigid rod shapes in STF can withstand contact forces and, therefore, provide more advances for shear thickening, whereas GNs with two-dimensional soft structures can be easily deformed. Therefore, CNTs are better for shear thickening behavior than GNs. The coexistence of CNTs and GNs on STF further demonstrates that CNTs predominate over GNs concerning suspensions. The viscosity of suspension increases with an increase in the CNTs/GNs ratio in a multi-phase STF. The results demonstrated the enhanced shear thickening behavior by additive incorporation.

The rheological behavior of a multi-phase STF with the incorporation of cellulose nanofibers (CNFs) was investigated by Ghosh et al. [54]. Different concentrations (0.1–0.3 wt.%) of CNFs were used for the preparation of the multi-phase STFs. The rheological measurements showed that the addition of CNFs (0.3 wt.%) to the STF leads to a considerable increase in the viscosity. Moreover, the stronger shear thickening behavior occurs at a lower critical shear rate. This is likely attributed to the large number of hydroxyl groups on the CNFs, which contribute to the formation of hydrogen bonding between the CNFs and silica particles. Increasing the amount of CNFs in the multi-phase STF leads to a reduction in the critical shear rate due to the more interaction between the CNFs with high aspect ratio and silica particles, which induced shear thickening at a lower shear rate. Indeed, the number of available hydroxyl groups increases by increasing the CNFs content, implying stronger interaction and entanglement between the silica particles and CNFs through the formation of a greater number of hydrogen bonds. Figure 3.5 shows the

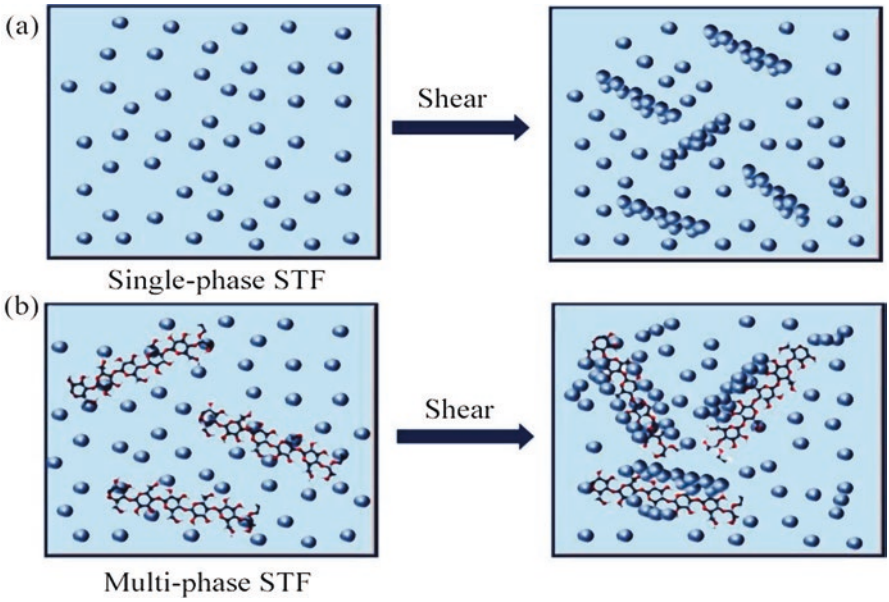

Fig. 3.5 Schematic representation of shear thickening behavior of (**a**) single-phase STF and (**b**) multi-phase STF before and after shear

schematic representation of shear thickening behavior in the multi-phase STF using CNFs as additives.

Sun et al. [55] investigated the rheological properties of a multi-phase STF based on zirconia nanoparticle additives. They found that the incorporation of zirconia nanoparticles into the STF (20% silica nanoparticles) leads to a growth in the shear thickening behavior while increasing the apparent viscosity level. The formation of a cluster of zirconia particles around the functional groups induces the shear thickening behavior and consequently increases the viscosity of the suspension. No regular changes are observed with increasing additive contents. In the multi-phase STF with zirconia content more than the cut-off point (12%), the initial viscosity and critical shear rate increase while the peak viscosity decreases. This is likely due to the hindering of the interaction of the silica nanoparticles by the excess amount of zirconia. Interestingly, the effect of temperature on the viscosity of the multi-phase STF becomes less pronounced when the content of zirconia increases. However, it still significantly influences the critical shear rate and shear thickening behavior.

The rheological behavior of a multi-phase STF was investigated by Sun et al. [56]. Neodymium oxide (Nd_2O_3) nanoparticles were used as an additive in the suspensions. They prepared various suspensions with different concentrations (9–15 wt.%) and found that an appropriate amount of Nd_2O_3 (12 wt.%) results in a significant increase in the peak viscosity by about 320%. The critical shear rate decreases by 75%. The investigation on the effect of temperature reveals a reduction

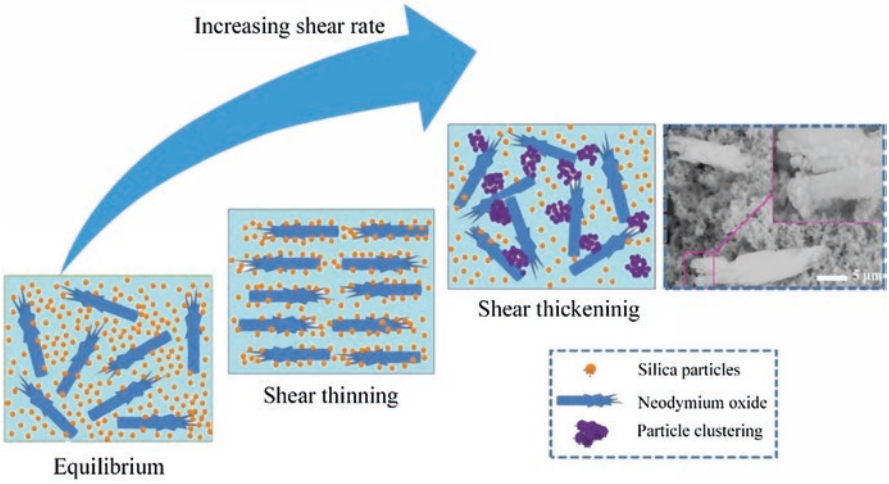

Fig. 3.6 Schematic representation of shear thickening behavior of Nd_2O_3-based multi-phase STF [56]. Reprinted by permission from Springer

in the peak viscosity with increasing temperature. Applying shear force to the multi-phase STF containing Nd_2O_3 particles with more mass fraction and larger size than silica particles results in the movement of Nd_2O_3 particles and adherence of silica particles to the Nd_2O_3 particles. By increasing shear force, the Nd_2O_3 particles are well organized and distributed uniformly, which leads to the shear thinning behavior. Further increase in shear force leads to a destroying effect in the layered structure of Nd_2O_3 particles. The silica particles form particle clusters by adhering to the Nd_2O_3 particles, which leads to a sharp increase in the viscosity of the Nd_2O_3-based multi-phase STF. Figure 3.6 shows the schematic illustration of the shear thickening mechanism. The results show that the incorporation of Nd_2O_3 particles significantly enhances the shear thickening effect especially at higher weight fractions and lower temperatures.

Although several studies have been carried out on the rheology of different multi-phase STF systems, further investigations are needed using various types of additives for a comprehensive understanding of the role of additives in the multi-phase STF. Table 3.3 summarizes the most relevant research works on the rheology of multi-phase STF. The effect of additives on the shear thickening behavior does not have the same trend each other as the literature provides only case-dependent studies. Some additives disrupt the shear thickening mechanism and some improve this behavior. However, it can be concluded that the rheology of multi-phase STF is dependent on various factors such as chemistry, material, geometry, weight fraction, aspect ratio, temperature, and mechanical properties.

Table 3.3 Multi-phase STF prepared by different additive particles

Single-phase STF		Multi-phase STF			
Particle (size)	Liquid medium (molecular weight)	Additive particles	Weight fraction (%)	Focus of the research	Ref.
Fumed silica (12 nm)	PEG (200 g/mol)	MWCNTs	0.4–1.2	Tuning STF rheology	[44]
Fumed silica (12 nm)	PEG (200 g/mol)	MWCNTs	0.2–1	Tuning STF rheology	[45]
Fumed silica (12 nm)	PEG (200 g/mol)	Oxygen-plasma-modified MWCNTs	0.02–0.06	Enhancing impact resistance of STF treated textiles	[46]
Fumed silica (14 nm)	PEG (200 g/mol)	GO	0–0.3	Tuning STF rheology	[49]
Fumed silica (12 nm)	PEG (200 g/mol)	GO and MWCNTs	0.002–0.02	Tuning STF rheology	[57]
Fumed silica (11 nm)	PEG (200 g/mol)	Halloysite nanotubes	1–5	Tuning STF rheology	[50]
Fumed silica (20 nm)	PEG (400 g/mol)	SiC particles	5–45	Tuning STF rheology	[47]
Spherical silica (300 nm)	PEG (400 g/mol)	SiC nanowires	0–1.25 (vol.%)	Tuning STF rheology	[58]
Spherical silica (650 nm)	PEG (200 g/mol)	GNs and CNTs	1–3	Tuning STF rheology	[53]
Spherical silica (500 nm)	PEG (200 g/mol)	CNFs	0.1–0.3	Tuning STF rheology	[54]
Spherical silica (12 nm)	PEG (200 g/mol)	ZrO_2 nanoparticles	9–20	Tuning STF rheology	[55]
Fumed silica (20 nm)	PEG (400 g/mol)	Al_2O_3 nanoparticles	5–45	Tuning STF rheology	[9]
Fumed silica (12 nm)	PEG (200 g/mol)	Nd_2O_3 nanoparticles	9–15	Tuning STF rheology	[56]

3.5 Conclusions

The unique rheological behavior of STF provides the opportunity for different various applications such as protective fabrics and mechanical dampers. Several attempts have been carried out to design multi-phase STF by adding particular additives. A detailed review of the rheological behavior of multi-phase STF is presented in this chapter. This chapter shows that there are many significant parameters influencing the shear thickening properties of multi-phase STF such as the shape, size, and weight fraction of additives as well as their interactions with the base particles and carrier liquid in STF. There is an increasing attention and necessity to understand the rheological characteristic of multi-phase STF to figure out and tune it

according to their special applications. Several micro and nano additives have been utilized for tuning the STF rheology including carbon based structures, metal oxides, and inorganic materials. Although the effect of additives on the shear thickening behavior of multi-phase STF does not have the same trend, they often lead to enhanced rheological properties in the optimum conditions. Hence, the fabrication of multi-phase STF with unique structural and rheological characteristics provides new possibilities for the design and development of efficient STF-based systems for various applications.

References

1. M. Hasanzadeh, V. Mottaghitalab, The role of shear-thickening fluids (STFs) in ballistic and stab-resistance improvement of flexible armor. J. Mater. Eng. Perform. **23**(4), 1182–1196 (2014)
2. M. Hasanzadeh, V. Mottaghitalab, M. Rezaei, Rheological and viscoelastic behavior of concentrated colloidal suspensions of silica nanoparticles: A response surface methodology approach. Adv. Powder Technol. **26**(6), 1570–1577 (2015)
3. K. Yu, H. Cao, K. Qian, L. Jiang, H. Li, Synthesis and stab resistance of shear thickening fluid (STF) impregnated glass fabric composites. Fibres Text East Eur. **95**(6), 126–128 (2012)
4. A. Srivastava, A. Majumdar, B.S. Butola, Improving the impact resistance performance of Kevlar fabrics using silica based shear thickening fluid. Mater. Sci. Eng. A **529**(1), 224–229 (2011)
5. E.V. Lomakin, P.A. Mossakovsky, A.M. Bragov, A.K. Lomunov, A.Y. Konstantinov, M.E. Kolotnikov, et al., Investigation of impact resistance of multilayered woven composite barrier impregnated with the shear thickening fluid. Arch. Appl. Mech. **81**(12), 2007–2020 (2011. [Internet]. 2011 Apr 11 [cited 2022 Aug 9]). https://doi.org/10.1007/s00419-011-0533-0
6. Y.S. Lee, E.D. Wetzel, N.J. Wagner, The ballistic impact characteristics of Kevlar® woven fabrics impregnated with a colloidal shear thickening fluid. J. Mater. Sci. **38**(13), 2825–2833 (2003. 3813 [Internet]. 2003 Jul 1 [cited 2022 Aug 9]). https://doi.org/10.1023/A:1024424200221
7. T.A. Hassan, V.K. Rangari, S. Jeelani, Synthesis, processing and characterization of shear thickening fluid (STF) impregnated fabric composites. Mater. Sci. Eng. A **527**(12), 2892–2899 (2010)
8. L.L. Sun, D.S. Xiong, C.Y. Xu, Application of shear thickening fluid in ultra high molecular weight polyethylene fabric. J. Appl. Polym. Sci. **129**(4), 1922–1928 (2013. [Internet] [cited 2022 Aug 9]). https://doi.org/10.1002/app.38844
9. S. Gürgen, M.A. Sofuoğlu, M.C. Kuşhan, Rheological compatibility of multi-phase shear thickening fluid with a phenomenological model. Smart Mater. Struct. **28**(3), 035027 (2019)
10. S. Gürgen, M.C. Kuşhan, W. Li, Shear thickening fluids in protective applications: A review. Prog. Polym. Sci. **75**, 48–72. [Internet] (2017). https://doi.org/10.1016/j.progpolymsci.2017.07.003
11. W.H. Boersma, P.J.M. Baets, J. Laven, H.N. Stein, Time-dependent behavior and wall slip in concentrated shear thickening dispersions. J. Rheol. (N Y N Y) **35**(6), 1093 (1998. [cited 2022 Aug 9], [Internet]). https://doi.org/10.1122/1.550167
12. M.J. Decker, C.J. Halbach, C.H. Nam, N.J. Wagner, E.D. Wetzel, Stab resistance of shear thickening fluid (STF)-treated fabrics. Compos. Sci. Technol. **67**(3–4), 565–578 (2007)
13. D.P. Kalman, J.B. Schein, J.M. Houghton, C.H.N. Laufer, E.D. Wetzel, N.J. Wagner, Polymer dispersion based shear thickening fluid-fabrics for protective applications. Int. SAMPE Symp. Exhib., 52 (2007)
14. S.R. Raghavan, S.A. Khan, Shear-thickening response of Fumed silica suspensions under steady and oscillatory shear. J. Colloid Interface Sci. **185**(1), 57–67 (1997)

15. H.A. Barnes, Shear-thickening ("dilatancy") in suspensions of nonaggregating solid particles dispersed in Newtonian liquids. J. Rheol. (N Y N Y) **33**(2), 329 (2000. [Internet, cited 2022 Aug 9]). https://doi.org/10.1122/1.550017
16. T.A. Hassan, V.K. Rangari, S. Jeelani, Sonochemical synthesis and rheological properties of shear thickening silica dispersions. Ultrason. Sonochem. **17**(5), 947–952. [Internet] (2010). https://doi.org/10.1016/j.ultsonch.2010.02.001
17. K. Yu, H. Cao, K. Qian, X. Sha, Y. Chen, Shear-thickening behavior of modified silica nanoparticles in polyethylene glycol. J. Nanopart. Res. **14**(3), 1–9 (2012. [Internet, cited 2022 Aug 9]). https://doi.org/10.1007/s11051-012-0747-2
18. Q.M. Wu, J.M. Ruan, B.Y. Huang, Z.C. Zhou, J.P. Zou, Rheological behavior of fumed silica suspension in polyethylene glycol. J. Cent. S. Univ. Technol. **13**(1), 1–5 (2006. [Internet, cited 2022 Aug 9]). https://doi.org/10.1007/s11771-006-0096-3
19. X.Z. Zhang, W.H. Li, X.L. Gong, The rheology of shear thickening fluid (STF) and the dynamic performance of an STF-filleddamper. Smart Mater. Struct. **17**(3), 035027 (2008., [Internet, cited 2022 Aug 9]). https://doi.org/10.1088/0964-1726/17/3/035027
20. T.J. Kang, C.Y. Kim, K.H. Hong, Rheological behavior of concentrated silica suspension and its application to soft armor. J. Appl. Polym. Sci. **124**(2), 1534–1541 (2012. [Internet, cited 2022 Aug 9]). https://doi.org/10.1002/app.34843
21. D.P. Kalman, R.L. Merrill, N.J. Wagner, E.D. Wetzel, Effect of particle hardness on the penetration behavior of fabrics intercalated with dry particles and concentrated particle-fluid suspensions. ACS Appl. Mater. Interfaces **1**(11), 2602–2612 (2009. [Internet, cited 2022 Aug 9]). https://doi.org/10.1021/am900516w
22. B.W. Lee, I.J. Kim, C.G. Kim, The influence of the particle size of silica on the ballistic performance of fabrics impregnated with silica colloidal suspension. J. Compos. Mater. **43**(23), 2679–2698 (2009. [Internet, cited 2022 Aug 9]). https://doi.org/10.1177/0021998309345292
23. A. Majumdar, B.S. Butola, A. Srivastava, Optimal designing of soft body armour materials using shear thickening fluid. Mater. Des. **1**(46), 191–198 (2013)
24. Houghton JM, Schiffman BA, Kalman DP, Wetzel ED, Wagner NJ. Hypodermic needle puncture of shear thickening fluid (STF)-treated fabrics. Int SAMPE Symp Exhib. 2007; 52 (October)
25. Y.S. Lee, N.J. Wagner, Rheological properties and small-angle neutron scattering of a shear thickening, nanoparticle dispersion at high shear rates. Ind. Eng. Chem. Res. **45**(21), 7015–7024 (2006. [Internet, cited 2022 Aug 9]). https://doi.org/10.1021/ie0512690
26. M. Takeda, T. Matsunaga, T. Nishida, H. Endo, T. Takahashi, M. Shibayama, Rheo-SANS studies on shear thickening in clay-poly(ethylene oxide) mixed solutions. Macromolecules **43**(18), 7793–7799 (2010. [Internet, cited 2022 Aug 9]). https://doi.org/10.1021/ma101319j
27. Y. Wu, S. Cao, S. Xuan, M. Sang, L. Bai, S. Wang, et al., High performance zeolitic imidazolate framework-8 (ZIF-8) based suspension: Improving the shear thickening effect by controlling the morphological particle-particle interaction. Adv. Powder Technol. **31**(1), 70–77 (2020)
28. M. Liu, W. Jiang, Q. Chen, S. Wang, Y. Mao, X. Gong, et al., A facile one-step method to synthesize SiO2@polydopamine core–shell nanospheres for shear thickening fluid. RSC Adv. **6**(35), 29279–29287 (2016)
29. W. Jiang, F. Ye, Q. He, X. Gong, J. Feng, L. Lu, et al., Study of the particles' structure dependent rheological behavior for polymer nanospheres based shear thickening fluid. J. Colloid Interface Sci. **413**, 8–16 (2014)
30. R.L. Hoffman, Explanations for the cause of shear thickening in concentrated colloidal suspensions. J. Rheol. (N Y N Y) **42**(1), 111 (1998. [Internet, cited 2022 Aug 15]). https://doi.org/10.1122/1.550884
31. W.H. Boersma, J. Laven, H.N. Stein, Viscoelastic properties of concentrated shear-thickening dispersions. J. Colloid Interface Sci. **149**(1), 10–22 (1992)
32. H.M. Laun, R. Bung, S. Hess, W. Loose, O. Hess, K. Hahn, et al., Rheological and small angle neutron scattering investigation of shear-induced particle structures of concentrated polymer

dispersions submitted to plane Poiseuille and Couette flowa. J. Rheol. (N Y N Y) **36**(4), 743 (1998. [Internet, cited 2022 Aug 15]). https://doi.org/10.1122/1.550314
33. R.L. Hoffman, Discontinuous and dilatant viscosity behavior in concentrated suspensions. II. Theory and experimental tests. J. Colloid Interface Sci. **46**(3), 491–506 (1974)
34. R.L. Hoffman, Discontinuous and dilatant viscosity behavior in concentrated suspensions. I. Observation of a flow instability. Trans. Soc. Rheol. **16**(1), 155 (2000. [Internet, cited 2022 Aug 15]). https://doi.org/10.1122/1.549250
35. J.W. Bender, N.J. Wagner, Optical measurement of the contributions of colloidal forces to the rheology of concentrated suspensions. J. Colloid Interface Sci. **172**(1), 171–184 (1995)
36. J. Bender, N.J. Wagner, Reversible shear thickening in monodisperse and bidisperse colloidal dispersions. J. Rheol. (N Y N Y) **40**(5), 899 (1998. [Internet, cited 2022 Aug 15]). https://doi.org/10.1122/1.550767
37. M. Zarei, J. Aalaie, Application of shear thickening fluids in material development. J. Mater. Res. Technol. **9**(5), 10411–10433 (2020)
38. B.J. Maranzano, N.J. Wagner, Flow-small angle neutron scattering measurements of colloidal dispersion microstructure evolution through the shear thickening transition. J. Chem. Phys. **117**(22), 10291 (2002. [Internet, cited 2022 Aug 15]). https://doi.org/10.1063/1.1519253
39. N.Y.C. Lin, B.M. Guy, M. Hermes, C. Ness, J. Sun, W.C.K. Poon, et al., Hydrodynamic and contact contributions to continuous shear thickening in colloidal suspensions. Phys. Rev. Lett. **115**(22), 228304 (2015. [Internet, cited 2022 Aug 14]). https://doi.org/10.1103/PhysRevLett.115.228304
40. I.R. Peters, S. Majumdar, H.M. Jaeger, Direct observation of dynamic shear jamming in dense suspensions. Nature **532**(7598), 214–217 (2016) [Internet, cited 2022 Aug 14]. Available from: https://www.nature.com/articles/nature17167
41. M. Wyart, M.E. Cates, Discontinuous shear thickening without inertia in dense non-brownian suspensions. Phys. Rev. Lett. **112**(9), 098302 (2014. [Internet, cited 2022 Aug 14]). https://doi.org/10.1103/PhysRevLett.112.098302
42. B.J. Maranzano, N.J. Wagner, The effects of particle size on reversible shear thickening of concentrated colloidal dispersions. J. Chem. Phys. **114**(23), 10514 (2001)
43. E.D. Wetzel, Y.S. Lee, R.G. Egres, K.M. Kirkwood, J.E. Kirkwood, N.J. Wagner, The effect of rheological parameters on the ballistic properties of shear thickening fluid (STF)-Kevlar composites. AIP Conf. Proc. **712**(1), 288 (2004. [Internet, cited 2022 Aug 9]). https://doi.org/10.1063/1.1766538
44. M. Hasanzadeh, V. Mottaghitalab, Tuning of the rheological properties of concentrated silica suspensions using carbon nanotubes. Rheol. Acta **55**(9), 759–766 (2016)
45. M. Wei, Y. Lv, L. Sun, H. Sun, Rheological properties of multi-walled carbon nanotubes/silica shear thickening fluid suspensions. Colloid Polym. Sci. **298**(3), 243–250 (2020)
46. D. Li, R. Wang, X. Liu, S. Fang, Y. Sun, Shear-thickening fluid using oxygen-plasma-modified multi-walled carbon nanotubes to improve the quasi-static stab resistance of Kevlar fabrics. Polymers (Basel). **10**(12), 1356 (2018)
47. S. Gürgen, M.C. Kuşhan, W. Li, The effect of carbide particle additives on rheology of shear thickening fluids. Korea Aust. Rheol. J. **28**(2), 121–128 (2016)
48. S. Gürgen, W. Li, M.C. Kuşhan, The rheology of shear thickening fluids with various ceramic particle additives. Mater. Des. **104**, 312–319 (2016)
49. W. Huang, Y. Wu, L. Qiu, C. Dong, J. Ding, D. Li, Tuning rheological performance of silica concentrated shear thickening fluid by using graphene oxide. Adv. Condens Matter Phys. **2015**, 734250 (2015)
50. P. Passey, M. Singh, S.K. Verma, D. Bhattacharya, R. Mehta, Steady shear and dynamic strain thickening of halloysite nanotubes and fumed silica shear thickening composite. J. Polym. Eng. **38**(10), 915–923 (2018. [Internet, cited 2022 Aug 9]). https://doi.org/10.1515/polyeng-2018-0043/html
51. A. Laha, A. Majumdar, Shear thickening fluids using silica-halloysite nanotubes to improve the impact resistance of p-aramid fabrics. Appl. Clay Sci. **132–133**, 468–474 (2016)

52. H. Barthel, Surface interactions of dimethylsiloxy group-modified fumed silica. Colloids Surf. A Physicochem. Eng. Asp. **101**(2–3), 217–226 (1995)
53. X. Sha, K. Yu, H. Cao, K. Qian, Shear thickening behavior of nanoparticle suspensions with carbon nanofillers. J. Nanopart. Res. **15**(7), 1–11 (2013. [Internet, cited 2022 Jul 29]). https://doi.org/10.1007/s11051-013-1816-x
54. A. Ghosh, I. Chauhan, A. Majumdar, B.S. Butola, Influence of cellulose nanofibers on the rheological behavior of silica-based shear-thickening fluid. Cellulose **24**(10), 4163–4171 (2017)
55. L. Sun, J. Zhu, M. Wei, C. Zhang, Y. Song, P. Qi, Effect of zirconia nanoparticles on the rheological properties of silica-based shear thickening fluid. Mater Res. Express. **5**(5), 055705 (2018)
56. L. Sun, Y. Lv, M. Wei, H. Sun, J. Zhu, Shear thickening fluid based on silica with neodymium oxide nanoparticles. Bull. Mater. Sci. **43**(1), 1–6., [Internet] (2020). https://doi.org/10.1007/s12034-020-02134-2
57. M. Zabet, K. Trinh, H. Toghiani, T.E. Lacy, C.U. Pittman, S. Kundu, Anisotropic nanoparticles contributing to shear-thickening behavior of Fumed silica suspensions. ACS Omega **2**(12), 8877–8887 (2017. [Internet, cited 2022 Aug 15]). https://doi.org/10.1021/acsomega.7b01484
58. J. Ge, Z. Tan, W. Li, H. Zhang, The rheological properties of shear thickening fluid reinforced with SiC nanowires. Results Phys **7**, 3369–3372 (2017). https://doi.org/10.1016/j.rinp.2017.08.065. [Internet]

Chapter 4
Multi-Functional Systems Based on Shear Thickening Fluid

Xinglong Gong, Junshuo Zhang, and Shouhu Xuan

4.1 Introduction

Shear thickening fluids (STFs) are dense granular suspensions with a drastic increase in viscosity as shear rate or stress increases and exceeds the critical shear rate [1–4]. When the applied loading is released, the viscosity would return to its initial state reversibly. In recent years, a large number of studies have been carried out on studying the rheological properties of STF, and several shear thickening mechanisms, e.g., ordered-disorder transition [5, 6], hydrocluster mechanism [7–10], and contact force [11–13], have been proposed. Although there is no unified explanation about the shear thickening mechanism, the STFs have been widely used in engineering due to their unique mechanical properties.

As an excellent energy-absorbing material, the traditional STFs have been applied in various damping systems. Typically, it was expected to enhance the anti-impact properties of textile-based armor. Wagner's et al. [14] firstly developed STF-based body armor by impregnating STF with high performance fabrics. It was found that the bulletproof performance of Kevlar fabric could be significantly improved by introducing STFs [15–25]. STF also can be integrated into damping systems to optimize and improve the dynamic performance [26–31]. Moreover, STF has been used in medical equipment to provide protection against external physical shocks [32].

Besides the traditional shear rate–dependent mechanical behavior, some types of STFs have special properties, such as shear thickening effects increased with temperature [33, 34] or color changed in response to external forces [35], which demonstrate an application potential in multi-functional devices. By adding conductive

X. Gong · J. Zhang · S. Xuan (✉)
Department of Modern Mechanics, University of Science and Technology of China, Hefei, China
e-mail: xuansh@ustc.edu.cn

S. Gürgen (ed.), *Shear Thickening Fluid*,
https://doi.org/10.1007/978-3-031-25717-9_4

materials, such as carbon nanotubes, carbon black, and graphene, or using ionic liquids [36] as dispersants [37–41], the STF not only exhibits an enhanced shear thickening performance but also possesses typical electrical conductivity. Therefore, the conductive STFs show sensing function and can be further applied in wearable devices. As a result, the multi-functional STFs exhibit wide potential in smart devices and structures by improving the mechanical and electrical properties of smart structures [42, 43]. In this chapter, a detailed overview of STF applications is given after a brief introduction to the multi-functional STF.

4.2 Multi-Functional STF

The shear thickening performance of STF is directly associated with the function and properties of dispersed phase and dispersed medium. Moreover, the additives also affect the rheological behavior of STF. Therefore, by adjusting the dispersed particles and carrier liquid, or using additives, STF can be endowed with multi-field coupling performance, such as force-thermal, force-optical, and force-electric coupling properties.

4.2.1 Traditional STF

The traditional STFs are prepared by dispersing uniform particles into disperse phase. The properties of STF are highly dependent on the dispersed phase, the dispersed media, and the additives. The rheology of STF is dramatically affected by the dispersed phase, such as volume fraction, particle size, size distribution, shape, and surface chemistry properties [44–47].

The dispersed phases used in shear thickening studies generally fall into two categories. The first category is inorganic particles, including clay, limestone, quartz powder, iron oxide pigment, silica, etc. [48–52]. The second category is organic particles, including cornstarch particles, polyvinyl chloride (PVC), polystyrene ethyl acrylonitrile (PS-AN), polystyrene (PSt), polymethyl methacrylate (PMMA), polystyrene ethyl acrylate (PST-EA), etc. [53–57].

Besides these factors itself, additive particles also exhibit a great influence on shear thickening mechanism. Various research teams carried out intensive works on shear thickening behavior by adding additive particles to the suspension [58–62]. Yang et al. [45] studied the pH-dependent rheological properties of titanium dioxide mixtures by adding HNO_3 or NaOH to change the particle surface charge. Gürgen et al. [58] added ceramic particles to silicon-based STF and found that ceramic particles in STF would reduce the shear thickening performance of STF, and the degree of reduction depended on the amount of additives and particle size, etc.

Ye et al. [62] studied the effect of surfactants on shear thickening behavior of STF by adding cationic, anionic, nonionic, and zwitterionic surfactants into STF. The results show that the surfactant affects the shear thickening rheology by altering the inter-particle and surface forces.

4.2.2 STF with Force-Thermal Coupling Characteristics

Shear thickening phenomenon is depended on fluid lubrication, frictional contact between particles, hydrogen bonding between particles and dispersed media. Generally, the shear thickening effect of STF decreases with increasing temperature [63–66]. However, by modifying the surface of dispersed particles or adding additives, the force between particles changes so that the shear thickening effect can be enhanced with the increase of temperature. Hsu et al. [33] prepared a silica colloid with different surface roughness at different temperatures. As shown in Fig. 4.1, the

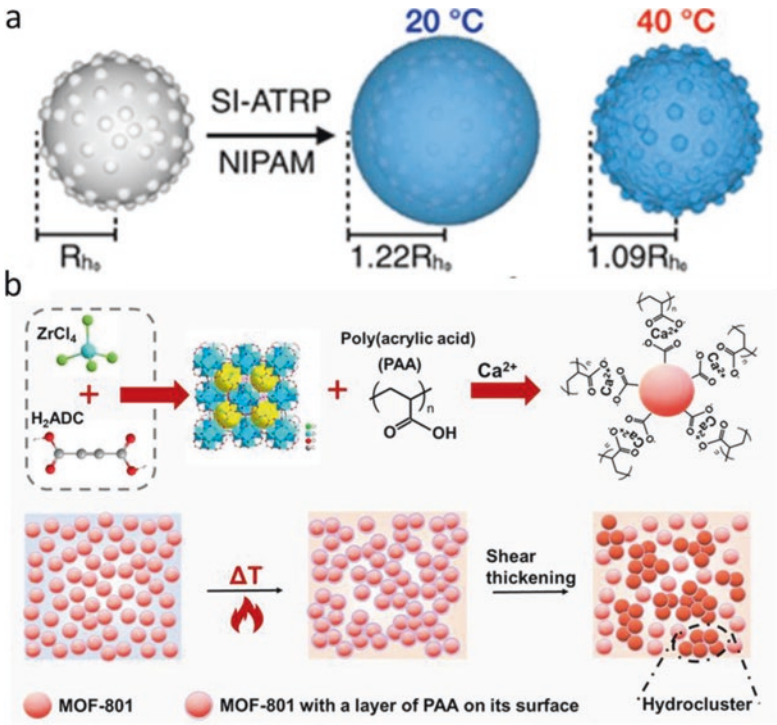

Fig. 4.1 (**a**) Schematics of the PNIPAM-grafted rough (RB) particles at 20 °C and 40 °C [33]. (**b**) Schematic diagram of M-STF shear thickening effect enhancement [34]. Reprinted by permission from Elsevier

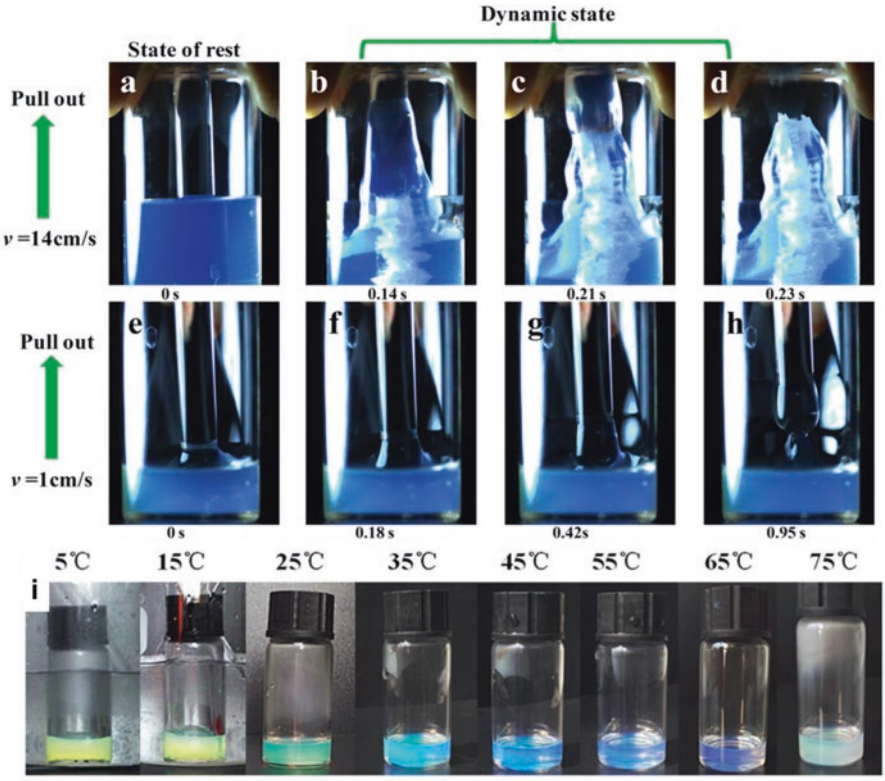

Fig. 4.2 The photographs taken when the glass bar was pulled out from the c-STF using fast speed (**a**–**d**) and low speed (**e**–**h**). (**i**) Photographs of the color changes in c-STF (the average diameter of SiO_2 nanospheres was about 200 nm) with the temperature changing [35]. Reprinted by permission from IOP Publishing

surface roughness of PNIPAM particles at 40 °C is greater than that at 20 °C. As a result, the shear thickening effect of STF prepared by PNIPAM particles at 40 °C is higher than that at 20 °C. Recently, Wu et al. [34] reported a new MOF-801-based STF with better thickening effect at high temperature based on the thermal resistance mechanism of thermophilic proteins (Fig. 4.2). MOF-801, which is rich in carboxyl groups on the surface, was used as the dispersed phase and added into the polyethylene glycol (PEG). By introducing polyacrylic acid (PAA) and Ca^{2+} into the dispersed medium, the hydrogen bonding, which is the internal force for the conventional STF, was replaced with the ionic and hydrophobic interactions. As a result, a novel MOF-801-based STF (M-STF) with enhanced shear thickening properties was developed at elevated temperature for the first time.

4.2.3 STF with Force-Optical Coupling Characteristics

Photonic crystals have become one of the most representative color materials because of their long-range ordered periodic microstructures. However, the color variation depends largely on the angle of view. [67, 68]. SiO_2 nanospheres can be synthesized by the Stöber hydrolysis technique [69–71], which is the most commonly used material for preparing STF, and it is also a photonic crystal material. However, in most cases, the polydispersity index (PDI) of SiO_2 nanospheres is not sufficiently small, and the surface chemical properties and refractive indexes of the SiO_2 are different from carrier fluid, which results in the opacity of STF.

Liu et al. [35] obtained SiO_2 nanospheres with PDI within 5% by controlling experimental conditions. Importantly, the SiO_2 was only cleaned with ethanol and the surface contained rich ethanol hydroxyl, which had good compatibility with PEG 200. In addition, the SiO_2 and PEG200 should have the same refractive index. As a result, the semitransparent and colorful STFs were obtained and the color of STF was related to the size and amount of SiO_2 particles. STF with different colors (c-STF) could be obtained by controlling the size and volume fraction of SiO_2 particles. Interestingly, the c-STF also changed its color under external loads. When the glass rod was pulled quickly (Fig. 4.2b-c) from the c-STF, the color changed from the initial translucent blue (Fig. 4.2a) to white. However, when the external influence was mild, there was no significant state and color change. The c-STF also showed different colors at different temperatures (Fig. 4.2i). Clearly, the ability to change color under different conditions endowed the STF with wide potential application in multi-functional soft armor defense materials.

4.2.4 STF with Force-Electric Coupling Characteristics

The CNTs exhibit great electrical conductivity, mechanical properties, and low density characteristics, and thus they are ideal nano-additives to reinforce and functionalize conventional materials [72–76]. By introducing CNTs into the dispersion, the conductive STF is obtained. In addition, as the networks formed by CNT restrict the particle motions, the thickening effect is enhanced [39–41]. The homogeneously dispersed CNTs within the SiO_2-based STF can be assembled to create conductive paths, thereby presenting typical electrical conductivity [77–79]. Therefore, it shows high potential in the field of wearable devices.

Moreover, the ionic liquid has a good chemical stability, thermal stability, low volatility, and electrical conductivity. It is suitable as a dispersed medium to fabricate high-performance STF with unique mechanic-conductive coupling performance. Qin et al. [36] used four ionic liquids, 1-Butyl-3-Methylimidazolium Tetraf luoroborate, 1-Butylpyridinium Tetrafluoroborate, 1-Butyl-3-Methylimidazolium Hexafluorophosphate, 1-Ethoxyl-3-Methylimidazolium Tetrafluoroborate, as the

dispersion medium to prepare a new type of shear thickening fluid. The electrical conductivity of STF was suppressed by including more silica microsphere in the suspension. When the concentration of silicon microsphere was 64%, the electrical conductivity of STF was about 2500 μS/cm (Fig. 4.5j). This kind of shear thickening fluid has a clearer shear thickening effect and has an excellent electric conductivity and thermal stability. It can be further interpreted into the Kevlar fabric and thus the smart body armor is developed.

4.3 Applications of the Multi-Functional STF Systems

In addition to the development of multi-functional STFs, STFs are also used as reinforcement materials for multi-functional systems. For example, the STFs can be used in lithium batteries, supercapacitors, motion sensors, and triboelectric nanogenerator (TENG) devices to improve the mechanical and electrical properties of smart structures.

4.3.1 Shear Thickened Electrolyte

Lithium ion batteries have been developed for several engineering applications ranging from biomedical devices to new energy vehicles [81–88]. Currently, commercial lithium ion batteries mostly use flammable electrolytes such as ethylene carbonate, propylene carbonate, and dimethyl carbonate [89–91]. However, when the electrolytes receive an impact damage, they may show spontaneous thermal reactions, fires, and explosions. Therefore, it is very important to enhance the impact resistance of electrolyte.

By adding fumed silica nanoparticles to a commercial electrolyte (1 M $LiFP_6$ in EC/DMC), Ding et al. [92] developed a multi-functional fluid with thickening properties that provide impact protection inherent to lithium ion batteries while serving as a highly conductive electrolyte in lithium-ion batteries. Typically, the conductivity of the STF electrolytes was higher compared to commercial electrolytes. As shown in Fig. 4.3a, the maximum conductivity increase for 1 M $LiPF_6$ in EC/DMC (1:1) is observed for the STF having a silica loading of 10.7 wt.%, with the value of $1.93 \times 10^{-2}\ \Omega^{-1}\ cm^{-1}$, which was greatly higher than the commercial electrolyte with no addition of fumed silica ($2 \times 10^{-3}\ \Omega^{-1}\ cm^{-1}$).

Furthermore, lithium-ion batteries using STF electrolytes provide enhanced capacity at high charge and discharge rates, and the batteries using STF electrolytes maintain their electrochemical capacity after successive impact conditions. As shown in Fig. 4.3b, lithium-ion batteries using STF electrolytes can withstand a shock energy up to 0.568 J, which is higher than 0.426 J that can be safely tolerated by lithium-ion batteries with normal electrolyte. Figure 4.3c-e shows the protective mechanism of STF electrolyte under impact conditions. It is seen that the silica

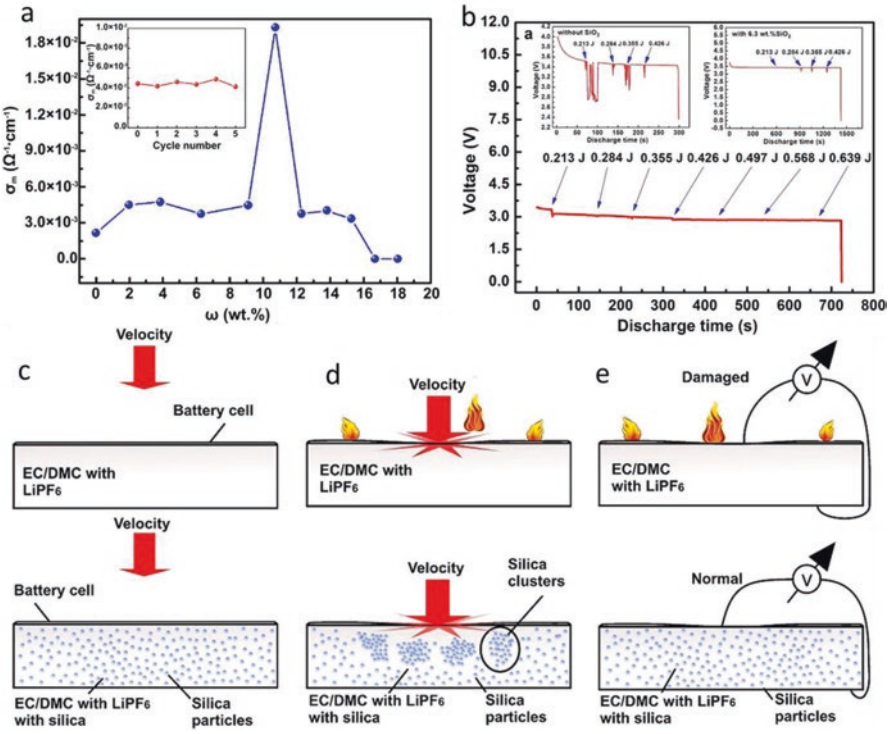

Fig. 4.3 (**a**) Room temperature variation of ionic conductivity of composite electrolytes (SiO_2/$LiPF_6$ in EC/DMC) versus weight fraction (ω) of fumed silica. Inset: Ionic conductivity of composite electrolyte with 9.1 wt.% SiO_2 after impact tests. (**b**) Discharge curve of $LiFePO_4$ electrode in the STF electrolyte of EC/DMC/$LiPF_6$ with 9.1 wt.% SiO_2. Impacts with different energies were applied to the cell during the discharge. For comparison, the discharge curves of $LiFePO_4$ electrode in bare EC/DMC/$LiPF_6$ electrolyte and composite electrolyte of EC/DMC/$LiPF_6$ with 6.3 wt.% SiO_2 (showing shear thinning effect) are also shown in the inset of (**b**). (**c**–**e**) Schematic representation of the protective mechanism of STF electrolyte [92]. Under the Creative Commons license

particles enhance the ionic conductivity due to their mutual repulsion. When the electrolyte is impacted, the silica nanoparticles overcome the inter-particle repulsive force and aggregate in the electrolyte, causing the electrolyte to be solid and show typical shear thickening phenomenon, resulting in the increase of suspension viscosity. Hooke's model proposes that the increase in viscosity slows down the energy dissipation due to the basic function of restoring force. The overall effect of this phenomenon is to slow down the rise in electrolyte temperature after impact and effectively increase the stiffness of the battery. Conversely, battery systems without shear thickening function are prone to undergo large deformations and a quick jump in temperature during the impact, igniting the solvent.

Liu et al. [93] developed an electrochemically stable shear thickening electrolyte to enhance the protection of LIBs. The electrolyte was designed by the integration of (3-aminopropyl)triethoxysilane (APTES) modified glass fiber additives and

typical liquid electrolyte. Compared with conventional electrolytes, shear thickening electrolytes behaved as solid materials on impact, preventing bullets from penetrating them. The half cells with STF electrolytes showed great cyclability, in which the capacity retention rate of STF electrolytes half battery was 95.2% after 500 cycles, while the capacity retention rate of conventional electrolytes half battery was 61.1% after 500 cycles. This phenomenon was most likely due to the functionalized glass fibers (mGFs) in STF electrolyte, which may be attributed to form torturous structure and slow down lithium dendrite growth. In order to further evaluate the impact resistance of STF electrolytes in the battery, the LFP-LTO bag battery with STF electrolytes was prepared. A steel ball was impacted on the bagged battery and the open-circuit voltage (OCV) of the bagged battery was tracked in real time. The voltage of the cell with the STF electrolytes was more stable than that of the bag cell with the conventional electrolytes. The impact test of the battery showed that the impact resistant battery can be realized by using STF electrolytes.

Recently, Wu et al. [94] developed an STF-filled organic gel electrolytes (PVA/STF) to prepare STF-enhanced supercapacitor (SSC). Due to the shear thickening rheology, the enhancement of SiO_2, and the hydrogen bonding in the PVA matrix, PVA/STF dissipates a large amount of energy during the impact process.

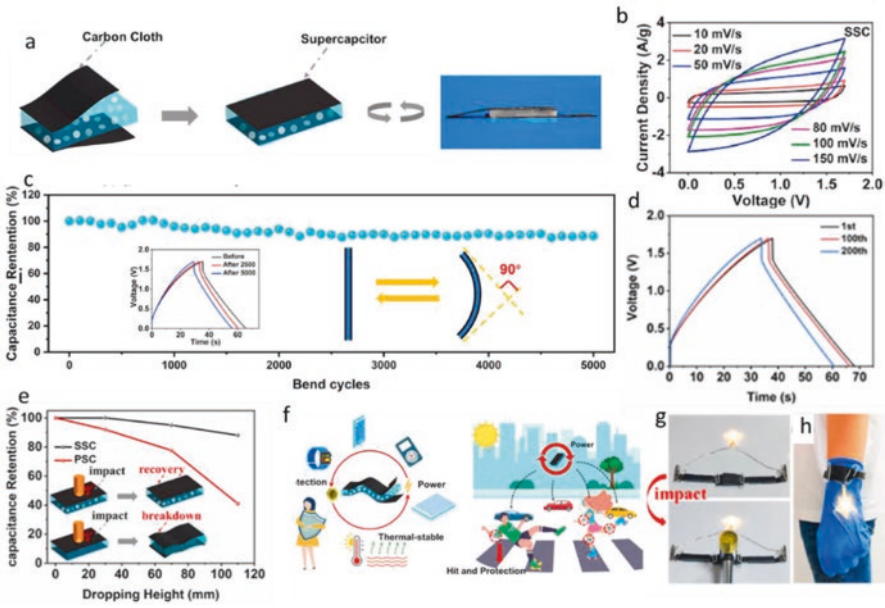

Fig. 4.4 (**a**) Schematic diagram and photograph of SSC. (**b**) CV curves of SSC. (**c**) Capacitance stability of the SSC after a number of bending cycles. (**d**) Capacitance stability of the SSC after a number of compression cycles. (**e**) Capacitance retention of SSC and PSC after different collisions. Insets: schematic diagram of SSC and PSC under impact. (**f**) Practical applications of SSC in daily life. (**g**) Photographs of the circuit with three SSCs before and after impact. A wearable wristband composed of three SSCs is used as (**h**) an energy storage device [94]. Reprinted by permission from Elsevier

Figure 4.4a shows the manufacturing steps for SSC, which is obtained by sandwiching PVA/STF between two carbon cloth clips. The voltage window of the SSC is extended to 1.7 V (Fig. 4.4b), almost twice that of a traditional hydrogel-based supercapacitor. SSC also has good bending and compression cycle stability. After bending to 90° for 5000 times, only 11% specific capacitance attenuation is observed (Fig. 4.4c). After 200 compression cycles, it still retains 90% capacitance (Fig. 4.4d). In addition, SSC has a good environmental stability and thermal stability. Due to the excellent impact resistance of the PVA/STF, the SSC maintains its integrity after impact with minimal capacitance loss. When the hammer drop height is 110 mm, the capacitance loss of SSC is only 12%, while the loss of ordinary hydrogel capacitor is 59% (Fig. 4.4e), illustrating the good capacitance retention of SSC. According to the results, SSC can be employed as a power source while providing flexible body protection (Fig. 4.4f). In addition, the SSC can be bent into a wristband as a wearable energy storage device (Fig. 4.4g-h). It can also protect humans from shock excitation. Therefore, SSC with good energy storage performance, high flexibility, and excellent mechanical properties shows broad application prospects in wearable devices, new power supplies, and protective structures.

4.3.2 Wearable Devices with STF

Nowadays, flexible sensors have attracted great attention due to their wide range of applications in wearable devices [95–97]. Flexible sensors can be applied to electronic skin, touch sensing, health motion detection, soft robots, etc. [98–104]. In addition, the STF has been applied in flexible sensors to improve the mechanical and electrical properties. In this case, Liu et al. [80] reported on a CNT-/STF-/Kevlar-based wearable electronic textile (ET) with sensing capabilities and protective properties. The yarn pull-out and stab resistance tests showed that the anti-impact performance of this material is improved due to the STF and CNT fillers. Compared to the neat textiles, the ET composite exhibited two times larger in peak impact force and 50% increment in the stab resistance. This indicates that the ET composite can be efficiently used under energy absorbing and anti-impact conditions. ET is conductive due to CNT addition into the composite material, and thus the prepared ET not only has an excellent protection performance but also shows excellent sensing characteristics. Figure 4.5a-b shows a conductive circuit consisting of ET fabric, LED bulb, and battery. When the circuit is connected, the LED bulb lights up, proving that the ET has a good electrical conductivity. Figure 4.5c-e shows the change in normalized resistance during the cyclic bending test. The results showed that the response signals under different bending angles and frequencies are distinguishable and stable after repeated cycles. Due to its high sensitivity to deformation, flexible ET can be used to monitor human movement. As shown in Fig. 4.5f-g, ET can clearly identify the movements of fingers and elbow joints, indicating that ET sensors have the potential to be applied to detect various movements of human or robot bodies. Figure 4.5h-i shows the sensing mechanism of ET. When

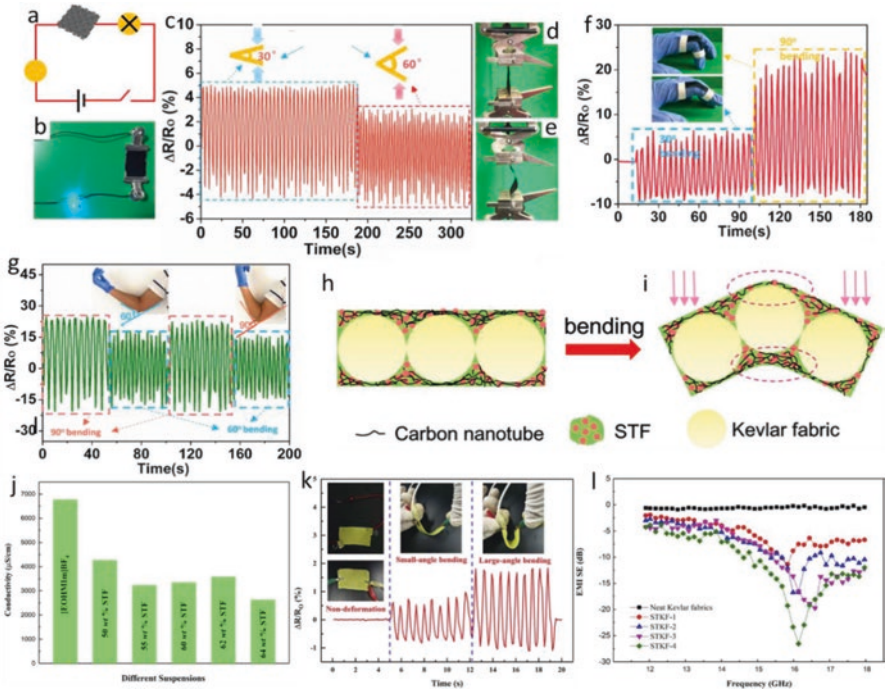

Fig. 4.5 Illustration (**a**) and photograph (**b**) of a conductive circuit composed of the ET fabric, an LED bulb, and a cell. Normalized resistance changes ($\Delta R/R_0$) of the ET sensor during a cyclic bending test (**c**). Photographs of the ET sensor on a steel clamp that undergoes a bending test (**d** and **e**). Relative normalized resistance change of the ET in monitoring movements of finger (**f**) and elbow at different angels (**g**). The illustration of partial magnification of the cross section of the yarns of the CNT/STF/Kevlar composite (**h** and **i**) [80]. (**j**) Conductivity for [EOHMIm] [BF_4] STFs with different concentrations of silica microsphere. (**k**) Normalized electrical resistance versus time for the STKF-3 during different bending circles and static non-deformation, respectively. (**l**) EMI SE dependencies of frequency for the STKF and the neat Kevlar fabric [36]. Reprinted by permission from Elsevier

CNT/STF/Kevlar composites are bent by external forces, some parts of CNT conductive paths are destroyed. In addition, when ET returns to its original shape, the conductive path also quickly recovers by the effect of fluidity. Therefore, the conductivity of ET sensor has a significant repeatability under external stimuli.

Qin et al. [36] developed a soft armor material (STKF) which is constructed by high-performance textiles treated with a recently developed STF composed of silica microsphere and ionic liquids (ILs). Besides the resistance to external loading, the STKF exhibits a stable electrical conductivity and high sensitivity to the applied deformation, which can be used to monitor the human body motions. The ILs are used as dispersion medium to prepare STF with a high electrical conductivity. As shown in Fig. 4.5k, the LED bulb is lighted up in a circuit composed of STKF, proving the conductivity of STKF. At the same time, the resistance of STKF is highly sensitive to the applied deformation, which provides an opportunity to develop new

types of armor with excellent protection and intelligent wearable characteristics. In addition, due to the good electrical conductivity of STKF, it has a certain EMI SE level, which can reach 27 dB near the 16 GHz frequency (Fig. 4.5l).

Zhang et al. [42] designed a novel STF/Ecoflex composite by encapsulating STF in Ecoflex-0030. The compression and drop tests proved that STF/Ecoflex composite has excellent impact resistance, and the increase in the STF amount is helpful to enhance the anti-impact behavior of the composite. The STF can be conductive by including CNTs into the suspension. Therefore, conductive STF/Ecoflex (C-STF/Ecoflex) with sensing properties under different conditions is designed by including CNTs into the STF. As shown in Fig. 4.6a, the electrical response of C-STF/Ecoflex becomes apparent as the compression displacement increases. In addition, C-STF/Ecoflex can respond to the impact signals in time under impact conditions (Fig. 4.6b), and its resistance that changes under impact conditions is directly related to the impact energy (Fig. 4.6c), indicating that C-STF/Ecoflex has the potential to be used as a sensor with protective capabilities under impact conditions. Then, the wearable multi-functional protective suit C-STF/Ecoflex/Kevlar is developed by

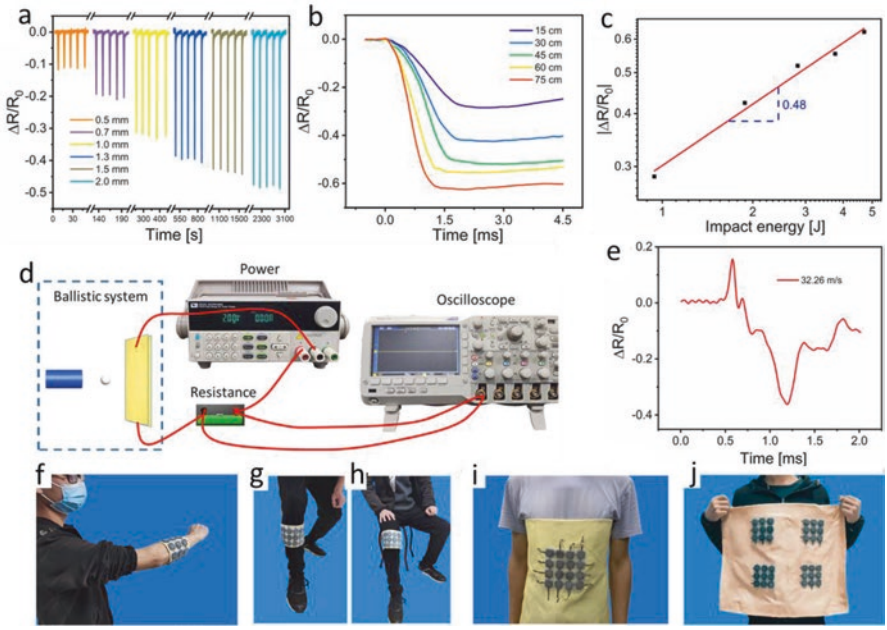

Fig. 4.6 (**a**) Resistance change rate under different compression displacements. (**b**) The $\Delta R/R_0$vs. time curves when the hammerhead fell from different heights. (**c**) The fitting curve of $|\Delta R/R_0|$ with impact energy in the logarithmic coordinate system. (**d**) Schematic of the system for recording the variation of C-STF/Kevlar resistance during the high-speed impact. (**e**) The curves of the resistance signal of C-STF/Kevlar under 32.26 m/s. Shape programmable photographs of C-STF/Ecoflex/Kevlar device: (**f**) worn on arm, (**g**) worn on leg, (**h**) worn on knee, (**i**) the overlying one provided higher protection effect, and (**j**) the arrays were integrated into one pad with larger protection area [42]. Reprinted by permission from Elsevier

combining C-STF/Ecoflex and Kevlar. Ballistic impact tests show that C-STF/Ecoflex/Kevlar can sense the impact behavior of projectiles (Fig. 4.6d-e). In addition, C-STF/Ecoflex/Kevlar is flexible and lightweight, which can be comfortably worn on people's arms (Fig. 4.6f), legs (Fig. 4.6g), knees (Fig. 4.6h), and waist (Fig. 4.6i). By bringing the four arrays together (Fig. 4.6j), a large scale area can be obtained. Therefore, C-STF/Ecoflex/Kevlar can be used as an intelligent wearable device with protective characteristics.

4.3.3 TENG Based on STF

More wearable electronic devices have been developed for daily life use. A battery is required to supply power to the wearable devices; however, the need of charge or replace of the power unit has been a challenging issue, apart from their heavy structures [105]. For this reason, triboelectric nanogenerators (TENGs) have been rising as a promising energy conversion device due to a list of advantages such as lightweight, easy fabrication, and low cost [106–113]. However, in order to obtain energy, TENG needs to maintain various mechanical excitation for a long time, such as compression, distortion, and friction, which is easy to damage the TENG equipment. Because of its unique shear thickening properties, the introduction of STF into TENG equipment is expected to enhance the structural durability and impact resistance of TENG equipment.

Wang et al. [43] developed a multi-mode energy-harvesting and safeguarding STF-based TENG (Fig. 4.7a-e). The TENG exhibits a high-energy harvesting effect in which the maximum power density is about 27.05 mW/m^2 under compression. As STF flows into the TENG, it rubs against the polymer, causing electron conversion and output current (Fig. 4.7f-h). Therefore, this portable TENG shows the potential of perceiving human movement due to the difference in amplitude and frequency of movement during human moving. In addition, the Ecoflex/CI housing can be magnetically driven to deform, collecting mechanical energy and outputting voltage signals during deforming (Fig. 4.7i). Because of the shear thickening property of STF, the TENG has a good protective performance. A drop hammer test is used to investigate the protective properties of TENG. Figure 4.7j shows that TENG has the lowest impact force. In addition, the TENG output voltage increases with the increase of impact height (Fig. 4.7k). These results indicate that TENG can be used as a protective self-supplied power sensor. Here, a TENG-based human hand array is developed (Fig. 4.7l). TENGs are able to detect bending excitation (Fig. 4.7m-n), and they can detect pressure in real time for finger bending, grasping ring boxes and apples. In addition, the wearable Kevlar/TENG composite fabric has been developed (Fig. 4.7o). The Kevlar/TENG composite with wearable shape adaptability has self-powered characteristics and protective effects, which can be used as intelligent clothing in the fields of robotics, human-computer interaction, healthcare, and protection. In conclusion, the STF-based TENG exhibits significant potentials in power sources, healthcare, smart systems, and safeguards.

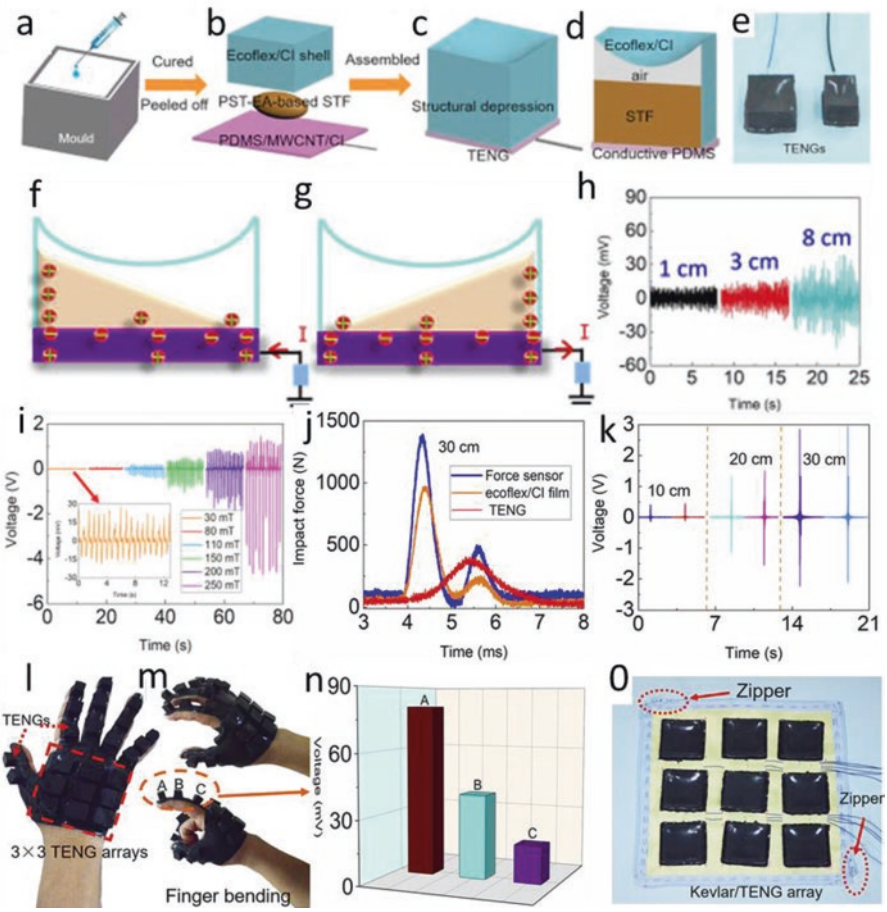

Fig. 4.7 (**a**) Preparation procedures of the TENG device: uncured Ecoflex/CI were dropped on the mold, (**b**, **c**, **e**) STF, Ecoflex/CI, and PDMS/MWCNT/CI were assembled and cured into TENG, (**d**) schematic of the components of TENG. (**f**, **g**) Electrons transferred during STF flowing process and (**h**) the corresponding voltages. (**i**) Magnetic-dependent triboelectric performance. (**j**) Representative force curves comparison of TENG, Ecoflex/CI, and force sensor impacted from 30 cm height. (**k**) The corresponding triboelectric voltages of TENG during loading process. (**l**) A TENG-based hand array, human gesture sensing performance of the device: (**m**) index finger bending and (**n**) the corresponding maximum voltages. (**o**) The wearable Kevlar/TENG array [43]. Reprinted by permission from Elsevier

Yun et al. [114] developed an STF-TENG benefitting from the shear thickening rheology (Fig. 4.8a). The STF-based TENG shows an inherent anti-impact performance, which is tested by dropping a steel ball on the device dropped from different heights. Durability tests for contact separation are also carried out and the output voltage does not decrease up to 102,600 cycles, indicating structural reliability and long-term durability of the STF-based TENG. An STF-TENG is able to monitor the

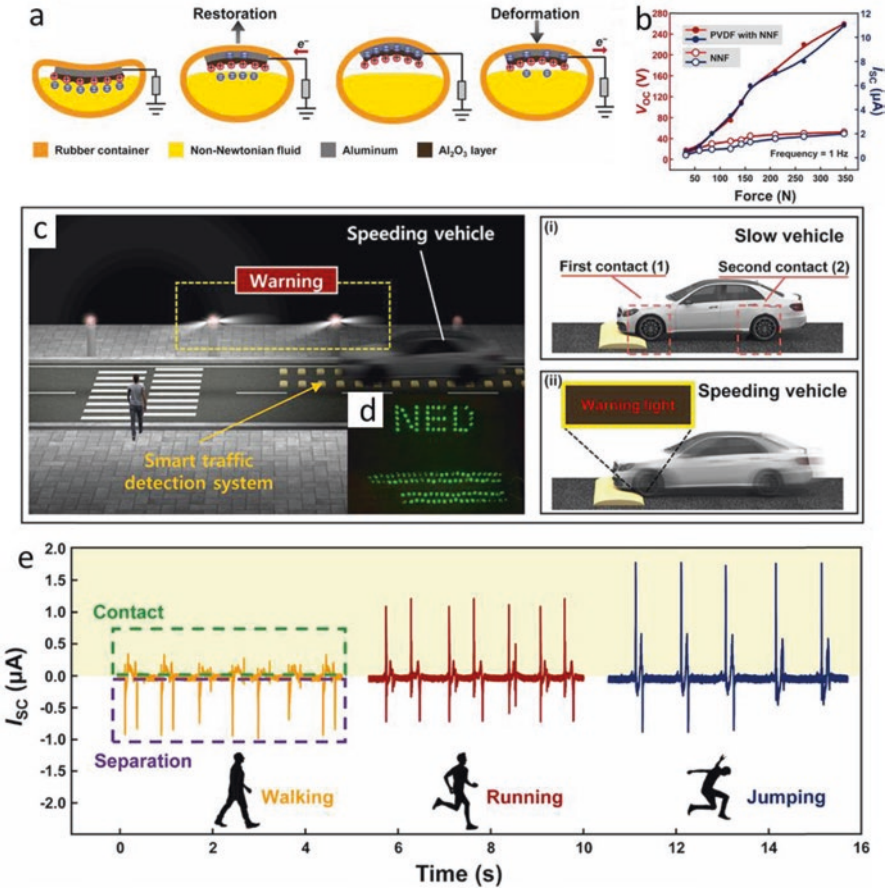

Fig. 4.8 (**a**) Working mechanism of the proposed NNFT. (**b**) Electrical output generated from the NNFT-P with the various applied forces. (**c**) The schematic illustration of the proposed NSTDS and its working mechanism. (**d**) Photograph of the simultaneously turning 126 LEDs on using the electricity generated from the NNFT-P. (**e**) The electrical output according to walking, running, and jumping acquired from the NNFT-P [115]. Reprinted by permission from Elsevier

daily human movements such as finger sliding, touching, bending, hand shaking, knee bending, ankle bending, elbow bending, and hand tapping. These characteristics exhibit the potential of the STF-based TENG as a self-powered multi-functional device. Finally, STF-TENG can be used as an impact monitoring system connected to a smartphone that provided a warning upon receiving a strong pulse on the device.

Recently, Kim et al. [115] fabricated triboelectric nanogenerator (NNFT) using the non-Newtonian fluid (NNF) with shear thickening rheology. The prepared NNFT was operated in a single-electrode mode, consisting of cornstarch and

water-based suspension, aluminum electrode, and rubber container, respectively. The operating mechanism of the system is depicted in Fig. 4.8a. When the WAO-treated aluminum electrode is taken out from the STF for the rubber container restoration, the balanced state of the electrical equilibrium is disrupted due to the negative charge effect on the STF surface. For this reason, the electrons flow to the WAO-treated aluminum electrode from the ground to establish an electrical equilibrium between the Al_2O_3 layer and WAO-treated aluminum electrode. Upon completing the restoration, the electrical equilibrium is restored. By applying the external loading again, the negative charge effect appears on the WAO-treated aluminum electrode while the electrons are flowing from the WAO-treated aluminum electrode to the ground for retaining the electrical equilibrium. Consequently, the AC electricity is generated from the NNFT. The PVDF, which has a chemical formula of $(C_2H_2F_2)_n$, can enhance the triboelectricity due to the rich fluorine content in the PVDF. The NNFT-P with stronger friction point effect is obtained by mixing the STF with PVDF. Compared with the electrical output generated from the NNFT, the NNFT-P is enhanced by 5.41 times for the V_{OC} while the increase is about 5.6 times for the I_{SC} (Fig. 4.8b). Finally, a self-powered traffic detection system (NSTDS) based on NNFT-P is developed, which alerts the pedestrians to the danger (Fig. 4.8c-d). In addition, the developed NNFT-P can be employed as a sensor for motion detection such as walking, running, and jumping on the road (Fig. 4.8e).

Wang et al. [116] fabricated a textile-based TENG by including STF, graphene, and SSG with high performance fabrics. The TENG shows excellent energy-harvesting capabilities. The triboelectric properties of the TENG are investigated with an oscillator system. The effect of load amplitude and frequency on triboelectric performance is studied. As the force increases, the electrical signal increases (Fig. 4.9a). This is mainly due to the increased contact interface between the TENG and PMMA. Afterward, the corresponding voltage signals of TENG at different input frequencies are given in Fig. 4.9b, exhibiting a similar growing trend. This increase is caused by the reduction of separation time and the accumulation of more generated charges on the electrodes. The TENG shows a quite good electrical stability in one thousand loading and unloading excitation cycles (Fig. 4.9c). As a power unit, the TENG effectively provides a power for lightening up the LED array (Fig. 4.9d). It can also charge the commercial capacitors through rectifier circuits (Fig. 4.9e-f). The TENG shows enhanced protection properties under impact loadings. On the other side, the TENG can produce voltage signals due to the self-powered sensing effect (Fig. 4.9g). The negative peak voltage increases with the increase of descending height. In summary, the TENG not only shows a good impact resistance but also has a self-supplied power sensing performance at low-velocity impact conditions. In addition, the impact protection performance of the TENG under high-velocity impact is further studied. The toy in the pristine textile suit is completely penetrated, causing serious injuries. Instead, the bullet is effectively stopped by the TENG-based textile suit (Fig. 4.9h). This result proves that the ready

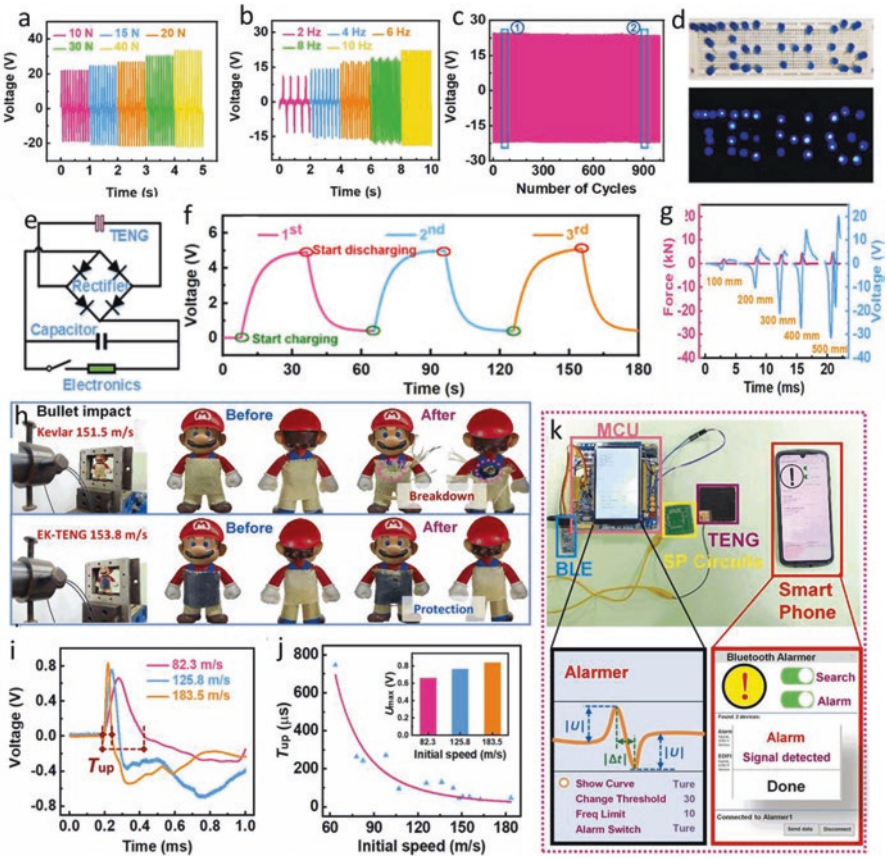

Fig. 4.9 (**a**) Force-dependent output voltages at 10 Hz. (**b**) Frequency-dependent output voltages at 10 N. (**c**) Cycling stability of TENG at 10 MΩ. (**d**) TENG-harvested mechanical energy and lit up LEDs. (**e**) Rectifier circuit diagram for charging the capacitors. (**f**) The cycle charge-discharge curves of 0.47 μF capacitor by TENG at 40 N and 10 Hz. (**g**) The impact force and voltage vs. time with impactor dropping from 100 to 500 mm. (**h**) The scenario of safeguarding properties of TENG-based suit under high-speed shooting. (**i**) Voltage signals of TENG generated by the bullet impacts with 82.3, 125.8 and 183.5 m/s. (**j**) Impact velocity-dependent voltage positive peak duration time and maximum positive voltage. (**k**) The sensing system contained TENG-based Bluetooth and the interface of microcontroller and smartphone [116]. Reprinted by permission from Elsevier

TENG is able to prevent high-velocity impact damages. It is seen that the increase in the impact velocity leads to a rise in the peak voltage, while the duration of the positive voltage (T_{up}) also shows a significant reduction (Fig. 4.9j). The results indicate that the TENG has also good self-powered sensing capabilities under high-velocity impact. At the end, a TENG-based wireless passive sensor alarm system is developed, which is able to detect various kinds of impacting threats (Fig. 4.9k).

4.4 Conclusions

The unique mechanical properties of STFs provide important applications in a wide range of engineering and scientific fields. In this chapter, multi-function STF and multi-function system based on STF are discussed. According to the previous section, the STF can obtain the ability of multi-physical field coupling by changing the morphology, roughness, and surface characteristics of dispersed phase particles, or by adding additives. The force-thermal-coupled STF can change the shear thickening effect of STF by adjusting the temperature, which expands the application fields of STF. The color of the force-optical-coupled STF reflects the magnitude of the applied load, and the ability to change color under different conditions provides a wide range of potential applications for the STF in multi-functional soft armor defense materials. Moreover, STF with force-electric coupling characteristics shows high potential in the field of wearable protective devices.

Due to the special characteristics of STF, it can be used in different multi-functional devices. The STF-based electrolyte significantly improves the impact resistance and electrochemical stability of lithium batteries and supercapacitors, confirming its applicability to protect lithium ion batteries and supercapacitors from severe shocks. Nowadays, flexible sensors based on STF have been used in human motion detection and impact monitoring. Due to the high sensitivity, advanced impact resistance, and good flexibility, it is an important candidate for developing the next generation of sensors with protective properties. TENG is considered to be a promising energy conversion device because of its simplicity, lightweight, and low cost. The introduction of STF into TENG equipment enhances the structural durability and impact resistance of TENG equipment. Hence, smart STF fabrication with unique rheological and multi-field coupling properties, or design of multi-functional systems based on STF, proposes a broad application prospect in different engineering and scientific fields.

References

1. W.H. Boersma, J. Laven, H.N. Stein, Shear thickening (dilatancy) in concentrated dispersions. AICHE J. **36**, 321–332 (1990)
2. Y.S. Lee, N.J. Wagner, Rheological properties and small-angle neutron scattering of a shear thickening, nanoparticle dispersion at high shear rates. Ind. Eng. Chem. Res. **45**, 7015–7024 (2006)
3. N.J. Wagner, J.F. Brady, Shear thickening in colloidal dispersions. Phys. Today **62**, 27–32 (2009)
4. Y.S. Lee, N.J. Wagner, Dynamic properties of shear thickening colloidal suspensions. Rheol. Acta **42**, 199–208 (2003)
5. R. Hoffman, Discontinuous and dilatant viscosity behavior in concentrated suspensions. II. Theory and experimental tests. J. Colloid Interface Sci. **46**, 491–506 (1974)

6. H.M. Laun, R. Bung, S. Hess, W. Loose, O. Hess, K. Hahn, et al., Rheological and small-angle neutron-scattering investigation of shear-induced particle structures of concentrated polymer dispersions submitted to plane Poiseuille and Couette flow. J. Rheol. **36**, 743–787 (1992)
7. J.W. Bender, N.J. Wagner, Optical measurement of the contributions of colloidal forces to the rheology of concentrated suspensions. J. Colloid Interface Sci. **172**, 171–184 (1995)
8. J. Bender, N.J. Wagner, Reversible shear thickening in monodisperse and bidisperse colloidal dispersions. J. Rheol. **40**, 899–916 (1996)
9. T.N. Phung, J.F. Brady, G. Bossis, Stokesian dynamics simulation of Brownian suspensions. J. Fluid Mech. **313**, 181–207 (1996)
10. R. Farr, J.R. Melrose, R. Ball, Kinetic theory of jamming in hard-sphere startup flows. Phys. Rev. E **55**, 7203–7211 (1997)
11. N.Y. Lin, B.M. Guy, M. Hermes, C. Ness, J. Sun, W.C. Poon, et al., Hydrodynamic and contact contributions to continuous shear thickening in colloidal suspensions. Phys. Rev. Lett. **115**, 228304 (2015)
12. R.L. Hoffman, Explanations for the cause of shear thickening in concentrated colloidal suspensions. J. Rheol. **42**, 111–123 (1998)
13. E. Brown, H.M. Jaeger, The role of dilation and confining stresses in shear thickening of dense suspensions. J. Rheol. **56**, 875–923 (2012)
14. D.P. Kalman, R.L. Merrill, N.J. Wagner, E.D. Wetzel, Effect of particle hardness on the penetration behavior of fabrics intercalated with dry particles and concentrated particle-fluid suspensions. ACS Appl Mater Inter **1**(11), 2602–2612 (2009)
15. A. Laha, A. Majumdar, Shear thickening fluids using silica-halloysite nanotubes to improve the impact resistance of p-aramid fabrics. Appl. Clay Sci. **132**, 468–474 (2016)
16. S. Gürgen, M.C. Kuşhan, The stab resistance of fabrics impregnated with shear thickening fluids including various particle size of additives. Compos Part A-Appl S **94**, 50–60 (2017)
17. S. Gürgen, M.C. Kuşhan, The ballistic performance of aramid based fabrics impregnated with multi-phase shear thickening fluids. Polym. Test. **64**, 296–306 (2017)
18. S.S. Cao, Q. Chen, Y.P. Wang, S.H. Xuan, W.Q. Jiang, X.L. Gong, High strain-rate dynamic mechanical properties of Kevlar fabrics impregnated with shear thickening fluid. Compos Part A-Appl S **100**, 161–169 (2017)
19. S.S. Cao, H.M. Pang, C.Y. Zhao, S.H. Xuan, X.L. Gong, The CNT/PSt-EA/Kevlar composite with excellent ballistic performance. Compos Part B-Eng **180**, 107793 (2020)
20. J.S. Zhang, Y. Wang, J.Y. Zhou, C.Y. Zhao, Y.X. Wu, S. Liu, et al., Intralayer interfacial sliding effect on the anti-impact performance of STF/Kevlar composite fabric. Compos Part A-Appl S **145**, 106401 (2021)
21. Q. Wang, R. Sun, M. Yao, M. Chen, Y. Feng, The influence of temperature on inter-yarns fictional properties of shear thickening fluids treated Kevlar fabrics. Composer Part A Appl S **116**, 46–53 (2019)
22. M.R. Sheikhi, S. Gürgen, Anti-impact design of multi-layer composites enhanced by shear thickening fluid. Compos. Struct. **279**, 114797 (2022)
23. S. Gürgen, F.A. Fernandes, R.J. Sousa, M.C. Kushan, Development of eco-friendly shock absorbing cork composites enhanced by a non-Newtonian fluid. Appl. Compos. Mater. **28**(1), 165–179 (2021)
24. Z.H. Tan, W.H. Li, W. Huang, The effect of graphene on the yarn pull-out force and ballistic performance of Kevlar fabrics impregnated with shear thickening fluids. Smart Mater. Struct. **27**(7), 075048 (2018)
25. M. Lin, C. Lou, J. Lin, T. Lin, J. Lin, Mechanical property evaluations of flexible laminated composites reinforced by high-performance Kevlar filaments: Tensile strength, peel load, and static puncture resistance. Compos Part B-Eng **166**, 139–147 (2019)
26. C. Fischer, S. Braun, P. Bourban, V. Michaud, C. Plummer, J.E. Månson, Dynamic properties of sandwich structures with integrated shear-thickening fluids. Smart Mater. Struct. **15**, 1467 (2006)

27. X. Zhang, W. Li, X. Gong, The rheology of shear thickening fluid (STF) and the dynamic performance of an STF-filled damper. Smart Mater. Struct. **17**, 035027 (2008)
28. S. Gürgen, M.A. Sofuoglu, Smart polymer integrated cork composites for enhanced vibration damping properties. Compos. Struct. **258**, 113200 (2021)
29. S. Gürgen, M.A. Sofuoglu, Vibration attenuation of sandwich structures filled with shear thickening fluids. Compos Part B-Eng **186**, 107831 (2020)
30. S. Liu, X.W. Fan, F. Yuan, M. Sang, J.Y. Zhou, J.S. Zhang, et al., Enabling thermally enhanced vibration attenuation via biomimetic Zr-fumarate MOF-based shear thickening fluid. Compos Part B-Eng **239**, 109964 (2022)
31. F. Pinto, M. Meo, Design and manufacturing of a novel shear thickening fluid composite (STFC) with enhanced out-of-plane properties and damage suppression. Appl Compos Mater **24**, 643–660 (2017)
32. A. Haris, B. Goh, T. Tay, H. Lee, A. Rammohan, V. Tan, On the effectiveness of incorporating shear thickening fluid with fumed silica particles in hip protectors. Smart Mater. Struct. **27**, 015021 (2017)
33. C.P. Hsu, J. Mandal, S.N. Ramakrishna, N.D. Spencer, L. Isa, Exploring the roles of roughness, friction and adhesion in discontinuous shear thickening by means of thermo-responsive particles. Nat. Commun. **12**(1), 1477 (2021)
34. Y.X. Wu, W.H. Wang, J.S. Zhang, M. Sang, Y.Q. Xu, J.Y. Zhou, et al., Liquid or solid? A biologically inspired concentrated suspension for protective coating. Chem. Eng. J. **428**, 131793 (2022)
35. M. Liu, W.Q. Jiang, S. Wang, S.H. Xuan, L.F. Bai, M. Sang, et al., Shear thickening fluid with tunable structural colors. Smart Mater. Struct. **27**, 095012 (2018)
36. J.B. Qin, B.R. Guo, L. Zhang, T.W. Wang, G.C. Zhang, X.T. Shi, Soft armor materials constructed with Kevlar fabric and a novel shear thickening fluid. Compos Part B-Eng **183**, 107686 (2020)
37. K.L. White, H. Yao, X. Zhang, H.J. Sue, Rheology of electrostatically tethered nanoplatelets and multi-walled carbon nanotubes in epoxy. Polymer **84**, 223–233 (2016)
38. R.B. Ladani, S.Y. Wu, A.J. Kinloch, K. Ghorbani, J. Zhang, A.P. Mouritz, et al., Multifunctional properties of epoxy nanocomposites reinforced by aligned nanoscale carbon. Mater Design **94**, 554–564 (2016)
39. X. Sha, K. Yu, H. Cao, K. Qian, Shear thickening behavior of nanoparticle suspensions with carbon nanofillers. J. Nanopart. Res. **15**(7), 1–11 (2013)
40. S. Gürgen, M.C. Kushan, W.H. Li, The effect of carbide particle additives on rheology of shear thickening fluids. Korea-Aust Rheol J **28**(2), 121–128 (2016)
41. B. Seifried, F. Temelli, Viscosity and rheological behavior of carbon dioxide-expanded fish oil fatty acid ethyl esters: Measurement using a rotational viscometer and modeling. J. Supercrit. Fluids **95**, 519–524 (2014)
42. J.S. Zhang, Y. Wang, H.X. Deng, J.Y. Zhou, S. Liu, J.P. Wu, et al., A high anti-impact STF/Ecoflex composite structure with a sensing capacity for wearable design. Compos Part B-Eng **233**, 109656 (2022)
43. S. Wang, S. Liu, J.Y. Zhou, F.X. Li, J. Li, X.F. Cao, et al., Advanced triboelectric nanogenerator with multi-mode energy harvesting and anti-impact properties for smart glove and wearable e-textile. Nano Energy **78**, 105291 (2020)
44. H.A. Barnes, Shear-thickening (dilatancy) in suspensions of nonaggregating solid particles dispersed in newtonian liquids. J. Rheol. **33**(2), 329–366 (1989)
45. H.G. Yang, C.Z. Li, H.C. Gu, T.N. Fang, Rheological behavior of titanium dioxide suspensions. J Colloid Interface Sci **236**(1), 96–103 (2001)
46. B.J. Maranzano, N.J. Wagner, The effects of particle-size on reversible shear thickening of concentrated colloidal dispersions. J. Chem. Phys. **114**(23), 10514–10527 (2001)
47. S.S. Zhang, Y.J. Zhang, H.W. Wang, Effect of particle size distributions on the rheology of Sn/ag/cu lead-free solder pastes. Mater Design **31**(1), 594–598 (2010)

48. R.G. Egres, F. Nettesheim, J. Wagnern, Rheo-SANS investigation of acicular-precipitated calcium carbon-ate colloidal suspensions through the shear thickening transition. J. Rheol. **50**(5), 685–709 (2006)
49. S. Majumdar, R. Krishnaswamy, A.K. Sood, Discontinuous shear thickening in confined dilute carbon nanotube suspensions. Proc. Natl. Acad. Sci. U. S. A. **108**(22), 8996–9001 (2011)
50. L.M. Zhang, T. Ma, J.L. Yang, Y. Huang, Rheological behavior of alumina suspensions. J. Inorg. Mater. **19**(5), 1145–1150 (2004)
51. M. Liu, Q. Chen, S. Wang, L.F. Bai, M. Sang, W.Q. Jiang, et al., PVP immobilized SiO_2 nanospheres for high-performance shear thickening fluid. J. Nanopart. Res. **19**, 234 (2017)
52. M. Liu, W.Q. Jiang, Q. Chen, S. Wang, Y. Mao, X.L. Gong, et al., A facile one-step method to synthesize SiO_2@polydopamine core-shell nanospheres for shear thickening fluid. RSC Adv. **6**, 29279–29287 (2016)
53. W.Q. Jiang, F. Ye, Q.Y. He, X.L. Gong, J.B. Feng, L. Lu, et al., Study of the particles' structure dependent rheological behavior for polymer nanospheres based shear-thickening fluid. J Colloid Interface Sci **413**, 8–16 (2014)
54. W.Q. Jiang, Y.Q. Sun, Y.L. Xu, C. Peng, X.L. Gong, Z. Zhang, Shear-thickening behavior of polymethyl-methacrylate particles suspensions in glycerine-water mixtures. Rheol. Acta **49**(11–12), 1157–1163 (2010)
55. Y. Otsubo, M. Fujiwara, M. Kouno, K. Edamura, Shear-thickening flow of suspensions of carbon nano-fibers in aqueous PVA solutions. Rheol. Acta **46**(7), 905–912 (2007)
56. H.L. Yang, J.M. Ruan, J.P. Zou, Q.M. Wu, Z.C. Zhou, Y.Y. Xie, Non-linear viscoelastic rheological properties of PCC/PEG suspensions. Chin. J. Chem. Phys. **22**(1), 46–50 (2009)
57. L. Albiston, K.R. Franklin, E. Lee, J. Smeulders, Rheology and microstructure of aqueous layered double hydroxide dispersions. J. Mater. Chem. **6**(5), 871–877 (1996)
58. S. Gürgen, W. Li, M.C. Kuşhan, The rheology of shear thickening fluids with various ceramic particle additives. Mater Design **104**, 312–319 (2016)
59. Y.L. Xu, X.L. Gong, C. Peng, Y.Q. Sun, W.Q. Jiang, Z. Zhang, Shear thickening fluids based on additives with different concentrations and molecular chain lengths. Chin. J. Chem. Phys. **23**, 342–346 (2010)
60. M. Kamibayashi, H. Ogura, Y. Otsubo, Shear-thickening flow of nanoparticle suspensions flocculated by polymer bridging. J. Colloid Interface Sci. **321**, 294–301 (2008)
61. G.V. Franks, Z.W. Zhou, N.J. Duin, D.V. Boger, Effect of interparticle forces on shear thickening of oxide suspensions. J. Rheol. **44**, 759–779 (2000)
62. F. Ye, W. Zhu, W.Q. Jiang, Z.Y. Wang, Q. Chen, X.L. Gong, et al., Influence of surfactants on shear-thickening behavior in concentrated polymer dispersions. J. Nanopart. Res. **15**, 2122 (2013)
63. X.Q. Liu, R.Y. Bao, X.J. Wu, W. Yang, B.H. Xie, M.B. Yang, Temperature induced gelation transition of a fumed silica/PEG shear thickening fluid. RSC Adv. **5**, 18367–18374 (2015)
64. J. Warren, S. Offenberger, H. Toghiani, C.U. Pittman, T.E. Lacy, S. Kundu, Effect of temperature on the shear-thickening behavior of fumed silica suspensions. ACS Appl. Mater. Interfaces **7**, 18650–18661 (2015)
65. T. Tian, G. Peng, W. Li, J. Ding, M. Nakano, Experimental and modelling study of the effect of temperature on shear thickening fluids. Korea-Aust Rheol J **27**, 17–24 (2015)
66. D. Rivero, L.M. Gouveia, A.J. Müller, A.E. Sáez, Shear-thickening behavior of high molecular weight poly(ethylene oxide) solutions. Rheol. Acta **51**, 13–20 (2012)
67. E. Yablonovitch, Inhibited spontaneous emission in solid state physics and electronics. Phys. Rev. Lett. **58**, 2059 (1987)
68. A. Blanco, E. Chomski, S. Grabtchak, M. Ibisate, S. John, S.W. Leonard, et al., Large-scale synthesis of a silicon photonic crystal with a complete three-dimensional bandgap near 1.5 micrometres. Nature **405**, 437–440 (2000)
69. M. Honda, T. Seki, Y. Takeoka, Dual tuning of the photonic band-gap structure in soft photonic crystals. Adv. Mater. **21**, 1801–1804 (2009)

70. A.C. Arsenault, D.P. Puzzo, I. Manners, G.A. Ozin, Photonic-crystal full-colour displays. Nat Photon **1**, 468–472 (2007)
71. W. Stöber, A. Fink, E. Bohn, Controlled growth of monodisperse silica spheres in the micron size range. J. Colloid Interface Sci. **26**, 62–69 (1968)
72. A.N. Golikand, E. Lohrasbi, M.G. Maragheh, M. Asgari, Carbon nano-tube supported Pt-pd as methanol-resistant oxygen reduction electrocatalyts for enhancing catalytic activity in DMFCs. J. Appl. Electrochem. **39**, 2421–2431 (2009)
73. M. Paradise, T. Goswami, Carbon nanotubes - production and industrial applications. Mater Design **28**, 1477–1489 (2007)
74. E. Svasand, K.D. Kristiansen, O.G. Martinsen, G. Helgesen, S. Grimnes, A.T. Skjeltorp, Behavior of carbon cone particle dispersions in electric and magnetic fields. Colloid Surf A **339**, 211–216 (2009)
75. O.S. Young, O.M. Kyung, K.T. Jin, Characterization and electrorheological response of silica/titania-coated MWNTs synthesized by sol-gel process. Colloid Surf A **436**, 354–362 (2013)
76. T. Makowski, M. Grala, W. Fortuniak, D. Kowalczyk, S. Brzezinski, Electrical properties of hydrophobic polyester and woven fabrics with conducting 3D network of multiwall carbon nanotubes. Mater Design **90**, 1026–1033 (2016)
77. A. Farjoud, E.A. Bagherpour, Electromagnet design for magneto-rheological devices. J Intel Mat Syst Str **27**(1), 51–70 (2016)
78. Y. Wang, S.H. Xuan, B. Dong, F. Xu, X.L. Gong, Stimuli dependent impedance of conductive magnetorheological elastomers. Smart Mater. Struct. **25**(2), 025003 (2016)
79. W. Xiaojie, F. Gordaninejad, M. Calgar, L. Yanming, J. Sutrisno, A. Fuchs, Sensing behavior of magnetorheological elastomers. J. Mech. Des. **131**(9), 091004 (2009)
80. M. Liu, S.S. Zhang, S. Liu, S.S. Cao, S. Wang, L.F. Bai, et al., CNT/STF/Kevlar-based wearable electronic textile with excellent anti-impact and sensing performance. Compos Part A-Appl S **126**, 105612 (2019)
81. M.A. Hannan, M.M. Hoque, A. Hussain, Y. Yusof, P.J. Ker, State-of-the-art and energy management system of lithium-ion batteries in electric vehicle applications: Issues and recommendations. IEEE Access **6**, 19362–19378 (2018)
82. L.G. Lu, X.B. Han, J.Q. Li, J.F. Hua, M.G. Ouyang, A review on the key issues for lithium-ion battery management in electric vehicles. J. Power Sources **226**, 272–288 (2013)
83. M.A. Hannan, M.S.H. Lipu, A. Hussain, A. Mohamed, A review of lithium-ion battery state of charge estimation and management system in electric vehicle applications: challenges and recommendations. Renew. Sust. Energ. Rev. **78**, 834–854 (2017)
84. G. Li, Z. Chen, J. Lu, Lithium-sulfur batteries for commercial applications. Chem **4**, 3–7 (2018)
85. Y. Wu, L. Yang, X. Tian, Y. Li, T. Zuo, Temporal and spatial analysis for end-of-life power batteries from electric vehicles in China. Resour. Conserv. Recycl. **155**, 104651 (2020)
86. M. Zarei, Portable biosensing devices for point-of-care diagnostics: Recent developments and applications. TrAC-Trends Anal Chem. **91**, 26–41 (2017)
87. A. Masias, J. Marcicki, W.A. Paxton, Opportunities and challenges of lithium ion batteries in automotive applications. ACS Energy Lett **6**(2), 621–630 (2021)
88. J. Benajes, A. García, J. Monsalve-Serrano, S. Martínez-Boggio, Emissions reduction from passenger cars with RCCI plug-in hybrid electric vehicle technology. Appl. Therm. Eng. **164**, 114430 (2020)
89. X. Duan, G. Naterer, Heat transfer in phase change materials for thermal management of electric vehicle battery modules. Int J Heat Mass Transf - Theory Appl **53**, 5176–5182 (2010)
90. R. Kizilel, A. Lateef, R. Sabbah, M. Farid, J. Selman, S. Al-Hallaj, Passive control of temperature excursion and uniformity in high-energy Li-ion battery packs at high current and ambient temperature. J. Power Sources **183**, 370–375 (2008)
91. R. Kizilel, R. Sabbah, J.R. Selman, S. Al-Hallaj, An alternative cooling system to enhance the safety of Li-ion battery packs. J. Power Sources **194**, 1105–1112 (2009)

92. J. Ding, T.F. Tian, Q. Meng, Z.P. Guo, W.H. Li, P. Zhang, et al., Smart multifunctional fluids for lithium ion batteries: Enhanced rate performance and intrinsic mechanical protection. Sci. Rep. **3**, 2485 (2013)
93. K.W. Liu, C.F. Cheng, L.Y. Zhou, F. Zou, W.F. Liang, M.Y. Wang, et al., A shear thickening fluid based impact resistant electrolyte for safe Li-ion batteries. J. Power Sources **423**, 297–304 (2019)
94. Y.X. Wu, S. Wang, M. Sang, Q. Shu, J.S. Zhang, S.H. Xuan, et al., A safeguarding and high temperature tolerant organogel electrolyte for flexible solid-state supercapacitors. J. Power Sources **505**, 0083 (2021)
95. Y. Wang, L. Wang, T. Yang, X. Li, X. Zang, M. Zhu, et al., Wearable and highly sensitive graphene strain sensors for human motion monitoring. Adv. Funct. Mater. **24**, 4666–4670 (2014)
96. Y. Yang, X. Yang, Y. Tan, Q. Yuan, Recent progress in flexible and wearable bio-electronics based on nanomaterials. Nano Res. **10**, 1560–1583 (2017)
97. X. Wang, Z. Liu, T. Zhang, Flexible sensing electronics for wearable/attachable health monitoring. Small **13**, 1602790 (2017)
98. H. Wang, H. Zhou, A. Gestos, J. Fang, H. Niu, J. Ding, et al., Robust, electro-conductive, self-healing superamphiphobic fabric prepared by one-step vapour-phase polymerisation of poly (3, 4-ethylenedioxythiophene) in the presence of fluorinated decyl polyhedral oligomeric silsesquioxane and fluorinated alkyl silane. Soft Matt **9**(1), 277–282 (2013)
99. D. Du, P. Li, J. Ouyang, Graphene coated nonwoven fabrics as wearable sensors. J Mater Chem C **4**(15), 3224–3230 (2016)
100. T.Q. Trung, N.E. Lee, Flexible and stretchable physical sensor integrated platforms for wearable human-activity monitoring and personal healthcare. Adv. Mater. **28**(22), 4338–4372 (2016)
101. R.E. Fernandez, Y. Umasankar, P. Manickam, J.C. Nickel, L.R. Iwasaki, B.K. Kawamoto, et al., Disposable aptamer-sensor aided by magnetic nanoparticle enrichment for detection of salivary cortisol variations in obstructive sleep apnea patients. Sci. Rep. **7**(1), 17992 (2017)
102. J. Kuang, Z. Dai, L. Liu, Z. Yang, M. Jin, Z. Zhang, Synergistic effects from graphene and carbon nanotubes endow ordered hierarchical structure foams with a combination of compressibility, super-elasticity and stability and potential application as pressure sensors. Nanoscale **7**(20), 9252–9260 (2015)
103. D. Vilarinho, A. Theodosiou, C. Leitão, A.G. Leal-Junior, M. Domingues, et al., POFBG-embedded cork insole for plantar pressure monitoring. Sensors **17**(12), 2924 (2017)
104. J. Wu, J. Wang, Y. Ling, H. Xu, An advanced hybrid technique of dcs and jsrc for tele monitoring of multi-sensor gait pattern. Sensors **17**(12), 2764 (2017)
105. W. Liu, J. Chen, Z. Chen, K. Liu, G. Zhou, Y. Sun, et al., Stretchable lithium-ion batteries enabled by device-scaled wavy structure and elastic-sticky separator. Adv. Energy Mater. **7**(21), 1701076 (2017)
106. S. Wang, L. Lin, Z.L. Wang, Triboelectric nanogenerators as self-powered active sensors. Nano Energy **11**, 436–462 (2015)
107. W.G. Kim, D.W. Kim, I.W. Tcho, J.K. Kim, M.S. Kim, Y.K. Choi, Triboelectric nanogenerator: Structure, mechanism, and applications. ACS Nano **15**(1), 258–287 (2021)
108. D.W. Kim, S.W. Kim, U. Jeong, Lipids: Source of static electricity of regenerative natural substances and nondestructive energy harvesting. Adv. Mater. **30**(52), 1804948 (2018)
109. K. Parida, V. Kumar, W. Jiangxin, V. Bhavanasi, R. Bendi, P.S. Lee, Highly transparent, stretchable, and self-healing ionic-skin triboelectric nanogenerators for energy harvesting and touch applications. Adv. Mater. **29**(37), 1702181 (2017)
110. J.Y. Zhou, S. Wang, F. Yuan, J.S. Zhang, S. Liu, C.Y. Zhao, et al., Functional kevlar-based triboelectric nanogenerator with impact energy-harvesting property for power source and personal safeguard. ACS Appl Mater Inter **13**, 6575–6584 (2021)
111. Y.T. Jao, P.K. Yang, C.M. Chiu, Y.J. Lin, S.W. Chen, D. Choi, et al., A textile-based triboelectric nanogenerator with humidity-resistant output characteristic and its applications in self-powered healthcare sensors. Nano Energy **50**, 513–520 (2018)

112. S. Wang, L. Ding, Y. Wang, X.L. Gong, Multifunctional triboelectric nanogenerator towards impact energy harvesting and safeguards. Nano Energy **59**, 434–442 (2019)
113. S. Wang, F. Yuan, S. Liu, J.Y. Zhou, S.H. Xuan, Y. Wang, et al., A smart triboelectric nanogenerator with tunable rheological and electrical performance for self-powered multi-sensors. J. Mater. Chem. C **8**, 3715–3723 (2020)
114. S.Y. Yun, I.W. Tcho, W.G. Kim, D.W. Kim, J.H. Son, S.W. Lee, et al., Mechanically robust triboelectric nanogenerator with a shear thickening fluid for impact monitoring. J. Mater. Chem. A **10**, 10383–10390 (2022)
115. Y. Kim, J. Yun, D. Kim, Robust and flexible triboelectric nanogenerator using non-Newtonian fluid characteristics towards smart traffic and human-motion detecting system. Nano Energy **98**, 107246 (2022)
116. W.H. Wang, J.Y. Zhou, S. Wang, F. Yuan, S. Liu, J.S. Zhang, et al., Enhanced Kevlar-based triboelectric nanogenerator with anti-impact and sensing performance towards wireless alarm system. Nano Energy **91**, 106657 (2022)

Chapter 5
Vibration Damping Systems with Shear Thickening Fluid

Mohammad Rauf Sheikhi, Selim Gürgen, and Melih Cemal Kuşhan

5.1 Introduction

Vibration is an undesired phenomenon due to the detrimental effects on structural stability, position control, materials performance, fatigue life, and noise reduction. This topic is of concern to a broad range of structures from automobiles to tall buildings. Vibration damping is a special field of interest to suppress the vibrations acting on the structures. Damping capacity and structural stiffness are desired to be increased in vibration damping studies [1].

Vibration damping systems use passive or active solutions to suppress the vibrational loadings on the structures. In passive solutions, materials with high damping characteristics are included into the structures. These materials provide an enhanced absorption capability to the vibrational energy acting on the structures. For example, vibrational energy can be transferred into mechanical deformation or heat loss on the damping materials, thereby providing passive vibration attenuation for the structures. On the other hand, active systems require an external power for the sensors and actuators that are used to counter the vibrations on the structures [1]. As a major advantage of active systems over passive ones, resonances can be avoided by tuning the damping systems, thereby preventing from structural collapses at natural frequencies.

M. R. Sheikhi
Key Laboratory of Traffic Safety on Track of Ministry of Education, School of Traffic & Transportation Engineering, Central South University, Changsha, Hunan, China

State Key Laboratory for Strength and Vibration of Mechanical Structures, Shaanxi ERC of NDT and Structural Integrity Evaluation, School of Aerospace Engineering, Xi'an Jiaotong University, Xi'an, China

S. Gürgen (✉) · M. C. Kuşhan
Department of Aeronautical Engineering, Eskişehir Osmangazi University, Eskişehir, Turkey
e-mail: sgurgen@ogu.edu.tr

S. Gürgen (ed.), *Shear Thickening Fluid*,
https://doi.org/10.1007/978-3-031-25717-9_5

Various materials are used in passive vibration damping systems. In general, viscoelastic properties are demanded from the materials. Polymers and rubbers are widely used for this purpose [2]. Vibrational energy is attenuated through heat loss by the effect of viscoelastic characteristics of the materials. In addition to viscoelasticity, microstructural defects in metal alloys such as dislocations, grain boundaries, and secondary phases are benefitted in vibration damping systems. In metal-based vibration damping systems, vibrational energy triggers the activation of defects such as slip motions and plastic deformations in metal alloys and consequently leading to vibration damping through energy conversion in the structures [3].

Due to its unique rheological behavior, shear thickening fluid (STF) has been adapted to different vibration damping systems in recent years. STF has low viscosity properties under rest or low frequency conditions; however, its viscosity significantly increases upper levels upon exciting by high-frequency loading. STF exhibits excellent viscous damping behavior as well as good elastic stiffness capabilities, and for this reason, it emerges as a passive dissipative material suitable for vibration damping systems [4–6]. Unlike active damping devices, STF does not require an additional power unit for activation because its rheological response naturally activates in case of an external stimulation [7, 8]. Tailoring the rheological response for the desired damping properties provides excellent advantages for the users, thereby eliminating the complexity as such in the fluid-based active damping systems requiring magnetic or electric fields.

Vibration control is an essential issue for many fields. However, three main application areas come to the forefront considering the STF-based vibration damping systems in the literature: structural components, machinery, and manufacturing. In this chapter, STF-based vibration damping systems are discussed for the given application areas.

5.2 STF-Based Vibration Damping in Structural Components

In order to enhance the vibration damping properties of structures, STF is generally merged into conventional components instead of using it as a single body because STF is a fluidic material. For this reason, holes and channels are typically designed in structural components to be filled with STF. Gürgen et al. [9] designed sandwich panels having an extruded polystyrene (XPS) core material between aluminum face sheets. A set of holes was drilled in the core material to contain STF. Modal analysis method was employed to find out the damping ratios in the sandwich structures. In this simple technique, structures are excited by hammer impacts to show their natural vibrations. An accelerometer is used to collect the free vibrations in terms of displacement, and then mass, damping, and stiffness metrics are calculated for overall system. Complex systems such as STF-included structures show multi-degree of freedom, which is transformed into a set of single-degree of freedom systems by

this way. Consequently, complex problems can be modeled as linear superposition of a number of single-degree of freedom systems in modal analysis. According to this work, STF integration into the sandwich structures leads to a significant increase in the damping ratios. Based on an early study [10], liquid addition into the structures contributes to the damping properties regardless of liquid rheology. Because the liquid acts as a viscous medium in the system and thereby provides a damping mechanism for the structures. Liquid sloshing lowers the vibrations acting on the structures [11]. Despite the conventional viscous effect in any liquid, STF provides an additional damping mechanism for the structures. When the STF-containing sandwich panels are excited by vibrational loading, STF in the holes starts flowing and particle interactions are observed in the microstructure. By the effect of vibrational stimulation, hydrodynamic interactions grow up in the flow field and, consequently, particles are forced to get close to each other. Particle contacts, which support the shear thickening effect, may be observed depending on the loading level. As particle contacts predominate the microstructure, shear thickening effect grows stronger. For this reason, STF shows stiffer characteristics under vibrational loading, thereby contributing to the damping properties of the structures [9].

Fischer et al. [12] investigated the vibration control properties of multi-layer composites intercalated with STF. The aim of this work was understanding the effect of STF inclusion on the stiffness and damping capacity of the composite under dynamic deformation. In line with this purpose, a layer of STF was spread between polyvinyl chloride (PVC) beams. The STF was fabricated by distributing hydrophilic fumed silica in a polypropylene glycol (PPG) pool. In the vibrating beam testing, one of the beam ends was fixed by a clamp while the other end was exposed to forced oscillations by a vibration generator. A laser velocity transducer was used for monitoring the displacement at the tip of the excited beam end. The amplitude of the stimulation was adjusted instantly to keep the displacement amplitude constant. A data recording unit was used to track the corresponding forces with respect to frequency for different levels of displacement amplitudes. From the experimental results, the relative motion of the PVC beam is heavily affected by the shear thickening rheology. Above a certain amplitude, which corresponds to the thickening point of STF, the natural frequency of the beam increases while growing the vibration damping performance in the multi-layer structure.

A similar beam design was proposed by Wei et al. [13]. Aluminum face sheets with an STF core layer were considered in this work. The dynamic characteristics were theoretically investigated by considering an external forced excitation. STF properties were taken into account while the governing equation for the beam was derived from the complex stiffness method and Timoshenko beam theory. In the calculations, the following were assumed: (1) the Euler-Bernoulli beam theory is valid for face sheet deformations, (2) low mode vibration is considered for the beam, (3) only shear deformations act in STF core, (4) all the layers (face sheets and STF core) show identical transverse displacements, and (5) no slip and delamination conditions for the interfaces during deformation. Various parameters were selected to understand their effects on the dynamic properties of the structure. These parameters were excitation frequency, excitation amplitude, excitation location, and

skin/core thickness ratio. According to the results, natural frequency is quite dynamic by integrating STF core into the beam unlike traditional structures. Moreover, natural frequency gets more sensitive at higher excitation amplitudes. In addition, the sensitivity of the natural frequency is prone to increase at lower excitation frequencies. On the other hand, the variation in the natural frequency gets bigger when the excitation location is near the mid-span of the structure. There is a certain relationship between the skin/core thickness ratio and natural frequency. When the skin/core thickness ratio increases, the natural frequency increases as well. To sum up, STF inclusion in the aluminum-based beams leads to a reduction in the vibration of the structures [14]. The non-Newtonian rheology of STF provides a thickened texture in the core of the beam under loading. From this change, stiffness and damping characteristics in the structures are enhanced and, consequently, vibration attenuation behavior is enhanced.

In another study, STF was incorporated into carbon fiber reinforced polymers (CFRP) tubes [15]. Although CFRP-based components are widely used in aerospace, automotive, sport, and medical equipment applications, this material needs an improvement in the vibration damping properties. The STF was made from natural products such as cornstarch and water. Three different cornstarch loadings (50%, 55%, and 60%) were used in the STF fabrication. After filling the CFRP tubes with STF, the specimens were tested in modal analysis. Two different clamping configurations were selected in the experimental setup as shown in Fig. 5.1. According to the results, the tubes without STF exhibit the lowest damping ratio while damping ratio increases by filling the tubes with higher cornstarch content mixtures. These results indicate that STF addition leads to a gain of performance for damping behavior. Moreover, vibration damping performance simply depends on the shear thickening effect. To understand the role of shear thickening effect, thickening ratio was calculated for all suspensions having different cornstarch amounts. Thickening ratio is a performance metric for the better understanding of shear thickening intensity in

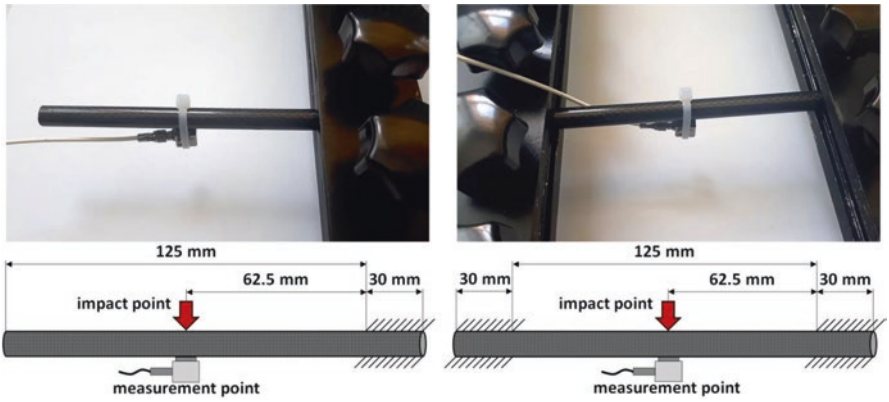

Fig. 5.1 Vibration test setup for single-fix end and double-fix end [15]. Reprinted by permission from Elsevier

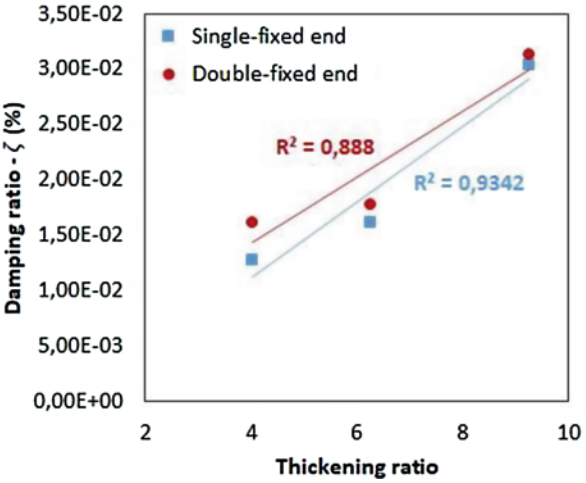

Fig. 5.2 Damping ratio vs thickening ratio [15]. Reprinted by permission from Elsevier

the suspensions. This metric is defined as the peak viscosity beyond the thickening point over the viscosity at the critical shear rate [16]. Figure 5.2 shows the correlation between the damping ratio of the tubes and the thickening ratio of the STFs. It is clearly seen in the chart that shear thickening intensity has a direct relationship with the vibration damping behavior of the structures. As the solid particle loading increases in the suspension, thickening ratio increases and, therefore, peak viscosity at the thickening regime reaches upper levels. Consequently, STF-included tubes behave in stiffer manner and damping properties get stronger by this means. The novel STF/CFRP design is suggested for unmanned aerial vehicle (UAV) structures to enhance the vibration isolation properties against flutter and undesired vibrations during flights.

The thickening ratio level regarding the particle loading aforementioned in the previous paragraph can be associated with the clustering mechanism in the suspension. In denser mixtures, clustering mechanism quickly takes place due to the increased hydrodynamic interactions. For this reason, lower critical shear rates are frequently encountered in the rheological measurements, which means that the onset of the thickening phenomenon can be easily observed at lower rate of external stimulations. In other words, thickening threshold in terms of shear forces can be reached at lower shear rates by adding more solid particles in the mixtures. This is due to the decreasing inter-particle distances, which enhance the particle interactions as well as overcoming the repulsive forces between the particles [17]. In addition to the hydrodynamic effect, dense suspensions are more prone to produce particle contacts in their microstructures especially at higher shear rates. Because small inter-particle distances lead to strong attraction forces between the particles and consequently physical contacts inevitably take place in the microstructures. From this formation, shear thickening effect gets stronger in the mixtures, thereby increasing stress transfer both in the suspension and at the STF/CFRP interfaces. As

a result of this process, vibration damping characteristics are enhanced in the STF-included structures [15].

The key point in benefiting from STF in vibration damping is tailoring the thickening phase to coincide with the structural resonance point. At the shear thickening regime, the suspension shows increased stiffness and thereby provides strong damping behavior at that state. Regarding this important issue, Neagu et al. [18] proposed a micromechanical approach to STF-integrated composite structures. In this work, a block of silicone was reinforced by a set of glass fiber/epoxy rods. The interfaces between the silicone matrix and reinforcing rods were nested for an STF made from spherical silica particles and polyethylene glycol (PEG). The composites were subjected to dynamic mechanical analyses to determine the dynamic properties. According to the experimental results, STF presence at the matrix/reinforcement interfaces significantly enhances the damping behavior of the composites. The dynamic properties are heavily dependent on frequency and applied external load amplitude. Damping peaks are observed at the shear thickening regime of the STF, which clearly proves that shear thickening provides an additional damping capability for the structures. In addition, the damping peak locations appear depending on the onset of shear thickening rheology in the STF. In this sense, STF-integrated composites are capable of stiffness/damping control for certain vibration frequencies. To do this, STF rheology can be tailored in many different ways. STF rheology depends on several factors, which can be manipulated for tuning the shear thickening behavior. Particle volume fraction, particle aspect ratio, particle size, particle roughness, particle modifications, liquid medium, temperature, and reinforcing fillers are the main factors providing an opportunity for rheological control [16, 19–21].

5.3 STF-Based Vibration Damping in Machinery

STF-based vibration control in machinery has been an interesting topic for two decades. A damper is a simple solution in conventional applications. From this point of view, researchers have made great efforts to integrate STF into a simple device and ultimately propose a passive adaptive damper for machinery applications. The first attempt about including STF in traditional dampers is replacing the hydraulic oil with STF. The viscoelastic damping characteristics of the dampers gain an adaptive behavior by this way.

Zhao et al. [22] proposed an STF-based damper for adaptive vibration attenuation in rotary systems. The STF was synthesized by distributing nano-size fumed silica in PEG medium. Then this smart suspension was filled in a damper, which was investigated in a rotary test setup as shown in Fig. 5.3. In the experimental stage, two STF dampers were attached to a rotor system in x and y directions to suppress the undesired vibrations generated by the rotary motion. Vibration frequencies and vibration amplitudes were investigated in this experimental work. Figure 5.4 shows the dynamic response of the rotary system. As shown in Fig. 5.4a and b, there are quite large displacements in the no-damper cases. By attaching one

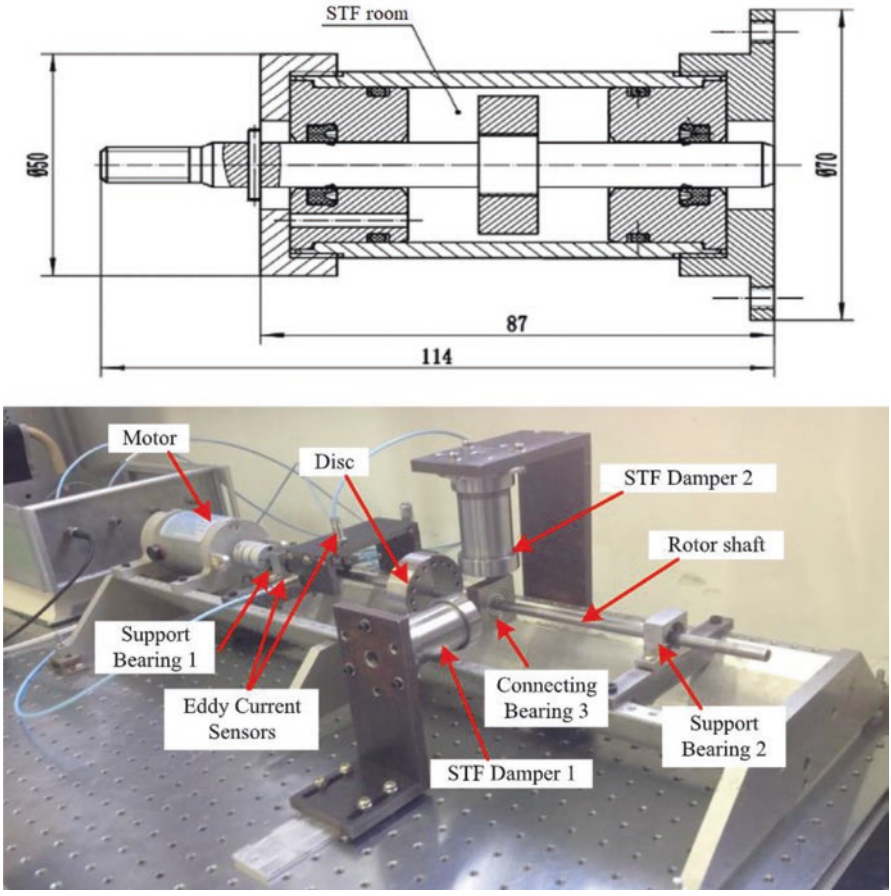

Fig. 5.3 Structural design of STF damper and vibration test setup [22]. Reprinted by permission from Elsevier

STF damper whether in x or y directions, the displacements are effectively restricted to a small area. Moreover, the displacements show higher restrictions in the STF damper installation directions. On the other hand, the displacements are significantly reduced and, thus, the stability of the rotary system is highly enhanced by using two STF dampers in both directions. From the chart given in Fig. 5.4c, it is possible to state that the first-order resonance amplitude of the rotary system is about 90 μm in x-direction for the no STF damper case. The resonance amplitude greatly reduces to about 15 μm and 40 μm by using an STF damper in x-direction and y-direction respectively. On the other hand, a significant reduction is obtained in the two STF damper case that the resonance amplitude shows only 4 μm by the effect of STF damping in both directions. Similar improvements are achieved in the resonance amplitudes in y-direction as shown in Fig. 5.4d. As given in the graph, the resonance amplitude of the system without a damper is about 400 μm, whereas it is

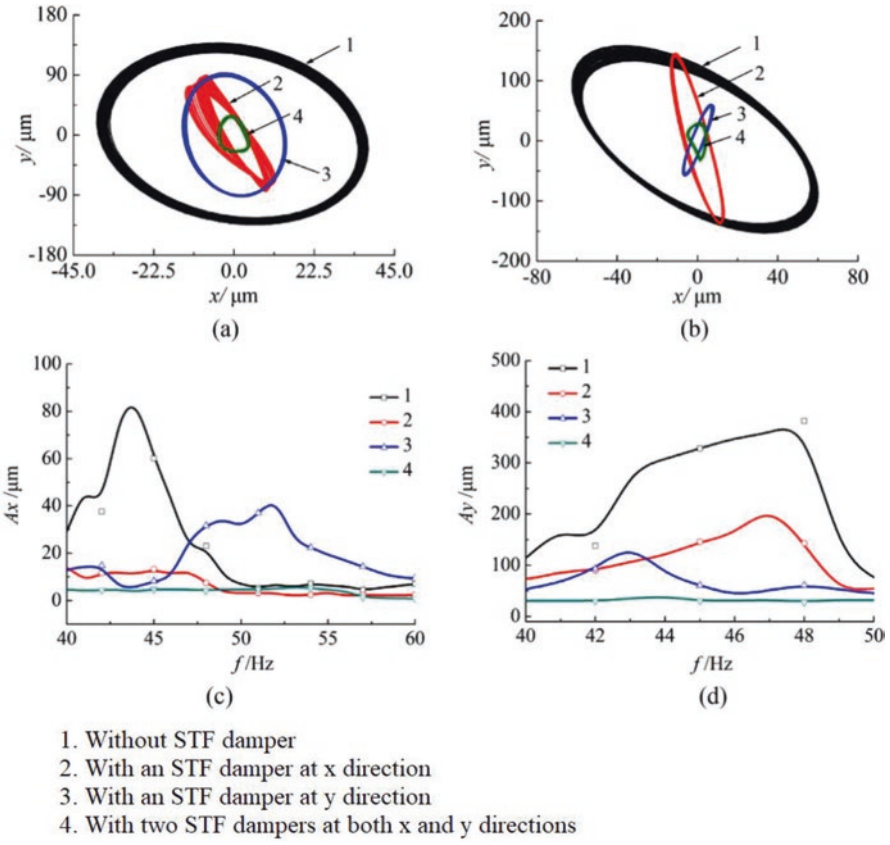

Fig. 5.4 Dynamic response of the rotary system: (**a**) axis orbits with a frequency of 42 Hz, (**b**) axis orbits with a frequency of 45 Hz, (**c**) x-direction amplitude response nearby resonance region, and (**d**) y-direction amplitude response nearby resonance region [22]. Reprinted by permission from Elsevier

about 220 μm and 140 μm for the one STF dampers attached in x-direction and y-direction, respectively. The highest suppression is achieved in the two STF damper case, which yields a resonance amplitude of about 30 μm. There is an obvious improvement in the vibration attenuation properties by using STF dampers in the rotary mechanism.

STF dampers have nonlinear characteristics due to the rate-dependent behavior of STF rheology and show large damping forces. For this reason, they provide enhanced energy absorption capabilities at natural frequencies in comparison to the conventional linear dampers. Furthermore, damping force in STF dampers can be increased significantly depending on the frequency and amplitude and, therefore, stronger vibration suppression properties are clearly obtained in these smart devices. Unbalanced vibrations in rotary systems especially at natural frequencies can be effectively attenuated by the nonlinear damping characteristics. STF dampers have

a great potential to be integrated into adaptive or semi-active vibration control systems [22].

In another STF damper study, Wei et al. [23] developed a phenomenological model for predicting the flow characteristics of STF. Then, an analytical model was proposed to simulate the dynamic characteristics of an STF damper by the aid of the developed phenomenological model for STF rheology. In the damper modeling, force-displacement curves were investigated for various amplitudes and frequencies. According to the results, peak damping forces greatly increase as the amplitudes and frequencies increase in the system. Contrary to the magnetorheological dampers, force-displacement curves in STF dampers do not follow stable characteristics under increasing excitations. At significantly large amplitudes and frequencies, damping forces are prone to get lower values beyond a critical point. Furthermore, the reduction in damping forces becomes prominent by decreasing the annular gap. For this reason, annular gap dimension is one of the key factors in STF damper design, especially for large amplitude and frequency applications.

Lin et al. [24] designed a damper filled with fumed silica and PEG-based STF. The damper was subjected to sinusoidal loadings while imposing different frequencies. The dynamic behavior of this smart damper was investigated by considering the force-displacement and force-velocity curves. From the results, damper forces exhibit a reduction by increasing the loading cycles for all frequencies. This effect grows upon long-term loadings. The root cause is found as the heat generation in the damper system and consequently increasing temperature. Based on the previous works [25–29], shear thickening behavior shows a degradation at elevated temperatures due to lower rate of hydrodynamic interactions. For this reason, a gradual reduction in peak viscosity develops as the loading is applied to the damper. As a result, damping properties show a loss of performance for long-term operations. Although STF inclusion in damper systems provides an improvement for the dynamic properties, temperature has a restrictive effect on STF performance. From this point of view, an attempt is required to control the heat generation in STF-based damping devices.

Apart from conventional damper devices, STF was brought together with a sliding friction (SF) isolator to benefit from shear thickening rheology [30]. This device is suggested for anti-seismic applications to keep the structures in a stable position during cyclic loadings. The STF-based SF isolator includes a traditional SF material and STF as well. Figure 5.5 shows the details of STF-based SF isolator. At low excitation energies, the SF material protects the structure from large vibrations and displacements. On the other hand, STF provides a large damping forces by dissipating the external energy acting at high excitation cases. Consequently, the relative motion between the upper plate and the lower member is restricted to keep the structure static. For better understanding of the concept, a mechanistic approach was made by building an analytical model based on the flow momentum equations. The system was subjected to cyclic loadings with various accelerations. From the chart given in Fig. 5.6a, the upper plate shows excessive displacement with reference to the base member when the isolator is assembled without SF material and STF. On the other hand, almost no displacements are visible in the STF and SF/STF

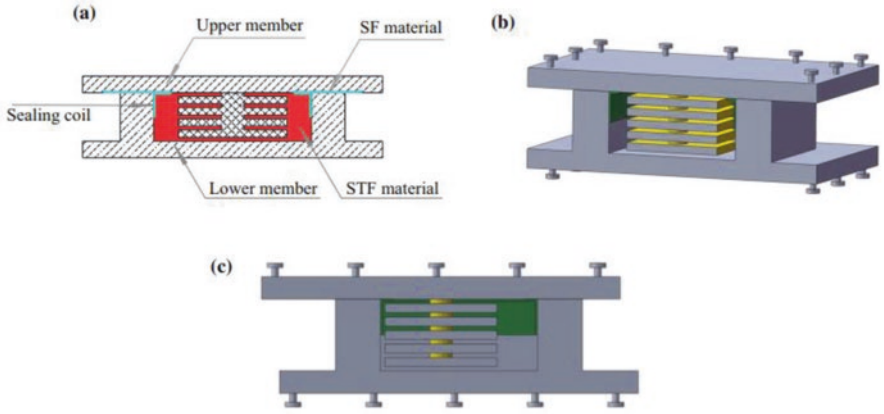

Fig. 5.5 (**a**) Cross-sectional view of STF-based sliding friction isolator, (**b**) three-dimensional view of STF-based sliding friction isolator, and (**c**) STF-based sliding friction isolator after deformation [30]. Reprinted by permission from Springer Nature

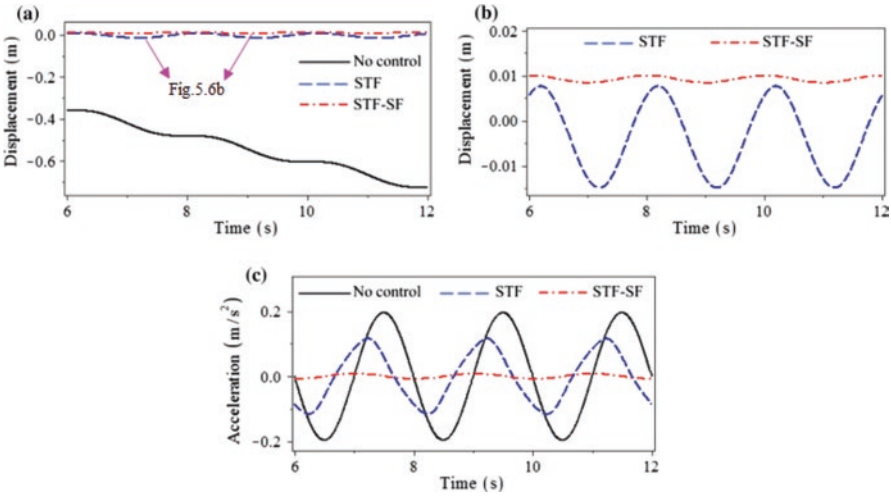

Fig. 5.6 (**a**) General displacement response, (**b**) magnified displacement response, and (**c**) acceleration response of the isolators under a cyclic excitation acceleration of 0.01 g [30]. Reprinted by permission from Springer Nature

cases. Figure 5.6b shows a detailed view of the displacement curves in the STF and SF/STF cases. It is clearly seen that the average displacement for the SF/STF isolator is about 0.01 m while the amplitude is only 0.001 m. On the other hand, average displacement is about 0.005 m; however, larger amplitudes about 0.01 m are visible in the STF case. From these results, it is possible to mention that the SF/STF isolator provides more stable characteristics for vibration damping. The acceleration response of each system is given in Fig. 5.6c. The system without SF material and

STF exhibits large acceleration peaks during the cyclic loading. The accelerations are varied in a range of ±0.2 m/s^2. In the STF case, the accelerations are suppressed to a range of ±0.1 m/s^2. On the other side, the system with the SF/STF isolator shows almost no accelerations, which means that the system is quite stationary under the harmonic excitations. It can be stated that STF inclusion in the SF isolators provides a gain of performance for suppressing the excitations; however, SF sealing at the interface of the upper and lower members significantly enhances the damping characteristics. It can be mentioned that STF inclusion in the conventional SF isolators adds a value in terms of damping properties. Smart device concept is introduced with the SF isolators by integrating STF into these devices. Although the SF/STF isolator shows excellent properties, the design of the device can be enhanced for gain of performance. As an example of improvement, the layered design of columnar structure in the STF room can be optimized for increased shear thickening formation.

Another vibration damping device for machinery is damping pads. In the conventional applications, damping pads are generally made from elastomers to suppress the undesired vibrations through viscoelastic damping. Damping pads are easy-to-use and cost-effective solutions for anti-vibration applications. These pads are used as a support element in the installation of a wide range of large machines such as machining centers, sewing machines, belt lines, rotary mixers, and shakers. In recent applications, STF-based anti-vibration pads have been designed to take advantage of the adaptive damping behavior of STF in vibration isolation.

Cork is a potential material for anti-vibration systems due to its excellent damping behavior. There are many applications with the usage of cork in vibration isolation applications especially damping in machinery. One of them is incorporating STF into cork panels to gain smart damping pads for machinery applications. Gürgen et al. [31] designed multi-layer cork structures by applying STF as an adhesive between the layers. The STF used in this work was based on nano-size fumed silica and PEG. They constructed 20 mm thick cork pads with different numbers of layers as shown in Fig. 5.7. Vibration attenuation properties of these novel pads

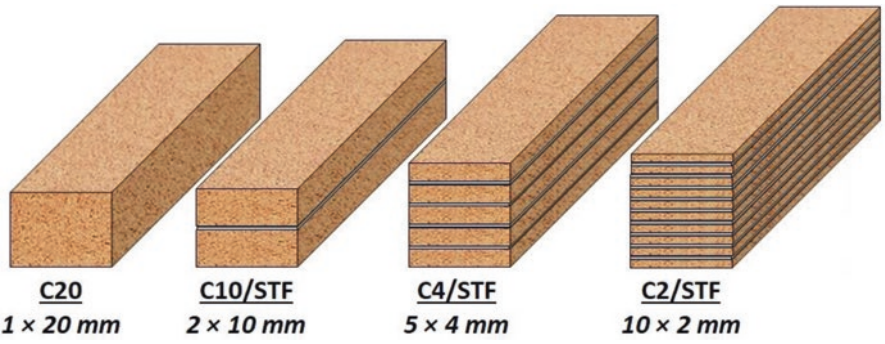

Fig. 5.7 STF-included cork pads for vibration isolation [31]. Reprinted by permission from Elsevier

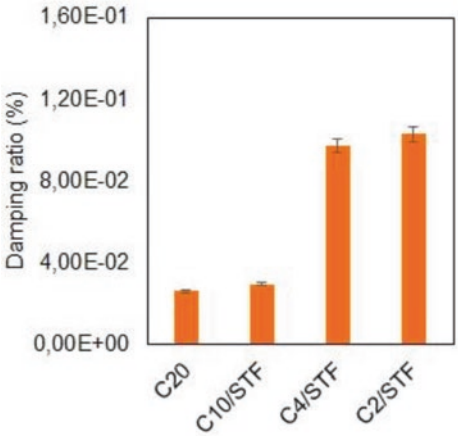

Fig. 5.8 Damping ratios for the multi-layer pads [31]. Reprinted by permission from Elsevier

were investigated by modal analysis considering the damping ratios. Figure 5.8 shows the damping ratios for the STF-included cork pads. From the results, there is a slight improvement in the damping behavior from the C20 to C10/STF pad. However, a clear jump in damping ratio is observed in the C4/STF and C2/STF pads. By using the STF at the cork layer interfaces, vibration suppression is enhanced and, furthermore, this effect is pronounced by increasing the number of STF intercalated layers in the pads. This is simply related to the STF amount increasing with the increased number of interfaces. For example, the C10/STF pad includes only 1 g of STF, whereas it is 9 g in the C2/STF pad. Replacing the C10/STF pad with the C2/STF one in a machinery application, shear thickening formation takes place in an increased number of layers within the structure. As a result of this, structural stiffness grows stronger in the C2/STF pad. From the microstructural aspect, silica particles introduce with hydrodynamic loading upon vibrational excitation. The particles are restricted in clusters within the liquid medium by the effect of hydrodynamic forces, thereby forming particle groups in the flow fields. For this reason, flowability is hindered and fluid viscosity increases as well. At this juncture, we should touch upon the significance of particle morphology because hydrodynamic effect gets bigger when the particles have complex morphologies as such in fumed silica [32, 33]. Since fumed silica is composed of branchy particles, hydrodynamic forces drastically increase on these particles, thereby contributing to the shear thickening formation in the suspensions. Furthermore, particle contacts are commonly observed in the mixtures upon shearing at high rates. At these rates, branchy particles lead to interlocking process in the mixtures and provide a booster effect for shear thickening rheology.

It is also important to mention that shear thickening rheology is able to be activated at small excitations without needing high-level loadings. Based on previous works [34, 35], shear thickening onset is visible even at quasi-static conditions, where the stresses are on the order of 10 to 100 Pa. From the rheological measurement results of an STF based on fumed silica and PEG [36], shear thickening onset

is observed at about 10 Pa stresses, which exhibits compatible results with the literature.

5.4 STF-Based Vibration Damping in Manufacturing

Vibration damping in manufacturing is quite a new field for STF; however, it possesses a good potential for smart manufacturing applications. Chatter is the main problem based on undesired vibrations in machining operations; however, STF-based solutions date back to only a couple of years. Hence, there is still a big gap to take advantage of shear thickening damping in manufacturing operations.

The first attempt was made by Gürgen et al. [37] in 2020. In this work, STF was integrated into a cutting tool by drilling a set of STF holes on the top and flank surface of the shank as shown in Fig. 5.9. The holes were covered by a tape after STF filling to prevent from spilling during machining. Modal analysis method was used to determine the damping ratio in the cutting tools. In addition, a set of machining tests was conducted by using different designs of cutting tools and then the surface roughness of the workpieces was measured to understand the role of STF inclusion into the cutting tool. Figure 5.10 shows the experimental setup for the machining and modal analysis system. From the modal analysis results, the damping ratio of the cutting tool increases by filling the holes with STF. However, the damping ratio depends on the hole directions in the cutting tool. The damping ratio is 0.0174% for the conventional tool, whereas it changes to 0.0392% and 0.0225% after STF filling

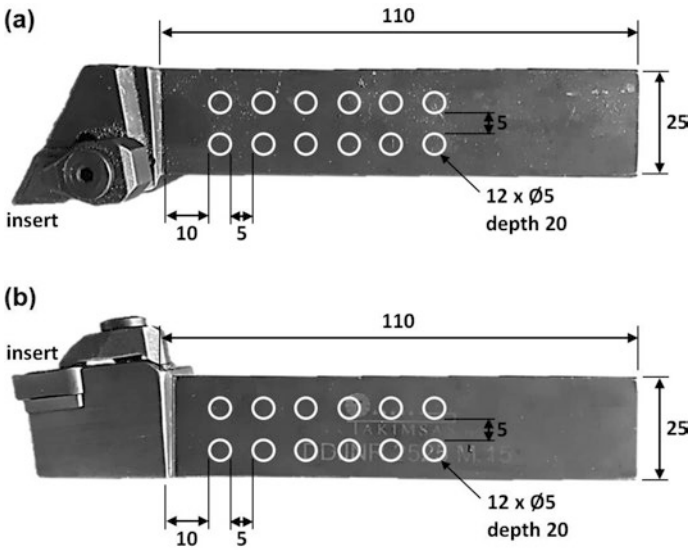

Fig. 5.9 STF holes on the (**a**) top and (**b**) flank surface of the shank [37]. Reprinted by permission from Elsevier

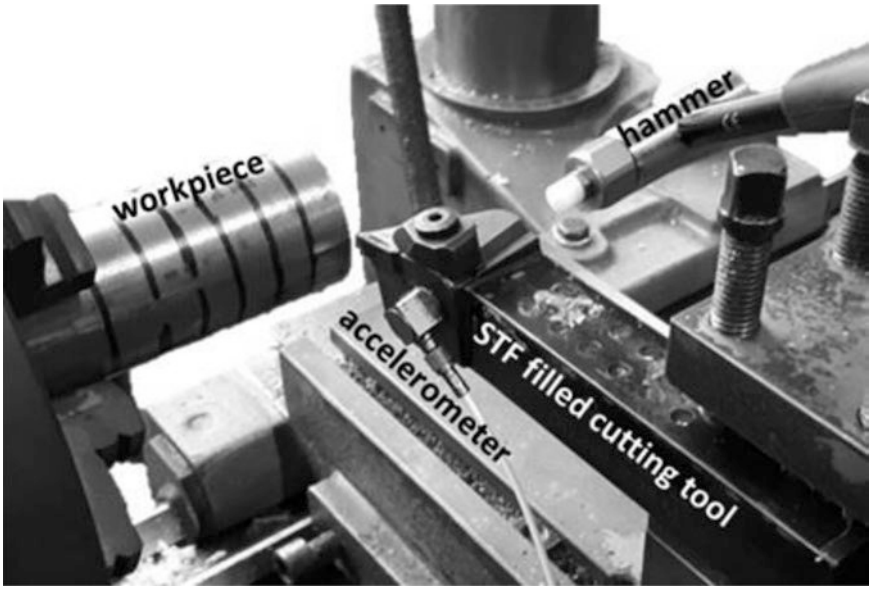

Fig. 5.10 Experimental setup for the machining and modal analysis system [37]. Reprinted by permission from Elsevier

in the top holes and flank holes, respectively. The damping capacity of the cutting tool increases for both STF cases. Figure 5.11 shows the surface topographies for the workpieces machined with different cutting tools. As shown in the images, STF integration leads to a smoother surface finish in comparison to the conventional tool. According to the surface roughness measurements, machining with the conventional tool yields Ra 1.27, while Ra 1.04 and Ra 1.20 are measured for the STF in top and flank holes, respectively. Although STF integration improves both the damping ratio of the cutting tool and the surface finish on the workpiece, hole directions have an importance in the applications.

According to Gürgen et al. [37], chatter-based vibrations act in the feed direction in the machining operation and, therefore, STF in the top holes is excited in the transverse direction, whereas excitation is realized in the longitudinal direction for the STF in the flank holes. It should be noted that particle clusters are able to reach the hole boundaries easily in the top holes compared to the flank holes. Because the peripheral walls in the top holes provide large holding areas for the clustering particles, shear thickening formation grows stronger. In other words, hole boundaries act as rigid bases for the particle clusters, thereby increasing the particle confinement in the suspension. As suggested in previous works [33], particle confinement produces increased shear thickening rheology because confined particle networks are capable of bearing higher stresses without structural breakdown in the particle-contacted microstructure. The mechanism related to this phenomenon is illustrated in Fig. 5.12.

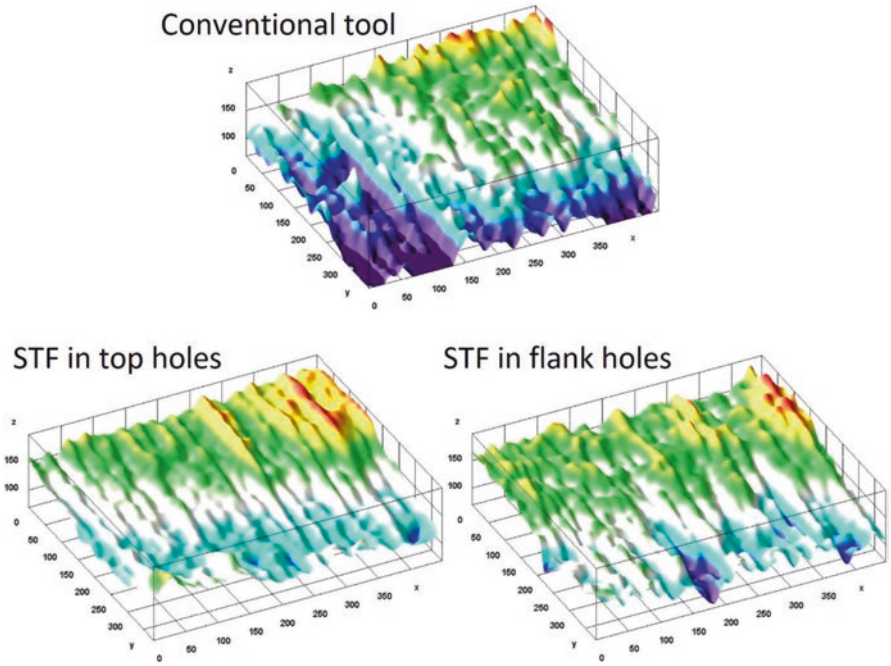

Fig. 5.11 Surface topographies for the workpieces machined with different cutting tools [37]. Reprinted by permission from Elsevier

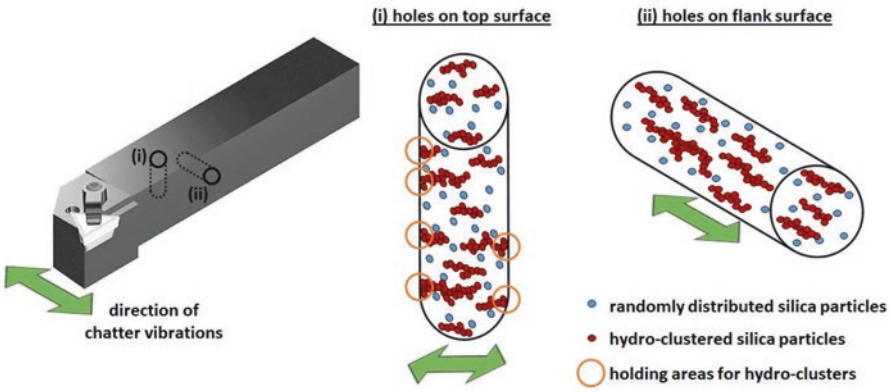

Fig. 5.12 Particle clustering in STF for different cases [37]. Reprinted by permission from Elsevier

Yuan et al. [38] proposed a novel concept regarding the STF-based vibration damping system for the milling of thin-walled parts. Milling is one of the essential operations for shaping the products into final sizes. However, chatter is a big challenge in milling especially for thin-walled parts. In this work, thin-walled parts were

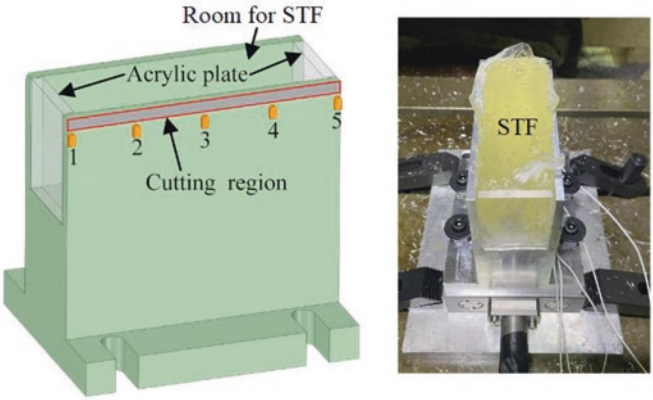

Fig. 5.13 Experimental setup for milling of thin-walled parts [38]. Reprinted by permission from Elsevier

supported by an STF filler behind the machining face. The outer face was machined by a two-edged carbide tool with 12 mm diameter and 55° helix angle. Feed rate, rotational speed, and cutting depth were 400 mm/min, 5000 rpm, and 0.1 mm, respectively. Five sensors were located at the vibration data collection points as shown in Fig. 5.13. Milling tests were conducted for two cases: (1) without STF and (2) with STF. Figure 5.14 shows the vibration amplitude results from the sensors located at the points 1, 2, and 3. It is clearly seen that vibration amplitudes are suppressed to a great extent by using STF support in the milling operations. At point-1, the peak amplitude is about 30 g without using STF in the machining. The peak amplitude lowers to about 10 g after STF support, which is only one-third of that in the non-STF case. Similar results are observed at points 2 and 3. Another result is the surface roughness on the workpiece after the milling operations. Machined surfaces show more stable surface finish in chatter-free operations. Figure 5.15 shows the surface roughness profiles for different cases. As shown in the charts, milled surfaces include sharp peaks and valleys in the non-STF operations. On the other hand, smoother surfaces are achieved after the milling operations with STF supports. Considering point-5, surface profile varies in a range of 15 μm without STF support, while the variation range is within only 2 μm by using STF support in the operation. For the same measurement point, average roughness is 1.352 μm for the non-STF case and it is lowered to 0.219 μm by adding STF support in the machining. It is also stated that STF provides a practical approach for chatter suppression in the machining of thin-walled products, which exhibit highly complex vibration characteristics. The product is subjected to different vibrational modes at different locations based on the cutter position. However, STF rheology provides an adaptive behavior for chatter suppression depending on the excitation level. As well as cutter

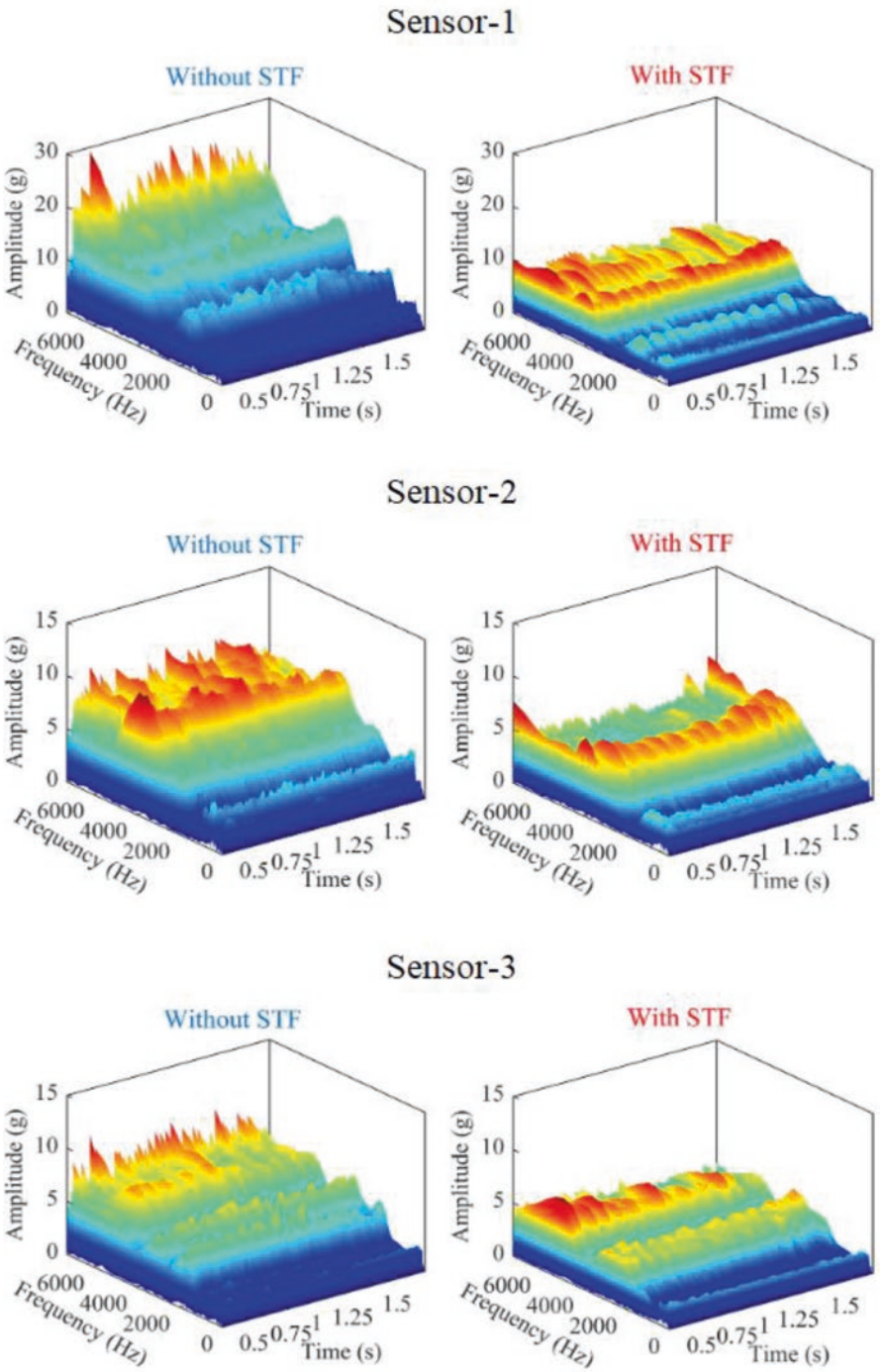

Fig. 5.14 Vibration amplitude results based on various sensors [38]. Reprinted by permission from Elsevier

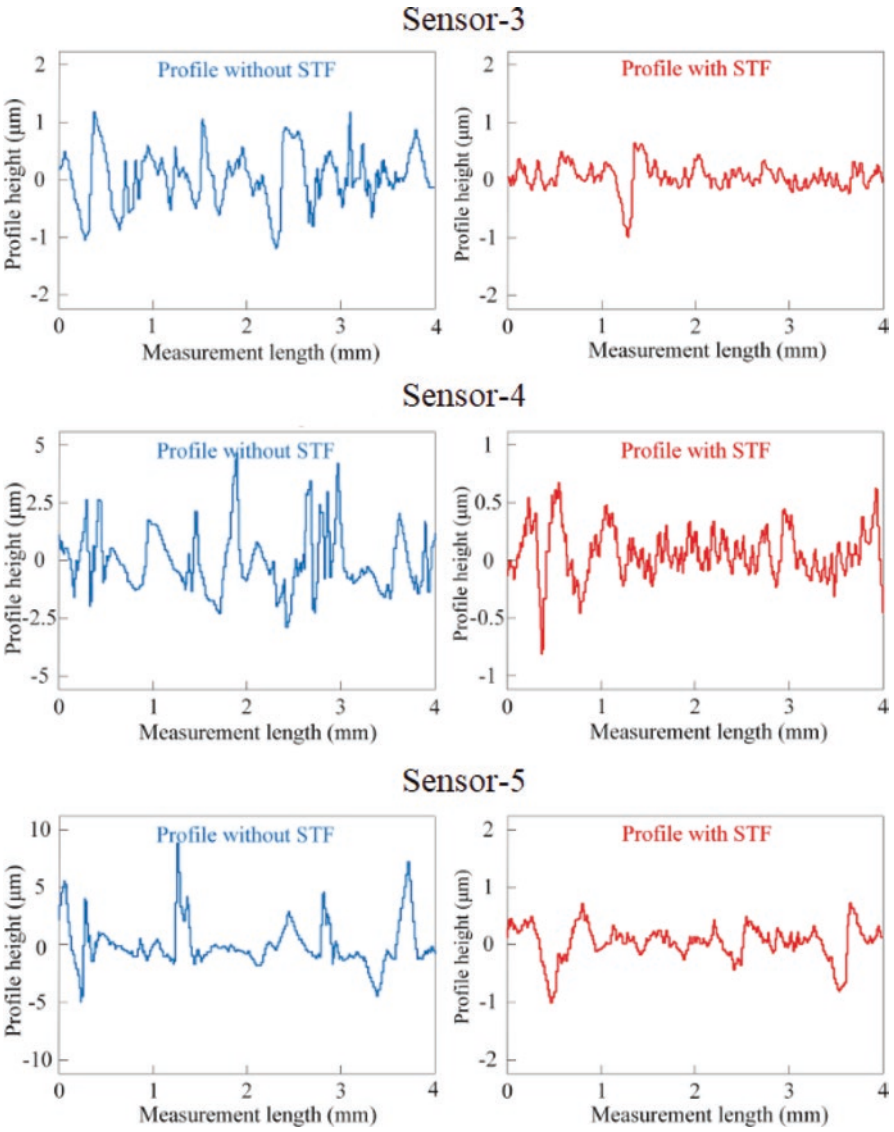

Fig. 5.15 Surface roughness profiles at different locations [38]. Reprinted by permission from Elsevier

position, cutting force frequency, and cutting force magnitude are determining factors of the vibration characteristics of the machining system. Based on this preliminary work, STF has a promising future in manufacturing applications especially for developing smart adaptive damping operations.

5.5 Conclusions

STF is one of the smart materials that shows adaptive rheological behavior for vibration damping systems. For this reason, STF has been adapted to different applications dealing with anti-vibration properties. It is possible to divide the STF-based anti-vibration applications into three groups based on the studies in the literature. A large part of the works is about integrating STF into structural components so that a self-damping behavior is obtained in the structures without requiring additional dampers. Another focus is modifying the conventional dampers by including STF in machinery applications. In general, hydraulic oils are replaced with STF in the conventional damper systems. The damper gets an adaptive damping characteristic by this way. In addition to damper systems, anti-vibration pads are quite common products for vibration attenuation in machinery systems. The latest area for STF-based vibration damping is manufacturing. Undesired vibrations and chatter formation are the most frequent problems in machining operations. STF usage is promising however, STF history is quite short in manufacturing that's why there are only two works in the literature. According to the literature survey conducted in this chapter, STF rheology is suitable for vibration damping systems. STF has a rate sensitive rheology, thereby providing adaptive stiffness and damping properties for anti-vibration applications. Another advantage is that STF is a passive vibration damping material that does not require external stimulation to activate the stiffness and damping behavior. Despite the promising results, there are some drawbacks regarding the STF usage in engineering applications. For example, temperature-dependent rheology in STF restricts the long-term use in damper applications. Nevertheless, STF has a great potential to be adapted to the vibration damping systems after a careful tailoring in the material properties.

References

1. D.D.L. Chung, Review: Materials for vibration damping. J. Mater. Sci. **36**(24), 5733–5737 (2001)
2. X.Q. Zhou, D.Y. Yu, X.Y. Shao, S.Q. Zhang, S. Wang, Research and applications of viscoelastic vibration damping materials: A review. Compos. Struct. **136**, 460–480 (2016 Feb)
3. H. Lu, X. Wang, T. Zhang, Z. Cheng, Q. Fang, Design, fabrication, and properties of high damping metal matrix composites—A review. Materials. **2**(3), 958–977 (2009 Aug 18)
4. C. Fischer, A. Bennani, V. Michaud, E. Jacquelin, J.A.E. Månson, Structural damping of model sandwich structures using tailored shear thickening fluid compositions. Smart Mater. Struct. **19**(3), 035017 (2010 Mar 1)
5. F. Galindo-Rosales, Complex fluids in energy dissipating systems. Appl. Sci. **6**(8), 206 (2016 Jul 25)
6. S. Gürgen, F.A.O. Fernandes, R.J.A. de Sousa, M.C. Kuşhan, Development of eco-friendly shock-absorbing Cork composites enhanced by a non-Newtonian fluid. Appl. Compos. Mater. **28**(1), 165–179 (2021 Feb)
7. S.S. Shenoy, N.J. Wagner, J.W. Bender, E-FiRST: Electric field responsive shear thickening fluids. Rheol. Acta **42**(4), 287–294 (2003 Jul 1)

8. S. Gürgen, A. Sert, Polishing operation of a steel bar in a shear thickening fluid medium. Compos. Part B Eng. **175**, 107127 (2019 Oct)
9. S. Gürgen, M.A. Sofuoğlu, Vibration attenuation of sandwich structures filled with shear thickening fluids. Compos. Part B Eng. **186**, 107831 (2020 Apr)
10. S.S. Iyer, R. Vedad-Ghavami, H. Lee, M. Liger, H.P. Kavehpour, R.N. Candler, Nonlinear damping for vibration isolation of microsystems using shear thickening fluid. Appl. Phys. Lett. **102**(25), 251902 (2013 Jun 24)
11. K.M. Shum, Closed form optimal solution of a tuned liquid column damper for suppressing harmonic vibration of structures. Eng. Struct. **31**(1), 84–92 (2009 Jan)
12. C. Fischer, S.A. Braun, P.E. Bourban, V. Michaud, C.J.G. Plummer, J.A.E. Månson, Dynamic properties of sandwich structures with integrated shear-thickening fluids. Smart Mater. Struct. **15**(5), 1467–1475 (2006 Oct 1)
13. M. Wei, G. Hu, L. Jin, K. Lin, D. Zou, Forced vibration of a shear thickening fluid sandwich beam. Smart Mater. Struct. **25**(5), 055041 (2016 May 1)
14. M. Wei, K. Lin, L. Sun, Shear thickening fluids and their applications. Mater. Des. **216**, 110570 (2022 Apr)
15. S. Gürgen, M.A. Sofuoğlu, Experimental investigation on vibration characteristics of shear thickening fluid filled CFRP tubes. Compos. Struct. **226**, 111236 (2019 Oct)
16. S. Gürgen, W. Li, M.C. Kuşhan, The rheology of shear thickening fluids with various ceramic particle additives. Mater. Des. **104**, 312–319 (2016 Aug)
17. S. Gürgen, An investigation on composite laminates including shear thickening fluid under stab condition. J. Compos. Mater. **53**(8), 1111–1122 (2019 Apr)
18. R.C. Neagu, P.E. Bourban, J.A.E. Månson, Micromechanics and damping properties of composites integrating shear thickening fluids. Compos. Sci. Technol. **69**(3–4), 515–522 (2009 Mar)
19. S. Gürgen, M.C. Kuşhan, W. Li, Shear thickening fluids in protective applications: A review. Prog. Polym. Sci. **75**, 48–72 (2017 Dec)
20. S. Gürgen, Tuning the rheology of Nano-sized silica suspensions with silicon nitride particles. J Nano Res. **56**, 63–70 (2019 Feb)
21. S. Gürgen, M.C. Kuşhan, W. Li, The effect of carbide particle additives on rheology of shear thickening fluids. Korea-Aust Rheol J. **28**(2), 121–128 (2016 May)
22. Q. Zhao, J. Yuan, H. Jiang, H. Yao, B. Wen, Vibration control of a rotor system by shear thickening fluid dampers. J. Sound Vib. **494**, 115883 (2021 Mar)
23. M. Wei, K. Lin, Q. Guo, H. Sun, Characterization and performance analysis of a shear thickening fluid damper. Meas Control. **52**(1–2), 72–80 (2019 Jan)
24. K. Lin, H. Liu, M. Wei, A. Zhou, F. Bu, Dynamic performance of shear-thickening fluid damper under long-term cyclic loads. Smart Mater. Struct. **28**(2), 025007 (2019 Feb 1)
25. S. Gürgen, M.A. Sofuoğlu, M.C. Kuşhan, Rheological compatibility of multi-phase shear thickening fluid with a phenomenological model. Smart Mater. Struct. **28**(3), 035027 (2019 Mar 1)
26. T. Tian, G. Peng, W. Li, J. Ding, M. Nakano, Experimental and modelling study of the effect of temperature on shear thickening fluids. Korea-Aust Rheol J. **27**(1), 17–24 (2015 Feb)
27. L. Sun, J. Zhu, M. Wei, C. Zhang, Y. Song, P. Qi, Effect of zirconia nanoparticles on the rheological properties of silica-based shear thickening fluid. Mater Res Express. **5**(5), 055705 (2018 May 15)
28. S. Gürgen, M.C. Kuşhan, Rheological properties of shear thickening fluids. J. Polytech. **19**(4), 409–414 (2016)
29. S. Gürgen, M.A. Sofuoğlu, M.C. Kuşhan, Rheological modeling of multi-phase shear thickening fluid using an intelligent methodology. J. Braz. Soc. Mech. Sci. Eng. **42**(11), 605 (2020 Nov)
30. M. Wei, G. Hu, L. Li, H. Liu, Development and theoretically evaluation of an STF–SF isolator for seismic protection of structures. Meccanica **53**(4–5), 841–856 (2018 Mar)
31. S. Gürgen, M.A. Sofuoğlu, Smart polymer integrated cork composites for enhanced vibration damping properties. Compos. Struct. **258**, 113200 (2021 Feb)

32. G. Bossis, J.F. Brady, The rheology of Brownian suspensions. J. Chem. Phys. **91**(3), 1866–1874 (1989 Aug)
33. S.R. Raghavan, S.A. Khan, Shear-thickening response of Fumed silica suspensions under steady and oscillatory shear. J. Colloid Interface Sci. **185**(1), 57–67 (1997 Jan)
34. M.J. Decker, C.J. Halbach, C.H. Nam, N.J. Wagner, E.D. Wetzel, Stab resistance of shear thickening fluid (STF)-treated fabrics. Compos. Sci. Technol. **67**(3–4), 565–578 (2007 Mar)
35. B.J. Maranzano, N.J. Wagner, The effects of interparticle interactions and particle size on reversible shear thickening: Hard-sphere colloidal dispersions. J. Rheol. **45**(5), 1205–1222 (2001 Sep)
36. S. Gürgen, R.J.A. de Sousa, Rheological and deformation behavior of natural smart suspensions exhibiting shear thickening properties. Arch Civ Mech Eng. **20**(4), 110 (2020 Dec)
37. S. Gürgen, M.A. Sofuoğlu, Integration of shear thickening fluid into cutting tools for improved turning operations. J. Manuf. Process. **56**, 1146–1154 (2020 Aug)
38. X. Yuan, S. Wang, X. Mao, H. Liu, Z. Liang, Q. Guo, et al., Forced vibration mechanism and suppression method for thin-walled workpiece milling. Int. J. Mech. Sci. **230**, 107553 (2022 Sep)

Chapter 6
Shear Thickening Fluid in Surface Finishing Operations

Ziyan Man and Li Chang

6.1 Introduction

Shear thickening is a non-Newtonian flow behavior mostly observed in highly dense suspensions [1–3], exhibiting sudden phase transitions between liquid and solid states due to the reversible changes in viscosity (Fig. 6.1) [5]. The term "shear thickening" describes a sudden increase in viscosity by increasing shear rate. Numerous efforts have been made to explain the rheological properties of this smart fluid: one is hydro-cluster theory, where the Brownian interactions between suspended particles make the fluid flow easily at low shear rates, while hydrodynamic effects on the particles increase with the increasing shear rate [6]. Over the years, more theories have been proposed to explain the shear thickening mechanism, such as disorder-order transition [7], jamming [8], and dilatancy [9]. Recent studies have led to a new model, namely contact rheology model, suggesting that contact forces increase for the thickening onset where the particles contact each other at high shear rates [10, 11]. Although being studied for a long time, STF has not been utilized for engineering applications until the last two decades, including smart dampers [12] and liquid/soft armors [13–15].

The introduction of STF into the field of manufacturing and surface finishing is a more recent and a very novel idea. The first description of shear thickening polishing (STP) was reported in a 2013 patent disclosure by a research team from the University of Sydney [16]. The suspension was an ethylene glycol–based STF filled with 60 wt% polymeric particles (BASF AG, Ludwigshafen, Germany), which were in its liquid state under static conditions so that the specimen could be fully immersed. Silicon carbide (SiC) particles with sizes in the range of 45–1000 μm

Z. Man (✉) · L. Chang
School of Aerospace, Mechanical and Mechatronic Engineering, The University of Sydney, Sydney, NSW, Australia
e-mail: zman4889@uni.sydney.edu.au

S. Gürgen (ed.), *Shear Thickening Fluid*,
https://doi.org/10.1007/978-3-031-25717-9_6

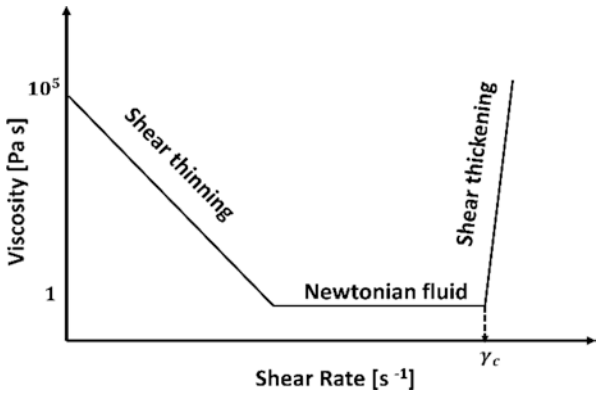

Fig. 6.1 Rheological behavior of dense suspensions [4]

were added to the STF as the abrasive medium. STP used the liquid- to solid-like characteristics of the STF when the rotational speed of the specimen reached the critical value, the surrounding STF substantially solidified, which firmly held the abrasive particles in place. Meanwhile, a normal force was also generated due to the shear thickening behavior of the STF. This leads to the formation of a "flexible fixed abrasive tool" [17] and, subsequently, the abrasive particles can polish all the surfaces of the specimen in contact with the STF simultaneously. It can be seen that STP enables the polishing of complex structures, for instance, curved surfaces, and surfaces at different heights or orientations, and even the potential of enabling inner surfaces to be polished simultaneously with the exterior surfaces.

In recent years, the STP method has been concept-proofed by different research groups [18, 19] and received increasing attention [20–22]. The process is currently used to polish the products with complex surfaces [23–25]. STP has great potential to address the limitations of the abovementioned non-conventional finishing methods. Compared to the traditional operations, common problems such as deep scratches on the surfaces, excessive plunge of abrasives, and drastic force increase are avoided due to the tough backing effect of the slurry in the process [26]. Nevertheless, up to now, there are still some limitations, for example, (1) difficulty in controlling shear thickening behavior in the optimal range with a nonlinear increase in the viscosity; (2) influenced machining efficiency and surface integrity due to the increasing contacting temperature within fluid [27]; and (3) larger agglomerates and poor surface integrity caused by shear induced clustering of particles [19].

STF has undergone a rapid development in the past decade, attributable to its great potential in surface finishing applications. Moreover, a large number of recent works has largely expanded this field and produced a new knowledge along with new methods such as chemistry-enhanced STP and magnetorheological STP. This chapter aims to provide the state-of-the-art literature studies on STF polishing from experimental, analytical, and numerical methods. It is anticipated to provide a better understanding of polishing mechanisms, improve the current processing systems, and broaden the applications of STP.

6.2 Fundamental Principles in Polishing with STF

Over the past decades, the surface qualities of components not only influenced their performance and life but also had a close relationship with the usability and reliability of the entire machine. The surface processing technology, as an effective method to promote surface qualities, has become one of the important ways to improve the serviceable performance and prolong lifespan of products [28]. Conventional finishing processes include grinding, polishing, shot peening, turning, milling, lapping, superfinishing, and honing. However, as it is quite challenging to control what happens in the processing and in that they entail the application of high pressures, deterministic machining could not always be ensured, and deep cracks on the finished surface are often generated [29]. To improve surface finishing quality, a large number of research studies have been carried out via the development of novel abrasive tools, for example, diamond whisker wheels, biomimetic grinding wheels, and fiber wheels [30]. Moreover, in the recent times, there has been a continuous development of non-conventional surface finishing to obtain ultra-precision surfaces with high surface quality and integrity (e.g., magnetorheological finishing, chemical mechanical polishing, electric emission machining, and abrasive flow machining) [31]. However, these methods may have certain limitations: (1) magnetorheological finishing is achieved by controlling viscosity with a magnetic field requiring a costly installation and large equipment, thus restricting its application in a much wider range; (2) chemical mechanical polishing requires chemical slurries that would impact on the environment; (3) surface finishing efficiency of the electric emission machining is limited by its nano or sub-nano level of material removal mechanism; and (4) rheological behavior of the polishing medium in the abrasive flow machining cannot be controlled externally, resulting in reduced accuracy and efficiency [26, 27, 32]. This, therefore, leads to searching for new surface processing techniques with higher quality and efficiency, environmental friendliness, and lower cost.

Very recently, STF has been introduced into the field, enabling a novel surface finishing technique for various engineering materials [16–25]. As schematically demonstrated in Fig. 6.2, the principle of STP process is based on the micro-level material removal actions [19]. Shear thickening effect of non-Newtonian fluids is triggered by flow velocity change (shear rate). The workpiece material is hard to be removed without shear thickening because of the insufficient dynamic force on the abrasive particles. Once the shear thickening occurs, the suspended particles in the slurry form particle clusters (i.e., hydroclusters), in which the abrasives are packed. The applied force on the abrasive particles is significantly increased to make the abrasive particles cut rather than rolling across the micro peak on the surface. After the removal of a small chip, hydrodynamic pressure increases, contributing to the increased dynamic force. Subsequently, more parts of the peak can be removed. As a result of the decreased peaks on the surfaces, the magnitude of shear thickening decreases as the abrasive particles pass over. Finally, as it approaches a smooth surface, the hydroclusters disintegrate.

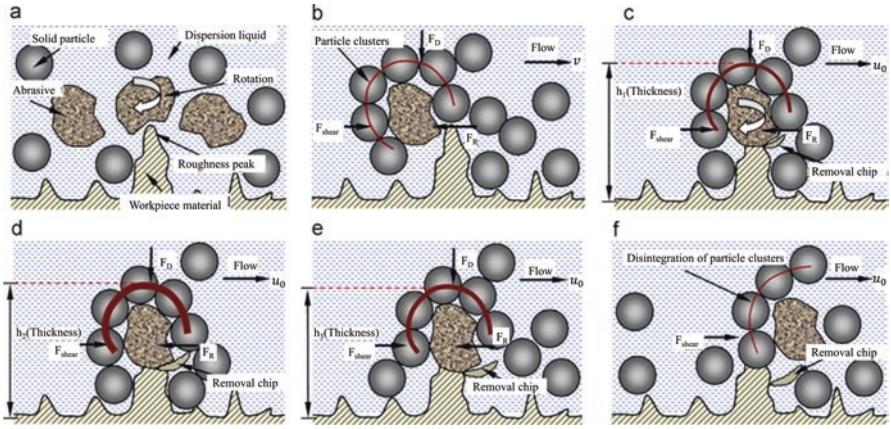

Fig. 6.2 Material removal mechanism in STP: (**a**) without shear thickening, (**b**) with shear thickening, (**c**) with a small removal chip sheared off by abrasive particle, (**d**) with a bigger removal chip under enhanced shear thickening, (**e**) material removal completed, and (**f**) disintegration of particle clusters [19]

According to recent studies, shear thickening behavior is governed by the contact forces between the particles rather than the hydrodynamic interactions at high shear rates [10]. The abovementioned mechanisms have been supplemented by Gürgen et al. [26]; at shear thckening regime, the inter-particle contact forces are added to the hydrodynamic forces, and thus, the abrasives are sufficiently supported by the shear thickened medium to realize the material removal from the workpiece. Besides, the fluid medium could provide a damping property in case of sudden force increases. Accordingly, excessive force generation and surface scratches are suppressed during the surface polishing process. It is also worth noting the work carried out by Span et al. [33], who firstly reported the shear-induced dynamic jamming mechanism in abrasive finishing applications. Within the context of their study, jamming refers to the formation of a localized, solid-like granular extensions of force chains at particle densities well below the critical value required for global jamming, with a characteristic feature of a significant increase in force when the jammed domain reaches and interacts with a rigid boundary [8].

6.3 Recent Advances in Polishing with STF

In recent years, numerous works have been performed on STP with a focus on the surface finishing of parts, aiming to achieve flexible polishing with higher efficiency and wider applications. In this section, the recent advances in STF finishing are reviewed about experimental characterization, numerical modelling and theoretical analysis.

6.3.1 Experimental Investigations

6.3.1.1 Materials and STF Preparation

In order to achieve high-efficiency polishing, emphasis should be firstly put on the preparation process of STP slurries, whose base liquid is a kind of non-Newtonian fluid added with abrasives, e.g., aluminum oxide (Al_2O_3), cerium dioxide (CeO_2), and diamond. From the relative literature, it is known that different compositions of STP slurries can result in various rheological properties, hence contributing to different surface finishing results. The most commonly used slurry is composed of the micro-sized multi-hydroxyl polymer as the first dispersion phase particle and deionized water as the dispersant. In Li et al.'s work [19], Al_2O_3 abrasives were added into the suspension, and the viscosity in terms of shear rate under different concentrations of abrasives was examined as shown in Fig. 6.3a. It is possible to mention that

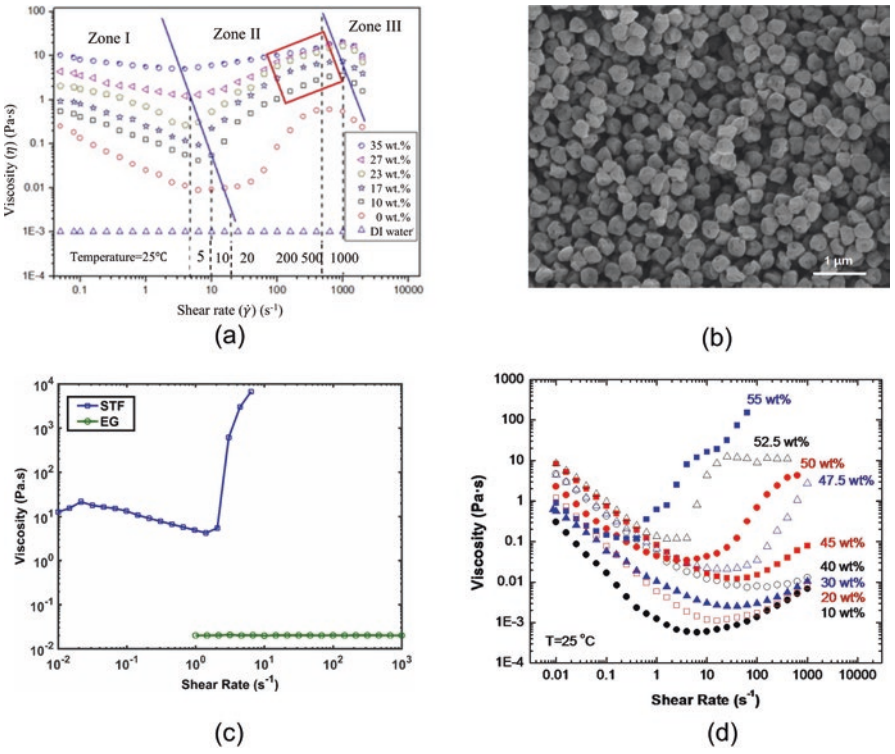

Fig. 6.3 (**a**) Variation of viscosity with respect to different shear rates for STP slurry with different concentration of Al_2O_3 abrasives [19]; (**b**) SEM image of styrene/acrylate particles [34]; (**c**) steady-state viscosity as a function of shear rate for EG and STF; (**d**) steady state shear rate ramp of cornstarch and water suspensions ranging in concentration from 10 to 55 wt.% [35]

the viscosity of deionized water was independent of the shear rate, while the slurries presented a shear thinning phase followed by a shear thickening regime. The inclusion of the particle abrasives interfered with the STF flow, which led to increased original viscosity of STF and decreased peak viscosity [36]. With increasing abrasive concentration, the shear rate at which shear thickening starts became lower and viscosity became larger.

Another well-studied slurry was prepared by dispersing micro- or nano-sized particles in polyethylene glycol (PEG) medium. For instance, in our previous study [34], we prepared styrene/acrylate particles (Fig. 6.3b) suspended in PEG. As shown in Fig. 6.3c, the viscosity of PEG almost remains constant with increasing shear strain rate, which indicates that the PEG is a Newtonian fluid. In comparison, STF exhibits a transition from shear thinning to shear thickening above a critical shear rate. In recent studies, nano-sized fumed silica was introduced, which showed a more beneficial effect on shear thickening behavior than the micron-sized colloidal particles [32]. This can be explained by the branchy particle structure of fumed silica and the increased surface area that contributes to a strong hydro-clustering mechanism of the suspension [26]. When comparing the multi-hydroxyl-based STF with fumed silica-based fluid, the maximum viscosities of neat slurry without abrasives were 0.6 Pa.s and 85.02 Pa.s, respectively. A similar observation has been made by Tian et al. [30], where the rheological properties of different dispersion systems were studied. The viscosity at the same shear rate differed by up to 11-fold when comparing 15 w.t.% and 20 w.t.% silica loadings. This was because the viscosity became large with increased particles and hydrogen bonds.

It is also worth noting a more accessible and environmentally friendly non-Newtonian fluid, i.e., cornstarch suspension, that has been utilized in multiple surface polishing applications [33, 37]. Its rheological behavior with different amounts are shown in Fig. 6.3d. Although being widely adopted, the size of starch agglomerates may vary in a very broad range for the suspension consisting of only starch and abrasives at high shear rates [38]. These larger starch agglomerates would greatly result in surface scratching during polishing. To address the issue, Zhu et al. [39] added polyacrylamide (PAM) into the mixture of starch and water to shift the thickening onset to a higher shear rate, which was attributed to the overall thinning effect in the suspension. Additionally, PAM polymer could form bridges between the destabilized particles, thereby developing hydroclusters [40] and promoting a stable suspension that enables both thickening mechanism by the starch and entangling of abrasive particles within the hydroclusters.

6.3.1.2 Polishing Systems with STF

Substantial experimental works have been conducted to assess STF surface finishing performance over the years; therefore, a range of experimental devices for STP process have been developed. As illustrated in Fig. 6.4, the polishing specimen is mounted and submerged to a cup filled with STP slurries, while the polishing tank is driven by a step motor. During the polishing process, the rotational speed and the

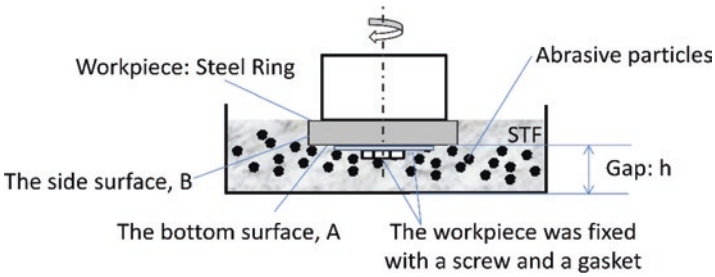

Fig. 6.4 Illustration of STP experimental configuration [41]

distance between the specimen and cup base are adjusted to guarantee the shear thickening conditions [19]. By using a similar setup, the impact of inclination angle on surface quality during the machining process has also been investigated by several researchers [20, 21]. In their studies, the workpiece was fixed with a certain tilt angle, i.e., the angle between the substrate surface and the horizontal plane. In some works, tribometers with pin-on-disk configurations have also shown the capability of STF polishing [26, 41]. All the above mentioned works mainly concentrate on full-aperture finishing by immersing the workpiece into a polishing slurry, which could simplify the industrial production equipment. However, deterministic polishing cannot be realized by such an apparatus. In order to achieve freeform surface polishing, a 7-axis CNC machine was utilized in Zhu et al.'s works, which offer great potential to have a controllable material removal process. In their studies, the A-axis and B-axis enabled different process angles and tool directions, while the workpiece was fixed to an XYZ translational stage on the other side [39, 42].

6.3.1.3 Effect of Processing Parameters

The shear thickening finishing is closely related to a number of processing variables such as polishing speed, abrasive grit size and particle loading, and impact angle. Li et al. [19] were among the pioneers who studied the effect of polishing speed in STP process. The experimental results showed that the material removal rate (MRR) presented a power-function rise with increasing polishing velocity, while surface roughness gradually decreased with time and reached a steady value at the final stage. Better surface finishing was achieved with higher speed during the same period of polishing. This could be explained by the enhanced shear thickening and cutting ability of abrasive particles surrounded firmly by colloidal particles. According to Span et al.'s study [33], the polishing speed not only gives the material removal rate but also directly influences the shear rate in STF [23], which determines the resultant force applied on the abrasive particles. The positive effect of polishing speed on STP has also been reported by the following researchers [22, 24]. Gürgen et al. [26] compared the polishing effect within different viscosity zones (i.e., shear thinning and shear thickening) by controlling the linear speed of

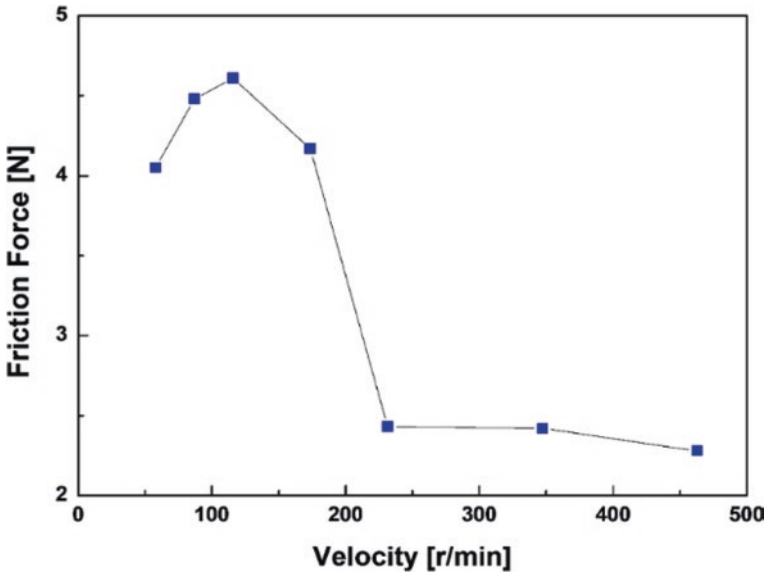

Fig. 6.5 Friction force under various rotation speeds [41]

specimen. It is found that an efficient surface finishing result can only be achieved when the velocity reflects the shear thickened regime. In a recent work [41], the friction force as a function of rotation speed was examined in a wider range as shown in Fig. 6.5, depicting the average friction values in the steady polishing phase. It is important to state that the friction force was initially increased with the rotation speed, which was attributed to the thickening effect owing to the increasing shear rate, with the growing friction force associating with shear jamming in STF. However, the friction force significantly dropped with the further increase in the rotation speed. Afterward, increasing velocity resulted in a much lower friction force, which may be due to the wall-slip behavior in the STF. Though the thickened STF exhibited a stable, smooth surface against the workpiece, no strong polishing ability was observed at higher rotational speeds.

Extensive studies have also been conducted to examine the influence of abrasive particles [19, 20]. Figure 6.6a shows that MRR has a linear rise with the increase of abrasive concentration, as the active number of abrasive particles is increasing. However, excessive amount of abrasives will suppress the polishing effect, which can be explained by the uneven agglomeration of particles that may result in damages on the surface. Interestingly, different conclusions based on the effect of abrasive size upon polishing performance were drawn by various research teams. For example, Li et al. [19] found that, although increasing grain size resulted in decreased MRR, it had a slight effect on the average surface roughness after polishing [19]. It is believed that large abrasive particles are similar to small abrasives in the sense that neither will cause visible scratches on the surface and can produce a smooth surface [43]. According to our previous study, the resultant surface

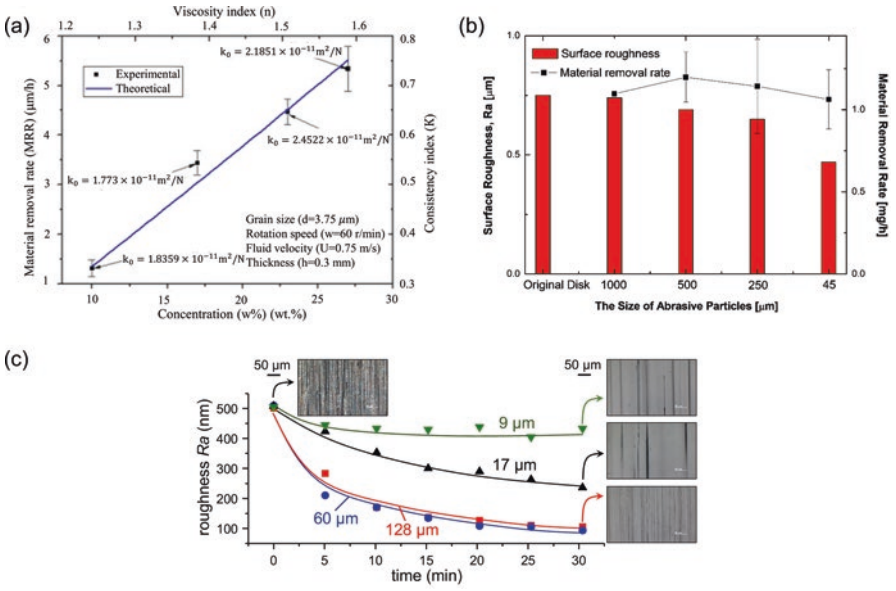

Fig. 6.6 Influence of abrasive particles on STP performance: (**a**) MRR as a function of abrasive concentration [19]; (**b**) surface roughness and MRR as a function of grain size [41]; (**c**) dependence of finishing performance on abrasive size [33]

roughness decreased by using finer particles, which was in agreement with the observation by Lyu et al. [23]. It is believed that a smaller size means more abrasive particles are included in the STP suspension under the same abrasive loading, leading to improved surface polishing efficiency. Yet the removal rate in the process was slightly affected by the size of particles (Fig. 6.6b). This may be because the friction force and normal pressure mainly depend on the mechanical properties of suspension beyond the thickening point. Those are the key factors in determining the MRR from the workpiece [41]. In comparison, different observations were obtained in the work by Span et al. [33] as shown in Fig. 6.6c; the coarser abrasives attributed to a better surface processing performance. It was obvious that relatively poor performance of the finer abrasive particles was due to their ineffectiveness in removing a few deep scratches on the workpiece surface. It is also claimed that the abrasive effect on surface processing may be related to the size and morphology of solid colloidal particles [19], which has been further proved by Li et al. [18] by performing STP under different ratios of abrasive particle size to polymer size. When the ratio was smaller than 0.5, material removal was predominated by plastic ploughing; thus, the workpiece ahead of the abrasive cutting edge was heavily squeezed and polished, causing the deterioration of surface quality. If the ratio was greater than 0.5, an increased ratio would lead to a better surface finish.

In addition, the effect of the inclination angle of specimen is often discussed, particularly in polishing complex-shaped parts [23, 39, 44]. It is known that the rapidly growing demand for complex surfaces requires high surface finishing and high-efficiency processing technologies, which have contributed to the research of

STP of cylindrical and complex workpieces over the past few years. According to the literature, the selection of angle range varied significantly, which is strongly dependent on workpiece geometries. In the work of STP for spherical steels by Nguyen et al. [22], the experimental results showed that surface roughness increased in the tilt angle ranging from 0° to 3° due to the smallest cutting pressure. Better surface finishing can be achieved with the increased inclination angle in the range of 5° and 15°. For inner raceway surface polishing, the overall roughness lowers significantly at tilt angles between 12.5° and 25°; however, further increase in angle brings uneven surface characteristics, indicating poor polishing quality [44]. It is also worth noting that the surface roughness has different levels on the workpiece surface. The smoothest surface was found near the top position of the component. This could be explained by the fact that the bottom surface of the polishing slurry tends to change into solid than the upper fluid layer and, therefore, the cutting pressure on the surface is larger. Similar phenomenon has been observed in other work, where the polishing effect varied upon different locations of gear surfaces [21]. Because of the less contact of the back surface with polishing fluid, the distributed pressure is smaller than the front gear surfaces, and the surface finishing is thus worse. It is also reported by Guo et al. [44] that the over-processing phenomenon at the entrance leads to uneven polishing, namely the edge effect in STP. To realize the uniformity and high quality of surface polishing, a guide block with the same angle as that of the ring cross-section is introduced in the fixture. Considering a series of processing parameters, some researchers extensively utilized the Taguchi experimental design method or the analysis of variance (ANOVA) to explore the optimization of multiple factors involved in the STP [20, 21, 45]. Results showed that by selecting the optimal combination of the polishing parameters, STP is an effective and feasible technique for surface finishing, even with complicated shapes.

6.3.2 Analytical Modeling

It can be seen that experimental investigations require specific workpieces and equipment, which can result in a heavy burden of resources and time. Therefore, numerous works have been performed to develop analytical models with high efficiency and low cost solutions for STP performance, and providing key estimation for the optimal selection of polishing parameters. To identify the polishing mechanism, it is of great significance to study the material removal. The Preston equation is a widely adopted empirical formula relating the MRR to work done by the friction force and guiding the precision finishing [46]. The Preston equation is expressed in Eq. (6.1).

$$\mathrm{MRR} = kPv = k_0 PU_0 \tag{6.1}$$

where k is a proportional constant ($k_0 = k_1 \times k_2 \times k_3$), P is the pressure on the specimen surface, and v is the abrasive velocity. Under specific process parameters, k_1, k_2, and

k_3 are the coefficients corresponding to the specimen material hardness, the coefficient related to abrasive particle size, and the coefficient influenced by other factors, respectively; U_0 is the relative velocity of the polishing fluid to the workpiece surface [19]. The theoretical prediction is normally verified by the experimentally obtained MRR, i.e.,

$$\mathrm{MRR} = \Delta m / \rho S \tag{6.2}$$

where Δm is the weight loss after polishing, ρ is the density, and S is the processing area [31].

Regarding STP, it is also essential to study the fluid field and calculate the pressure acting on the workpiece [45]. According to the rheological flow mechanics, STP suspension can be characterized as non-Newtonian power-law fluid with the assumption of being homogeneous, isotropic, and incompressible in nature [19]. Li et al. [18] firstly developed a mathematical model with dynamic pressure to analytically govern the Reynolds equation for predicting MRR. As an extension to the MRR model, a surface roughness model was then developed, which can predict the surface evolution process. The model was proposed based on the workpiece Brinell hardness, shear thickening mechanism, and plastic indentation on abrasive wear theory. Additionally, Li et al. [27] recently established a subsurface damage predictive model for adaptive shearing-gradient thickening polishing. According to the results, the theoretical calculation is verified by the experiments, being close to that from experimental data, and the maximum difference between experimental and analytical results is no greater than 12.02% [18]. In Zhu et al. [42]'s study, the STP slurry was considered as incompressible viscous laminar flow governed by Navier-Stokes equations, and then the equivalent principal stress, as well as the material removal, was estimated. Nevertheless, it is pointed out that the varying viscosity of non-Newtonian slurry couples with fluid velocity and dynamic pressure, which affects the stress field distribution [39]. Hence, Reynolds approximation in the lubrication-based model cannot make an accurate prediction of MRR due to the overestimation of fluid stress. In a recent study by Zhu et al. [39], a comprehensive model describing the dynamic couplings of pressure and velocity and microscopic abrasive removal mechanism correlating to the suspension rheology is proposed, offering a generic and flexible model for STP process.

6.3.3 Numerical Simulation

With the rapid growth of computational methods and computer science, numerical simulations have been widely used to predict the stress distribution, rheological flow, and material removal behavior, which are quite complicated to measure by direct experimental effort. Considering the multiple influential factors that are discussed in the last section, the numerical study also enables the optimization of polishing parameters more efficiently. Most finite element simulation is carried out by

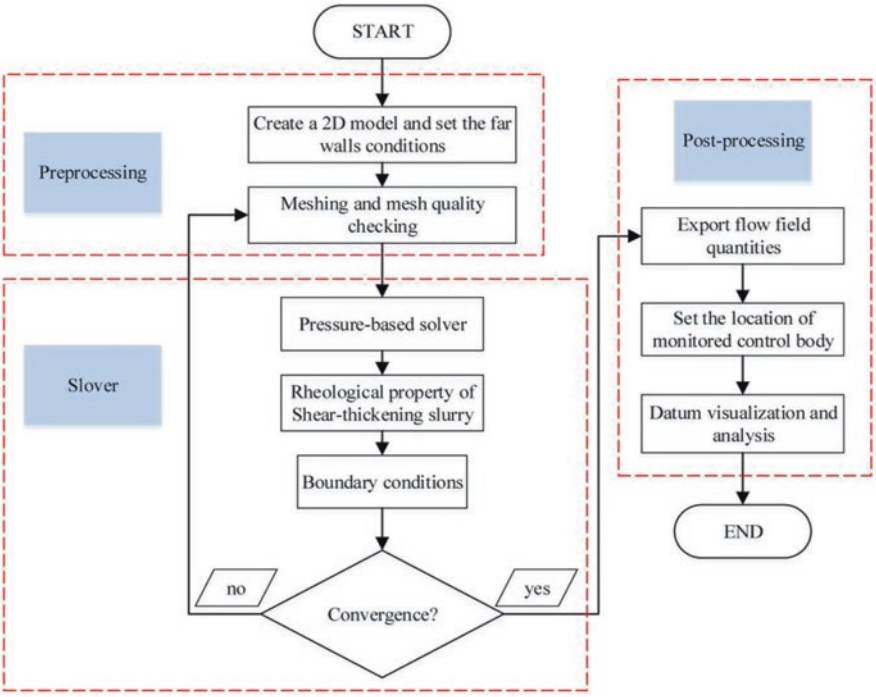

Fig. 6.7 Flowchart of numerical calculation process [44]

computational fluid dynamics (CFD) software such as ANSYS CFX [21, 24], and a representative flowchart of the simulation analysis is demonstrated in Fig. 6.7. In Guo et al. [44]'s work, a 2D model was established to simplify the numerical work with the assumption of a rectilinear flow through the channel. In the literature, as STP is commonly utilized for complex-shaped surfaces, such an assumption is not always valid. Hence, 3D models are more frequently created based on the geometry of the workpiece [24, 47]. Before the simulation work, the STF flow curve is input to the software, which can also be described as the specific consistency coefficient and flow index of the shear thickening slurry [21]. In addition, boundary conditions, including the parameters of the liquid inlet, the liquid outlet, the polishing cup and the workpiece, are required to be specified. Mostly, the constant velocity of low corresponding to the non-Newtonian power-law is set at the inlet, and the outlets are set to constant pressure.

As known from the experimental results, polishing angle heavily influences the flow field distribution of polishing slurry, which affects the velocity and pressure distribution on the workpiece surface. Accordingly, the MRR and surface quality are directly influenced by the pressure and velocity distribution. Therefore, numerical works investigate the distribution of velocity (v) and pressure (P) in terms of different processing parameters [22, 24, 44]. For example, by investigating the normalization of P.v value at different impact angles through numerical methods, it is

found that using an inclination angle of 45° would contribute to the highest P.v value and the lowest variance on the surface, as well as the best removal efficiency and polishing quality. The numerical results have shown consistency with the experimental data [44]. Apart from velocity and pressure, the maximum principal stress and maximum tool deformation are also used as output for simulation analysis [39]. Zhu et al. [42] studied the shear stress and equivalent principal stress in a tool contact region with regard to the varying working gap and tool rotation speed. The results also proved the simulation analysis to be a powerful methodology to predict the STF polishing results.

6.3.4 Engineering Applications

STP method, utilizing the shear thickening behavior, has developed recently to process complicated surfaces with high quality, high efficiency, and low cost. However, it should be noted that the quality and efficiency of surface processing are restricted since the material removal is driven by the mechanical action of the abrasives [48]. This is particularly significant for hard and brittle crystals with a lack of chemical mechanisms. Therefore, Li et al. [32] proposed an approach with the combination of shear thickening based micro-cutting and chemo-physical friction for ultra-precision finishing optical materials, lithium niobite ($LiNbO_3$). The formation of chemical soft reaction layers can effectively lower the surface hardness of $LiNbO_3$, realizing the polishing action of the "polymer-Al_2O_3-network." Their results show that an ultra-precision high-accuracy surface with roughness Ra 1.46 nm and low subsurface damage (<5 nm of damage depth) can be attained, proving to be a novel STF processing concept for optical crystal materials.

Regarding the machining of optical materials, another factor that should be taken into account is reducing subsurface damage, which would heavily influence the mechanical strength and optical quality [49]. In Li et al. [32]'s study, a novel adaptive shearing-gradient surface finishing method is first developed for enhanced surface quality and suppressed subsurface damage on $LiNbO_3$. The STP system includes thermo-sensitive particles and a temperature-controlling device, in order to achieve the concept of fluid-workpiece contacting temperature-induced gradient thickening mechanism. The results showed different levels of jamming with changing temperatures, while the subsurface damage depth and surface roughness were lowered to a minimum critical threshold of 1 nm under certain conditions.

In order to improve the efficiency of STP, some researchers observed that the magnetic field could raise the shear rate in STF, thus resulting in a liquid with a higher yield stress, which affects the polishing effect. Ren et al. [50] and Ming et al. [51] introduced carbonyl iron particles into STF, and it was found that the shear thickening behavior of magnetorheological STF contributes to the particle clustering due to magnetic chains and hydrogen bonds. Under the magnetic field, the shear stress becomes higher, and the maximum MRR is approximately 5.96 μm/h, which is 95.4% higher than that of neat STP. In addition, the magnetic-assisted STF did not

cause any damage to the processed zirconia surface, providing characteristics of non-destructive, adaptive and ultra-precision processing of ceramic-based brittle and hard materials [52].

Apart from the abovementioned applications of STP, STF was also applied to improve other surface finishing methods. For instance, abrasive flow machining is a technique for polishing complex components by extruding abrasive media. However, conventional abrasive media with shear-thinning properties present poor capacities of anti-deformation and carrying abrasives under high shear rate conditions [53]. By changing media to STF, the MRR increases from 69 to 351 mg/h, and the value of Ra reduces from 19.49 nm to 6.48 nm, appearing with fewer machining strokes. Another concept of using cornstarch mixture in a cutting-based vibration attenuation system was proposed by Wang et al. [37]. In the milling operation of thin-walled structures, vibrations induced by the cutting forces could lead to low surface quality and static deflections. By comparing milled workpieces immersed with and without cornstarch mixture, the average maximum amplitudes of the acceleration signals are decreased by 90% by using the cornstarch loading rate of 48% or more in the slurry.

6.4 Conclusions

This chapter reviews recent advances in developing new surface finishing technology by utilizing STF. It can be stated that a lot of experimental work has demonstrated that the new technology is promising to polish complex structures having curved surfaces. Compared with the conventional mechanical polishing process, it is less dependent on the geometric features of the treated surface. Further, a polishing pad is not required, as the abrasive particles are held by solidified STF. In this case, the polishing process relies on the shear thickening behavior of the STF, depending on operation parameters such as speed and working gap. Besides the experiment work on surface finishing with STF, the chapter also reviews the theoretical modeling for understanding the underlying mechanisms. Finally, some practical applications of this new polishing technology are discussed.

References

1. H.A. Barnes, Thixotropy—A review. J. Non-Newtonian Fluid Mech. **70**(1), 1–33 (1997)
2. Y.S. Lee, N.J. Wagner, Dynamic properties of shear thickening colloidal suspensions. Rheol. Acta **42**(3), 199–208 (2003)
3. S. Gürgen, M.C. Kuşhan, W. Li, Shear thickening fluids in protective applications: A review. Prog. Polym. Sci. **75**, 48–72 (2017)
4. L. Chang et al., Shear-thickening behaviour of concentrated polymer dispersions under steady and oscillatory shear. J. Mater. Sci. **46**(2), 339–346 (2011)

5. L. Chang, Z. Man, L. Ye, A study on the mechanical polishing technique by using shear thickening fluids. Journal of Micromechanics and Molecular Physics **6**(3), 25–29 (2021)
6. N.J. Wagner, J.F. Brady, Shear thickening in colloidal dispersions. **62**(10), 27–32 (2009)
7. R.L. Hoffman, Discontinuous and dilatant viscosity behavior in concentrated suspensions--1. Observation of a flow instability. Trans. Soc. Rheol. **16**(1), 155–173 (1972)
8. E. Brown, H.M. Jaeger, Shear thickening in concentrated suspensions: Phenomenology, mechanisms and relations to jamming. Rep. Prog. Phys. **77**(4), 046602 (2014)
9. E. Brown, H.M. Jaeger, The role of dilation and confining stresses in shear thickening of dense suspensions. **56**(4), 875–923 (2012)
10. R. Seto et al., Discontinuous shear thickening of frictional hard-sphere suspensions. Phys. Rev. Lett. **111**(21), 218301 (2013)
11. R. Mari et al., Shear thickening, frictionless and frictional rheologies in non-Brownian suspensions. **58**(6), 1693–1724 (2014)
12. J. Lim, S.-W. Kim, Enhanced damping characteristics of carbon fiber reinforced polymer–based shear thickening fluid hybrid composite structures. J. Intell. Mater. Syst. Struct. **31**(20), 2291–2303 (2020)
13. Y.S. Lee, E.D. Wetzel, N.J. Wagner, The ballistic impact characteristics of Kevlar® woven fabrics impregnated with a colloidal shear thickening fluid. J. Mater. Sci. **38**(13), 2825–2833 (2003)
14. S. Gürgen, M.C. Kuşhan, The stab resistance of fabrics impregnated with shear thickening fluids including various particle size of additives. Compos. A: Appl. Sci. Manuf. **94**, 50–60 (2017)
15. J. Qin et al., Soft armor materials constructed with Kevlar fabric and a novel shear thickening fluid. Compos. Part B **183**, 107686 (2020)
16. Chang, L, Klaus Friedrich, Lin Ye, Method, Systems and Compositions for polishing. International Patent WO/2013/016779, 2013
17. M. Wei, K. Lin, L. Sun, Shear thickening fluids and their applications. Mater. Des. **216**, 110570 (2022)
18. M. Li et al., Evolution and equivalent control law of surface roughness in shear-thickening polishing. Int. J. Mach. Tools Manuf. **108**, 113–126 (2016)
19. M. Li et al., Shear-thickening polishing method. Int. J. Mach. Tools Manuf. **94**, 88–99 (2015)
20. B.H. Lyu et al., Shear thickening polishing of black lithium tantalite substrate. Int. J. Precis. Eng. Manuf. **21**(9), 1663–1675 (2020)
21. D.-N. Nguyen et al., Machining parameter optimization in shear thickening polishing of gear surfaces. J. Mater. Res. Technol. **9**(3), 5112–5126 (2020)
22. D.-N. Nguyen, Simulation and experimental study on polishing of spherical steel by non-Newtonian fluids. Int. J. Adv. Manuf. Technol. **107**(1), 763–773 (2020)
23. B.H. Lyu et al., Experimental study on shear thickening polishing of cemented carbide insert with complex shape. Int. J. Adv. Manuf. Technol. **103**(1), 585–595 (2019)
24. Q. Shao et al., Shear thickening polishing of the concave surface of high-temperature nickel-based alloy turbine blade. J. Mater. Res. Technol. **11**, 72–84 (2021)
25. M. Li, B. Karpuschewski, O. Riemer, High-efficiency nano polishing of steel materials. Nanotechnol. Rev. **10**(1), 1329–1338 (2021)
26. S. Gürgen, A. Sert, Polishing operation of a steel bar in a shear thickening fluid medium. Compos. Part B **175**, 107127 (2019)
27. M. Li et al., Adaptive shearing-gradient thickening polishing (AS-GTP) and subsurface damage inhibition. Int. J. Mach. Tools Manuf. **160**, 103651 (2021)
28. S. Yang, W. Li, H. Chen, *Surface finishing theory and new technology.* (Springer, 2018)
29. L. Heng et al., A Review on Surface Finishing Techniques for Difficult-to-Machine Ceramics by Non-Conventional Finishing Processes. **15**(3), 1227 (2022)
30. Y. Tian et al., Development of novel high-shear and low-pressure grinding tool with flexible composite. Mater. Manuf. Process. **36**(4), 479–487 (2021)
31. Q. Shao et al., Shear thickening polishing of quartz glass. Micromachines **12**(8), 956 (2021)
32. M. Li et al., Origin of material removal mechanism in shear thickening-chemical polishing. Int. J. Mach. Tools Manuf. **170**, 103800 (2021)

33. J. Span et al., Dynamic jamming in dense suspensions: Surface finishing and edge honing applications. CIRP Ann. **66**(1), 321–324 (2017)
34. K. Fu et al., Confined compression behaviour of a shear thickening fluid with concentrated submicron particles. Composites Communications **10**, 186–189 (2018)
35. N.C. Crawford et al., Shear thickening of corn starch suspensions: Does concentration matter? J. Colloid Interface Sci. **396**, 83–89 (2013)
36. S. Gürgen, W. Li, M.C. Kuşhan, The rheology of shear thickening fluids with various ceramic particle additives. Mater. Des. **104**, 312–319 (2016)
37. S.Q. Wang et al., Vibration-free surface finish in the milling of a thin-walled cavity part using a corn starch suspension. J. Mater. Process. Technol. **290**, 116980 (2021)
38. P. Bubakova, M. Pivokonsky, P. Filip, Effect of shear rate on aggregate size and structure in the process of aggregation and at steady state. Powder Technol. **235**, 540–549 (2013)
39. W.-L. Zhu, A. Beaucamp, Generic three-dimensional model of freeform surface polishing with non-Newtonian fluids. Int. J. Mach. Tools Manuf. **172**, 103837 (2022)
40. B. Xiong et al., Polyacrylamide degradation and its implications in environmental systems. Npj clean. Water **1**(1), 17 (2018)
41. L. Chang, Z. Man, L. Ye, A study on the mechanical polishing technique by using shear thickening fluids. Journal of Micromechanics and Molecular Physics **06**(03), 25–29 (2021)
42. W.-L. Zhu, A. Beaucamp, Non-Newtonian fluid based contactless sub-aperture polishing. CIRP Ann. **69**(1), 293–296 (2020)
43. I.D. Marinescu, E. Uhlmann, T. Doi, *Handbook of Lapping and polishing* (CrC Press, 2006)
44. L. Guo et al., Shear-thickening polishing of inner raceway surface of bearing and suppression of edge effect. Int. J. Adv. Manuf. Technol. (2022)
45. W. Yao et al., Modeling of material removal based on multi-scale contact in cylindrical polishing. Int. J. Mech. Sci. **223**, 107287 (2022)
46. F.W. Preston, The theory and design of plate glass polishing machines. J. Soc. Glass Tech. **11**(44), 214–256 (1927)
47. D.-N. Nguyen et al., Simulation and optimization study on shear thickening polishing of complex surfaces, in *Proceedings of the 2nd Annual International Conference on Material, Machines and Methods for Sustainable Development (MMMS2020)*, (Springer International Publishing, Cham, 2021)
48. J. Wang et al., Chemistry enhanced shear thickening polishing of Ti–6Al–4V. Precis. Eng. **72**, 59–68 (2021)
49. S. Agarwal, P.V. Rao, Experimental investigation of surface/subsurface damage formation and material removal mechanisms in SiC grinding. Int. J. Mach. Tools Manuf. **48**(6), 698–710 (2008)
50. Y. Ren et al., Research on the rheological characteristic of magnetorheological shear thickening fluid for polishing process. Int. J. Adv. Manuf. Technol. **117**(1–2), 413–423 (2021)
51. Y. Ming et al., A novel non-Newtonian fluid polishing technique for zirconia ceramics based on the weak magnetorheological strengthening thickening effect. Ceram. Int. **48**(5), 7192–7203 (2022)
52. Y. Ming et al., Rheological properties of magnetic field-assisted thickening fluid and high-efficiency spherical polishing of ZrO2 ceramics. Int. J. Adv. Manuf. Technol. **121**(1–2), 1049–1061 (2022)
53. H. Wei, H. Gao, X. Wang, Development of novel guar gum hydrogel based media for abrasive flow machining: Shear-thickening behavior and finishing performance. Int. J. Mech. Sci. **157-158**, 758–772 (2019)

Chapter 7
Shear Thickening Fluid–Based Protective Structures Against Low Velocity Impacts

Unsanhame Mawkhlieng, Mukesh Bajya, and Abhijit Majumdar

7.1 Introduction

The application of shear thickening fluid (STF) for protective structures has been researched extensively in the past couple of decades [1–5]. Specifically for textile structures intended for low velocity impact applications, STF has been found to be advantageous on many occasions [6, 7]. STF is a category of non-Newtonian fluid that hardens temporarily upon being impact. The opposite of quicksand, STF responses to sudden impact by forming a clustered mass that can resist and absorb the impact energy. This unique behavior of the fluid prompted researchers at the University of Delaware and the US Army Research Laboratory to explore its suitability for impact application [8, 9]. Since the use of STF with Kevlar® fabric revived in 2003 in the University of Delaware, many researchers have explored the possibility of a commercially feasible "liquid" armor [10]. Shear thickening is a triggered and reversible phenomenon, which means that under normal circumstances, STF does not affect the stiffness of the fabrics. STF has been studied extensively and a series of hypotheses have been proposed as an

U. Mawkhlieng
Department of Textile Design, National Institute of Fashion Technology Shillong, Shillong, India

Department of Textile and Fiber Engineering, Indian Institute of Technology Delhi, New Delhi, India

M. Bajya · A. Majumdar (✉)
Department of Textile and Fiber Engineering, Indian Institute of Technology Delhi, New Delhi, India
e-mail: majumdar@textile.iitd.ac.in

S. Gürgen (ed.), *Shear Thickening Fluid*,
https://doi.org/10.1007/978-3-031-25717-9_7

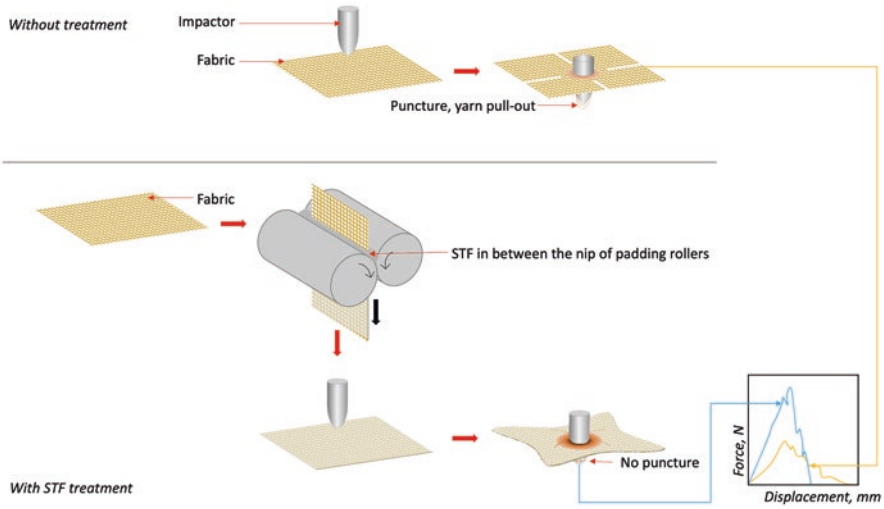

Fig. 7.1 A typical protocol adopted for impact test of (**a**) neat; (**b**) STF-treated fabrics

explanation to this reversible phenomenon of shear thickening. Several reviews [11–15] have been put forth to consolidate the works that have been carried out in the exploration of STF as a novel fluid as well as in its application for stab and impact resistances.

A quick overview explaining the common methodology of energy absorption assessment is presented here. Fabrics are treated with STF and then subjected to impact, the speed of which can vary significantly. The most followed protocol is depicted in Fig. 7.1. Most of the works report the behavior of STF-treated fabrics against low velocity impacts in the form of a drop tower test. In essence, an indenter or impactor in the shapes of knives, spikes, needles, blunt impactors, and flat impactors is made to fall from a certain height, carrying a certain amount of potential energy. The fabric that is placed at the bottom of the indenter absorbs much, if not all of its energy. The energy absorbed is then recorded. Sometimes, researchers present the values in terms of specific energy absorption which is a weight normalized figure. For higher velocity impact test by a projectile or bullet, the experimental setup is different. The target is usually placed at a certain distance away from the source of impact, usually separated by a velocity measuring system (VMS), say entry VMS. When energy absorption is considered, then another set of system, say exit VMS is placed after the target. On the other hand, when the behind armor blunt trauma (the indentation that occurs behind the armor if the bullet is stopped by the target) is assessed, then only the entry VMS is present. A representation of the test setups is shown in Fig. 7.2.

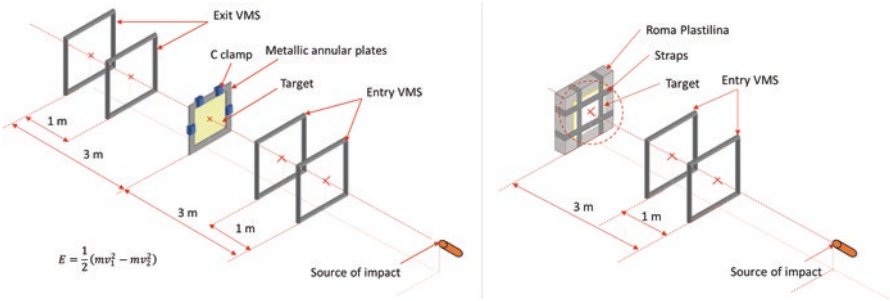

Fig. 7.2 A typical setup of a ballistic test for (**a**) exit velocity or energy absorption; (**b**) back face signature evaluation

7.2 Approaches to Improve the Energy Absorption of STF-Treated Structures

Researches have stretched in different directions with the sole purpose of improving the performance of STF-treated structures either in terms of energy absorption or reduction of weight and stiffness for a given level of performance. An extensive literature survey [16–21] reveals that the entire research is broadly concentrated in two different directions. Some works focus on improving the energy absorption capacity of the STF itself, while others, on enhancing the combined effect of STF and the structure in which it is integrated. Figure 7.3 depicts the different approaches that pertain to the use of STF-based protective structures against low velocity impacts.

In the first approach, some noteworthy steps that have been taken with the intent to tune the rheological behavior of the STF include the following:

1. Varying the contents of the fluid, either the dispersed phase (solid phase) or the dispersion medium (liquid phase). Here, either the contents are changed altogether, or the quantity of the content is altered.
2. Mixing two or more solid particles, either of the same material but with different sizes, or of completely different materials.
3. Introducing "foreign" additives in addition to the usual contents of the fluid to improve the "peak" viscosity. These foreign additives are either in the nano- or micro-scale.

In the second approach, the structure, mostly fabric, is modified to improve its overall energy absorption behavior after its treatment with STF. In this domain, several steps have been explored majorly aiming at optimizing the interaction of the fabric structure with the STF. Some of the approaches reported in literature include the following [22–24]:

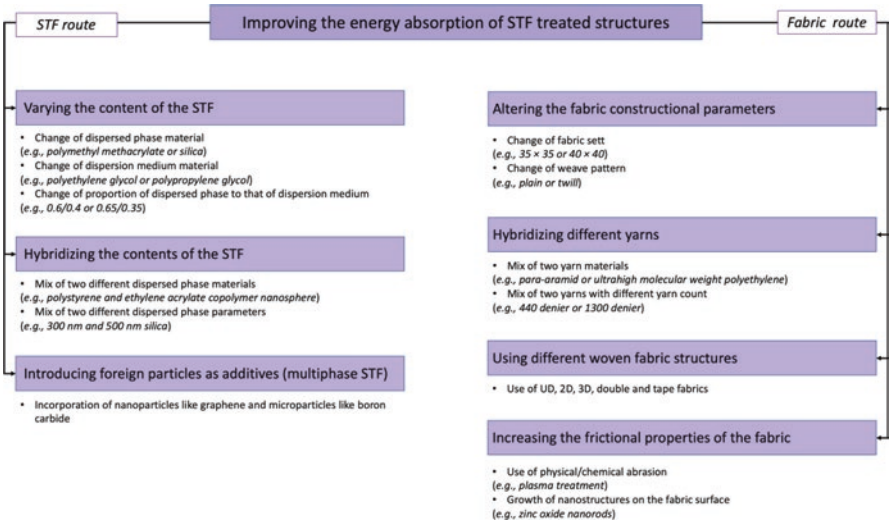

Fig. 7.3 Approaches to improve the energy absorption of STF-treated structures

1. Altering the fabric construction through parameters such as fabric sett (ends per inch and picks per inch) and weave pattern, which by extension, alters the areal density and the porosity of the structure.
2. Hybridizing different yarns, either of the same materials but with different parameters (mostly, yarn count) or of different materials altogether.
3. Exploring structure other than the conventional 2-dimensional (2D) fabric, such as unidirectional (UD), double, and 3-dimensional (3D) fabrics.
4. Increasing the internal friction of the fabric through physical and chemical roughening such as plasma treatment, or through the growth of nanostructures on the fabric surface.

7.2.1 STF Route

7.2.1.1 Varying the Content of the STF

Rheological properties of STF can be modified by changing the constituent parameters of the dispersed phase or dispersion medium or by varying the ratio of the two [25–27].

Rheological properties of STF are modified by changing the dispersed phase of the STF or the parameters thereof. Researchers have explored various materials such as silica (SiO_2), polymethylmethacrylate (PMMA), and polystyrene-ethyl acrylate nanoparticles as dispersed phase. Each particle type is expected to cause a different response in the flow behavior of the fluid due to the change in the interaction between the two phases in the STF. In fact, several research works show that when a fabric is treated with different STFs, their response to low velocity impact is

different. In general, the low velocity impact response depends on two factors: (1) types of particles and (2) types of low velocity impact. As far as particle type is concerned, the major deciding factor is particle hardness [28, 29]. Several review articles [12, 13, 30] have briefed about this aspect. However, the role of particle hardness seems to be relevant when the impact velocity is low and when the type of impact is knife-stab, involving severing of the structure. This is seen in the work of Gong et al. [31, 32], who found that for puncture type of impact involving major yarn pull-out, the fabrics treated with harder SiO_2-based STF did not perform better than those treated with softer polystyrene-ethyl acrylate based STF. Here, the role of fabric friction comes to play, and it is observed that those fabrics with the most internal friction, as estimated through tests such as yarn pull-out, tend to absorb higher puncture energy [31].

Shear thickening has also been tuned by changing the dispersion medium, keeping the dispersed phase constant. This aspect has been concisely reviewed by Gürgen et al. [12] and Mawkhlieng and Majumdar [11] in their respective progresses. A general understanding that emerges from the conclusion of different studies is that the dispersion medium not only "carries" the dispersed phase, but also has an interactive effect on the rheological behavior of the STF. In general, the study of Gong et al. [31] shows that a low viscous, low molecular weight medium is preferred to form the STF. This is probably because with the lower molecular weight medium, the trigger time for the STF to shear thicken is longer which is compatible with low velocity impacts. Additionally, the distribution of the dispersed phase is uniform and the level of penetration of the fluid inside the fabric structure during treatment through the process of padding is expected to be enhanced when the viscosity of the carrier fluid is least. However, a balance between low viscosity for ease of handling and high viscosity for better shear thickening must be maintained. Hence, the result from this study suggests the use of ethylene glycol instead of polyethylene glycol of higher molecular weights, at least for knife and stab impact conditions comparable to their work.

The proportions of dispersed phase and medium are changed by altering the solid fraction, the effect of which on the rheological behavior of STF is well grounded and documented. Hence, this aspect is not discussed in this chapter. However, a different but crucial perspective to note here is that the major contributing factor is the "volume fraction" and not "weight fraction." Since the same level of STF viscosity is achieved with much lower solid fraction (<20%) when fumed nanoparticles SiO_2 are used than when solid SiO_2 submicron particles (~65%) are used supports this logic.

7.2.1.2 Hybridizing the Content of STF

Hybridization of different dispersed phases is not readily available in literature. This is probably an extension of the knowledge gained from varying the properties of the same dispersed phase within the same STF. When the same dispersed phase, say SiO_2 is varied in terms of size, for instance, and mixed to form an STF, the shear thickening propensity reduces. In fact, when the difference between the particles is

largely varied, shear thickening almost ceases to occur altogether. Hence, the exploration of combining two types of dispersed phases is of little interest to the research fraternity working in the domain of increasing low velocity impact resistance of structures through STF treatment. However, there are a few reported papers working in this area. For instance, in a unique approach, a different form of hybridization of the dispersed phase is explored by Son et al. [33] who prepared a special spherical particle of polystyrene surrounded by a poly (2-hydroyethyl methacrylate) shell. It is also claimed that this STF with polystyrene to poly (2-hydroyethyl methacrylate) ratio of 4:1 produces higher viscosity than equivalent polymer-based STFs. Such an STF ought to be researched further to check its applicability in real-life impact resistance applications. However, as of the day, the application of this STF has not been reported. The same authors have also developed an STF from the colloidal suspension of polystyrene-poly (acrylamide) and polystyrene-poly (2-hydroyethyl methacrylate) particles dispersed in ethylene glycol. Synthesized by emulsion polymerization method, this STF is again reported to exhibit enhanced shear thickening due to the presence of abundant hydrogen bond donor groups of polystyrene-poly(acrylamide) [34]. Chen et al. [35] also explored this approach of hybridizing two different dispersed phases using polystyrene and ethylene acrylate copolymer nanosphere in a suspension of ethylene glycol. Unfortunately, in both the works, the prepared STFs were not yet explored as energy-absorbing supplements in high performance fabrics for impact or stab resistance applications.

Hybridizing two variants of the same dispersed phase was explored by Mawkhlieng and Majumdar [36] who mixed two different sizes of SiO_2 in polyethylene glycol. As reported by Alince and Lepoutre in 1983 [37] also, the authors found that the mixture of widely different particles works against the purpose of achieving a high peak viscosity STF. Although the STFs prepared glaringly displayed weak shear thickening, the authors extended their study to observe the applications of such STFs through a drop tower experiment. As expected, the study revealed that those with only one type of dispersed phase in them suit the application better.

7.2.1.3 Introducing Foreign Particles as Additives

Hybridization by adding an extra foreign constituent to a “regular” STF has been explored thoroughly, if not systematically. Several additives, mostly nanoparticles and nano and micro fibers such as halloysite nanotubes, graphene, graphene oxides, graphene nanoplatelets, and carbon nanotubes, and microparticles such as boron carbide, silicon carbide, and aluminum oxide have been reported [38–42]. Such STFs are frequently referred to as multi-phase STFs. However, the flow behavior of multi-phase STFs varies based on the additives, a trend that is not understood to this day. This is probably due to the lack of a thorough and systematic experimental investigation. However, a few pioneering works surfacing the last 5 years or so are worth mentioning. For instance, Gürgen et al. [39, 43] studied the effect of carbide microparticles on the rheological behavior of STF. The results follow a similar logic

of hybridizing two variants of the same dispersed phase, probably because the interparticle interaction in the STF is predominantly physical and not chemical. Hence, when the amount of carbide microparticles and particle size are increased, shear thickening reduces or almost ceases to appear. It is important to remember that the overall viscosity may be amplified when the amount is increased due to the general upsurge in solid content; however, when the viscosity versus shear rate curve is studied, it is seen that the sudden "jump" in viscosity or the characteristic discontinuous shear thickening rapidly diminishes. Gürgen et al. [39] describe this intensity of viscosity rise as thickening ratio, defined as the peak viscosity divided by the viscosity at critical shear rate. Gürgen and Kuşhan [44] furthered the experiment to investigate if such STFs would be practical for impact applications. The results show that the performance of STF-treated fabrics improves since the depth of penetration of knife and spike reduces with the presence of silicon carbide additives. While the outcome of the study shows improvement in performance, the scarcity of research suggests that this approach is yet to gain acceptance and popularity. The present authors anticipate the imbalance between increased performance and cost as one of the major causes that limits the research in this direction. However, more in-depth studies are important to arrive at any tangible conclusion.

The additives in the nanoscopic range have been explored more elaborately; however, the results vary widely. Largely, there is a lack of understanding on how these additives supplement the STF. It is understood that the rheological response of the fluid is influenced by many other factors other than the mere presence of the nanoparticles itself. The major factors that are often not accounted for are the inevitable increased in solid content, the effect of particle shape and size, and the interaction with the STF itself. Since it is complex to isolate the effect of each parameter, therefore, the increased in viscosity of STF upon inclusion of nanoparticles cannot be fully attributed only to the increased surface area of interaction, although this may be one of the major contributors. Further, the study of such STFs is often limited to their flow behavior although a few have explored beyond. Laha and Majumdar [45] studied the flow behavior of halloysite-reinforced STFs and the application thereof against low velocity drop tower impact. The results favored the use of the novel multi-phase STFs as expected since the STFs compounded with halloysite exhibited higher viscosity. The authors also hypothesized that the presence of the halloysites shorten the distance needed to be travelled by the particles to cluster and shear thicken. Similarly, Mawkhlieng and Majumdar [46] conducted an experiment exploring the use of graphene nanoplatelets, while keeping the overall solid fraction of the STF constant. As the amount of graphene nanoplatelets increased, the amount of SiO_2 originally present in the neat STF was adjusted accordingly. It is reported that the viscosity increased substantially when the nanoparticles were present and that the fabrics treated with more "viscous" STFs showed better energy absorption. In fact, when the panels were made and subjected to a bullet impact of higher impact speed (~165 m/s), the panels treated with the multi-phase STFs outperformed those that were not. As discussed in Sect. 7.2.1.1, the volume fraction played a major role here since the bulk density of graphene nanoplatelets is relatively lower. A simplistic representation of different types of STFs is shown in Fig. 7.4.

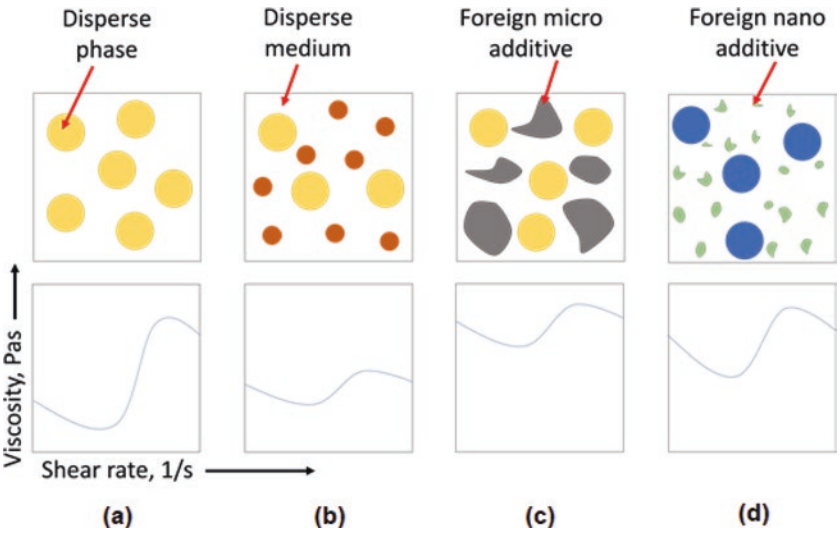

Fig. 7.4 Varying and hybridizing the solid content of STF. (**a**) Mono dispersed phase; (**b**) two variants of the same dispersed phase; (**c**) microscopic additives; (**d**) nanoscopic additives. Below each representation is the corresponding typical rheological behavior

However, the major question that is left unanswered is whether this positive response of multi-phase STF-treated fabrics is a mere consequence of the rise in viscosity or does the presence of the nanoparticles physically contribute to anything. A study in this direction is important as it will justify the use of nanoparticles which are generally expensive and toxic.

7.2.2 Fabric Route

7.2.2.1 Changing the Parameters of the Fabric

Altering the structure of the fabric by varying the fabric sett and weave are the common approaches that researchers have resorted to in order to maximize the energy absorption. Much work has been dedicated to fabric structure in isolation as well as its effect with STF. A detailed analysis of fabric sett was done by Arora et al. [22] experimenting on ultra-high molecular weight polyethylene (UHMWPE) fabrics. From this study, an important conclusion is drawn highlighting the interactive effect of STF and fabric structure. It is then understood that STF treatment on a high performance fabric is beneficial only when the fabric conditions are favorable. Until that time, the general practice for researchers is to procure commercially available *p*-aramid fabrics and then treat them with STF. However, Arora et al. [22] showed that STF depicts positive effect when the sett is such that the fabric is neither too tight nor too loose. In fact, Laha and Majumdar [47] had shown prior to this that

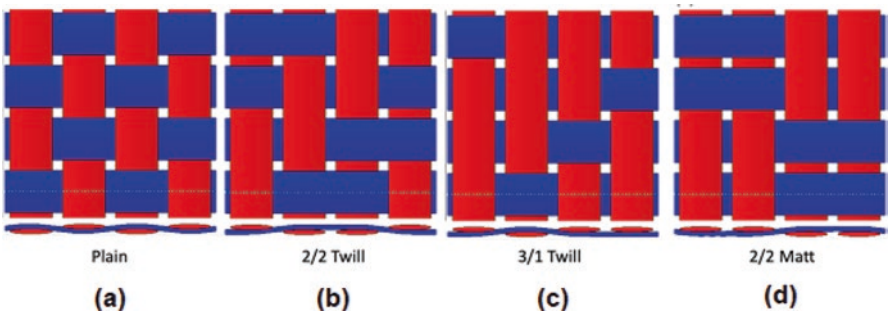

Fig. 7.5 Fabrics with: (**a**) plain; (**b**) 2/2 twill; (**c**) 3/1 twill; (**d**) matt weaves

STFs lose their effectiveness when the fabric structure is jammed. Similarly, in the works of Mawkhlieng et al. [36] and Bajya et al. [48], two grades of Kevlar® fabrics are often explored: one low sett Kevlar® 802F and the other high sett Kevlar® 363. It is often observed that the percentage increment in energy absorption from untreated fabric to STF-treated fabric is substantially large in the case of Kevlar® 802F.

The effect of weave is also expected to be significant since fabric weave alters the openness or looseness of the structure (Fig. 7.5), even when the fabric sett is constant. The effect of weave has been discussed by Mawkhlieng and Majumdar [11] in detail in their textile progress. Various studies reveal that plain weave generally outperforms other weaves due to an optimized balance between the isotropic nature and firmness of the structure. However, from the works of Laha and Majumdar [45, 47, 49], Chu and Chen [50], and Shimek and Fahrenthold [51], the effect of fabric structure is seen to also depend on the type of impact, the yarn count, and number of layers in the panel. An oversimplified generalization is to have a tight plain-woven structure for low velocity puncture type of impact to resist the incoming impacting object from windowing through the structure (Fig. 7.6). However, for a panel of many layers against higher velocity impact, a balance between tight weaves and low yarn crimp has to be met. While the former ensures structural integrity, the latter ensures rapid wave propagation from the impact point. This is probably why Shimek and Fahrenthold [51] observed a harness satin four weave to be superior to the plain weave. Noting that the testing conditions in various studies differ from each other, it is evident to conclude that the impact resistance of a fabric is highly dependent on structure. The complexity of structural effect only increases when STF is added.

Structural integrity of a fabric is a term that is used often in literature to qualitatively assess the firmness of the structure [23, 52]. In the first, Mawkhlieng et al. [23] attemptted to add a numerical figure to this term in their work on STF-treated fabrics against low velocity impact. However, the approach was addressed toward 3D-woven fabrics only. For 2D structures, the authors considered the number of binding points per repeat unit as the major factor contributing to integrity. The integrity factor, as they call it, relates to the energy absorption of the different structure. However, the calculation did not consider the effect of STF add-on, an important

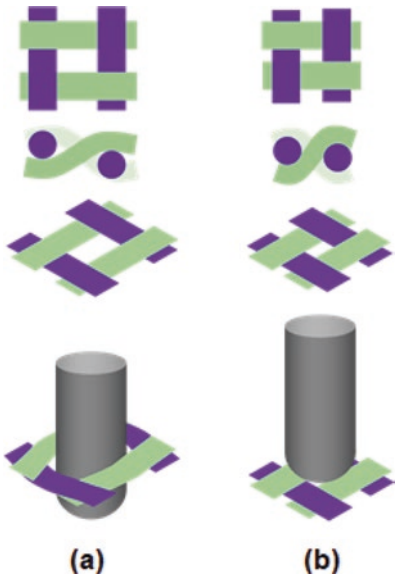

Fig. 7.6 Structure dependent low velocity impact for: (**a**) low fabric sett (windowing effect); (**b**) high fabric sett

aspect since STF treatment "consolidates" or "binds" the structure. Further research along this line is therefore crucial and worthwhile [53].

7.2.2.2 Using Different Woven Structures

The suitability of UD, 2D, and 3D fabric structures for impact resistance has all been explored, if not to the same degree. The structure difference among the three is simplified in Fig. 7.7. UD fabrics outperform any other structure [54–61]. However, such fabrics are often stiff and inflexible. They are mainly advised to be used against high velocity impact in an assembled panel especially at the front and back. At the front, the monolithic nature of the structure helps to deform the bullet by blocking it and rapidly propagating the massive stress waves through the structure, which is effective due to lack of crimp. At the back, the UD laminates restrict the outward deflection of the panel thus, minimizing the behind armor blunt trauma. One of the reasons for the superiority of UD fabrics is the absence of interlacement which causes: (1) maximum accommodation of fibers or filaments in a given area and (2) elimination of interstices that can work as weak spots. While this property is beneficial in many ways, however, this type of void-free structure limits the application of STF, which is probably why research in this area is almost nonexistent. As per the knowledge of the presenting authors, there is only one trial that has been reported recently. Mishra et al. [62] investigated the treatment of STF on UD UHMWPE fabric against the high velocity projectile. Figure 7.8 clearly shows that UD fabric exhibits improved ballistic performance in terms of energy absorption

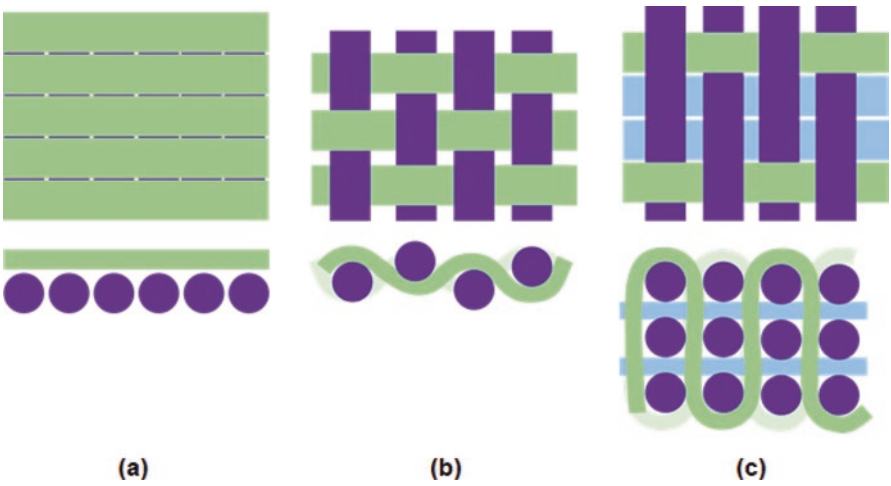

Fig. 7.7 Structural difference among: (**a**) 2 ply UD laminate; (**b**) 2D plain-woven fabric; (**c**) 3-layered orthogonal 3D-woven fabric. Here, green represents the lengthwise yarns (warp in 2D or binder in 3D), purple represents the widthwise yarns (weft), and blue represent the stuffer yarns in 3D

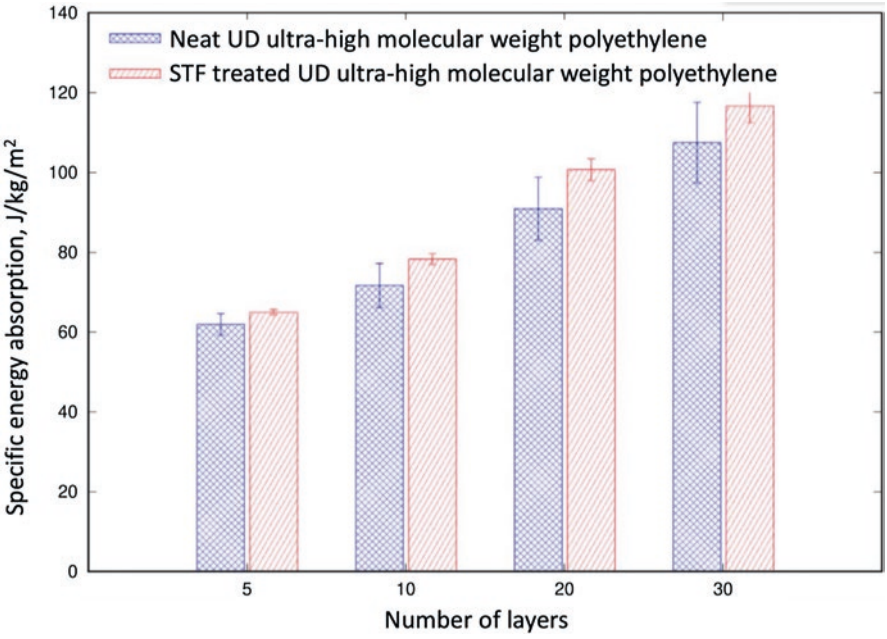

Fig. 7.8 Ballistic performance of neat and STF-treated UD UHMWPE fabrics in terms of specific energy absorption [62]. Reprinted by permission from Elsevier

(13%) and ballistic limit (5%) at varying number of UD laminates when STF is added. The percentage increase in energy absorption is however nowhere close what is commonly observed in the case of 2D woven fabrics.

For STF treatment, 2D- and 3D-woven fabrics dominate. 2D fabrics have been explored extensively, contributing to much of the work reported. The exploration of double fabrics and 3D structures have also begun to surface. The advantage of woven structures is the presence of the interlacements that enables the STF to act as a friction enhancer as one its role. The deposition of STF on the interstices and surface of the fabric helps achieve a certain level of firmness and generates friction when the yarns of the fabrics are pulled. The mechanism is illustrated in Fig. 7.9. Hence, it is not wrong to conclude that in a condition where there is no yarn pull-out, STF is anticipated to help merely through shear thickening.

From the work of Mawkhlieng et al. [23], it is seen that a judiciously designed double fabric can perform better than 2D fabric at least in neat form, if not in the STF-treated state. However, a preliminary study like this and probably the first paper that reported on double fabrics for impact applications can only be a guiding step for future and advanced work. Hence, unless a detailed study is conducted, the potential suitability of double fabrics cannot be undermined. 3D fabrics in general have been seen to underperform 2D counterparts of comparable areal density on multiple occasions at least against low velocity impact. This is because 3D fabrics cannot be woven as tightly as 2D fabrics because of the interlacement nature of three sets of yarns, implying that yarns can be pulled out with ease during impact. However, with STF addition, the performance enhances substantially. Although 3D fabrics are not as attractive for these applications as are 2D fabrics, there is an added advantage of these architectures, particularly the angle interlocks. Their moldability has been explored successfully for designing female body armor [63–65].

Knit structures have also been explored as suitable candidates although to a much lesser extent than woven structures. This is due to the openness of the

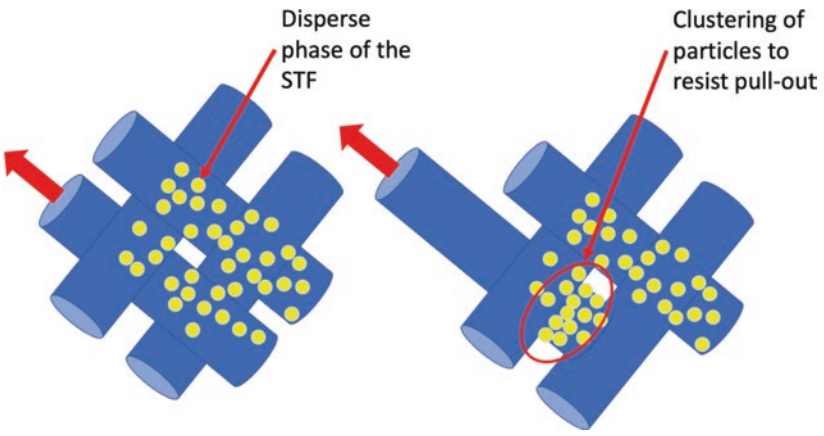

Fig. 7.9 STF treatment enhances fabric friction during yarn pull-out

structure, restricting its applicability in impact resistance applications. Nonetheless, it can potentially be used as a backing material in a hybrid panel. For instance, Lu et al. [66] studied the compressive behavior of neat and STF-filled warp-knitted spacer fabrics when subjected to quasi-static compression and low velocity impact. The STF-filled warp-knitted spacer fabric shows higher energy absorption and a lower peak load as compared to neat fabric. However, further research in this direction is almost missing.

7.2.2.3 Hybridizing Different Yarns

Hybrid fabrics consisting of different yarns have gained the attention of the research fraternity. The yarns can vary either in material or in terms of yarn parameters. Again, this aspect has been dealt in a number of reviews [11, 13, 67–69]. The purpose of hybridization is to synergistically combine the strong features of different materials or different variants of the same material, often driven by cost reduction without compromising on the performance. If some portion of an excellent expensive material can be safely replaced with a lower grade cost-effective alternative, then the manufacturing cost can be reduced. Alternately, the performance of a certain inferior material can be significantly improved by incorporating another superior alternative with it. For example, when lower grade UHMWPE is hybridized with superior *p*-aramid yarns in the same fabric, substantial improvement is expected [23]. Sometimes, hybridization is carried out to achieve a certain objective as in the case of Chitrangad [70] who suggested the use of warps and wefts with different failure strain so that both can break together at the time of impact. In the case of 3D fabrics, different yarns play varying roles. Stuffer and weft yarns are expected to absorb energy whereas binder yarns majorly consolidate the structure. Because of the path they take which is in the Z-direction along the height, the use of finer yarns for binders is suggested [23].

7.2.2.4 Increasing the Fabric Friction

Treatment with STF increases friction as supported by yarn pull-out test results. Friction has also been increased through other techniques such as plasma treatment and growth of nanostructures [71–77]. These approaches have not been reported as successful as STF treatment. This may confirm that STF plays dual roles. Combining both STF treatment and growth of nanostructures has also been explored. Dixit et al. [78] found that fabric treated with both exhibited superior resistance to low velocity impact. Again, progressive work has not been reported in this area.

7.3 STF Treatment of High Performance Fabrics

STF-treated structures have been tested for their impact resistance at varying speeds from impactor drops to low velocity bullet shots. There is a consistent and strong evidence to support that STF structures are resistible against such impacts. Since the revival of the inception of liquid armor in 2003, STF has proven to be an effective alternative to augment the energy absorption capacity of high performance fabrics. However, the use of STF is limited due to a number of reasons, which means that a "liquid armor" in its true sense is far from reality. An initial attempt was to have the fluid stored in pouches that were inserted either before, after, or in between layers of Kevlar® as shown in Fig. 7.10. However, the most successful combination was obtained when the fabric was immersed or impregnated with the fluid. From Fig. 7.10, it is also clear that the presence of fabric layers at the front or strike face is crucial for the success of the invention.

Further, the STF treatment process is crucial. When the fabrics are simply soaked in the fluid, handling and containing the fluid is naturally a challenge. Hence, excess STF has to be removed. The most common procedure reported in literature are as follows: (1) soaking the fabric in STF for a given time and then calendaring and (2) padding. In either case, it is understood that the application should be even to ensure uniformity in the properties of the treated fabrics in all

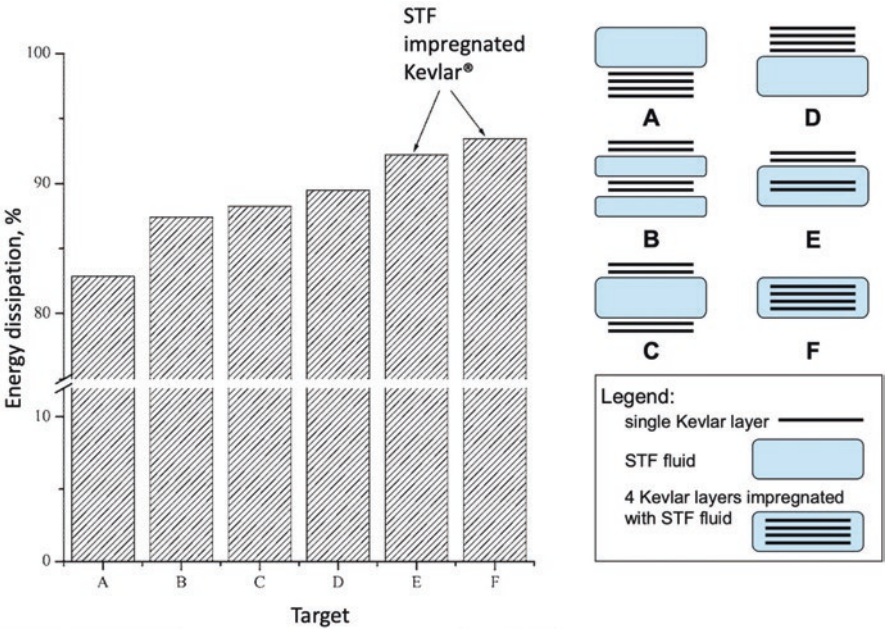

Fig. 7.10 Different combinations of STF and fabrics and their performance in the terms of penetration depth [79]. Reprinted by permission from Springer

directions. Also, the level of penetration, i.e., how deep the fluid impregnates the fabric is important as this decides the concentration of the fluid in the fabric—either at the surface or in the interstices. The implication of this aspect is not thoroughly researched, but it has been observed that the yarn pull-out results are often related to the distribution of the solid particles of the STF in the fabric. Consequently, Majumdar et al. [80] attempt to optimize STF-treated structures through a Box-Behnken design of experiment to obtain the best combination of SiO_2 concentration, padding pressure, and diluent to STF ratio to achieve maximum energy absorption for Kevlar® fabrics. The authors also proposed a two-step sequential padding to ensure the best results. A similar trial has been carried out by Bajya et al. [81] for UHMWPE fabrics. It is critical to note the conclusions of these two studies that more STF add-on does not translate to better energy absorption. The energy absorption evaluation in both these studies was through a drop tower dynamic impact experiment with an impact speed below 5 m/s. Based on these results, it can be extrapolated that the same independency is expected at higher speeds as well. Therefore, it is clear that although STF treatment is beneficial, its undue incorporation either in the form of the liquid itself inside pouches or in terms of excess add-on is not useful. On the contrary, the extra weight addition hinders the practical applicability of the treated structures.

After padding, the STF-treated fabrics are often dried before assembling into a panel. Thus, the fabrics are dry and do not differ in appearance to the untreated fabrics significantly. The only noticeable difference is the matt finish appearance that results from the deposition of the solid particles of the fluid. In fact, the handle of the fabric in terms of stiffness does not change [75]. The STF treatment process quickly changes the phase of STF from fluid form in the literal sense to a fine coating that is barely visible by the naked eye. Hence, this aspect enforces many to speculate if shear thickening plays a significant role as it is supposed to. Rather, its appearance in the fabric suggests that the solid particles' mere adherence to the surface of the fabric simply improves the friction. An "ideology" as such poses several questions to the successful works done before and to those that will be carried in the future as well. If STF merely enhances friction, then other methods of friction enhancement such as plasma treatment and in situ nanostructure growth should be equally efficacious. However, none of these are as successful a story as is the use of STF. Mawkhlieng and Majumdar [36] conducted an experiment to understand this aspect through an indirect approach by relating the rheological flow behavior, fabric friction, and energy absorption. It was found that the low velocity energy absorption relates to the fluid flow behavior and not to the fabric friction. The observation was valid for two sets of fabrics explored. Hence, it is conclusive that STF plays dual roles; while its does improve friction, shear thickening as a mechanism also helps.

7.4 STF-Treated Structures Against Low Velocity Impact

Before furthering the discussion of suitability of STF-treated structures for low velocity impact, it is important to define what low velocity covers. While the speed of "low velocity" impacts can be subjective and can vary based on contexts, this chapter considers impact speeds below 450 m/s as low. For armor applications, the National Institute of Justice (NIJ) is drafting a standard, NIJ 0101.07 that classifies armor types based on the level of protection they provide [82]. The new standard uses acronyms such as HG for handgun and RF for rifle to distinguish the type of weapon used to fire the bullet, a classification that automatically takes bullet speed into consideration also. This chapter covers all impact speeds that pertain up to those that are propelled from a handgun. Rifle shots (~847 m/s and above) can be classified as high velocity impact and are therefore, not included in this chapter.

For stab and spike impacts, STF-treated structures have been reported as successful. An excerpt of a pioneering work is reproduced here in Fig. 7.11a,b. For both knife and spike drop tower tests, the effect of STF is demonstrated through images of the fabric appearance with and without STF treatment post impact. Clearly, the addition of STF remarkably improves the resistance against both impactors. There is evidence in the case of knife impact that no yarns were severed after STF treatment (Fig. 7.11a). Similarly, in the case of spike impact, there was little to no yarn fracture after STF is incorporated. In both cases, after STF treatment, the affected area was much lower, and the damage was hardly visible from the rear side. In case of blunt impact, there was formation of a dome that resulted in substantial energy absorption as displayed in Fig. 7.12. The untreated fabric failed through windowing and yarn pull-out without the real involvement of the yarns whereas in the STF-treated fabrics, the yarns participated in failure by deformation and rupturing. The way STF binds the fabric is witnessed through the involvement of secondary yarns, those that are not directly contacted by the falling impactor.

For higher velocity impacts around 450 m/s, the response depends on the placement of the STF-treated structure in the panel. STF-treated fabrics when placed toward the rear provide better protection in terms of back face signature. It is hypothesized that this arrangement allows sufficient time for the bullet's speed to reduce from the front to the back of the panel so that the rear layers are subjected to a relatively low speed. When placed at the front, the results do not seem to differ than when untreated fabric layers serve as the strike face [48]. Similarly, in the case of hybrid panels, where different materials are used, it has been observed that the replacement of neat fabrics in the back layers with those that treated with STF has an added advantage in reducing the back face signature [65]. An important point to note here is that when the panels are compared on the basis of equivalent weight, the number of fabric layers can be reduced when STF-treated fabrics are used to replace the untreated counterparts. Treatment with STF involves cost, whereas reduction in the number of layers of high performance can reduce cost significantly particularly in bulk production. Hence, cost comparison must be considered, keeping in mind that the performance should be optimum. Consequently, a Memorandum of

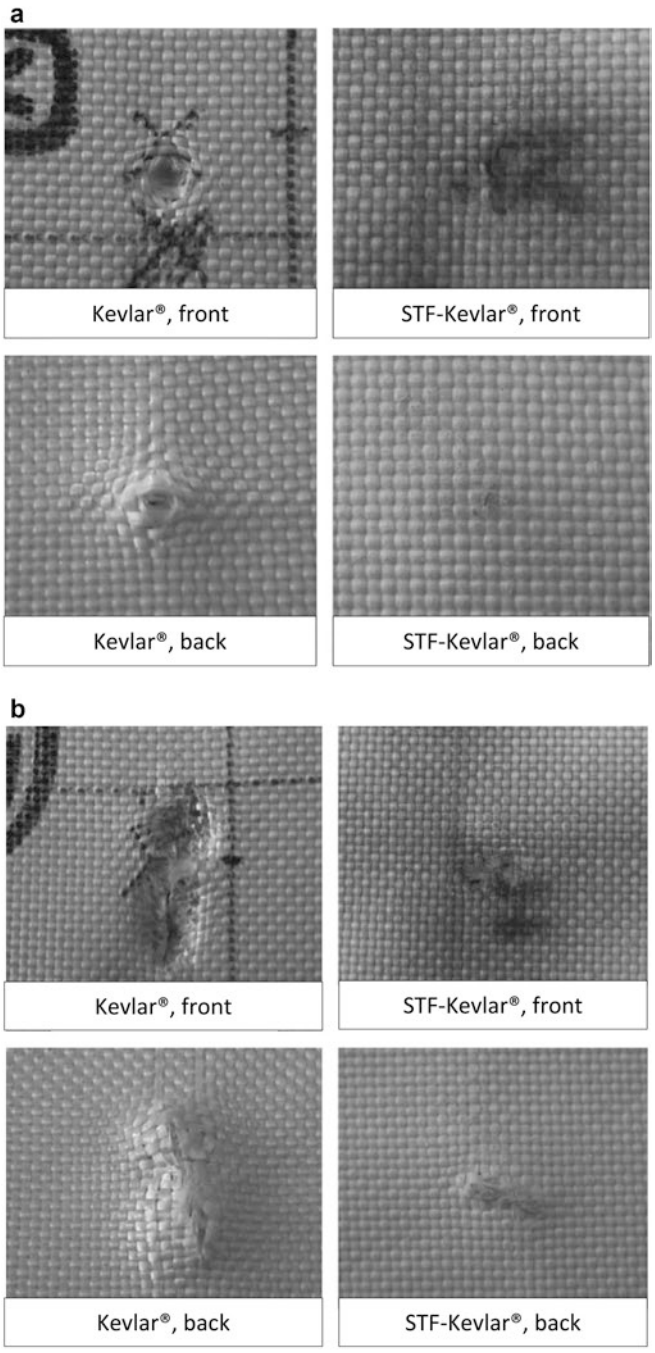

Fig. 7.11 Photographs of neat Kevlar® and STF-treated Kevlar® fabrics after: (**a**) knife; (**b**) spike drop tower test with mass 2.33 kg and height 0.75 m [83]. Reprinted by permission from Elsevier

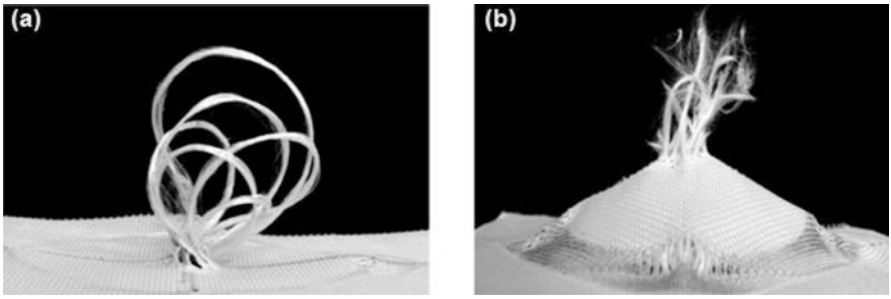

Fig. 7.12 Photographs of (**a**) neat Kevlar® and (**b**) STF-treated Kevlar® after impact [84]. Reprinted by permission from Elsevier

Understanding (MoU) was signed in 2017 between BAE Systems and Helios Global Technologies to commercialize this technology [85]. BAE Systems is an international defense, aerospace, and security company, whereas Helios Global Technologies is a designer, manufacturer, and distributor of technologies related to hazardous worker safety. This is the latest news concerning the "liquid armor" that is known to the day this chapter is written. It is not clear as of now if all the layers of the armor will be treated with STF or if only a portion of the STF-treated layers are to replace the neat layers. Researches show that for low velocity impact where the number of layers required is substantially low, replacing all the woven layers with STF-treated alternatives may be beneficial. This conclusion is drawn from the results of several research works that report on the effectiveness of STF on single layer fabrics. Further, the panels experimented by Mawkhlieng and Majumdar [46] against an impact velocity of ~165 m/s consisted of three layers, and the superior panel that was able to stop maximum number of bullets had all STF-treated layers. However, for higher velocity impact, the replacement of all layers is not required. Realistically, to maintain the panel weight, there is a balance between the replaceable number of layers and the corresponding reduction in the total number of layers. From the work of Bajya et al. [48], it can be extrapolated that for low velocity impact, a superior panel may be composed of neat high performance fabrics with a few layers at the back replaced with STF-treated substitutes without changing the panel weight. The exact number of layers depends on the type of impactor, the velocity of impact, and level of protection required, for which a trial must be conducted considering the findings of existing works. The design strategy of placing a layer of UD laminate or two behind the STF-treated layers may also be followed where reduction of back face signature is crucial [65]. Here, it is also important to mention the cost incurred in STF treatment, an aspect crucial from a commercial standpoint. Therefore, an optimized level of STF treatment in terms of the number of layers has to be considered. Several review papers [15, 86, 87] are dedicated specifically to stab and spike resistance of STF-based armor which can be read further.

Another important consideration is the packaging of STF-treated fabrics. STF when left exposed in atmospheric conditions for several days can absorb water,

resulting in the reduction in the effective solid fraction and consequently, in viscosity. This effect when STF is added to fabrics is still unknown as there is no study at present that investigates this matter. A detailed and extended study on the effect of exposure of STF-treated fabrics in atmosphere for a given number of days will be helpful to throw light on the longevity of the effect of such treatment, if any. Although in practice, the fabric layers are sealed in a water-resistant nylon carriage fabric that are later used as armor panels, this study will suggest the number of days the STF-treated fabrics can be safely placed unpacked from the time of treatment to the time of assembling and sealing. In a number of unreported works by the present authors, it has been observed that when the panels are isolated in an airtight seal, then then effect of moisture can be eliminated. In fact, when the same sealed panels were tumbled under adverse humid conditions, a process called as accelerated ageing, the performance of panels dropped only slightly.

Furthermore, hybridization at the panel stage is also advised. A hybrid panel is an assemble of different layers of materials that can be judiciously designed so that the performance can be improved within the limitations of cost and weight. Such a panel may be represented by Fig. 7.13. The image is only representative and hence, does not reflect the actual number of layers or the exact sequence to be used.

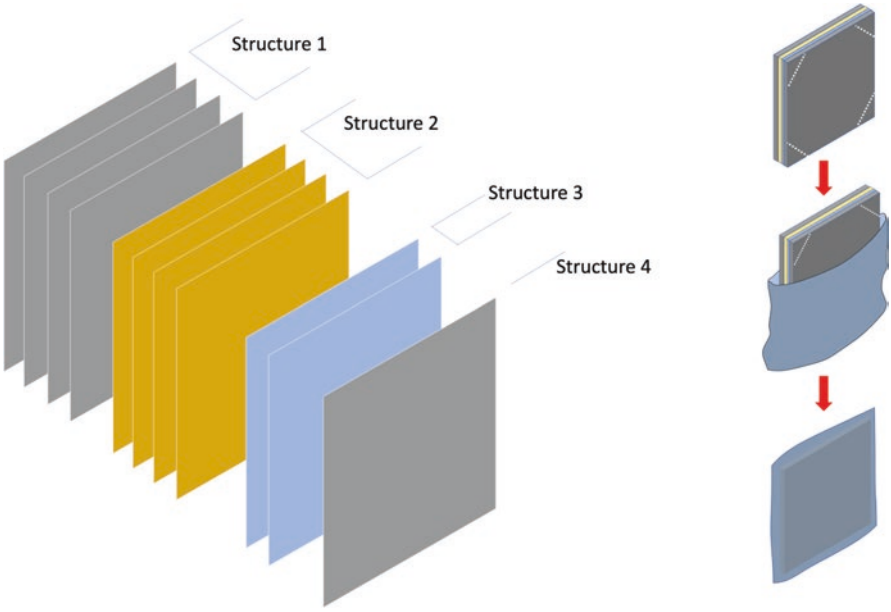

Fig. 7.13 Representative assembly of different materials strategically sequenced. Here, structure represents either UD laminates, 2D- or 3D- woven structures, either in neat or STF-treated conditions. Also, the panel is stitched and sealed in a water-resistant carriage

7.5 Summary

In this chapter, the important facets of various types of STF and protective structures have been summarized against low velocity impacts. The introduction section provides a concise summary of the measurement system for low and high velocity impacts. The methods of augmenting energy absorption are categorically routed through the improvement of shear thickening or viscosity of STF or through the thoughtful construction of fabric. The STF route briefly describes the methods to prepare an effective STF for protective application either by varying or hybridizing the contents, or by incorporating additives. The fabric route illustrates the approaches to alter the structure. This chapter focuses on the STF treatment of high performance 2D-, UD-, and 3D-woven fabric structures of aramid and UHMWPE and their performances against low velocity impact. The failure modes of STF-treated fabrics depend on the type of impactor and its speed (spike, knives, blunt indenter, or bullet). For bullet type of impact with high velocity, the arrangement of STF-treated layer in the panel is an important aspect to consider.

References

1. A. Laha, A. Majumdar, Shear thickening fluids using silica-halloysite nanotubes to improve the impact resistance of p-aramid fabrics. Appl. Clay Sci. **132–133**, 468–474 (2016)
2. S. Gürgen, M.C. Kuşhan, The ballistic performance of aramid based fabrics impregnated with multi-phase shear thickening fluids. Polym. Test. **64**, 296–306 (2017)
3. H. Liu, H. Zhu, K. Fu, et al., High-impact resistant hybrid sandwich panel filled with shear thickening fluid. Compos. Struct. **284**, 115208 (2022)
4. A. Ghosh, A. Majumdar, B.S. Butola, Modulating the rheological response of shear thickening fluids by variation in molecular weight of carrier fluid and its correlation with impact resistance of treated p-aramid fabrics. Polym. Test. **91**, 106830 (2020)
5. Y. Ma, Z. Lei, G. Huang, et al., Energy absorption analysis of STF/Kevlar composite fabric based on 3D morphology of impact basin under low-speed impact. Compos. Struct. **283**, 115152 (2022). https://doi.org/10.1016/j.compstruct.2021.115152
6. A. Majumdar, A. Laha, Effects of fabric construction and shear thickening fluid on yarn pull-out from high-performance fabrics. Text. Res. J. **86**, 2056–2066 (2016)
7. S. Gürgen, T. Yıldız, Stab resistance of smart polymer coated textiles reinforced with particle additives. Compos. Struct. **235**, 111812 (2020). https://doi.org/10.1016/j.compstruct.2019.111812
8. R.G. Egres Jr., Y.S. Lee, J.E. Kirkwood, et al., "liquid armor": Protective fabrics utilizing shear thickening fluids. 4th International Conference on Safety and Protective Fabrics, 1–8 (2004)
9. Y.S. Lee, E.D. Wetzel, R.G. Egres Jr., NJW, Advanced body armor utilizing shear thickening fluids. J. Chem. Inf. Model, 1689–1699 (2013)
10. N. Wagner, ED. Wetzel, Advanced body armor utilizing shear thickening fluids. US 7.498,276 B2, US, (2009)
11. U. Mawkhlieng, A. Majumdar, Soft body Armour. Text. Prog. **51**, 139–224 (2020)
12. S. Gürgen, M.C. Kuşhan, W. Li, Shear thickening fluids in protective applications: A review. Prog. Polym. Sci. **75**, 48–72 (2017)
13. U. Mawkhlieng, A. Majumdar, A. Laha, A review of fibrous materials for soft body Armour applications. RSC Adv. **10**, 1066–1086 (2020)

14. K. Patel, S.H. Chikkali, S. Sivaram, Ultrahigh molecular weight polyethylene: Catalysis, structure, properties, processing and applications. Prog. Polym. Sci. **109**, 101290 (2020). https://doi.org/10.1016/j.progpolymsci.2020.101290
15. K. Bilisik, Ballistic and stabbing protection: A review. Text Res. **87**, 2275–2304 (2017)
16. V.B.C. Tan, T.E. Tay, W.K. Teo, Strengthening fabric Armour with silica colloidal suspensions. Int. J. Solids Struct. **42**, 1561–1576 (2005)
17. B.-W.W. Lee, I.-J.J. Kim, C.-G.G. Kim, The influence of the particle size of silica on the ballistic performance of fabrics impregnated with silica colloidal suspension. J. Compos. Mater. **43**, 2679–2698 (2009)
18. C. Fischer, S.A. Braun, P.E. Bourban, et al., Dynamic properties of sandwich structures with integrated shear-thickening fluids. Smart Mater. Struct. **15**, 1467–1475 (2006)
19. M. Hasanzadeh, V. Mottaghitalab, M. Rezaei, et al., Numerical and experimental investigations into the response of STF-treated fabric composites undergoing ballistic impact. Thin-Walled Struct. **119**, 700–706 (2017)
20. L. Lam, W. Chen, H. Hao, et al., Numerical study of bio-inspired energy-absorbing device using shear thickening fluid (STF). Int. J. Impact Eng. **162**, 104158 (2022)
21. H. Mahfuz, F. Clements, V. Rangari, et al., Enhanced stab resistance of armor composites with functionalized silica nanoparticles. J. Appl. Phys. **105**, 3086431 (2009). https://doi.org/10.1063/1.3086431
22. S. Arora, A. Majumdar, B.S. Butola, Structure induced effectiveness of shear thickening fluid for modulating impact resistance of UHMWPE fabrics. Compos. Struct. **210**, 41–48 (2018)
23. U. Mawkhlieng, M. Gupta, A. Majumdar, An exposition of shear thickening fluid treated double and 3D woven fabrics with a new integrity factor for enhanced impact resistance. Compos. Struct. **270**, 114086 (2021)
24. Q. Hu, G. Lu, N. Hameed, et al., Dynamic compressive behaviour of shear thickening fluid-filled honeycomb. Int. J. Mech. Sci. **229**, 107493 (2022)
25. A. Khodadadi, G. Liaghat, A. Taherzadeh-Fard, et al., Impact characteristics of soft composites using shear thickening fluid and natural rubber–a review of current status. Compos. Struct. **271**, 114092 (2021)
26. T.A. Strivens, The shear thickening effect in concentrated dispersion systems. J. Colloid Interface Sci. **57**, 476–487 (1976)
27. A. Srivastava, A. Majumdar, B.S. Butola, Improving the impact resistance performance of Kevlar fabrics using silica based shear thickening fluid. Mater. Sci. Eng. A **529**, 224–229 (2011)
28. D.P. Kalman, R.L. Merrill, N.J. Wagner, et al., Effect of particle hardness on the penetration behavior of fabrics intercalated with dry particles and concentrated particle-fluid suspensions. ACS Appl. Mater. Interfaces **1**, 2602–2612 (2009)
29. D.P. Kalman, J.B. Schein, J.M. Houghton, et al., Polymer dispersion based shear thickening fluid-fabrics for protective applications. Int. SAMPE Symp Exhib. **52**, 1–9 (2007)
30. J. Ding, P. Tracey, W. Li, et al., Review on shear thickening fluids and applications. Text. Light Ind. Sci. Technol. **2**, 161–173 (2013)
31. X. Gong, Y. Xu, W. Zhu, et al., Study of the knife stab and puncture-resistant performance for shear thickening fluid enhanced fabric. J. Compos. Mater. **48**, 641–657 (2014)
32. Y.L. Xua, X.L. Gong, C. Peng, et al., Shear thickening fluids based on additives with different concentrations and molecular chain lengths. Chinese J. Chem. Phys. **23**, 342–346 (2010)
33. H.S. Son, K.H. Kim, J.H. Kim, et al., High-performance shear thickening of polystyrene particles with poly(HEMA). Colloid Polym. Sci. **296**, 1591–1598 (2018)
34. H.S. Son, K.H. Kim, J.H. Song, et al., Enhanced shear thickening of polystyrene-poly(acrylamide) and polystyrene-poly(HEMA) particles. Colloid Polym. Sci. **297**, 95–105 (2019)
35. Q. Chen, W. Zhu, F. Ye, et al., PH effects on shear thickening behaviors of polystyrene-ethylacrylate colloidal dispersions. Mater. Res. Express **1**, 015303 (2014). https://doi.org/10.1088/2053-1591/1/1/015303

36. U. Mawkhlieng, A. Majumdar, Deconstructing the role of shear thickening fluid in enhancing the impact resistance of high-performance fabrics. Compos. Part B Eng. **175**, 107167 (2019)
37. B. Alince, P. Lepoutre, Viscosity, packing density and optical properties of pigment blends. Colloids Surf. **6**, 155–165 (1983)
38. A. Ghosh, A. Majumdar, B.S. Butola, Role of surface chemistry of fibres additives on rheological behavior of ceramic particle based shear thickening fluids. Ceram. Int. **44**, 21514–21524 (2018)
39. S. Gürgen, W. Li, M.C. Kuşhan, The rheology of shear thickening fluids with various ceramic particle additives. Mater. Des. **104**, 312–319 (2016)
40. M. Zojaji, A. Hydarinasab, S.H. Hashemabadi, et al., Rheological behaviour of shear thickening fluid of graphene oxide and SiO2 polyethylene glycol 400-based fluid with molecular dynamic simulation. Mol. Simul. **47**, 317–325 (2021)
41. L. Liu, M. Cai, X. Liu, et al., Ballistic impact performance of multi-phase STF-impregnated Kevlar fabrics in aero-engine containment. Thin-Walled Struct. **157**, 107103 (2020)
42. M. Hasanzadeh, V. Mottaghitalab, Tuning of the rheological properties of concentrated silica suspensions using carbon nanotubes. Rheol. Acta **55**, 759–766 (2016)
43. S. Gürgen, M.C. Kuşhan, W. Li, The effect of carbide particle additives on rheology of shear thickening fluids. Korea Aust. Rheol. J. **28**, 121–128 (2016)
44. S. Gürgen, M.C. Kuşhan, The stab resistance of fabrics impregnated with shear thickening fluids including various particle size of additives. Compos. Part A Appl. Sci. Manuf. **94**, 50–60 (2017)
45. A. Laha, A. Majumdar, Shear thickening fluids using silica-halloysite nanotubes to improve the impact resistance of p-aramid fabrics. Appl. Clay Sci. **132–133**, 468–474 (2017)
46. U. Mawkhlieng, A. Majumdar, D. Bhattacharjee, Graphene reinforced multiphase shear thickening fluid for augmenting low velocity ballistic resistance. Fibers Polym. **22**, 213–221 (2021)
47. A. Laha, A. Majumdar, Interactive effects of p -aramid fabric structure and shear thickening fl uid on impact resistance performance of soft armor materials. Mater. Des **89**, 286–293 (2016)
48. M. Bajya, A. Majumdar, B.S. Butola, et al., Design strategy for optimising weight and ballistic performance of soft body Armour reinforced with shear thickening fluid. Compos. Part B **183**, 107721 (2020)
49. A. Laha, A. Majumdar, I. Biswas, et al., Role of fabric geometry in ballistic performance of flexible Armour panels. Procedia Eng. **173**, 747–754 (2017)
50. C.K. Chu, Y.L. Chen, Ballistic-proof effects of various woven constructions. Fibres Text. East. Eur **83**, 63–67 (2010)
51. M. Shimek, E. Fahrenthold. Effects of weave type on ballistic performance for aramid, UHMWPE, and hybrid fabrics. In: 53rd AIAA/ASME/ASCE/AHS/ASC Structures, Structural Dynamics and Materials Conference 20th AIAA/ASME/AHS Adaptive Structures Conference 14th AIAA. Reston, Virigina: American Institute of Aeronautics and Astronautics, 1–12
52. F. Boussu, I. Cristian, S. Nauman, General definition of 3D warp interlock fabric architecture. Compos. Part B Eng. **81**, 171–188 (2015)
53. S. Arora, A. Majumdar, B.B. Singh, Interplay of fabric structure and shear thickening fluid impregnation in moderating the impact response of high-performance woven fabrics. J. Compos. Mater. **54**, 4387–4395 (2020)
54. Y.Yang, Study on ballistic performance of hybrid soft Body armour. Ph.D. Thesis. University of Manchester, (2015). https://www.research.manchester.ac.uk/portal/files/61848779/FULL_TEXT.PDF
55. J.L. Park, B.I. Yoon, J.G. Paik, et al., Ballistic performance of p -aramid fabrics impregnated with shear thickening fluid; Part I–Effect of laminating sequence. Text. Res. J. **82**, 527–541 (2012)
56. J.L. Park, Y.S. Chi, T.J. Kang, Ballistic performance of hybrid panels composed of unidirectional/woven fabrics. Text. Res. J. **83**, 471–486 (2013)

57. M. Bajya, A. Majumdar, B.S. Butola, et al., Mitigating the blunt trauma of soft Armour panels using polycarbonate sheets: A cost-effective solution. Appl. Compos. Mater. **28**, 1089–1109 (2021)
58. M. Bajya, A. Majumdar, B.S. Butola, et al., Efficacy of various structural forms of disentangled polyethylene laminates against low velocity impact. J. Thermoplast. Compos. Mater. (2022). https://doi.org/10.1177/08927057221145573
59. M. Karahan, A. Jabbar, N. Karahan, Ballistic impact behavior of the aramid and ultra-high molecular weight polyethylene composites. J. Reinf. Plast. Compos. **34**, 37–48 (2015)
60. F. Boussu, T. Kanit, D. Crepin, et al., Behaviour of a warp interlock fabric subjected to ballistic impact : Experimental analysis. 12th World Text Conf. AUTEX, 1–7 (2012)
61. X. Chen, D. Sun, Y. Wang, et al., 2D/3D woven fabrics for ballistic protection. 4th World Conf. 3D Fabr. Their Appl., 1–12 (2012)
62. V.D. Mishra, A. Mishra, A. Singh, et al., Ballistic impact performance of UHMWP fabric impregnated with shear thickening fluid nanocomposite. Compos. Struct. **281**, 114991 (2022)
63. F. Boussu, I. Cristian, S. Nauman, et al., Effect of 3D-weave architecture on strength transfer from tow to textile composite. 2nd World Conf 3D Fabr. their Appl., 2–8 (2009)
64. M.A. Abtew, F. Boussu, P. Bruniaux, et al., Engineering of 3D warp interlock p-aramid fabric structure and its energy absorption capabilities against ballistic impact for body Armour applications. Compos. Struct. **225**, 111179 (2019)
65. U. Mawkhlieng, A. Majumdar, Designing of hybrid soft body Armour using high-performance unidirectional and woven fabrics impregnated with shear thickening fluid. Compos. Struct. **253**, 112776 (2020)
66. Z. Lu, X. Jing, B. Sun, et al., Compressive behaviors of warp-knitted spacer fabrics impregnated with shear thickening fluid. Compos. Sci. Technol. **88**, 184–189 (2013)
67. A. Srivastava, A. Majumdar, B.S. Butola, Improving the impact resistance of textile structures by using shear thickening fluids: A review. Crit. Rev. Solid State Mater. Sci. **37**, 115–129 (2012)
68. G. Nilakantan, J.W. Gillespie, Yarn pull-out behavior of plain woven Kevlar fabrics: Effect of yarn sizing, pullout rate, and fabric pre-tension. Compos. Struct. **101**, 215–224 (2013)
69. M. Bajya, A. Majumdar, B.S. Butola, Criticality of inter-yarn friction in high-performance fabrics for the design of soft body Armour. Compos. Commun. **29**, 100984 (2022)
70. M V, Chitrangad, Nelson PEA. Hybrid ballisitc fabric. US5187003A, US, (1993)
71. Y. Chu, *Surface Modification to Aramid and UHMWPE Fabrics to Increase Inter-Yarn Friction for Improved Ballistic Performance.PhD Thesis* (University of Manchester, 2015). https://www.escholar.manchester.ac.uk/uk-ac-man-scw:264414
72. Y. Chu, X. Chen, L. Tian, Modifying friction between ultra-high molecular weight polyethylene (UHMWPE) yarns with plasma enhanced chemical vapour deposition (PCVD). Appl. Surf. Sci. **406**, 77–83 (2017)
73. H.S. Hwang, M.H. Malakooti, B.A. Patterson, et al., Increased interyarn friction through ZnO nanowire arrays grown on aramid fabric. Compos. Sci. Technol. **107**, 75–81 (2015)
74. S. Arora, A. Majumdar, B.S. Butola, Deciphering the structure-induced impact response of ZnO nanorod grafted UHMWPE woven fabrics. Thin-Walled Struct. **156**, 106991 (2020)
75. D. Sun, X. Chen, Plasma modification of Kevlar fabrics for ballistic applications. Text. Res. J. **82**, 1928–1934 (2012)
76. Y. Chu, X. Chen, D.W. Sheel, et al., Surface modification of aramid fibers by atmospheric pressure plasma-enhanced vapor deposition. Text. Res. J. **84**, 1288–1297 (2014)
77. A. Hazarika, B.K. Deka, D.Y. Kim, et al., Growth of aligned ZnO nanorods on woven Kevlar® fiber and its performance in woven Kevlar® fiber/polyester composites. Compos. Part A Appl. Sci. Manuf. **78**, 284–293 (2015)
78. P. Dixit, A. Ghosh, A. Majumdar, Hybrid approach for augmenting the impact resistance of p-aramid fabrics: Grafting of ZnO nanorods and impregnation of shear thickening fluid. J Mater Sci. **54**, 13106–13117 (2019). https://doi.org/10.1007/s10853-019-03830-z
79. Y.S. Lee, E.D. Wetzel, N.J. Wagner, The ballistic impact characteristics of Kevlar® woven fabrics impregnated with a colloidal shear thickening fluid. J. Mater. Sci. **38**, 2825–2833 (2003)

80. A. Majumdar, B.S. Butola, A. Laha, et al., Improving the impact resistance of p-aramid fabrics by sequential impregnation with shear thickening fluid. Fibers Polym. **17**, 0–6 (2016)
81. M. Bajya, A. Majumdar, B.S. Butola, et al., Parametric optimisation of shear thickening fluid treatment for ultra-high molecular weight polyethylene woven fabric. J. Ind. Text. **52**, 152808372211267 (2022)
82. Ballistic Resistance of Body Armor, NIJ standard-0101.07.2018
83. M.J.J. Decker, C.J. Halbach, C.H. Nam, et al., Stab resistance of shear thickening fluid (STF)-treated fabrics. Compos. Sci. Technol. **67**, 565–578 (2006)
84. A. Majumdar, B.S. Butola, A. Srivastava, An analysis of deformation and energy absorption modes of shear thickening fluid treated Kevlar fabrics as soft body Armour materials. Mater. Des. **51**, 148–153 (2013)
85. https://www.baesystems.com/en-ca/article/liquid-armour-to-become-a-future-choice-for-protecting-soldiers
86. M. Wei, K. Lin, L. Sun, Shear thickening fluids and their applications. Mater. Des. **216**, 110570 (2022)
87. R. Nayak, I. Crouch, S. Kanesalingam, et al., Body armor for stab and spike protection, part 1: Scientific literature review. Text. Res. J. **88**, 812–832 (2018)

Chapter 8
Shear Thickening Fluid-Based Protective Structures Against High Velocity Impacts

Neelanchali Asija Bhalla

8.1 Introduction

Shear thickening fluid (STF) is an important class of non-Newtonian fluids, which exhibit transition from low viscosity to high viscosity under shear forces. The shear thickening phenomenon is reversible, making the STF revert to the initial low viscosity state upon the removal of applied shear [1]. Due to this remarkable feature, STF is extensively used in vibration damping systems [2–4], hip protection pads [5], and anti-impact applications [6–9]. In the last two decades, STF has been integrated into personal protection equipment to develop liquid body armor. In this regard, advanced protective textiles are treated with STF and efficiently used against various threats such as knives, spikes, and projectiles [10–12]. Although there is an extensive literature available on the low strain rate response of STF [13–15], there is a limited literature on STF characterization under high strain rate conditions. In this field, initial studies were conducted by Lim et al. [16] using split Hopkinson pressure bar (SHPB) technique for high strain rate characterization of STF. Lim et al. [17] reported the phenomenological modeling of the SHPB results to predict the mechanical response of STF under dynamic squeeze flow loading conditions. Thereafter, Asija et al. [18, 19] investigated the effect of particle size on the low and high strain rate behavior of STF, as well as reporting the mechanical characterization of STF under high strain rate dynamic compressive loading.

This chapter presents a review on the protective applications of STF under high velocity impact conditions. According to the outline of the chapter, the next section deals with the detailed description and classification of impacts in different

N. A. Bhalla (✉)
Mechanical Engineering Department, Bennett University, Greater Noida, Uttar Pradesh, India

Center for Nanosensors and Nanomedicine, Bennett University,
Greater Noida, Uttar Pradesh, India
e-mail: neelanchali.bhalla@bennett.edu.in

S. Gürgen (ed.), *Shear Thickening Fluid*,
https://doi.org/10.1007/978-3-031-25717-9_8

categories based upon impact velocities. The subsequent sections explain the various characterization techniques and test methods to determine the efficacy of STF at high strain rate conditions. Then, various STF impregnation techniques and their efficacy are discussed considering the protective applications. Furthermore, there is a discussion on the stability of STF under different environmental conditions such as high temperature, humidity, and ultraviolet (UV) radiation.

8.2 Classification of Impacts

The term "impact" can be defined as striking of an object forcibly onto another object. The degree of impact is measured in terms of severity of impact, i.e., damage occurred. Based upon the impact velocity, there are different categories: low velocity (large mass), intermediate velocity, high velocity, and hypervelocity impact as shown in Fig. 8.1.

It is important to categorize the impacts since there are drastic changes in the energy transfer phenomenon between the projectile and target. Furthermore, energy dissipation and damage mechanisms show variations by the change of impact velocity [20, 21]. Low velocity impacts occur at the velocities less than 10 m/s. Impacts occurring in the velocity range of 10–50 m/s are called intermediate velocity impacts, and impacts occurring at the velocity range of 50–1000 m/s are called high velocity impacts. Hypervelocity impacts are observed in the velocity range of 2–5 km/s [22].

8.3 Characterization of STF Under High Velocity Impacts

High velocity impact conditions produce high strain rate deformations in the materials. Figure 8.2 shows the classification of strain rates. For high strain rate levels, a special testing system namely split Hopkinson pressure bar (SHPB) test is used to characterize materials. In this testing procedure, strain rates from 10^2 to 10^4 s^{-1} are observed in the impact conditions. Figure 8.3 shows a typical SHPB testing system for high velocity impact conditions. As depicted in the figure, SHPB system

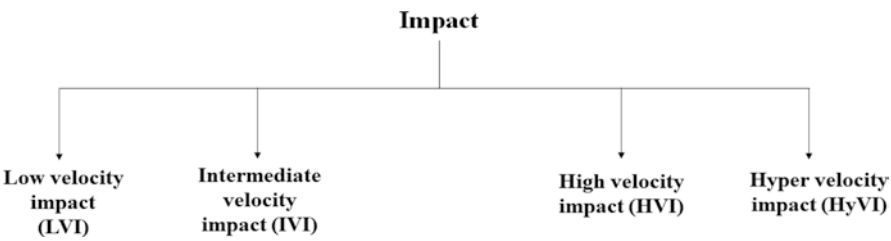

Fig. 8.1 Classification of impact based upon velocity

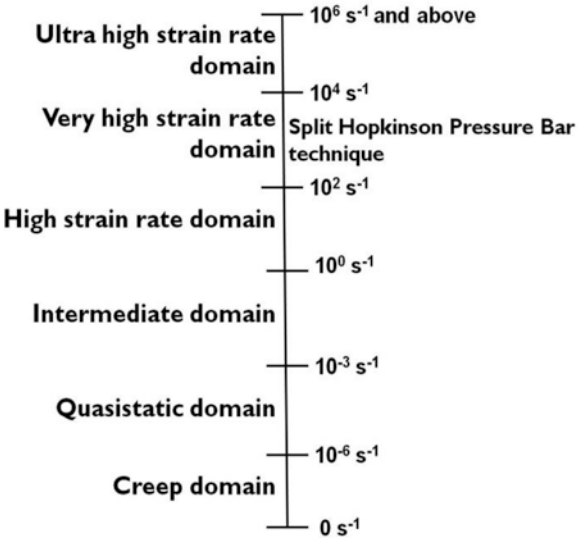

Fig. 8.2 Classification of strain rates

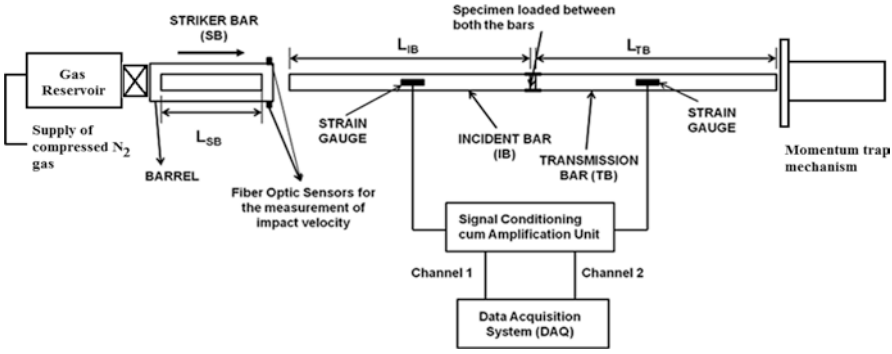

Fig. 8.3 Schematic illustration of an SHPB testing system

comprises three bars: striker bar, incident bar, and transmission bar. During the tests, striker bar is propelled through a long barrel under the pressure driven by a gas compressor. During striking on the incident bar, a part of the loading pulse is reflected back while the remaining part is carried through the transmission bar. The reflected and transmitted pulses are dependent on the mismatch of the acoustic impedance between the sample and bar. The term "acoustic impedance" is one of the materials properties that can be defined as the resistance by the medium in the propagation of longitudinal sound waves. Acoustic impedance depends upon the density and speed of sound through the material as given in Eq. (8.1).

$$Z = \rho \cdot C \tag{8.1}$$

where ρ is the density of the material, C is the speed of longitudinal waves in the material, and Z is the acoustic impedance of the material.

In the selection of bar material, the difference in the acoustic impedances of the sample and the bar is desired to be minimum to have a strong transmitted signal. For testing an STF in an SHPB system, the bar is generally made from AA6063 since the acoustic impedance of this alloy is quite close to that of STF. To have a successful SHPB test with an STF, the following conditions should be met.

1. The sample should be under a stable laminar flow.
2. The sample should be in a force equilibrium, i.e., the sum of the incident and reflected strains measured by the strain gauges should be equal to the transmitted strain.
3. A strong transmission signal should be obtained.

The satisfaction of above conditions contributes to the precise characterization of STF under high strain rate loadings. Prior to each test, a pulse shaper generally made of elastic rubber is placed at the impacting surface of the incident bar to increase the loading time since the pulse shaper deforms slower than the bar. This enables to have distinctive incident and reflected pulses while obtaining a near trapezoidal loading pulse (ε_i). The reflected and transmitted pulses are denoted by ε_r and ε_t, respectively. The magnitude of these pulses (ε_i, ε_r, and ε_t) is measured with strain gauges attached at the center of each bar. The specimen stress and strain are determined by using the SHPB equations, Eqs. (8.2, 8.3 and 8.4) given below;

$$\text{Compressional strain rate}: \ \dot{\varepsilon}s(t) = \left(\frac{2C_0}{Ls}\right)\varepsilon_r(t) \tag{8.2}$$

$$\text{Average strain}: \varepsilon s(t) = \pm\left(\frac{2C_0}{Ls}\right)\int_0^t \varepsilon_r(t)dt \tag{8.3}$$

$$\text{Average stress}: \sigma(t) = \pm E\frac{A_B}{A_S}\varepsilon t(t) \tag{8.4}$$

where, Co is the elastic wave velocity in the bars, Ls is the length of the sample, A_B is the cross-sectional area of the bar, A_S is the cross-sectional area of the sample, t is the duration, and E is the modulus of elasticity of the bar material.

The following assumptions are made in the relationships regarding the SHPB testing [23–25].

- Frictional and radial inertial effects are negligible.
- Wave propagation is considered by the one-dimensional wave theory with negligible wave dispersion.
- States of stress and strain are homogeneous in the sample.
- Sample is perfectly in contact with the bars during the impact.

Table 8.1 Experimental parameters in a typical SHPB system

Parameter	Value
Length of barrel	2000 mm
Material of bars	AA6063
Length of incident and transmission bar	1200 mm
Length of striker bar	85 mm
Diameter of incident and transmission bar	15.5 mm
Elastic modulus of bar material	68.9 GPa
Density of bar material	2.7 g/cm^3
Speed of sound in bar	5052 m/s
Thickness of sample	0.35 mm
Diameter of sample	15.5 mm

Table 8.1 shows the experimental parameters for a typical SHPB system. The gap size between the incident and transmission bars corresponds to the thickness of sample. However, STF is a fluidic sample and, therefore, this size is obtained by the application of Kuzma's dynamic squeeze flow model as given in Eq. (8.5) [16, 26].

$$F = \frac{\pi R^4}{4}\left[\frac{3\rho}{5h}\left(\ddot{U}_1 - \ddot{U}_2\right) + \frac{15\rho}{14h^2}\left(\dot{U}_1 - \dot{U}_2\right)^2 + \frac{6\mu}{\mathrm{h}^3}\left(\dot{U}_1 - \dot{U}_2\right)\right] \tag{8.5}$$

where,

F is the total force applied to the sample.
h is the instantaneous thickness of the sample (Hs (1-ε)).
Hs is the thickness of the sample.
ε is the strain in the sample.
μ is the viscosity.
ρ is the density of the sample.
$\left(\ddot{U}_1 - \ddot{U}_2\right)$ is the gap closing acceleration between the bars.
$\left(\dot{U}_1 - \dot{U}_2\right)$ is the gap closing speed between the bars.

The terms "gap closing speed" and "gap closing acceleration" are illustrated in Fig. 8.4. As given in the schematic, U_1 is the displacement of the incident bar, U_2 is the displacement of the transmission bar, and h is the instantaneous thickness of the fluid sample. Since the thickness of the fluid sample varies continuously during the loading and unloading period, instantaneous sample thickness is considered as a function of time while depending on the strain. From Fig. 8.4, it is clear that the fluid sample initially undergoes an axial compression during the loading phase of the cycle when the incident bar moves axially. Thereafter, the fluid sample undergoes a squeezing and radially expanding phase between the bars.

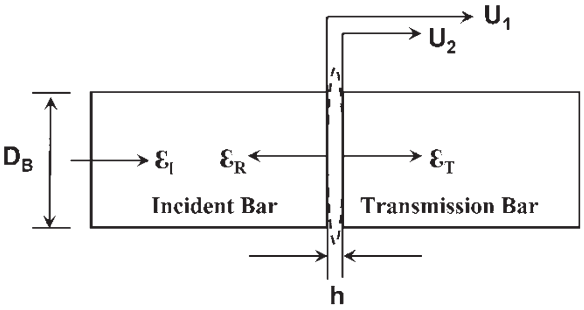

Fig. 8.4 Squeezing of the fluid sample under dynamic compressive loading

To determine the appropriate thickness of the fluid sample, the squeeze flow model is validated by using a standard fluid with a known viscosity. The viscous force in Eq. (8.5) can be written as in Eq. (8.6).

$$F_{\text{viscous}} = \frac{\pi R^4}{4}\left[\frac{6\mu}{h^3}\left(\dot{U}_1 - \dot{U}_2\right)\right] \tag{8.6}$$

By rearranging the terms in Eq. (8.6), the viscous force is obtained in Eq. (8.7).

$$\left(\frac{2h^3}{3\pi R^4}\right)F_{\text{viscous}} = \mu\left(\dot{U}_1 - \dot{U}_2\right) \tag{8.7}$$

All the terms in Eq. (8.7) are known except for the viscosity, which is the slope for the given relationship. Asija et al. [18] investigated a standard viscosity oil, N4000, to validate the sample thickness. The density and viscosity of the oil were known at different temperatures in accordance with ISO 17025 as provided by the manufacturer. To determine the sample thickness experimentally, the gap width between the incident and transmission bars was maintained at the desired value using a feeler gauge. The gap width was varied from 0.30 to 0.45 mm while firing each shot by keeping the pressure of the compressed gas constant at 0.2 bar. All the forces; the transient inertial force, bulk inertial force, viscous force, and experimental force were calculated for each shot. Figure 8.5 shows the relationship between the viscous force and gap closing speed based on the data obtained from the SHPB tests. The slope of the curve was calculated to determine the viscosity for different gap widths. The viscosities experimentally obtained from the graphs were compared with the viscosity given in the manufacturer's specifications. Based on the results, the experimental viscosity obtained for the gap width of 0.35 mm was the closest one to the viscosity given in the product sheet. Hence, sample thickness for SHPB testing was determined based on this procedure. Since the sample was a fluid, all the cross-sectional area of the bars was covered with the sample and, therefore, the diameter of the sample was considered as the diameter of the bars.

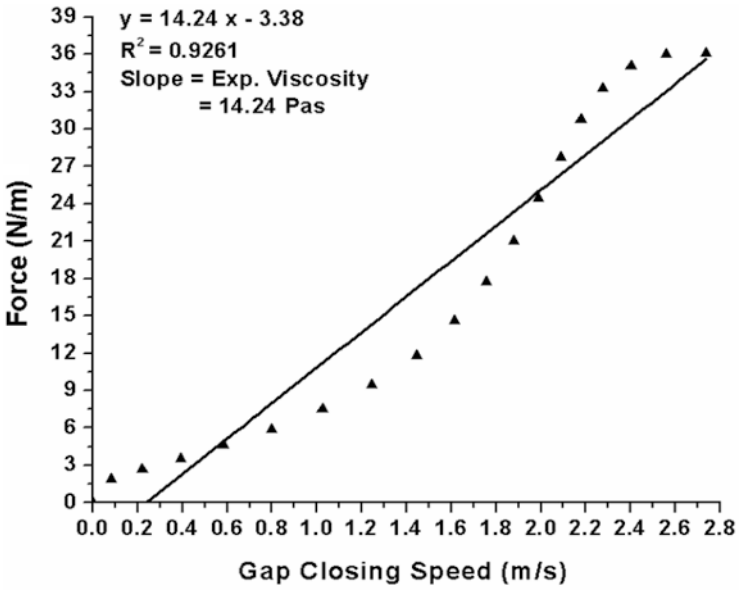

Fig. 8.5 Viscous force vs gap-closing speed for the standard oil N4000

After deciding on the dimensions of the sample, there is a list of steps followed to carry out the testing. The first step is calibration for ensuring reliable results. Calibration is done for two key points: (1) force calibration and (2) pressure-velocity calibration. In the force calibration procedure, the test is run without a sample between the incident and transmission bars. Since there is no specimen, there is no acoustic mismatch at the interface of the bars, thereby resulting in a complete passing of the stress pulse from the incident bar to the transmission bar without generating any reflected pulse. If the force measured by the strain gauge mounted on the incident bar equals to the force measured by the strain gauge mounted on the transmission bar upon running the test, stress states in the both bars become identical, which means that the system is perfectly aligned and ready for testing. On the other hand, the relationship between the impact velocity of the striker bar and the gas pressure of the gun is obtained in the pressure-velocity calibration. The impact velocity is measured with the help of fiber optic sensors, which are mounted at the specific locations with certain distances from each other.

A high-speed counter module equipped with programmable logic controller (PLC) is used to determine the time period between the sensors as the striker bar passes through the beam of the sensors before hitting the incident bar. This helps to compute the impact velocity of the striker bar. Figure 8.6 shows the schematic illustration of an impact velocity measurement system in the SHPB system.

After completing both calibration procedures, STF is applied at the interface of the incident and transmission bars by adjusting the gap width by the help of a feeler gauge. After applying the sample, the striker bar is fired by releasing the compressed

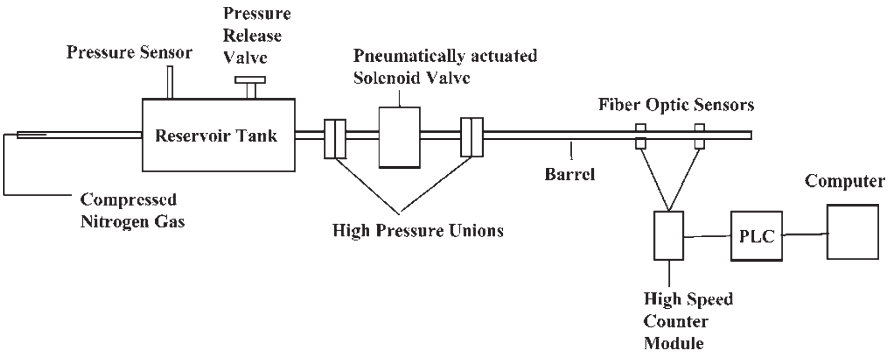

Fig. 8.6 Impact velocity measurement system in the SHPB system [18]. Reprinted by permission from Elsevier

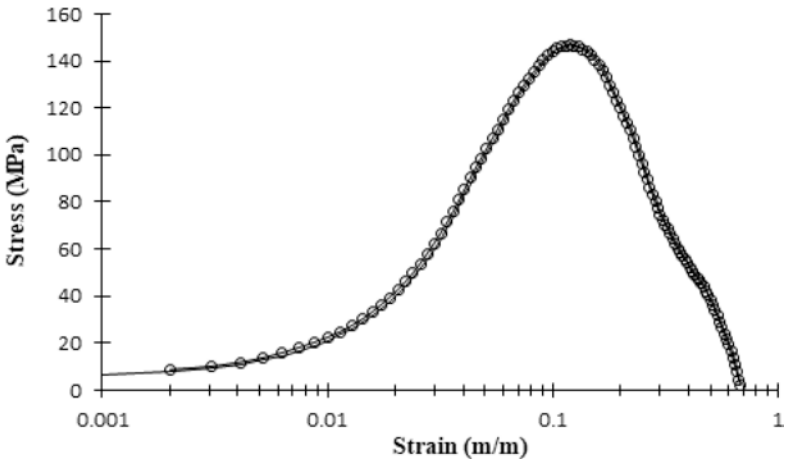

Fig. 8.7 Stress vs strain curve for an STF

gas. It is important to note that the test should be started immediately after the sample application to avoid STF leakage between the bars. Because STF is a viscous fluid, it shows loading and unloading cycles under dynamic compressive loading. For STF characterization on SHPB apparatus, one of the outputs is the stress and strain relationship during the impact. A typical graph of the stress vs strain curve for an STF is given in Fig. 8.7. It is clearly seen that there is a sharp increase in the stress beyond the critical strain. The stress induced in the sample is a measure of the capability to resist the deformation. Hence, higher stress magnitudes exhibit higher resistance to dynamic compressive impact. Since the stress is calculated from the magnitude of transmitted strain as given in Eq. (8.4), it is desirable to have a strong transmission signal in the SHPB testing. Another output is the relationship between strain rate and strain in the SHPB testing. Figure 8.8 shows a typical strain rate vs strain curve for an STF obtained from the SHPB testing. Similar to the

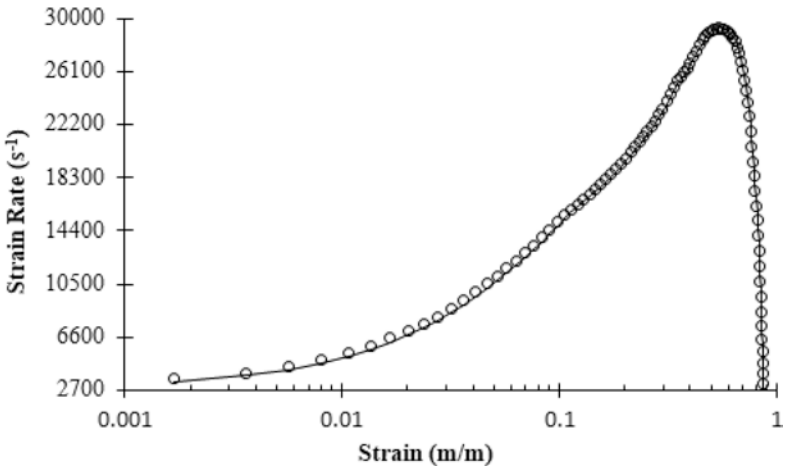

Fig. 8.8 Strain rate vs strain curve for an STF

relationship between stress and strain, strain rate curve increases beyond the critical point. The strain rate can be calculated by using Eq. (8.2) and requires the magnitude of the reflected pulse. The strain rate is a measure of loading rate for the sample, which implies how fast the sample is loaded to the peak value of the stress. To sum up, it is obvious that there is an increase in both stress and strain rate beyond a critical strain, which point out the onset of shear thickening phenomenon under dynamic compressive loading. This is completely analogous with the steady shear testing conducted with a rheometer, wherein the critical shear rate triggers the onset of the shear thickening behavior.

Characteristic transition time (CTT) is defined as the time required by STF to make the transition from the low viscosity state to high viscosity state. CTT is a characteristic feature of STF and provides more about the STF in addition to the stress and strain curves. CTT is influenced by all the parameters, which play a crucial role in the rheological behavior of STF such as particle size, particle size distribution, particle shape, particle hardness, and liquid medium. CTT is an important metric for the STF-included structures under dynamic loading. Generally, the CTT of an STF varies on a scale from microseconds to milliseconds. Technically, it is not possible to determine the CTT by using a commercial rheometer due to the operation timescales of milliseconds. For this reason, CTT is obtained from the SHPB testing. Figure 8.9 shows the compressive acceleration curve of an STF indicating the CTT on the graph. In the SHPB testing, the onset of shear thickening leads to the deceleration of the bars during the loading part of the stress cycle. The compressive acceleration is computed by taking the time derivative of the gap-closing speed at each instant and then subsequently plotting it with respect to time. The instance of the first deceleration in the plot, as seen in Fig. 8.9, indicates the onset of shear thickening phenomenon while providing the CTT of the STF. This information can only be deduced from the SHPB testing.

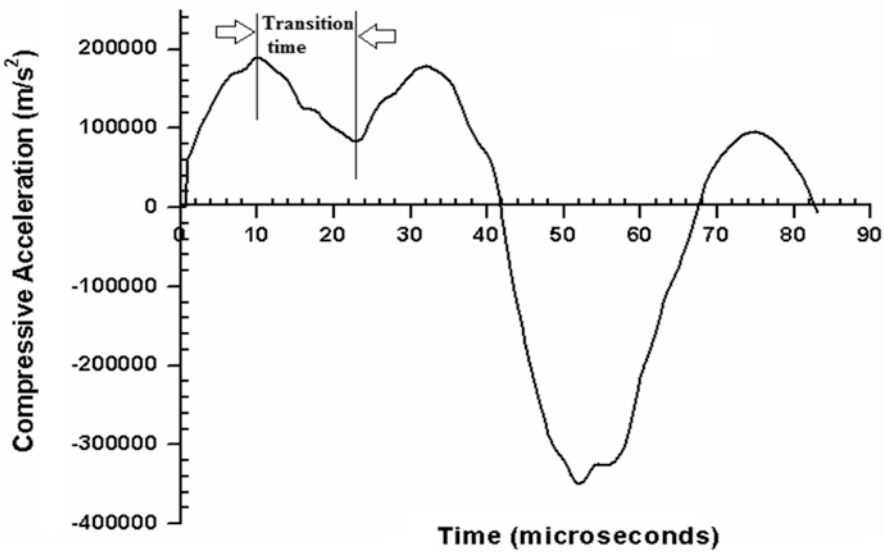

Fig. 8.9 CTT of an STF in the compressive acceleration curve

8.4 STF Applications in High Velocity Impact Resistant Protective Structures

As given in the previous sections, high velocity impact falls in the category of impact velocity range from 50 to 1000 m/s. In a high velocity impact event, it is very crucial to determine the strain rates and the CTT of the STF. Without knowing these parameters, it is highly difficult to ascertain the efficacy of STF under dynamic loading conditions.

Packaging technique of STF in protective structures is very crucial as it dictates the deformation and failure kinetics under high velocity impacts. According to the literature, STF-based protective structures can be produced in two different ways. In the first method, advanced engineering textiles are impregnated with STF by soaking the fabrics in a diluted STF pool. Then, the fabrics are rested to remove the excessive liquid and diluting agent. In the other method, STF is packed as a bulk liquid in a container and used as a liquid component in the structures. The use of STF in personal protection systems requires the development of special design to facilitate the incorporation of STF in different ways [27]. In the STF-integrated structures, it is imperative that the entire system is leak proof to prevent any leakage of STF in the impact events, thereby sustaining the anti-impact properties of the complete system. The structures can be modular in such a way that they may show the STF leakage only at a localized impacted area while preserving the efficacy of the remaining structure. Wisniewski et al. [27] proposed such kind of structural design including STF. It was observed that the STF-containing modules, which

were made of ballistic fabrics, performed better against high velocity impacts in comparison to the other designs including STF-impregnated fabrics.

There are several studies discussing the high velocity impact behavior of STF-included structures. De Goede et al. [28] reported the capability of complex non-Newtonian fluids to stop or retard the projectiles under high velocity impacts. It was stated that impact resistance can be attributed to the viscoelastic nature of the fluids rather than the shear thickening or shear thinning behavior. Hence, for the fabrication of liquid body armors, the focus shifted to use of polymeric viscoelastic fluids for an enhanced ballistic resistance. However, it was also observed that the anti-impact performance was higher with shear thickening suspensions in comparison to the other polymeric fluids. Kim et al. [29] studied the impact resistance of two different ballistic fabrics after impregnating with STF. The fabrics were also coated with a multi-purpose adhesive. Yarn pull-out tests and high velocity ballistic tests were conducted to characterize the fabrics. It was observed that STF impregnation provides no change in the flexibility of the ballistic fabrics; however, the yarn pull-out force as well as the energy absorption per unit areal density shows higher levels for adhesive-coated fabrics. Wei et al. [30] studied the effect of silica morphology on the stab resistance of STF-impregnated textile composites under dynamic impact conditions. Spherical silica-based STF was found to perform better as compared to the irregular-shaped silica STF in terms of induced stress and post-shear thickening viscosity under impact. Liu et al. [31] investigated the ballistic impact performance of multi-phase STF-impregnated high-performance fabrics against the titanium projectiles with the impact velocity of 250 m/s. Three different multi-phase STFs were fabricated by including graphene oxide (GO), carbon nanotubes (CNT), and a mixture of both in the suspensions. It was observed that multi-phase STFs exhibit enhanced yarn pull-out forces, lower value of critical shear rates, and post-shear thickening viscosity as compared to the single-phase STF. Moreover, the GO-based STF exhibited the highest energy absorption capability under high velocity impact testing among the investigated suspensions. With an objective to develop a low cost and biocompatible armor, Cho et al. [32] designed a bulletproof composite comprising composite panels and cornstarch-based STF. Contrary to the common STF applications, the composite panels were not impregnated with STF. In the target design, STF was kept in a sealed plastic bag, which was further encapsulated in a plastic container. It was observed that the normalized perforated area of the ballistic composite decreased with the increase in the thickness of STF layers as compared to the neat composite layers.

In addition to the impact resistance performance, there are various works dealing with the durability of STF in anti-impact structures. Since the protective structures are mainly used in open to atmospheric conditions, some key factors such as temperature, humidity, and UV radiation gain importance. Soutrenon et al. [33] studied the effect of processing methods and storage on the efficacy of STF. The efficacy was studied in terms of the change in critical shear rate and post-shear thickening viscosity. In their study, STF was prepared using hand mixing technique followed by sonication in an ultrasonic bath, jar rolling, and simply hand mixing the suspension followed by a vacuum degassing step. According to the results, increasing the

processing duration in sonication leads to a marginal increase in the viscosity at low shear rates while increasing the magnitude of shear thickening behavior, i.e., growing the peak viscosity. On the other hand, critical shear rate is significantly reduced by prolonging the sonication process. In order to investigate the storage conditions, STF samples were kept in different conditions as given below:

1. In a chamber with 22% relative humidity at ambient temperature for 45 days
2. In a chamber with 100% relative humidity at ambient temperature for 45 days
3. In a chamber with nitrogen gas at ambient temperature for 15 days
4. In a chamber at −24° C for 45 days
5. In a chamber at ambient temperature by encapsulating between two silicone layers for 15 days

It was observed that glycols are extremely hydrophilic in nature. They have high tendency to absorb moisture from the environment, thereby contaminating STF and causing deterioration in the shear thickening properties. As the molecular weight of glycols increases, the tendency to absorb moisture decreases. The STF at −24° C could preserve the shear thickening properties for the entire test duration. Since these conditions can only be found in laboratory, the efficacy of STF was checked in an encapsulation also. It was found that encapsulating STF in silicone tends to keep the shear thickening properties. From these results, it can be stated that STF encapsulation technique ensures to avoid any contact with air or contaminants in the ambient in order to have a prolonged service life of STF used in harsh conditions. Żurowski et al. [34] explored the influence of UV radiation on the shear thickening behavior. The synthesized STF samples were subjected to accelerated aging conditions with UV exposure for a total time period of 167 h, which corresponds to a natural aging period of 15.5 weeks. It was observed that prolonged exposure to UV radiation changes the oligomer structure to be degraded, thereby converting the liquid texture of STF into a solid phase. Consequently, the shear thickening behavior is completely lost. From these studies, it can be concluded that STF is susceptible to environmental conditions and, therefore, shear thickening properties are heavily affected by the ambient. In general, protective structures are used in harsh conditions including extremely low or high temperatures, humidity, and UV exposure; therefore, STF included protective systems should be designed taking all these issues into consideration.

8.5 Conclusions

There is a vast literature available on the rheological characterization of STF under steady and dynamic shear conditions. Researchers have also studied the anti-impact performance of advanced textiles with STF treatments; however, there is a limited literature discussing the efficiency of STF under high velocity impacts. For the STF usage against high velocity impacts, it is imperative to characterize the STF under high shear rates. The SHPB testing is a good way to do so. The information

delivered from the rheological tests are sometimes insufficient to ascertain the STF efficacy under high strain rate conditions. Moreover, it is also necessary to conduct investigations on the durability of STF in addition to the high strain rate characterizations. These studies help to determine the effect of environmental factors on the shear thickening behavior. As STF essentially comprises oligomers as the carrier fluid, its viscosity, and eventually shear thickening behavior, is drastically affected by the change in temperature. Similar to the temperature effect, humidity and UV exposure directly influence the microstructural properties of STF and thereby alter the shear thickening characteristics in the suspension. Because protective structures are mostly used in open to atmospheric conditions, they are subjected to various harsh conditions. For this reason, it is important that STF-based protective systems should be designed by considering the environmental effects on the shear thickening mechanism. Furthermore, STF should be isolated from the environmental exposures to avoid degradation in the shear thickening behavior.

References

1. S. Gürgen, M.C. Kuşhan, W. Li, The effect of carbide particle additives on rheology of shear thickening fluids. Korea Aust Rheol J. **28**(2), 121–128 (2016)
2. C. Fischer, A. Bennani, V. Michaud, E. Jacquelin, J.A.E. Månson, Structural damping of model sandwich structures using tailored shear thickening fluid compositions. Smart Mater. Struct. **19**(3), 035017 (2010)
3. C. Fischer, S.A. Braun, P.E. Bourban, V. Michaud, C.J.G. Plummer, J.A.E. Månson, Dynamic properties of sandwich structures with integrated shear-thickening fluids. Smart Mater. Struct. **15**(5), 1467 (2006)
4. S. Gürgen, M.A. Sofuoğlu, Experimental investigation on vibration characteristics of shear thickening fluid filled CFRP tubes. Compos. Struct. **226**, 111236 (2019)
5. S.N. Robinovitch, W.C. Hayes, T.A. McMahon, Energy-shunting hip padding system attenuates femoral impact force in a simulated fall. J. Biomech. Eng **117**, 409–413 (1995) http://biomechanical.asmedigitalcollection.asme.org/
6. M.J. Decker, C.J. Halbach, C.H. Nam, N.J. Wagner, E.D. Wetzel, Stab resistance of shear thickening fluid (STF)-treated fabrics. Compos. Sci. Technol. **67**(3–4), 565–578 (2007)
7. S. Gürgen, M.C. Kuşhan, Improvement of spall liner performance with smart fluid applications. Thin-Walled Struct. **180**, 109854 (2022)
8. M.R. Sheikhi, S. Gürgen, Deceleration behavior of multi-layer cork composites intercalated with a non-Newtonian material. Arch. Civ. Mech. Eng **23**(1), 1–11 (2023)
9. V.B.C. Tan, T.E. Tay, W.K. Teo, Strengthening fabric Armour with silica colloidal suspensions. Int. J. Solids Struct. **42**(5–6), 1561–1576 (2005 Mar)
10. S. Gürgen, T. Yıldız, Stab resistance of smart polymer coated textiles reinforced with particle additives. Compos. Struct. **235**, 111812 (2020)
11. S. Gürgen, F.A.O. Fernandes, R.J.A. de Sousa, M.C. Kuşhan, Development of eco-friendly shock-absorbing Cork composites enhanced by a non-Newtonian fluid. Appl. Compos. Mater. **28**(1), 165–179 (2021)
12. D.P. Kalman, R.L. Merrill, N.J. Wagner, E.D. Wetzel, Effect of particle hardness on the penetration behavior of fabrics intercalated with dry particles and concentrated particle-fluid suspensions. ACS Appl. Mater. Interfaces **1**(11), 2602–2612 (2009)
13. S. Gürgen, M.C. Kuşhan, The effect of silicon carbide additives on the stab resistance of shear thickening fluid treated fabrics. Mech. Adv. Mater. Struct. **24**(16), 1381–1390 (2017)

14. S.R. Raghavan, S.A. Khan, Shear-thickening response of Fumed silica suspensions under steady and oscillatory shear. J. Colloid Interface Sci. **185**, 57 (1997)
15. H. Yang, J. Ruan, J. Zou, Q. Wu, Z. Zhou, Z. Zhou, Rheological responses of fumed silica suspensions under steady and oscillatory shear. Sci. China Technol. Sci **52**(4), 910–915 (2009 Apr)
16. A.S. Lim, S.L. Lopatnikov, J.W. Gillespie, Implementing the Split-Hopkinson pressure bar technique for shear thickening fluid evaluation. AIP Conf Proc **1027**, 689–691 (2008)
17. A.S. Lim, S.L. Lopatnikov, N.J. Wagner, J.W. Gillespie, Phenomenological modeling of the response of a dense colloidal suspension under dynamic squeezing flow. J. Nonnewton Fluid Mech **166**(12–13), 680–688 (2011 Jul)
18. N. Asija, H. Chouhan, S.A. Gebremeskel, N. Bhatnagar, High strain rate characterization of shear thickening fluids using Split Hopkinson pressure Bar technique. Int J Impact Eng **110**, 365–370 (2017a)
19. N. Asija, H. Chouhan, S.A. Gebremeskel, N. Bhatnagar, Influence of particle size on the low and high strain rate behavior of dense colloidal dispersions of nanosilica. J Nanopart Res. **19**(1), 3723 (2017b)
20. S. Gürgen, The influence of boundary condition on the impact behavior of high performance fabrics. Adv. Electron. Forum **28**, 47–54 (2018)
21. N.K. Naik, P. Shrirao, Composite structures under ballistic impact. Compos. Struct. **66**(1–4), 579–590 (2004 Oct)
22. S.N.A. Safri, M.T.H. Sultan, N. Yidris, F. Mustapha, Low velocity and high velocity impact test on composite materials-a review. Int. J. Eng. Sci **3**(9), 50–60 (2014) Available from: www.theijes.com
23. H. Kolsky, An Investigation of the Mechanical Properties of Materials at very High Rates of Loading. Proc. Phys. Soc. **62**, 676–699 (1949)
24. N.K. Naik, V. Ch, V.R. Kavala, Hybrid composites under high strain rate compressive loading. Mater. Sci. Eng. A **498**(1–2), 87–99 (2008)
25. S.C. Woo, T.W. Kim, High-strain-rate impact in Kevlar-woven composites and fracture analysis using acoustic emission. Compos. Part B Eng **60**, 125–136 (2014)
26. A.S. Lim, S.L. Lopatnikov, J.W. Gillespie, Development of the split-Hopkinson pressure bar technique for viscous fluid characterization. Polym. Test. **28**(8), 891–900 (2009)
27. W. Adam, P. Dawid, Z. Pawel, W. Lukasz, K. Joanna, Z. Dorota, et al., Optimization of material systems with shear thickening fluids, in *28th International Symposium on Ballistics*. Atlanta, GA, (2014), pp. 1–10
28. T.C. de Goede, K.G. de Bruin, D. Bonn, High-velocity impact of solid objects on Non-Newtonian Fluids. Sci Rep **9**(1), 1250 (2019)
29. Y.H. Kim, S.K. Sathish Kumar, Y. Park, H. Kwon, C.G. Kim, *High-Velocity Impact onto a High-Frictional Fabric Treated with Adhesive Spray Coating and Shear Thickening Fluid Impregnation*, vol 185 (Compos B Eng., 2020), p. 107742
30. R. Wei, B. Dong, F. Wang, J. Yang, Y. Jiang, W. Zhai, et al., Effects of silica morphology on the shear-thickening behavior of shear thickening fluids and stabbing resistance of fabric composites. J. Appl. Polym. Sci. **137**(24), 1–7 (2020)
31. L. Liu, M. Cai, X. Liu, Z. Zhao, W. Chen, Ballistic impact performance of multi-phase STF-impregnated Kevlar fabrics in aero-engine containment. Thin-Wall. Struct **157**(29), 107103 (2020). https://doi.org/10.1016/j.tws.2020.107103
32. H. Cho, J. Lee, S. Hong, S. Kim, Bulletproof performance of composite plate fabricated using shear thickening fluid and natural fiber paper. Appl. Sci. **10**(1), 88 (2020)
33. M. Soutrenon, V. Michaud, J.A.E. Manson, Influence of processing and storage on the shear thickening properties of highly concentrated monodisperse silica particles in polyethylene glycol. Appl. Rheol. **23**(5), 20–28 (2013)
34. R. Żurowski, M. Tryznowski, S. Gürgen, M. Szafran, A. Świderska, The influence of UV radiation aging on degradation of shear thickening fluids. Materials **15**(9), 3269 (2022)

Index

A
Additives, 34, 38, 40–48, 54, 55, 59, 69, 117, 120–122, 134

E
Extensional flow, 18, 20

H
High velocity impacts, 124, 130, 134, 148–150

L
Liquid armor, 128, 132
Low velocity impact, 115–134

M
Multi-functional systems, 1, 2, 53–69
Multi-phase STF, 2, 34, 35, 40–48, 120–122, 149

N
Non-Newtonian fluid, 34, 35, 66, 103, 104, 115
Non-Newtonian rheology, 80

P
Polishing, 2, 21, 99–112

R
Rheology, 1, 2, 4, 17, 23, 24, 35, 38–48, 54, 55, 60, 65, 66, 79, 82, 84, 85, 88, 90, 92, 95, 99, 109

S
Shear flow, 5–17, 20
Shear thickening fluid (STF), 1, 2, 5–24, 34–40, 42–45, 47, 48, 53–69, 77–95, 99–112, 115–134, 139–151
Smart materials and structures, 34
Surface finishing, 2, 99–112

V
Vibration damping, 2, 36, 77–95, 139
Viscosity, 4–8, 10, 11, 15, 17, 19–23, 34, 35, 37–46, 53, 59, 78, 81, 85, 88, 99–101, 103–105, 109, 117, 119–122, 133, 134, 139, 143, 144, 147, 149–151

S. Gürgen (ed.), *Shear Thickening Fluid*,
https://doi.org/10.1007/978-3-031-25717-9_2